

Electronic Thesis and Dissertation Repository

8-14-2014 12:00 AM

The Roles of Matrix-Associated Periostin in an In Vitro Model of Hypertrophic Scarring

Justin D. Crawford
The University of Western Ontario

Supervisor
Dr. David O'Gorman
The University of Western Ontario

Graduate Program in Biochemistry
A thesis submitted in partial fulfillment of the requirements for the degree in Doctor of Philosophy
© Justin D. Crawford 2014

Follow this and additional works at: <https://ir.lib.uwo.ca/etd>



Part of the [Biochemistry Commons](#)

Recommended Citation

Crawford, Justin D., "The Roles of Matrix-Associated Periostin in an In Vitro Model of Hypertrophic Scarring" (2014). *Electronic Thesis and Dissertation Repository*. 2228.
<https://ir.lib.uwo.ca/etd/2228>

This Dissertation/Thesis is brought to you for free and open access by Scholarship@Western. It has been accepted for inclusion in Electronic Thesis and Dissertation Repository by an authorized administrator of Scholarship@Western. For more information, please contact wlsadmin@uwo.ca.

THE ROLES OF MATRIX-ASSOCIATED PERIOSTIN IN AN *IN VITRO* MODEL OF
HYPERTROPHIC SCARRING

(Thesis format: Monograph)

by

Justin David Crawford

Graduate Program in Biochemistry

A thesis submitted in partial fulfillment
of the requirements for the degree of
Doctor of Philosophy

The School of Graduate and Postdoctoral Studies
The University of Western Ontario
London, Ontario, Canada

© Justin D Crawford, 2014

Abstract

Abnormal scarring is a type of benign fibrosis of the skin that can restrict mobility, dexterity and quality of life. There are few, if any, truly effective treatment options for these conditions. Hypertrophic scarring is a common form of abnormal scarring characterized by increased fibroblast proliferation and differentiation of apoptosis-resistant and hypercontractile myofibroblasts that promote excessive deposition and contracture of the extracellular matrix (ECM). Periostin, a secreted ECM protein, is transiently expressed during normal cutaneous wound repair, but is abnormally abundant and persistent in abnormal scars and other benign fibroses that display enhanced fibroblast proliferation and myofibroblast differentiation. The objectives of this study were to elucidate the effects of periostin on fibroblast proliferation, myofibroblast differentiation and myofibroblast persistence in an *in vitro* human fibroblast model of hypertrophic scarring. Primary fibroblasts derived from patients with hypertrophic scars (HTS) or normal skin (NS) were cultured in two- and three-dimensional collagen cultures to more closely mimic their *in vivo* microenvironment. A series of *in vitro* techniques, including adenoviral transduction, WST-1 assays, stressed fibroblast populated collagen lattices (sFPCLs), western immunoblotting and immunofluorescence confocal microscopy were employed to assess periostin effects on fibroblast proliferation and myofibroblast differentiation under these culture conditions. Periostin treatment was shown to enhance HTS fibroblast proliferation in compliant 2D collagen cultures through Akt and Rho kinase dependent pathways. When subjected to isometric tension in sFPCLs, periostin enhanced myofibroblast differentiation, as evidenced by increases in collagen contraction, alpha smooth muscle actin (α SMA) and the formation of supermature focal adhesions. In contrast, no discernible effects of periostin treatment were evident in NS fibroblasts. Periostin signalling maintained α SMA levels in HTS fibroblasts in an environment of decreasing ECM tension, and this was correlated with changes in focal adhesion kinase, cofilin and myosin light chain activities. These studies are the first to identify periostin as a mediator of excessive proliferation, myofibroblast differentiation and persistence in human fibroblasts derived from hypertrophic scars. The findings reported here suggest that novel therapeutic interventions designed to deplete periostin levels in the dermis of hypertrophic scars may have utility for attenuating fibroblast proliferation and depleting myofibroblast populations, and thereby enhance scar resolution.

Keywords

Hypertrophic scarring; periostin; fibroblasts; *in vitro* human model; proliferation; myofibroblast differentiation and persistence; cell signalling; focal adhesions

Acknowledgments

“It’s good for the soul”

- Dr. David O’Gorman, 2009

First and foremost, I would like to thank my supervisor Dr. David O’Gorman. David it has been a great pleasure to work with you over the past six years. I am truly grateful for all your patience, support, and guidance and for giving me the opportunity to present my research on numerous occasions across Europe. Your advice and encouragement has been invaluable in my development as a scientist and I could not ask for a better mentor.

To the members of my advisory committee Dr. Frederick Dick and Dr. David Litchfield, thank you for your time and guidance. Your advice and feedback contributed greatly to the design and preparation of this thesis.

This thesis would not have been possible without the assistance, support and friendship provided by the staff and students at the Lawson Health Research Institute. In particular, I would like to thank Christina Raykha with whom I have worked alongside in the O’Gorman lab for the past six years. Thank you for your friendship and support throughout this project. I wish you all the best in your future endeavors.

For the past nine years, I have had the privilege of being a student at the University of Western Ontario. My time at Western would not have been the same without Colin Carruthers, Chase McLean, Jessica Willson, Michelle Nieuwesteeg and Mario Cepeda. Thank you for your friendship and wonderful memories that have made my time in London an enjoyable experience.

Lastly, I would like to thank my parents Dave and Angie and my sister Tiffany for their endless love and support throughout my university studies. Thank you for instilling in me the value of hard work and dedication. You have been exceptional role models and I would not be where I am today if not for you.

Table of Contents

Certificate of Examination.....	ii
Abstract.....	ii
i	
Acknowledgments.....	iv
List of Tables	x
List of Figures.....	xi
List of Appendices	xiv
List of Abbreviations	xv
Chapter 1.....	1
1 Introduction.....	1
1.1 The integumentary system.....	1
1.1.1 The epidermis.....	1
1.1.2 The dermis	2
1.2 Normal cutaneous wound repair.....	3
1.2.1 Hemostasis and the inflammatory phase.....	3
1.2.2 The proliferation phase	5
1.2.3 Myofibroblast differentiation.....	6
1.2.4 Remodelling phase.....	9
1.3 Abnormal cutaneous wound healing.....	10
1.3.1 Clinical features of abnormal cutaneous wound healing	10
1.3.2 Histological features of abnormal cutaneous wound healing	12
1.3.3 Epidemiological features of abnormal cutaneous wound healing	12
1.3.4 Treatments.....	13
1.4 TGFβ-1 is a difficult therapeutic target	14

1.5	Identification of TGF β -1-inducible proteins in abnormal wound healing.....	15
1.6	Periostin	16
1.6.1	Gene and protein structure	16
1.6.2	Classification as a matricellular protein.....	19
1.7	Periostin in normal cutaneous wound healing	22
1.8	Periostin in abnormal wound healing	25
1.9	Assessing the function of periostin in hypertrophic scar formation in an <i>in vitro</i> model system	26
1.10	Hypothesis and objectives.....	29
Chapter 2	30
2	Materials and Methods.....	30
2.1	Materials	30
2.1.1	Biochemicals.....	30
2.1.2	Cell culture.....	30
2.1.3	Cell proliferation assay	32
2.1.4	Protein chemistry	33
2.1.5	Polymerase Chain Reaction (PCR).....	37
2.1.6	Flow cytometry	38
2.1.7	Immunoprecipitation.....	38
2.1.8	Nickel magnetic bead precipitation	39
2.1.9	Loss-of-function studies.....	40
2.1.10	Immunofluorescence confocal microscopy	40
2.2	Methods.....	42
2.2.1	Clinical specimen collection.....	42
2.2.2	Primary cell culture.....	42
2.2.3	Preparation of rat tail type I collagen.....	43

2.2.4	WST-1 cell proliferation assay	43
2.2.5	Fibroblast Populated Collagen Lattices (FPCLs)	44
2.2.6	Western immunoblotting	45
2.2.7	PCR.....	47
2.2.8	Flow Cytometry	48
2.2.9	Immunoprecipitation (IP).....	49
2.2.10	Nickel magnetic bead precipitation	51
2.2.11	Loss-of-function studies.....	52
2.2.12	Immunofluorescence (IF) confocal microscopy	54
2.2.13	Statistical analyses	56
Chapter 3	57
3	<i>In vitro</i> analysis of the effects of periostin on fibroblast proliferation in hypertrophic scarring.....	57
3.1	Rationale	57
3.2	Assessment of <i>POSTN</i> expression and periostin levels in fibroblasts derived from hypertrophic scar tissue.....	57
3.3	Identification of <i>POSTN</i> variants in fibroblasts derived from hypertrophic scar tissue	58
3.4	Assessment of the basal proliferation rates of hypertrophic scar- and normal skin-derived fibroblasts in 2D collagen cultures	61
3.5	Assessment of the effects of periostin on hypertrophic scar and normal skin fibroblast proliferation in 2D collagen cultures	61
3.6	Identification of the signalling pathway(s) utilized by periostin to induce hypertrophic scar fibroblast proliferation in 2D collagen cultures	63
3.6.1	Assessment of PI3K inhibition effects on periostin-induced HTS fibroblast proliferation.....	63
3.6.2	Assessment of Akt inhibition effects on periostin-induced HTS fibroblast proliferation.....	63
3.6.3	Assessment of Glycogen synthase kinase - 3 beta (GSK-3 β) inhibition effects on periostin-induced HTS fibroblast proliferation	66

3.6.4	Assessment of Rho kinase (ROCK) inhibition effects on periostin-induced HTS fibroblast proliferation.....	68
3.6.5	Extracellular signal-regulated kinase (ERK) inhibition effects on periostin-induced HTS fibroblast proliferation	68
3.7	Discussion	71
Chapter 4	79
4	<i>In vitro</i> analysis of the effects of periostin on myofibroblast differentiation and persistence in hypertrophic scarring.....	79
4.1	Rationale	79
4.2	Assessment of the basal contractility of hypertrophic scar- and normal skin-derived fibroblasts in stressed fibroblast populated collagen lattices (sFPCL)	80
4.3	Assessment of the effects of periostin on the contractility of HTS and NS fibroblasts in sFPCLs	80
4.4	Identification of the mechanisms utilized by periostin to enhance HTS fibroblast contractility	83
4.4.1	Assessment of the effects of periostin on cell viability in sFPCLs.....	83
4.4.2	Assessment of the effects of periostin on proliferation in sFPCLs.....	83
4.4.3	Assessment of the effects of periostin on adhesion and 3D migration in rFPCLs	86
4.4.4	Assessment of the effects of periostin on myofibroblast differentiation in sFPCLs	86
4.5	Assessment of the effects of periostin-depletion of HTS myofibroblast differentiation in sFPCLs	89
4.5.1	Assessment of <i>POSTN</i> expression and periostin levels in HTS fibroblasts following adenoviral transduction with shRNAs against <i>POSTN</i>	89
4.5.2	Assessment of the effects of periostin depletion on HTS myofibroblast differentiation in sFPCLs	89
4.6	Assessment of NS fibroblast responses to periostin	91
4.6.1	Assessment of the effects of TGFβ-1 priming on NS fibroblast contractility	91
4.6.2	Assessment of the effects of HTS-conditioned media on NS fibroblast contractility in sFPCLs	95

4.6.3	Identification of potential periostin interactors in HTS- conditioned media	95
4.7	Assessment of the effects of periostin on HTS myofibroblast persistence in sFPCLs	97
4.8	Discussion	100
Chapter 5	106
5	<i>In vitro</i> analysis of the mechanisms utilized by periostin to induce myofibroblast differentiation and persistence in hypertrophic scarring	106
5.1	Rationale	106
5.2	Immunoprecipitation analyses of receptor interactions with periostin in HTS fibroblasts.....	106
5.3	Assessment of the effects of periostin on integrin-associated signalling molecules in HTS-derived fibroblasts.....	108
5.3.1	Assessment of the effects of periostin on FAK activation in HTS fibroblasts cultured in sFPCLs	110
5.3.2	Assessment of the effects of ROCK inhibition on periostin-induced HTS myofibroblast differentiation	110
5.3.3	Assessment of the effects of periostin on cofilin activation in HTS fibroblasts cultured in sFPCLs	113
5.3.4	Assessment of the effects of periostin on MLC activation in HTS fibroblasts cultured in sFPCLs	116
5.4	Supermature focal adhesions	119
5.4.1	Assessment of the effects of periostin on the formation of supermature focal adhesions.....	119
5.5	Discussion	120
Chapter 6	129
6	Conclusion	129
References	139
Appendix	165
Curriculum Vitae	166

List of Tables

Table 2.1 Buffers and medium for cell culture	31
Table 2.2 Inhibitors for cell proliferation assays	32
Table 2.3 Buffers for protein analysis.....	34
Table 2.4 Primary antisera for western immunoblotting	35
Table 2.5 Secondary antisera for western immunoblotting	37
Table 2.6 TaqMan gene expression assay primers	38
Table 2.7 Antisera for immunoprecipitation.....	38
Table 2.8 Buffers and solutions for immunoprecipitation	39
Table 2.9 Buffers for Nickel Magnetic Bead precipitation.....	40
Table 2.10 Adenoviral shRNA constructs	40
Table 2.11 Buffers for immunofluorescence confocal microscopy.....	41
Table 2.12 Antisera for immunofluorescence confocal microscopy	41
Table 2.13 Spectral properties of molecular probes and LSM 510 Duo Vario confocal microscope	42

List of Figures

Figure 1.1 Schematic representation of the phases of cutaneous wound repair.	4
Figure 1.2 Schematic representation of the events required for myofibroblast differentiation.	8
Figure 1.3 Clinical presentation of hypertrophic and keloid scars.	11
Figure 1.4 Schematic representation of the human <i>POSTN</i> gene and domain structures.....	18
Figure 1.5 <i>POSTN</i> expression and periostin levels are increased in hypertrophic scars.	27
Figure 3.1 <i>POSTN</i> expression and periostin levels are abundant in primary fibroblasts derived from hypertrophic scar tissue.	59
Figure 3.2 <i>POSTN</i> variant 1 is the most abundant transcript in hypertrophic scar fibroblasts	60
Figure 3.3 Periostin enhances the proliferation of hypertrophic scar-derived fibroblasts.	62
Figure 3.4 Inhibition of phosphoinositide 3-kinase attenuates periostin-induced and basal hypertrophic scar fibroblast proliferation.	64
Figure 3.5 Inhibition of Akt attenuates periostin-induced hypertrophic scar fibroblast proliferation.....	65
Figure 3.6 Glycogen synthase kinase-3 beta inhibition had no effect on hypertrophic scar fibroblast proliferation.	67
Figure 3.7 Rho kinase inhibition attenuates periostin-induced hypertrophic scar fibroblast proliferation.....	69
Figure 3.8 Extracellular signal-regulated kinase inhibition had no effect on basal or periostin- induced hypertrophic scar fibroblast proliferation.....	70
Figure 4.1 Hypertrophic scar-derived fibroblasts have enhanced contractility relative to normal skin-derived fibroblasts.	81

Figure 4.2 Periostin enhances collagen lattice contraction in abnormal scar-derived fibroblasts.....	82
Figure 4.3 Periostin had no effect on hypertrophic scar fibroblast viability in stressed fibroblast populated collagen lattices.....	84
Figure 4.4 Periostin had no effect on hypertrophic scar fibroblast proliferation in stressed fibroblast populated collagen lattices.....	85
Figure 4.5 Periostin had no effect on hypertrophic scar fibroblast adhesion and migration in three dimensional collagen cultures.....	87
Figure 4.6 Periostin enhances myofibroblast differentiation in hypertrophic scar-derived fibroblasts.....	88
Figure 4.7 <i>POSTN</i> expression and periostin levels are significantly depleted in hypertrophic scar fibroblasts transduced with adenovirus expressing shRNAs against <i>POSTN</i>	90
Figure 4.8 Periostin depletion had no effect on collagen lattice contraction in hypertrophic scar-derived fibroblasts.....	92
Figure 4.9 Periostin depletion significantly decreases α SMA levels in fibroblasts derived from a subset of HTS patients.....	93
Figure 4.10 Periostin depletion had no significant effects on myofibroblast markers in keloid scar fibroblasts.....	94
Figure 4.11 Fibrosis-associated growth factors are required to induce periostin sensitivity in normal skin fibroblasts.....	96
Figure 4.12 Identification of potential periostin interactors in hypertrophic scar conditioned media.....	98
Figure 4.13 Periostin maintains myofibroblasts in a differentiated state under conditions of decreasing ECM tension.....	99

Figure 5.1 Schematic representation of the proposed signalling pathway utilized by periostin to induce myofibroblast differentiation and persistence.	107
Figure 5.2 Immunoprecipitation analyses of receptor interactions with periostin in HTS fibroblasts.....	109
Figure 5.3 Periostin enhances focal adhesion kinase phosphorylation.....	111
Figure 5.4 Rho kinase inhibition significantly attenuates hypertrophic scar fibroblast contraction of stressed fibroblast populated collagen lattices.....	112
Figure 5.5 Periostin enhances cofilin phosphorylation in conditions of decreasing ECM tension in a subset of patients.	115
Figure 5.6 Periostin depletion reduces myosin light chain phosphorylation in HTS myofibroblasts cultured in sFPCLs in a subset of individuals.....	118
Figure 5.7 Periostin enhances supermature focal adhesion formation in hypertrophic scar-derived fibroblasts.....	121
Figure 5.8 Periostin enhances focal adhesion length and supermature focal adhesion formation in hypertrophic scar-derived fibroblasts.....	122
Figure 6.1 Schematic representation of the roles of periostin in hypertrophic scarring.	130

List of Appendices

Appendix A: Ethics Approval Notice	165
--	-----

List of Abbreviations

2D	two-dimensional
3D	three-dimensional
α MEM	Alpha modified Eagle's medium
ANOVA	Analysis of variance
α SMA	Alpha smooth muscle actin
Akti	Akt inhibitor VIII
ATP	Adenosine-5'-triphosphate
AU	Arbitrary units
β ig-h3	TGF β -induced gene clone 3
bp	Base pairs
BSA	Bovine serum albumin
CM	Conditioned media
DI	Aspartic acid-Isoleucine
DMSO	Dimethyl sulfoxide
ECM	Extracellular matrix
EMI	Emilin-like
EMT	Epithelial-mesenchymal transition
ERK	Extracellular signal-regulated kinase
ERKi	Extracellular signal-regulated kinase inhibitor, PD98059
FA	Focal adhesion

FAK	Focal adhesion kinase
FAS1	Fasciclin 1
FBS	Fetal bovine serum
GAP	GTPase activating protein
GDP	Guanosine-5'-diphosphate
GEF	Guanine nucleotide exchange factor
GSK-3 β	Glycogen synthase kinase - 3 beta
GSK-3 β i	Glycogen synthase kinase - 3 beta inhibitor VIII
GTP	Guanosine-5'-triphosphate
hrPN	Human recombinant periostin
HTS	Hypertrophic scar
IP	Immunoprecipitation
KS	Keloid scar
LAP	Latency-associated peptide
LC-MS/MS	Liquid chromatography tandem mass spectrometry
LTBP-1	Latent TGF β -1 binding protein-1
MLC	Myosin light chain
MMP	Matrix metalloproteinase
MOI	Multiplicity of infection
MW	Molecular weight
Ni	Nickel
NLS	Nuclear localization signal

NS	Normal skin
Pa	Pascals
PBS	Phosphate buffered saline
pCofilin	Phosphorylated cofilin
PCR	Polymerase chain reaction
pFAK	Phosphorylated focal adhesion kinase
PI3K	Phosphatidylinositide 3-kinase
PI3Ki	Phosphatidylinositide 3-kinase inhibitor, LY294002
pMLC	Phosphorylated MLC
PMN	Polymorphonuclear cells
PN	Periostin
RGD	Arginine-Glycine-Aspartic acid
rFPCL	Relaxed fibroblast populated collagen lattice
ROCK	Rho kinase
ROCKi	Rho kinase inhibitor, Y27632
RQ	Relative quantification
SDS-PAGE	Sodium dodecyl sulfate – polyacrylamide gel electrophoresis
SEM	Standard error of the mean
sFPCL	Stressed fibroblast populated collagen lattice
suFA	Supermature focal adhesion
TGF β	Transforming growth factor beta
UV	Ultraviolet

Veh	Vehicle
WB	Western immunoblot
WST-1	Water soluble tetrazolium-1

Chapter 1

1 Introduction

1.1 The integumentary system

The integumentary system, which is comprised of the skin and its appendages, is the largest organ in the body and accounts for up to 15% of the total adult body weight (1, 2). The main function of the skin is to provide a physical, chemical, and adaptive barrier to protect the body from external damage (1, 3, 4). The skin also plays important roles in hydration, sensation, thermoregulation, vitamin D synthesis, immune function and ultraviolet radiation protection (2, 5). This unique tissue is composed of two morphologically and functionally distinct layers: the epidermis and the dermis (1, 6).

1.1.1 The epidermis

The superficial protective layer known as the epidermis is largely composed of stratified epithelium that continuously renews itself (1). The epidermis is mostly comprised of keratinocytes (90-95%) that originate from progenitor cells adjacent to the dermis. These cells undergo progressive differentiation resulting in flattened, anucleated, keratin-rich cells that form the physical barrier of the skin (1, 5). The epidermis also contains Langerhan's cells, melanocytes, Merkel cells, and lymphocytes (1, 2). Immune function in the epidermis is maintained by lymphocytes and Langerhan's cells, which are dendritic cells that process and present antigens to T-cells (1, 2). Melanocytes produce the protein melanin, which is responsible for skin colour and protection from ultraviolet radiation (1, 2). Lastly, Merkel cells are mechanoreceptors that make contact with sensory neurons and are involved with the sensation of touch (1, 2).

The epidermis is typically composed of four, and in some cases five, continuous layers known as stratum. From lower to upper epidermis, they are the stratum basale (the only layer capable of cell division), stratum spinosum, stratum granulosum, stratum lucidum (a layer only found in the palms and soles) and the stratum corneum (1, 2, 6). Since the epidermis is avascular, it relies on the vasculature in the adjacent dermis to provide nutrients. Therefore, as keratinocytes divide and move up through the epidermal layers

and away from the dermis, they receive fewer nutrients, undergo terminal differentiation and are ultimately shed by abrasion (1, 2). The epidermis is connected to the underlying dermis by the dermal-epidermal junction that facilitates the exchange of metabolic products between the stratum basale and the dermis (1, 2).

1.1.2 The dermis

The primary role of the dermis is to provide structure and tensile strength to the skin (1, 2, 6). The dermis is divided into 2 layers, the papillary and reticular dermis (1, 2, 6). The papillary region is adjacent to the epidermis and contains the vasculature that allows for the exchange of metabolic products between the epidermis and dermis (1, 2, 6). The papillary dermis is also rich in nerves and nerve endings, both of which are responsible for transmitting the sensation of heat and touch (1, 6). The deeper reticular dermis is composed of fibroblasts, blood vessels, lymphatic vessels and extracellular matrix (ECM) proteins including collagens and elastins (1, 6). Fibroblasts are the heterogeneous population of cells of mesenchymal origin that synthesize and secrete collagens, proteoglycans, fibronectin, matrix metalloproteinases (MMPs) and other ECM proteins that make up the papillary and reticular dermal layers (7). The organization of these ECM proteins provides tensile strength and structure to the skin (2). The reticular dermis also supports the skin's appendages including hair follicles and various glands, including sweat glands (1, 2, 6).

Below the dermis is a layer known as the hypodermis that primarily consists of subcutaneous fat. Although not technically part of the skin, the hypodermis functions to anchor the skin to the underlying muscle and bone, and supplies the dermis with blood vessels and nerves (1, 6). Other than adipocytes, the hypodermis is also home to mast cells, lymphocytes, and fibroblasts, and contributes to thermoregulation, energy storage, immune response, and protection from mechanical injuries (1, 6).

Since the skin acts as a physical, chemical, and adaptive barrier to external insults, damage to the skin can leave an individual susceptible to a number of pathological conditions (8). Upon injury, the body needs to rapidly and effectively repair the wound to prevent infection and restore integrity to the skin (8).

1.2 Normal cutaneous wound repair

Integumental injuries are defined as any insult or disruption to the normal structure and function of the skin (9, 10). These injuries can range from a small break that disrupts epithelial integrity to injuries extending deep into the dermis and subcutaneous tissue (11, 12). The complex process required to repair injury, wound repair, is divided into 3 overlapping phases: the inflammatory, proliferation and remodelling phases (Figure 1.1, (10)). In each phase, several important molecular, humoral and cellular events occur in order to regenerate the protective barrier of the skin (10). The important features of each phase of normal cutaneous wound repair are described in the following sections.

1.2.1 Hemostasis and the inflammatory phase

Immediately after insult to the dermis, the inflammatory phase begins with a process known as hemostasis, characterized by the formation of a blood clot and cessation of bleeding (8). Fibrin, platelets and disrupted blood vessels play an important role in mediating this process. Minutes after injury, a clot is formed comprised mainly of fibrin and platelets (8). The formation of the clot not only prevents blood flow, it also acts as a provisional matrix for inflammatory cells and fibroblasts to infiltrate the wound (12). This provisional matrix is also a repository for growth factors and cytokines (12). During hemostasis, activated platelets in the provisional matrix excrete the growth factors and cytokines in their granules. One of these cytokines is transforming growth factor (TGF) β , a molecule that is utilized by numerous cell types in all phases of wound healing (8, 13, 14). In addition to the formation of a fibrin clot, vasoconstriction occurs at the site of injury, thereby preventing blood flow and contributing to hemostasis (8).

Vasoconstriction lasts upwards of 15 minutes and is mediated by the release of vasoactive amines from injured cells (15, 16). Local vasoconstriction, in concert with activated platelets, allows for the accumulation of growth factors and cytokines in the provisional matrix and promotes the recruitment of inflammatory cells and fibroblasts to the wound (10).

Once hemostasis is achieved, vascular changes occur that result in vasodilation and increased capillary permeability (8). The increased blood flow into the wound facilitates

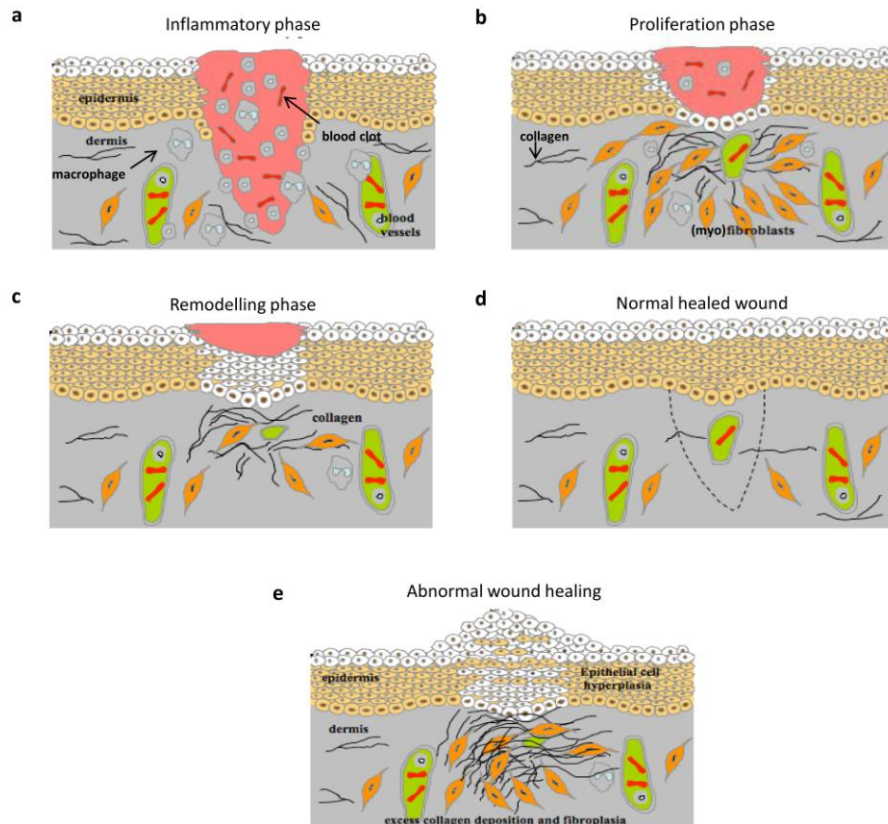


Figure 1.1 Schematic representation of the phases of cutaneous wound repair.

Normal cutaneous wound repair progresses through three overlapping phases following insult to the dermis. (a) The inflammatory phase is characterized by clot formation, vascular changes and recruitment of inflammatory cells, including macrophages, to the wound. Inflammatory cells are a major source of growth factors and cytokines that promote the proliferation phase. (b) The proliferation phase is marked by reepithelialization, angiogenesis, fibroblast migration and proliferation, collagen deposition and myofibroblast-mediated wound closure. (c) During the remodelling phase, collagen synthesis, degradation and ECM remodelling occur in order to restore strength to the wound. As the wound heals and the mechanical tension in the ECM is reduced, myofibroblasts and inflammatory cells undergo apoptosis. (d) The net result is a mature scar with high tensile strength. (e) When wound healing signals persist, excessive fibroblast proliferation and myofibroblast differentiation promote “overhealing” characterized by excessive ECM deposition and remodelling leading to the formation of abnormal scars.

the migration of inflammatory cells (8), such as polymorphonuclear cells (PMNs) and macrophages, that are attracted to the wound by growth factors and cytokines such as TGF β -1 (10, 12, 16, 17). PMNs and activated macrophages remove cellular debris, foreign particles and bacteria, and are a major source of the proinflammatory cytokines (13, 16, 18, 19) that regulate the inflammatory phase and initiate the proliferation phase (8, 13, 20, 21).

1.2.2 The proliferation phase

The proliferation phase is characterized by the formation of granulation tissue, dermal re-vascularization and the re-establishment of the protective barrier of the skin. Fibroblasts play a vital role in the proliferation phase as they produce the ECM proteins, including collagens, that make up the granulation tissue (8). The provisional matrix is initially devoid of fibroblasts, therefore fibroblast migration, proliferation, and ECM deposition are vital for the regeneration of a functional dermis (8). Plasma-derived fibronectin (22) and TGF β -1 are components of the provisional matrix that stimulate fibroblast migration to the wound (13, 23). Once within the wound, fibroblasts secrete components of the ECM, including collagens and fibronectin, and growth factors that regulate the function of other cells in the matrix (8). The ECM provides a scaffold for cell adhesion and regulates the growth, migration, and differentiation of the cells within it (24, 25). Collagen production begins approximately 3-5 days after injury and is stimulated by a number of cytokines including TGF β -1 (13, 16). In normal skin and mature scars, dermal collagen is composed of 80-90% type I collagen and 10-20% type III collagen. In the early stages of wound healing, the proportion of type III collagen increases to approximately 30% (8). Collagen deposition not only provides strength to the wound but also provides structural support for capillary formation and re-epithelialization (8).

The revascularization of the wound is a complex, but important, component of the proliferation phase. Cytokines, including TGF β -1 (26), activate endothelial cells at the wound site, resulting in the release of proteolytic enzymes, such as MMPs, that dissolve the basal lamina (10). This allows the activated endothelial cells to proliferate and migrate within the wound. These newly built vessels interconnect with each other

forming a vessel loop (10). These new vessels differentiate into arteries and venules and restore blood flow to the newly formed granulation tissue (10).

Re-epithelialization is another important process in the proliferation phase and is required to restore the protective barrier of the skin. Keratinocyte migration across the provisional matrix and newly formed granulation tissue is stimulated by a lack of contact inhibition and growth factor stimulation (8, 10). As migration proceeds, keratinocyte proliferation occurs at the wound edge to replace the cells and provide more cells for the migrating sheet (8, 10). Migration ceases when cells from opposing sides of the wound come in contact (8, 10). Once contact inhibition is established, the keratinocytes proliferate and differentiate to re-establish the stratified epithelium, thus restoring the skin's protective barrier (8, 10).

1.2.3 Myofibroblast differentiation

A major event in the proliferation phase is the differentiation of fibroblasts into contractile myofibroblasts. Myofibroblasts are the primary ECM producing cells in normal cutaneous wound healing and are responsible for the contracture of the granulation tissue during repair (27, 28). The myofibroblast was first identified in granulation tissue over forty years ago as a fibroblastic cell with a prominent endoplasmic reticulum and contractile microfilament bundles (29). The primary distinguishing feature of myofibroblasts is the neo-expression of alpha smooth muscle actin (α SMA) in stress fibres, allowing these cells to exhibit a hyper-contractile phenotype (30). Myofibroblasts are generally negative for smooth muscle myosin heavy chain, desmin, h-caldesom, and smoothelin, thereby distinguishing myofibroblasts from smooth muscle cells (31). In addition to fibroblasts, pericytes, vascular smooth muscle cells, cells undergoing epithelial-mesenchymal transition (EMT) and fibrocytes have all been implicated as precursors for myofibroblasts (32-37). Myofibroblasts combine the contractile features of smooth muscle cells with the extensive ECM production of fibroblasts (29, 31) thus allowing for deposition, contraction, and remodelling of the granulation tissue.

Fibroblasts in unwounded skin are stress shielded by the highly organized and cross-linked ECM that surrounds them. Following insult to the dermis, the initial contraction of

the wound by the tractional forces imposed by migrating fibroblasts, increases the mechanical tension in the granulation tissue (29, 38). This increase in ECM tension promotes the differentiation of fibroblasts into “proto”-myofibroblasts, characterized by the formation of stress fibres containing β and γ actin, mature focal adhesion formation, and *de novo* expression of the fibronectin splice variant, ED-A fibronectin (38, 39). Stress fibres connect to the ECM through integrin-associated focal adhesion complexes, while cell-cell interactions occur through *de novo* N-cadherin expression. The net result is an environment under high mechanical tension that allows the fibroblasts to stabilize their proto-myofibroblast phenotype (37).

Three events are required for the differentiation of proto-myofibroblasts into differentiated myofibroblasts characterized by the *de novo* expression of α SMA in their stress fibres (Figure 1.2, (30)). The first is the accumulation of cytokines such as active TGF β -1, which induces α SMA expression (40, 41). Platelet granules, immune cells, and fibroblasts secrete TGF β -1 in a latent form that is activated by increased mechanical tension within the ECM and by ECM-associated proteases (13, 42). Second, an accumulation of ED-A fibronectin in the ECM is required for myofibroblast differentiation (39). Lastly, the cells need to be stimulated by the increase in ECM tension generated by ECM remodelling (30). Specialized cell-ECM junctions termed fibronexus (*in vivo*) or “supermature” focal adhesions (*in vitro*) mediate this mechanoperception (43). The rigidity of the ECM determines the size of these cellular attachments to the ECM (43). α SMA can only become incorporated into pre-existing actin stress fibres once the ECM is stiff enough to allow the formation of supermature focal adhesions (suFAs, (43)). The formation of suFAs in combination with α SMA induction allows myofibroblasts to exert a 2-4 fold higher contractile stress on the ECM (43). A feedback loop between enhanced suFA formation and an ECM tension that is above threshold levels can maintain myofibroblasts in a differentiated state (43, 44).

In addition to secreting ECM proteins into the granulation tissue, myofibroblasts utilize their contractile machinery to achieve wound closure. This contractile force is generated by contractile stress fibres composed of actin bundles, non-muscle myosin, and actin-binding proteins, and is regulated by myosin light chain (MLC) phosphorylation

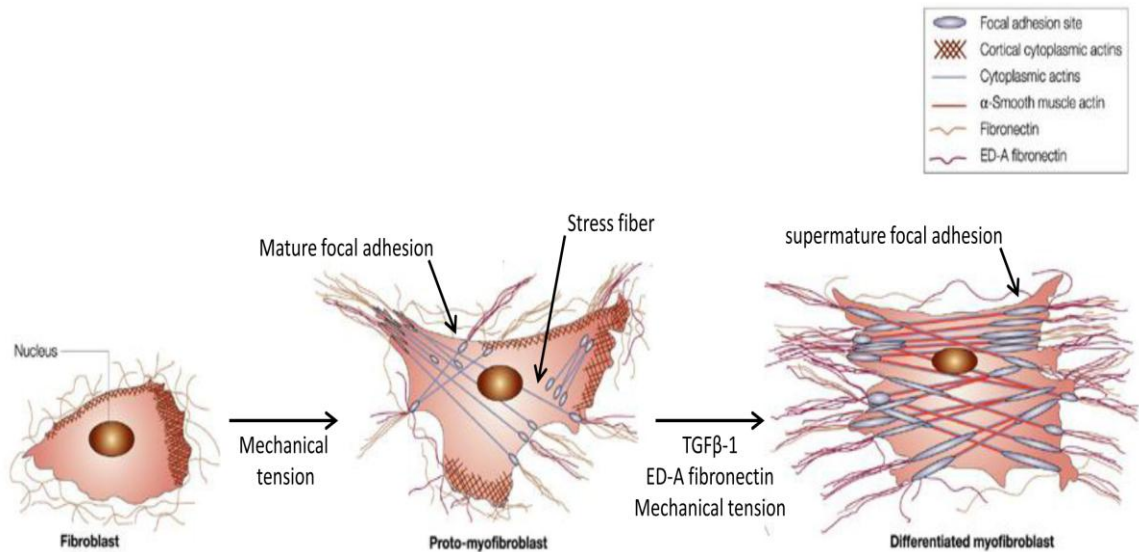


Figure 1.2 Schematic representation of the events required for myofibroblast differentiation. Fibroblasts in unwounded tissue are void of stress fibers and focal adhesions. Upon wounding, initial closure of the wound by migratory fibroblasts increases ECM tension leading to the formation of proto-myofibroblasts. Proto-myofibroblasts are characterized by the formation of stress fibers, mature focal adhesions and *de novo* expression of the fibronectin splice variant, ED-A fibronectin. Contractile forces generated by proto-myofibroblasts increase the mechanical tension in the ECM resulting in the formation of supermature focal adhesions and increased levels of active TGFβ-1 and ED-A fibronectin. The presence of mechanical tension, TGFβ-1 and ED-A fibronectin leads to myofibroblast differentiation characterized by *de novo* expression and incorporation of alpha smooth muscle actin into their stress fibers, giving these cells a hypercontractile phenotype. Figure adapted with permission from the authors from Tomasek et al (30).

(30, 45-47). Myofibroblasts utilize two signalling pathways to regulate MLC phosphorylation, the calcium dependent MLC kinase pathway and the Rho kinase (ROCK) pathway. An increase in intracellular concentrations of calcium activates MLC kinase, which promotes myofibroblast contraction through direct phosphorylation of MLC (46, 48). Since increased calcium levels are often transient, this contraction is rapid and short-lived and is actively inhibited by the effects of MLC phosphatase on MLC (30). In the ROCK pathway, guanosine-5'-triphosphate (GTP) bound RhoA activates ROCK (49, 50), which leads to increased MLC phosphorylation by two mechanisms. The first mechanism is by direct phosphorylation of MLC (51). The second mechanism is through MLC phosphatase inhibition (52, 53). Since MLC phosphatase activity is required for terminating myofibroblast contraction, its inhibition results in sustained contraction (30). Myofibroblast contractility in combination with ECM synthesis and degradation leads to connective tissue remodelling that includes the irreversible and long-term contracture events that result in wound closure and increased wound strength.

1.2.4 Remodelling phase

The remodelling phase represents a balance between collagen synthesis, collagen degradation, and collagen remodelling (8, 12) with the net result of increasing the strength of the wound. Net collagen production by fibroblasts peaks around three weeks after wounding, after which collagen production decreases (8, 16). As collagen production decreases, collagen degradation increases and several remodelling processes are initiated to enhance the strength of the wounded skin. Type III collagen and proteoglycan levels decrease while fibroblasts secrete increasing amounts of type I collagen, which imposes greater mechanical strength (8, 10). In the early stages of wound repair, the collagen is arranged haphazardly, resulting in the visual appearance of a "scar" (8). As the scar matures, wound strength increases as the collagen fibers become shorter, thicker, more organized and cross-linked due to contraction by myofibroblasts (8, 12). A mature scar has approximately 80% of the strength of unwounded skin (8, 12), indicating that wound repair falls short of true skin "regeneration". As the wound heals and mechanical stress of the ECM is relieved, the number of myofibroblasts and macrophages is reduced via apoptosis (8, 12). Over time, capillary growth ceases and blood flow to the

wound site decreases, resulting in reduced metabolic activity within the wound site (12). The net result is a relatively acellular and avascular mature scar with high tensile strength that approaches, but does not achieve, that of unwounded skin.

1.3 Abnormal cutaneous wound healing

Potentially, non-healing chronic wounds or excessive cutaneous scarring can arise from any aberration of processes that contribute to normal cutaneous wound healing.

Abnormalities in cell migration, proliferation, inflammation, ECM secretion, cytokine synthesis, and apoptosis can prevent normal wound repair (54) or conversely, contribute to excessive scar formation (55). Factors that promote excessive fibroblast proliferation and myofibroblast persistence leads to an “overhealing” phenomenon characterized by excessive collagen deposition at the site of injury, termed fibrosis (10), and contracture of the ECM (56, 57) that result in raised, collagenous scars. The associated pathological contracture of the skin can cause major clinical problems, and there are few treatment options. Abnormal cutaneous scarring can be divided into two broad categories, hypertrophic scarring and keloid scarring. The following sections will discuss the clinical, histological, and epidemiological characteristics of both hypertrophic and keloid scars and their treatment options.

1.3.1 Clinical features of abnormal cutaneous wound healing

Hypertrophic scars are clinically defined as raised collagenous scars that are confined to the borders of the initial wound (58). These scars occur 4-8 weeks following insult to the dermis, have a rapid growth phase of up to six months, then gradually regress over a period of years, eventually leading to a flat scar (59). In contrast, keloid scars extend beyond the borders of the initial wound, may develop several years after injury, or spontaneously, and do not regress over time (Figure 1.3, (58, 59)). Hypertrophic scars tend to occur at areas of high tension such as the shoulders, neck, pre-sternum, knees and ankles (59). In comparison, keloid scars tend to form on the shoulders, anterior chest, ear lobes, upper arms and the cheeks (59). Recurrence of hypertrophic scars following surgical incision is rare, however recurrence rates are high with keloid scars (59). Other than imposing a financial burden, these conditions impose morbidity that is difficult to

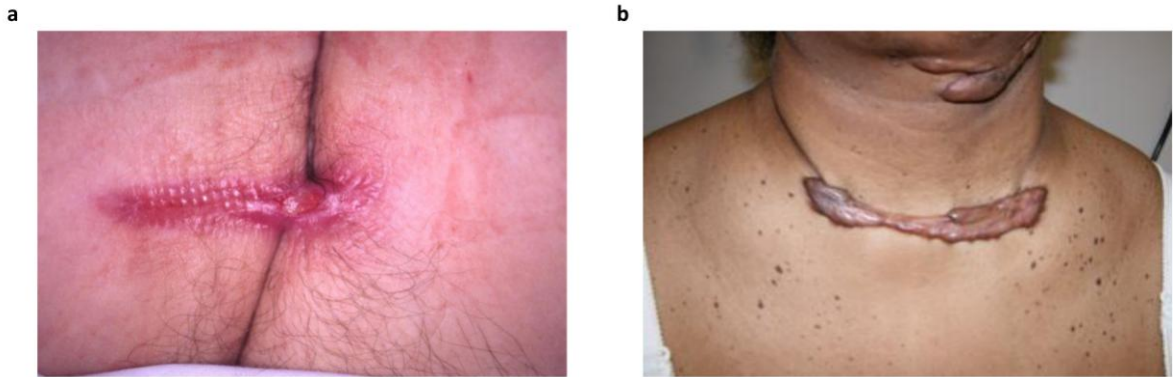


Figure 1.3 Clinical presentation of hypertrophic and keloid scars. (a) Clinical presentation of hypertrophic scarring following lymph node resection in the inguinal region. Hypertrophic scars present as raised collagenous scars that are confined to the borders of the initial wound. (b) Clinical presentation of keloid scarring on the anterior chest and the neck. In contrast to hypertrophic scars, keloid scars are able to extend beyond the borders of the initial wound. Photographs c/o Roth|McFarlane Hand and Upper Limb Centre.

quantify, including pain and loss of mobility, especially if the scar is associated with a joint (60). Furthermore, these scars are disfiguring and can adversely affect a patient's quality of life both physically and psychologically (60, 61).

1.3.2 Histological features of abnormal cutaneous wound healing

Histologically, both hypertrophic and keloid scars contain excessive amounts of collagen (59). Hypertrophic scars contain primarily type III collagen fibres arranged in a wavy pattern parallel to the epidermal surface (58). These scars also contain abundant nodules of myofibroblasts, small blood vessels, and large extracellular collagen filaments (58, 59). In contrast, keloid scars are composed of disorganized type I and III collagen fibres randomly oriented to the epidermal surface (59). These scars have poor vasculature, contain hypocellular collagen bundles and lack the excessive numbers of myofibroblasts evident in hypertrophic scars (59). Proliferating cell nuclear antigen, p53 and adenosine-5'-triphosphate (ATP) levels are elevated in keloid scars, suggesting that they are primarily the result of excessive fibro-proliferation and potentially explaining why they grow beyond the site of the original injury (62, 63). Both hypertrophic and keloid scars display increased immune cell infiltration, increased levels of TGF β -1 and myofibroblast persistence, however these features decline over time in hypertrophic scars and may explain why hypertrophic scars regress (58, 59, 62).

1.3.3 Epidemiological features of abnormal cutaneous wound healing

Hypertrophic and keloid scars have equal sex distribution and have the highest incidence rates in the second and third decade of life (59). Hormones may affect hypertrophic and keloid scar formation, as these scars tend to occur during puberty and pregnancy and the scars can decrease in size following menopause (59, 64, 65). The incidence of hypertrophic scars is probably higher than keloid scars, however there is currently insufficient data available to make robust comparisons (62). Incidence rates for hypertrophic scars vary from 40-70% following surgical incision and up to 91% following burns (66, 67). With the exception of albino individuals, keloid scars can develop in people of any skin color, however, dark skinned individuals are more susceptible with incidence rates as high as 16% in African populations (59). The

formation of hypertrophic scars does not appear to have any association with skin pigmentation (68). The notion of genetic predisposition has been suggested, as patients with keloid scars report a positive family history that is strongly associated with keloid formation at multiple anatomical sites (59, 69). In contrast, patients with hypertrophic scars typically report no family history of scar development (59).

1.3.4 Treatments

Increased tension at wound margins has been implicated in the development of hypertrophic scars, and several prophylactic approaches have been implemented on this basis to reduce hypertrophic scar development (59). Pressure therapy and silicone gel sheeting have been used to apply continuous pressure to the scar during wound repair. These approaches have shown little success and cause discomfort leading to reduced patient compliance (70). TGF β -3, which has been shown to reduce connective tissue deposition and is induced during the late stages of wound healing (71-73), has been used as a prophylactic approach to prevent scar formation. While initial studies showed evidence for the benefits of recombinant TGF β -3, further independent studies revealed that this treatment was unsuccessful in improving scar resolution (74). Current treatment strategies include corticosteroid injections, cryotherapy, surgical resection, radiotherapy, and laser therapy. These treatment strategies have varied success rates in the resolution of hypertrophic and keloid scars and can be associated with painful and disfiguring side effects, risk of malignancy (in the case of radiotherapy), and high recurrence rates (surgical and laser therapy) (59, 70). Emerging treatment strategies include interferon injections, which reduces collagen synthesis, and 5'-fluorouracil treatment to increase fibroblast apoptosis. These treatments have also demonstrated varied success rates and can present painful and harmful side effects (59, 70).

Although some treatments have been shown to be effective in reducing hypertrophic and keloid scar formation in individuals, few of these studies have been supported by well-designed studies with adequate control groups (59). Despite numerous studies, both *in vitro* and *in vivo*, there is limited information available regarding the cellular mechanisms that induce hypertrophic and keloid scar formation (59). One reason for our lack of knowledge of the cellular and molecular mechanisms involved in the development of

abnormal scars is a lack of representative and physiologically relevant animal models of hypertrophic scar formation (59). Therefore, gaining a better understanding of the biochemical processes involved in abnormal wound healing is crucial if we hope to achieve normal skin repair or, optimally, true skin regeneration in patients prone to abnormal scarring.

1.4 TGF β -1 is a difficult therapeutic target

As highlighted in the previous sections, TGF β -1 plays essential roles in normal cutaneous wound healing. In addition to these roles, excessive signalling by this cytokine has been implicated in hypertrophic and keloid scar formation (58, 59, 62). TGF β -1 has proven to be a difficult therapeutic target in many disease processes including abnormal scar formation, as it can exert pleiotropic effects on different cell types that can be diverse and, in some cases, seemingly paradoxical (75, 76). While TGF β -1 is one of several cytokines that attract PMNs and macrophages to the wound (10, 12, 16, 17), depletion of TGF β -1 in *Tgfb* null mouse models results in a lethal and widespread inflammatory response, revealing an essential anti-inflammatory role for this cytokine (77, 78). Knockdown of TGF β -1, its receptor, or signalling components in mouse models inhibits normal repair in the dermis (79-82), whereas TGF β -1 promotes matrix formation for keratinocyte migration while inhibiting keratinocyte proliferation (83, 84). *In vitro* studies demonstrate that TGF β -1 can promote fibroblast proliferation without affecting myofibroblast differentiation or myofibroblast differentiation without affecting proliferation, in the same cell line (75). These apparently paradoxical outcomes are likely to be the result of concurrent activation of other signalling pathways that modify and supplement the downstream effects of TGF β -1 signalling intermediates. For this reason, the identification of TGF β -1-inducible proteins that supplement, enhance or modify TGF β -1 signalling to promote pathological, rather than normal, fibroblast proliferation and/or myofibroblast differentiation may have greater utility as therapeutic targets than TGF β -1 itself.

1.5 Identification of TGF β -1-inducible proteins in abnormal wound healing

During cutaneous wound healing, TGF β -1 is released into the ECM by platelet granules, inflammatory cells and fibroblasts (13, 83) in an inactive form in association with latency-associated peptide (LAP) and latent TGF β -1 binding protein-1 (LTBP-1) (31). Extracellular matrix proteins associate with LTBP-1 creating a reservoir of latent TGF β -1 (85-87). Latent TGF β -1 bound in the ECM can interact with cells through integrin binding sites located in the LAP (85, 88). Stress applied to these integrins, either by stretching the ECM or by inducing cellular contraction, results in a conformational change in the large latent complex allowing the release of TGF β -1 in an active form (42). Mechanical activation of TGF β -1 enhances tissue remodelling by translating the level of ECM stiffness into pro-fibrotic signals (31). Therefore, the ECM is an important regulator of TGF β -1 activation in both normal and abnormal wound healing.

The ECM is comprised of both structural and non-structural proteins (89, 90). Structural proteins, such as collagens and fibronectin, provide strength to the dermis and act as scaffolds for migrating cells and as reservoirs for growth factors (8). Non-structural proteins within the ECM include cytokines like TGF β -1 and the family of “matricellular” proteins that modify cell signalling in response to extracellular stimuli, such as changes in mechanical tension of the ECM (40, 42, 90). Given the well-established roles of the ECM in scar formation, studies were focused on the roles of non-structural proteins in the ECM that might be activated by and/or act in combination with TGF β -1 to promote excessive scarring.

Initial studies in our laboratory showed increased expression of genes encoding ECM proteins in Dupuytren’s Disease, a fibro-contractile disease of the palmar fascia that has many similarities to abnormal scarring. Microarray analyses of tissues derived from patients with or without Dupuytren’s disease identified *POSTN*, encoding the matricellular protein periostin, as a very highly upregulated transcript (91). Subsequent *in vitro* experiments demonstrated that periostin induced fibroblast survival and myofibroblast differentiation in primary fibroblasts derived from Dupuytren’s disease

tissue and induced proliferation of fibroblasts derived from “pre-diseased” palmar fascia (91). As excessive fibroblast proliferation and increased myofibroblast differentiation and persistence are also characteristics of hypertrophic scarring (56, 57, 92-94), further studies were performed to investigate whether periostin expression was abundant in hypertrophic scar tissue. Western immunoblotting, immunohistochemistry and *in-situ* hybridization data performed by our laboratory (95, 96) and reports by other groups (97-99) demonstrated that *POSTN* expression was upregulated in the basal stratum of hypertrophic and keloid scar tissue relative to mature normal scar tissue. Levels of the translated product of *POSTN* mRNA, periostin, were also upregulated in the dermis (but not the basal stratum) of hypertrophic and keloid scar tissue relative to normal mature scars. Based on these studies, it was proposed that periostin might contribute to excessive fibroblast proliferation and myofibroblast differentiation in hypertrophic scarring.

1.6 Periostin

1.6.1 Gene and protein structure

Periostin was originally identified as osteoblast-specific factor 2, a novel cell-adhesion molecule, in a mouse osteoblastic cell line (100, 101). Using murine cDNAs as probes, human homologs encoding a protein with a molecular weight of up to 93 kDa were subsequently identified in placental and osteosarcoma cDNA libraries (100, 102). Osteoblast-specific factor 2 was later renamed periostin due to its preferential expression in cells of mesenchymal origin located in the collagen rich ECM surrounding the periosteum and periodontal ligament (101). The murine periostin gene, *Postn*, located on chromosome three and the human gene, *POSTN*, located on chromosome 13, are highly homologous. Amino acid identity between the two species is 89.2% for the entire protein and 90.1% for the mature processed forms (100). *POSTN* encodes 23 protein-coding exons over a genetic footprint of 36 kilobases (102). *POSTN* expression is upregulated by a number of factors involved in wound healing including TGF β -1, interleukins, platelet-derived growth factor and fibroblast growth factor (101, 103, 104).

The N-terminal signal sequence of periostin consists of 23 amino acids and lacks a transmembrane domain, suggesting that periostin is a secreted protein (100). This is consistent with pronounced immunoreactivity to periostin in the ECM surrounding the periosteum and periodontal ligaments (101). Following the signal sequence is a cysteine-rich Emilin-like (EMI) domain encoded by exons two and three (100, 102). EMI domains are typically involved in protein-protein interactions (105) and protein multimerization, and periostin dimers have been reported in some studies (106). Adjacent to the EMI domain are four repeated regions of 150 amino acids encoded by exons 3-14 (100, 102). These repeats share homology with the insect axon guidance protein fasciclin 1 (FAS1), an adhesion module (100, 107). Since periostin contains FAS1 domains, it has been assigned to the fasciclin family of proteins that includes stabilin 1 and 2, and TGF β -induced gene clone 3 (β ig-h3) (108). Each FAS1 domain contains two conserved regions of 13-14 amino acids that have high sequence similarity. However, the conserved repeats between the FAS1 domains have relatively low sequence homology (100). Each FAS1 domain contains glutamate residues and contains N-terminal recognition sites for γ -glutamylcarboxylase, an enzyme responsible for posttranslational modification of glutamate residues (109). The FAS1 domains are believed to be involved in cell adhesion and protein-protein interactions, as bone morphogenic protein-1, tenascin C, and integrins have been suggested to bind this region of periostin (110-112). Interestingly, periostin does not contain any canonical Arg-Gly-Asp (RGD) integrin binding motifs, suggesting that integrin binding by periostin is independent of these motifs (102). β ig-h3, which has a domain structure similar to periostin (102), has been demonstrated to bind $\alpha_3\beta_1$ integrins at sites that are independent of the RGD motif (112). This interaction occurs by two pentapeptides containing a central Asp-Ile (DI) dimer located in the second and fourth FAS1 domain (112). The DI dimer has a similar conformation to the RGD binding motif (113) and suggests a mechanism for periostin-integrin interactions (102).

Lastly, exons 16-23, accounting for 182 amino acids, make up the hydrophilic or C-terminal domain (102). This region is devoid of known domains, contains few known sequence motifs and contains a C-terminal nuclear localization signal at exon 22-23 (102), suggesting that periostin may also have intracellular functions (114). Exons 17-21

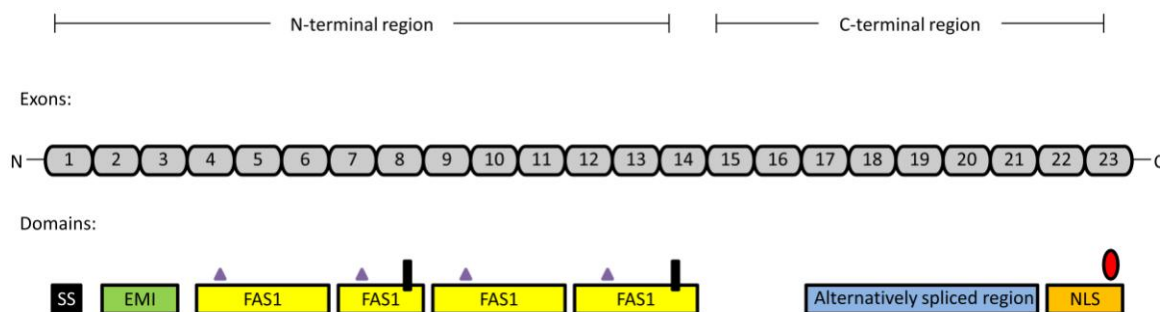


Figure 1.4 Schematic representation of the human *POSTN* gene and domain structures. The human *POSTN* gene contains 23 protein-coding exons. Exon 1 encodes a signal sequence (SS), characteristic of secreted proteins. Exons 2-3 encode for the Emilin-like (EMI) domain involved in protein-protein interactions and protein multimerization. Exons 3-14 encode four repeated fasciclin 1 (FAS1) domains involved in cellular adhesion and protein-protein interactions. Purple arrows represent recognition sites for γ -glutamylcarboxylase and vertical black bars represent proposed integrin binding sites in FAS1 repeats 2 and 4. Exons 17-21 present themselves as exon cassettes that can be present or deleted in mature mRNA through alternative splicing events. Exons 22-23 encode a C-terminal nuclear localization signal (NLS). Red oval represents heparin binding site in exon 23.

can be considered as “exon cassettes” that can be included or deleted in mature mRNA in various combinations through alternative splicing events (100-102). This results in several periostin isoforms ranging in size from 83-93 kDa (115). The number of nucleotide residues in each exon cassette is a multiple of three, and therefore deletion or inclusion of any of these cassettes in the mature mRNA does not result in frameshift mutations (100). Initial studies identified four periostin isoforms in mouse and five isoforms in human tissues (100, 101), with additional studies expanding the latter to eight isoforms (116, 117). These isoforms appear to be differentially expressed during development and injury and appear to be tissue, developmental stage or disease specific (114, 118-121). However, the function(s) of each individual isoform remain unclear. Secondary structure predictions demonstrate consecutive beta strands as the predominant structure in the C-terminal domain (102). β ig-h3, which lacks this domain, has not been reported to interact with collagen or fibronectin. Therefore it has been proposed that the C-terminal domain’s beta strand structure may facilitate periostin binding to collagen and fibronectin (102). Periostin contains similar repeats to those found in various bacteria that are able to bind fibronectin through an extended beta zipper (102, 122). Therefore, the strength of periostin’s interaction with the ECM would be influenced by the number of beta strands present in the mature protein determined by alternative splicing (102). Lastly, the C-terminal domain contains a heparin binding site in exon 23, creating a potential binding site for glycoproteins and proteoglycans (Figure 1.4, (101)).

1.6.2 Classification as a matricellular protein

Periostin has been classified as a matricellular protein (123), i.e. one of a family of structurally unrelated ECM proteins that do not serve a structural role in the ECM but instead serve as a link between the ECM and cells and modify cell behavior in response to external stimuli (90, 124). Originally, this family of proteins consisted of thrombospondin, tenascin-C and SPARC but recent studies have classified osteopontin, periostin and members of the CCN family, including CCN2, as matricellular proteins (125). Several characteristics have been identified for the classification of matricellular proteins. 1) Matricellular proteins interact with structural components of the ECM,

receptors, growth factors and proteases thereby allowing these proteins to regulate cellular signalling cascades (125). 2) Matricellular proteins promote an intermediate cellular adhesive state (126) that activates survival signals and increases expression of genes associated with adaptation and repair (125). 3) In normal adult tissue, expression of matricellular proteins is low, but is upregulated in response to injury or during development (125). 4) Mice with targeted disruption in matricellular genes have subtle abnormalities in the absence of injury. However, loss of these proteins results in a wide range of alterations in injured and remodelled tissue (125).

The first characteristic of matricellular proteins is their ability to bind ECM proteins, proteases and growth factors and to transmit external signals to the cell to modulate cellular phenotypes through receptor-mediated activation. Periostin has been demonstrated to bind several structural ECM proteins including type I and V collagen and fibronectin as well as other matricellular proteins including tenascin-C (104, 106). Bone morphogenic protein-1, a metalloproteinase, interacts with periostin inducing the cleavage and activation of lysyl oxidase required for collagen cross linking (127). Periostin has been shown to bind integrins $\alpha_v\beta_3$, $\alpha_v\beta_5$, $\alpha_5\beta_1$, β_1 and $\alpha_6\beta_4$ in various systems (127-135), presumably through its FAS1 domains. Integrins mediate cell-ECM interactions and transmit signals from the ECM to modulate cell behavior (136, 137). Periostin signalling through $\alpha_v\beta_3$ and $\alpha_6\beta_4$ has been shown to promote tumour cell survival through PI3K/Akt in human colon cancer cells and pancreatic ductal adenocarcinoma cells cultured on tissue culture plastic (129, 130). Periostin signalling through $\alpha_v\beta_3$ and $\alpha_v\beta_5$ can promote the migration of human ovarian epithelial cells, pancreatic ductal adenocarcinoma cells and mouse smooth muscle cells through Akt and FAK dependent pathways (128, 130, 134). Additionally, periostin has been shown to signal through $\alpha_v\beta_3$, $\alpha_v\beta_5$ and β_1 integrins to induce the proliferation of rat cardiomyocytes (132). It should be noted, however, that very few of these signalling intermediates and pathways were assessed on physiologically relevant culture substrates or within an ECM, where periostin could act as a matricellular molecule.

The second characteristic of matricellular proteins is their ability to promote cellular de-adhesion that activates survival signals and induces expression of genes associated with repair. Periostin has been implicated in promoting a “de-adhesive” state in the stroma of cancers and its presence is correlated with malignant tumor invasion and metastasis (*128, 129, 138-141*). In the presence of periostin, tumour cells enhance their invasive activity by forming fewer stress fibres and increasing motility (*128*). Periostin transfected cancer cells demonstrate morphological changes and increased mesenchymal cell markers suggesting that periostin may induce cancer cell invasion through EMT (*142*). Periostin has also been shown to promote survival through ECM-receptor activation in cancers, bone and periodontal ligaments. Enhanced survival induced by periostin in cancers is mediated through PI3K and Akt activation (*129, 130*). In the periosteum and periodontal ligament, periostin-null mice have reduced expression of Notch 1 and its downstream effector Bcl-xL (*143, 144*). Notch proteins are transmembrane receptors that play an important role in cell survival under mechanical stress (*145*). Periostin binding to notch under stressed conditions increases expression of Bcl-xL leading to inhibition of apoptosis (*121*). Periostin expression has also been correlated with proteins associated with repair. Studies utilizing periostin-null mice have demonstrated reduced collagen fibrillogenesis and α SMA levels in cardiac repair and normal cutaneous wound healing (*106, 120, 133*). Collagen remodelling and myofibroblast differentiation are important processes in normal wound repair.

The expression of matricellular proteins is usually low in most normal adult tissues but is upregulated during embryonic development and in response to injury. Periostin is highly expressed by fibroblasts in the embryonic myocardium and developing neonatal heart. In adult hearts, periostin expression is decreased and is primarily localized to the supporting structures of the heart valves that are subjected to mechanical tension. (*123, 146, 147*). In mouse skin, periostin is highly expressed during embryonic development in keratinocytes, at the basement membrane and in the dermis, however expression significantly decreases in adult mice (*97*). Unlike most matricellular proteins that are expressed at low levels in adult tissue, periostin expression in adult tissue is high in collagen-rich tissues under mechanical stress such as the periosteum, periodontal

ligaments, tendons, cardiac valves, and the skin (98, 101, 106, 123). A marked increase in periostin is seen in patients with myocardium infarction, advanced heart failure, and atherosclerotic and rheumatic valve disease (120, 148, 149). Up-regulation of periostin in myocardium infarction plays an important role in early scar formation by promoting migration, myofibroblast differentiation and collagen deposition thereby preventing cardiac rupture (120, 150). Periostin expression is also upregulated during cutaneous wound healing (98, 151, 152) and its roles in this process will be discussed in more detail in the following section.

The final unifying characteristic of matricellular proteins is that their deletion in mouse models generally results in subtle abnormalities in the absence of injury, but much more obvious abnormalities following injury. Despite high levels of periostin during embryonic development in the periosteum, periodontal ligament and heart valves, periostin-null mice are not embryonic-lethal and appear grossly normal at birth (150, 153). Three to four weeks after birth, periostin-null mice display growth retardation and dental defects (153). Approximately 15% of periostin-null mice die in the first three weeks due to cardiac defects (153, 154). Alterations in repair are evident following injury in periostin-null mice. Following myocardium infarction, periostin-null mice have increased rates of cardiac rupture resulting from impaired collagen fibrillogenesis and myofibroblast differentiation (120, 150). Defects in collagen fibrillogenesis and osteoclast inactivation are evident in the periosteum resulting in decreased bone formation and mass (121, 155). In normal cutaneous wound healing, periostin-null mice displayed delayed wound healing caused by defective re-epithelialization and decreased myofibroblast populations (133, 151, 152). These studies suggest that periostin fulfills the requirements of a matricellular protein and has roles in tissue repair.

1.7 Periostin in normal cutaneous wound healing

Several groups have assessed the expression of *POSTN* and periostin during normal cutaneous wound repair using murine excisional wound healing models. *POSTN* expression is detectable in the wound at Day 1 after injury, with peak expression at Day 7

with an ongoing decrease thereafter approaching baseline levels by Day 18 (152). Periostin expression is evident in the granulation tissue and in migrating keratinocytes as early as three days post wounding (98, 151). As increased periostin expression correlates with increased α SMA levels in the granulation tissue at Day 7 post wounding, some authors have suggested that periostin may contribute to normal myofibroblast differentiation (98). By Day 21, periostin expression is absent in keratinocytes and is only evident in the remodeled ECM (98, 152) and levels return to baseline by Day 28 (98). The expression pattern of *POSTN* and periostin over time are currently unclear in human cutaneous wound healing, due to obvious ethical restrictions in using humans as *in vivo* wound healing models.

Only three groups have utilized periostin-null mice in excisional wounding studies to investigate the roles of periostin during cutaneous wound repair. Periostin-null mice display delayed wound closure (133, 151, 152) suggesting that periostin may have a role in re-epithelialization or granulation tissue formation. As periostin-null mice displayed decreased re-epithelialization despite evidence that periostin does not affect keratinocyte proliferation or migration (151), it is likely that loss of periostin impairs re-epithelialization through an indirect mechanism.

Of the three groups to report excisional wound healing studies in periostin-null mice, only one has investigated the effects of periostin in the dermis (133). This group demonstrated that the granulation tissue in periostin-null mice displayed decreased expression of α SMA and its gene, *Acta2*, at Day 7 post wounding relative to wild type controls (133). Similar results were identified *in vitro*, with decreased α SMA levels observed in periostin-null fibroblasts cultured in anchored collagen lattices, which resembles the matrix stiffness of granulation tissue (133, 156). The decrease in myofibroblast populations in the granulation tissue in these *in vivo* studies was not due to impaired fibroblast migration or proliferation (133). However, *in vitro* studies using embryonic mouse fibroblasts provided conflicting data, as periostin-null fibroblast exhibited decreased proliferation, while over expression of periostin induced their proliferation (152). It is difficult to draw conclusions from these studies as they lacked

parallel *in vivo* experiments and utilized embryonic fibroblasts that may have characteristics that are distinct from adult murine fibroblasts (157). *In vitro* and *in vivo* experiments demonstrated that periostin-null dermal fibroblasts were significantly less contractile than wild type fibroblasts and that the addition of recombinant periostin was able to rescue this effect (133). This effect was blocked in the presence of inhibitors against integrin β 1 and FAK and addition of periostin induced FAK phosphorylation (133, 152). These studies suggest that periostin contributes to normal murine cutaneous wound healing by facilitating myofibroblast differentiation and contraction through an integrin-focal adhesion dependent pathway (133).

While these studies suggest that periostin can facilitate myofibroblast differentiation in murine wound healing models, the substantial differences between mouse and human skin make it unclear if these findings can be translated to normal human cutaneous wound healing. Mouse skin is covered in dense hair, lacks rete ridges and adipose sweat glands, has a thinner epidermis and dermis, has a faster keratinocyte turnover rate and is significantly more compliant than human skin (158, 159). In contrast, human skin has a thicker epidermis and dermis, less hair follicles, is relatively stiffer and is adherent to the underlying subcutaneous tissue (158-161). Mice and humans also heal cutaneous wounds by different mechanisms. Mice have a muscle layer below the hypodermis in the flanks, known as the panniculus carnosus, that is absent in most areas of human skin (158). This muscle layer allows mice to rapidly contract wounds following injury and enhances skin regeneration with minimal scarring. In contrast, human cutaneous wounds lacking a similar muscle layer heal through the formation of granulation tissue and re-epithelialization, typically leading to the formation of a scar (158, 160, 162). These profound differences in wound healing mechanisms between mice and humans make it unclear if the roles of periostin in murine excisional wound healing can be translated to normal, or particularly abnormal, cutaneous repair in humans.

1.8 Periostin in abnormal wound healing

Currently, there are no studies in the literature investigating the roles of periostin in the development of hypertrophic scars in humans. The molecular mechanisms implicated in the development of excessive scarring remain poorly understood. One reason for this is a lack of truly representative and physiological relevant animal models of human hypertrophic scar formation (59). Hypertrophic scarring does not normally occur in animals (163), and our current understanding of the mechanisms that promote excessive scarring are largely based on studies of chemically and/or genetically manipulated mice (164-166). These models can be very useful for investigating the cell types and molecules involved in scar formation at specific time points. More recently, animals with skin that more closely resembles human skin, such as the red Duroc pig (167), have been used as models with and without chemical or other treatments to induce scarring. While more physiologically relevant than mice, they cannot capture the multifactorial influences, such as age, sex, wound site and genetic predisposition that promote abnormal scarring in human patients. Since using humans as wound healing models is not ethically feasible, the next best option is analyze human scar tissue from patients undergoing surgical resections. By utilizing primary samples derived from human normal and abnormal scar tissue, we are able to perform a “top down” approach to identify factors that are elevated during abnormal scar formation relative to normal skin. Upon identification of such factors, *in vitro* studies can be performed on primary human fibroblasts that exhibit many clinically relevant features of both normal and abnormal scarring. As an *in vitro* model, these cells have the disadvantage of being obtained after scar formation has occurred, and are therefore unlikely to be informative of the initial stages of scar development, such as those induced by inflammation (59). However, primary fibroblasts derived from surgically resected hypertrophic tissue can provide clinically relevant models of the cellular processes that cause the abnormal persistence of scars for months or years, compared to normal skin wounds that typically heal in weeks.

In situ hybridization studies performed by our lab demonstrated that *POSTN* expression was upregulated and persistent in the basal epithelium of human hypertrophic scar (Figure 1.5a) and keloid scar tissue relative to normal mature scars (96), consistent with

previous reports (99). Immunohistochemistry studies performed by our laboratory (95, 96) and other groups (97, 98) have shown that periostin levels are abnormally abundant and localized to dermis in hypertrophic scars (Figure 1.5b and c) and keloid scars. Periostin is absent in the epidermis, despite clear evidence of *POSTN* expression, suggesting that the epidermis may be an additional source of dermal periostin in abnormal scarring conditions. Based on these findings, we hypothesize that the increased and persistent levels of periostin in the dermis of hypertrophic and keloid scars may contribute to excessive fibroblast proliferation and myofibroblast differentiation and persistence in these fibrotic conditions.

1.9 Assessing the function of periostin in hypertrophic scar formation in an *in vitro* model system

In order to assess the role(s) of a matricellular molecule like periostin in abnormal scar formation *in vitro*, studies must be performed in a model system that closely resembles the granulation tissue during wound healing *in vivo*. Excisional wound healing models and *in vitro* studies have been utilized to measure the stiffness of the ECM during wound healing. Matrix stiffness can be represented by Young's modulus, which is the ratio of stress to strain of an elastic substrate. The Young's modulus of the provisional matrix is 10-1000 Pascals (Pa), indicating that it is very compliant (31). The proto-myofibroblast phenotype is only evident when matrix stiffness reaches 3000 Pa (168). The stiffness of granulation tissue in seven day old rat granulation tissue is approximately 18 000 Pa, consistent with α SMA being incorporated into stress fibers at a Young's modulus of 16 000 - 20 000 Pa (31). Fibrotic tissue and contracting granulation tissues can exhibit a matrix stiffness of 25 000 – 50 000 Pa (169). Tissue-culture plates provide an extremely stiff substrate (~3 gPa, or 3 000 000 000 Pa (170)). A culture substrate of this stiffness inevitably induces robust and non-physiological influences on myofibroblast differentiation (31) that has the potential to overshadow any other effects of potential inducers of myofibroblast formation (133). Despite its routine use for culturing fibroblasts, tissue culture plastic is a very non-physiological model system in which to assess cellular processes that are sensitive to matrix tension. To address this issue, our

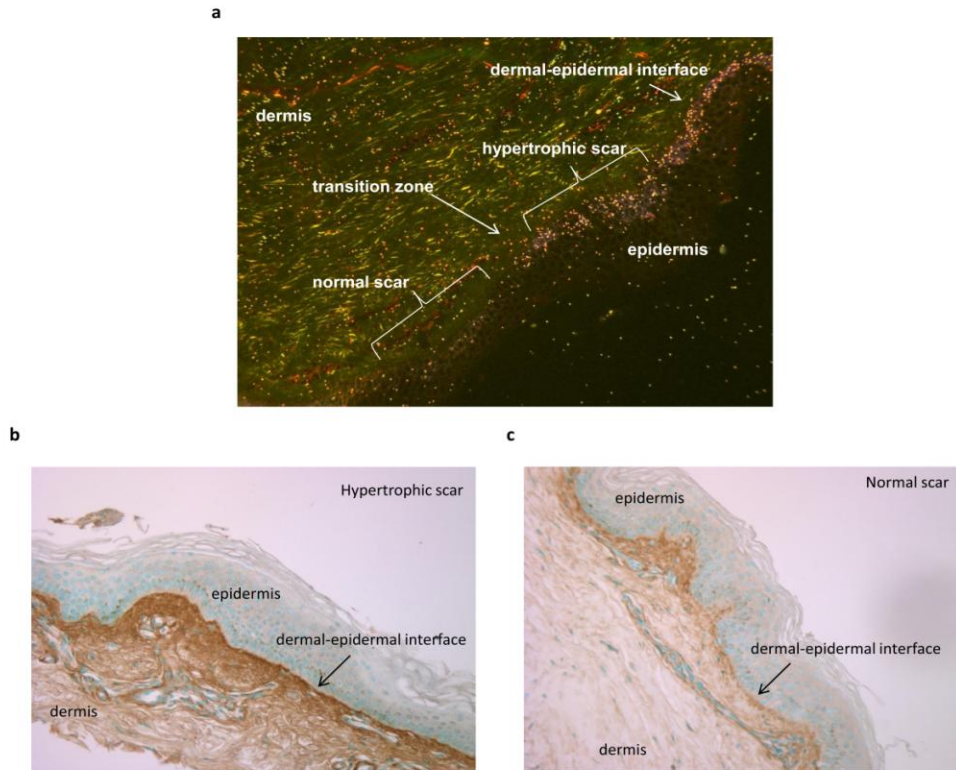


Figure 1.5 POSTN expression and periostin levels are increased in hypertrophic scars. (a) *In situ* hybridization studies were performed using S^{35} labeled sense and antisense transcripts derived from a 391-bp fragment from the 5' end of a *POSTN* cDNA. Paraffin-embedded mixed scar derived from a patient with a phenotypically normal scar at one edge transitioning to a hypertrophic scar at the opposite edge was exposed to antisense *POSTN* mRNA probe to compare *POSTN* expression across the normal-abnormal scarring transition zone (indicated with an arrow). Silver grains deposited due to exposure to S^{35} labeled transcripts are evident as white specks under dark field microscopy. As shown, *POSTN* expression is much more abundant in the basal epithelium along the hypertrophic scar section of the mixed scar relative to the normal scar area. Immunohistochemistry of paraffin-embedded (b) hypertrophic scar and (c) normal scar tissue with a periostin polyclonal antibody. Periostin immunoreactivity is evident as brown staining from di-amino precipitation. Periostin is more abundant in hypertrophic scars relative to normal scars and expression extends deep into the dermis. Images c/o Cell and Molecular Biology Laboratory, Roth|McFarlane Hand and Upper Limb Centre.

laboratory takes the approach of routinely culturing primary fibroblasts on type I collagen substrates. Type I collagen is the most abundant collagen in the skin and mature scars (8) and our laboratory has demonstrated that the change in substrate stiffness induced by culture on collagen substrates can modify gene expression and protein levels in primary fibroblasts relative to the same cells cultured on stiff tissue culture plastic (91, 171). Based on these observations, the effects of periostin on fibroblast proliferation and myofibroblast differentiation were assessed in two- (2D) and three-dimensional (3D) collagen-based cultures in this thesis to more closely mimic the ECM and substrate stiffness experienced by these fibroblasts *in vivo*.

Currently, three dimensional collagen lattices are utilized for examining *in vitro* the mechanical interactions that occur between cells and the ECM and how these interactions induce myofibroblast differentiation (47, 156). When cultured within a collagen lattice, fibroblasts experience a more complex environment and geometry compared to cells cultured on plastic (172). Fibroblast attachment, spreading, and migration through the collagen lattice generate mechanical signals that can modulate cellular phenotype. If the collagen lattice is mechanically restrained, such as in stressed Fibroblast Populated Collagen Lattices (sFPCLs) (47), tension develops as tractional forces compact the collagen fibers (30, 172). As the mechanical tension progressively increases in the collagen lattice, the fibroblasts will form stress fibers and focal adhesions associated with proto-myofibroblast and myofibroblast differentiation (156) similar to ECM remodelling *in vivo* (30). This tension is sustained in the lattice until it is released from its points of attachment (30). Newly polymerized 2D and 3D collagen gels have a matrix stiffness of 300-400 Pa (173), which is similar to that seen in the provisional fibrin matrix (31). The Young's modulus has not been reported for sFPCLs; however, it is believed to closely mimic the mechanical environment of the granulation tissue in Day 7 rat wounds, i.e. approximately 18 000 Pa (31, 44, 156). Using collagen substrates, periostin can be incorporated into collagenous ECM matrices to mimic its localization *in vivo* and provide a reproducible culture system to investigate periostin effect(s) on fibroblast proliferation and myofibroblast differentiation and persistence under physiological relevant conditions.

1.10 Hypothesis and objectives

When wound healing signals become abnormal, excessive fibroblast proliferation and myofibroblast persistence can be induced, resulting in excessive ECM deposition and remodelling and hypertrophic scarring (56, 57, 92-94). TGF β -1 is a potent inducer of myofibroblast differentiation in this context, however it is also implicated in regulating many of the processes that are essential for normal wound healing (13, 41, 174-177), making this cytokine a difficult therapeutic target. Therefore, TGF β -1-inducible proteins that act in combination with and/or sequentially to TGF β -1 signalling to promote pathological, rather than normal, fibroblast proliferation and/or myofibroblast differentiation may have greater utility as therapeutic targets. Periostin is a novel matricellular protein that is upregulated in the ECM of hypertrophic scars and may have potential as such a target. Although several studies have demonstrated that periostin regulates fibroblast proliferation and myofibroblast differentiation in other systems (91, 132, 133, 152, 178-180), the roles of periostin in hypertrophic scar formation in human fibroblasts has not been assessed. Therefore, this thesis focuses on identifying the role(s) of periostin on hypertrophic scar fibroblast proliferation and myofibroblast differentiation and persistence in 2D and 3D collagen cultures.

The central hypothesis of this thesis is that ECM-associated periostin contributes to hypertrophic scar formation by promoting excessive fibroblast proliferation and myofibroblast differentiation and by maintaining myofibroblasts in a differentiated state.

The following objectives were designed to test this hypothesis:

Objective 1: To assess the effects of periostin on the proliferation of normal skin and hypertrophic scar derived fibroblasts

Objective 2: To assess the effects of periostin on the differentiation of fibroblasts derived from normal skin and hypertrophic scar tissues

Objective 3: To identify the mechanism(s) utilized by periostin to induce and maintain hypertrophic scar myofibroblasts in a differentiated state

Chapter 2

2 Materials and Methods

2.1 Materials

2.1.1 Biochemicals

Bovine serum albumin (BSA)	Sigma-Aldrich, St. Louis, MO
Glycine	Fisher Scientific, Hampton, NH
Sodium hydroxide	Sigma-Aldrich, St. Louis, MO
Hydrochloric acid	Merck KGaA, Darmstadt, GER
Sodium dodecyl sulfate (SDS)	Sigma-Aldrich, St. Louis, MO
Tris Base	Fisher Scientific, Hampton, NH
Sodium chloride (NaCl)	Fisher Scientific, Hampton, NH
Glacial acetic Acid	Fisher Scientific, Hampton, NH
Potassium chloride (KCl)	Fisher Scientific, Hampton, NH
Potassium phosphate (KH ₂ PO ₄)	Fisher Scientific, Hampton, NH
Sodium phosphate, monobasic (NaH ₂ PO ₄)	Fisher Scientific, Hampton, NH
Sodium phosphate, dibasic (Na ₂ HPO ₄)	Fisher Scientific, Hampton, NH
Imidazole	Sigma-Aldrich, St. Louis, MO
Glycerol	Fisher Scientific, Hampton, NH
Bromophenol blue	Fisher Scientific, Hampton, NH
<h5>2.1.2 Cell culture</h5>	
100 mm and 24-well tissue culture plates	Becton Dickinson, Franklin Lakes, NJ
Alpha Modified Eagle's medium (α MEM)	Life Technologies, Carlsbad, CA

Dulbecco's modified Eagle's medium (DMEM)	Life Technologies, Carlsbad, CA
100x L-glutamine	Life Technologies, Carlsbad, CA
100x antibiotic-antimycotic	Life Technologies, Carlsbad, CA
Fetal bovine serum (FBS)	Life Technologies, Carlsbad, CA
Trypsin-EDTA	Life Technologies, Carlsbad, CA
Type I rat tail collagen	Made in our laboratory
Waymouth medium	Sigma-Aldrich, St. Louis, MO
Dimethyl sulfoxide (DMSO)	Sigma-Aldrich, St. Louis, MO
Recombinant human periostin	R&D systems, Minneapolis, MN
Recombinant human TGF β -1	R&D systems, Minneapolis, MN
Hank's balanced salt solution	Sigma-Aldrich, St. Louis, MO
Collagenase	Sigma-Aldrich, St. Louis, MO
Nalgene® cryogenic vials	Thermo Scientific, Waltham, MA
Sircol collagen quantification assay	Biocolor Ltd., Carrickfergus, UK

Table 2.1 Buffers and medium for cell culture

Buffer/medium	Application	Composition
Phosphate buffered saline (PBS)	Wash buffer	8 g NaCl, 0.2 g KCl, 1.44 g Na ₂ HPO ₄ , 0.24 g KH ₂ PO ₄ , reverse osmosis (R.O) H ₂ O up to 1 L, pH 7.4
Freezing Medium	Primary cell storage	50% FBS, 35% α MEM, 15% DMSO

2.1.3 Cell proliferation assay

Cell Proliferation Reagent WST-1

Roche Diagnostics, Mannheim, GER

96-well tissue culture plates

Becton Dickinson, Franklin Lakes, NJ

Table 2.2 Inhibitors for cell proliferation assays

Inhibitor	Mode of Action	Concentration	Vehicle	Supplier
PI3K inhibitor, LY294002	Inhibition is competitive with respect to ATP binding site	10 μ M	DMSO	Cell Signaling Technologies, Danvers, MA
AKT inhibitor VIII	Binds pleckstrin homology domain and prevents activation by PI3K	0.5 μ M	DMSO	Merck KGaA, Darmstadt, GER
GSK3 β inhibitor VIII	Inhibition is competitive with respect to ATP binding site	1 μ M	DMSO	Merck KGaA, Darmstadt, GER
Rho Kinase inhibitor, Y27632	Inhibition is competitive with respect to ATP binding site	10 μ M	H ₂ O	Sigma Aldrich, St. Louis, MO
ERK 1/2 inhibitor, PD98059	Binds to ERK specific MAP kinase, MEK, preventing activation of ERK 1/2 by MEK	20 μ M	DMSO	Sigma Aldrich, St. Louis, MO

2.1.4 Protein chemistry

RIPA lysis buffer	Teknova Inc., Hollister, CA
Proteinase inhibitor cocktail	Sigma-Aldrich, St. Louis, MO
Phenylmethanesulfonylfluoride (PMSF)	Sigma-Aldrich, St. Louis, MO
Sodium fluoride (NaF)	Sigma-Aldrich, St. Louis, MO
Sodium orthovanadate (Na ₃ VO ₄)	Sigma-Aldrich, St. Louis, MO
Pierce® BCA protein assay kit	Thermo Scientific, Waltham, MA
30% Acrylamide/Bis solution (29:1)	BioRad, Hercules, CA
Ammonium persulfate	BioRad, Hercules, CA
N,N,N',N'-tetramethylethylenediamine (TEMED)	BioRad, Hercules, CA
Dithiothreitol (DTT)	Sigma-Aldrich, St. Louis, MO
polyvinylidene difluoride (PVDF) – plus, 0.45 micron transfer membranes	Santa Cruz Biotechnology, Santa Cruz, CA
Tween®20	Merck KGaA, Darmstadt, GER
Novex sharp molecular weight markers	Life Technologies, Carlsbad, CA
Immobilon™ western chemiluminescent HRP substrate	Millipore Corporation, Billerica, MA

Table 2.3 Buffers for protein analysis

Buffer	Application	Composition
RIPA lysis buffer	Cell lysis	150 mM NaCl, 1% Triton X-100, 1% sodium deoxycholate, 0.1% SDS, 50 mM Tris-HCl (pH 7.5), 2 mM EDTA (pH 8.0)
SDS gel-loading buffer	SDS-PAGE	R.O. H ₂ O with 50 mM Tris-HCl (pH 6.8), 100 mM DTT, 2% SDS, 0.1% bromophenol blue, 10% glycerol
1.0 M Tris	SDS-PAGE stacking gel	121.0 g Tris base dissolved in R.O. H ₂ O to 1 L, pH 6.8
1.5 M Tris	SDS-PAGE resolving gel	181.65 g Tris base dissolved in R.O. H ₂ O to 1 L, pH 8.8
5x electrophoresis running buffer	SDS-PAGE	15.1 g Tris Base, 94.0 g glycine, 25 ml 20% (w/v) SDS, R.O. H ₂ O up to 1 L
10x electrophoresis transfer buffer	SDS-PAGE	30.3 g Tris base, 144.4 g glycine, R.O. H ₂ O up to 1 L
1x electrophoresis transfer buffer	SDS-PAGE	1 part 10x electrophoresis transfer buffer, 2 parts methanol, 7 parts R.O. H ₂ O
10x Tris buffered saline (TBS)	Western immunoblotting	80.8g NaCl, 60.6 g Tris Base, R.O. H ₂ O up to 1 L, pH 7.4
TBS/tween20	Western immunoblotting	1x TBS with 0.1% Tween@20

Table 2.4 Primary antisera for western immunoblotting

Antibody	Description	Antibody dilution (western blotting)	Supplier
Phospho-Akt	Rabbit anti-phospho-Akt (ser 473), polyclonal	1:1000 in 5% BSA, TBS/tween20	Cell Signaling Technology, Danvers, MA
Total Akt	Rabbit anti-Akt, polyclonal	1:1000 in 5% BSA, TBS/tween20	Cell Signaling Technology, Danvers, MA
Phospho-GSK-3 β	Rabbit anti-phospho-GSK-3 β (ser 9), polyclonal	1:1000 in 5% BSA, TBS/tween20	Cell Signaling Technology, Danvers, MA
Total GSK-3 β	Mouse anti-GSK-3 β , clone 7/GSK-3b, monoclonal	1:1000 in 5% non-fat milk, TBS/tween20	BD Biosciences Canada, Mississauga, ON
β -catenin	Rabbit anti- β -catenin, polyclonal	1:1000 in 5% non-fat milk, TBS/tween20	Millipore Corporation, Billerica, MA
Phospho-ERK 1/2	Rabbit anti-phospho-p44/42 MAPK (Thr 202, Tyr 204)	1:1000 in 5% BSA, TBS/tween20	Cell Signaling Technology, Danvers, MA
Total ERK 1/2	mouse anti-p44/42 MAPK (ERK1/2), clone L34F12, monoclonal	1:1000 in 5% non-fat milk, TBS/tween20	Cell Signaling Technology, Danvers, MA
Alpha smooth muscle actin (α SMA)	Mouse anti- α SMA, monoclonal	1:1000 in 5% non-fat milk, TBS/tween20	Sigma-Aldrich, St. Louis, MO
OB cadherin	Mouse anti-Cadherin 11, clone 5B2H5, monoclonal	1:1000 in 5% non-fat milk, TBS/tween20	Life Technologies, Carlsbad, CA
Periostin	Rabbit anti-periostin, clone H-300, polyclonal	1:1000 in 5% non-fat milk, TBS/tween20	Santa Cruz Biotechnology, Santa Cruz, CA

Phospho-Focal adhesion Kinase (FAK)	Rabbit anti-phospho-FAK (Tyr 397), polyclonal	1:500 in 5% BSA, TBS/tween20	Cell Signaling Technology, Danvers, MA
Total FAK	Rabbit anti-FAK, polyclonal	1:500 in 5% BSA, TBS/tween20	Cell Signaling Technology, Danvers, MA
Phospho-myosin light chain (MLC)	Rabbit anti-phospho-MLC 2 (ser 19), polyclonal	1:500 in 5% BSA, TBS/tween20	Thermo Scientific, Rockford, IL
Total MLC	Rabbit anti-MLC 2, polyclonal	1:500 in 5% BSA, TBS/tween20	Thermo Scientific, Rockford, IL
Phospho-cofilin	Rabbit anti-phospho-cofilin (Ser 3), clone 77G2, monoclonal	1:500 in 5% BSA, TBS/tween20	Cell Signaling Technology, Danvers, MA
Total cofilin	Rabbit anti-cofilin, clone D3F9, monoclonal	1:500 in 5% non-fat milk, TBS/tween20	Cell Signaling Technology, Danvers, MA
Alpha V integrin (α_v)	Rabbit anti- α_v , clone Q-20, polyclonal	1:1000 in 5% non-fat milk, TBS/tween20	Santa Cruz Biotechnology, Santa Cruz, CA
Alpha 5 integrin (α_5)	Rabbit anti- α_5 , polyclonal	1:1000 in 5% non-fat milk, TBS/tween20	Cell Signaling Technology, Danvers, MA
β -actin	Mouse anti- β -actin, HRP-linked, clone C4, monoclonal	1:2500 in 5% non-fat milk, TBS/tween20	Santa Cruz Biotechnology, Santa Cruz, CA

Table 2.5 Secondary antisera for western immunoblotting

Antibody	Description	Antibody dilution (western blotting)	Supplier
Mouse secondary	Horse anti-mouse IgG, HRP-linked	1:1000 in 5% non-fat milk, TBS/tween20	Cell Signaling Technology, Danvers, MA
Rabbit Secondary	Goat anti-rabbit IgG, HRP-linked	1:1000 in 5% non-fat milk, TBS/tween20	Cell Signaling Technology, Danvers, MA

2.1.5 Polymerase Chain Reaction (PCR)

RNeasy mini kit	Qiagen, Venlo, Netherlands
High-capacity cDNA archive kit	Life Technologies, Carlsbad, CA
10X PCR buffer, minus Mg	Life Technologies, Carlsbad, CA
50 mM Magnesium chloride	Life Technologies, Carlsbad, CA
Custom primers	Sigma Aldrich, St. Louis, MO
Platinum® Taq DNA polymerase	Life Technologies, Carlsbad, CA
100 mM dNTP set, PCR grade	Life Technologies, Carlsbad, CA
UltraPure™ Agarose	Life Technologies, Carlsbad, CA
QIAEX® II Gel extraction kit	Qiagen, Venlo, Netherlands
MicroAmp Optical 384-well reaction plate	Life Technologies, Carlsbad, CA
TaqMan universal PCR master mix	Life Technologies, Carlsbad, CA
TaqMan gene expression assay primers	Life Technologies, Carlsbad, CA

Table 2.6 TaqMan gene expression assay primers

Primer	Protein Encoded	Assay ID
<i>POSTN</i>	Periostin	Hs00170815_m1
<i>CCND1</i>	Cyclin D1	Hs00765553_m1
<i>BCL2</i>	Bcl2	Hs00608023_m1
<i>BAX</i>	Bax	Hs00180269_m1
<i>GAPDH</i>	GAPDH	Hs99999905_m1
<i>ACTB</i>	β -actin	Hs99999903_m1

2.1.6 Flow cytometry

Guava ViaCount® reagent

Millipore, Billerica, MA

MCDB 105 medium

Sigma-Aldrich, St. Louis, MO

2.1.7 Immunoprecipitation

Protein A/G magnetic beads

Thermo Scientific, Waltham, MA

Coomassie brilliant blue R-250

Fisher Scientific, Hampton, NH

Amicon® Ultra centrifugal 10 kDa filters

Millipore Corporation, Billerica, MA

Table 2.7 Antisera for immunoprecipitation

Antibody	Description	Antibody Concentration	Suppliers
Periostin	Rabbit anti-periostin, clone H-300, polyclonal	2 μ g / 500 μ g total cell lysate	Santa Cruz Biotechnology, Santa Cruz, CA
IgG	Rabbit anti-human IgG3, clone H-270, polyclonal	2 μ g / 500 μ g total cell lysate	Santa Cruz Biotechnology, Santa Cruz, CA
IgG	Anti-human IgG from rabbit serum	2 μ g / 500 μ g total cell lysate	Sigma-Aldrich, St. Louis, MO

Table 2.8 Buffers and solutions for immunoprecipitation

Buffer	Application	Composition
Lysis buffer	Cell lysis	R.O. H ₂ O with 20 mM Tris-HCl (pH 8.0), 137 mM NaCl, 1% Triton® X-100, 2 mM EDTA
Wash buffer	Wash buffer	TBS with 0.05% Tween®20 and 0.5 M NaCl
Elution buffer	Protein elution	4 parts lysis buffer, 1 part SDS gel-loading buffer
Gel fixation solution	Fixing polyacrylamide gels	50% methanol, 10% acetic acid, 40% R.O. H ₂ O
Coomassie brilliant blue concentrated stain solution	Protein staining	12.0 g coomassie brilliant blue, 300 ml methanol, 60 ml acetic acid
Coomasie brilliant blue staining solution	Protein staining	500 ml methanol, 30 ml coomassie brilliant blue concentrated stain solution, 400 ml R.O H ₂ O, 100 ml acetic acid, filtered using 0.22 µm filter
Destaining solution	Wash solution	45% methanol, 10% acetic acid, 45% R.O. H ₂ O
Gel storage solution	Polyacrylamide gel storage	R.O. H ₂ O with 5% acetic acid

2.1.8 Nickel magnetic bead precipitation

37% formaldehyde

Merck KGaA, Darmstadt, GER

10x glycine solution

Cell Signaling Technology, Danvers, MA

Nonidet P40 (NP-40)

Merck KGaA, Darmstadt, GER

PureProteome™ nickel magnetic beads

Millipore, Billerica, MA

Table 2.9 Buffers for Nickel Magnetic Bead precipitation

Buffer	Application	Composition
Lysis buffer	Cell lysis	R.O. H ₂ O with 50 mM NaH ₂ PO ₄ , 300 mM NaCl, 10 mM imidazole (pH 8), 0.1% NP-40
Wash buffer	Wash buffer	R.O. H ₂ O with 50 mM NaH ₂ PO ₄ , 300 mM NaCl, 20 mM imidazole (pH 8), 0.1% NP-40
Elution Buffer	Protein elution	R.O. H ₂ O with 50 mM NaH ₂ PO ₄ , 300 mM NaCl, 300 mM imidazole (pH 8)

2.1.9 Loss-of-function studies

Table 2.10 Adenoviral shRNA constructs

Construct	Promoter	Targeting sequence	Multiplicity of infection (MOI)	Supplier
Ad-GFP-U6-h-POSTN-shRNA	U6	CGGTGACAGTATA ACAGTAA	25	Vector Biolabs, Philadelphia, PA
Ad-U6-RNAi-GFP	U6	GACACGCGACTTG TACCACT	25	Vector Biolabs, Philadelphia, PA

2.1.10 Immunofluorescence confocal microscopy

35 mm, poly-D-lysine coated glass bottom tissue culture plates (No. 1.5 coverslip, 10 mm glass diameter)

Paraformaldehyde 16% solution

Electron Microscopy Sciences, Hatfield, PA

Background Sniper	Biocare Medical, Concord, Ca
Dako antibody diluent	Dako Canada Inc., Burlington, ON
Negative control mouse IgG1	Dako Canada Inc., Burlington, ON
Hoeschst 33342	Life Technologies, Carlsbad, CA
ProLong® Gold antifade reagent	Life Technologies, Carlsbad, CA
18 x 18 mm, No.1 coverslips	Fisher Scientific, Hampton, NH

Table 2.11 Buffers for immunofluorescence confocal microscopy

Buffer	Application	Composition
Immunofluorescence phosphate buffered solution (IF-PBS)	Wash buffer	0.2 g NaH ₂ PO ₄ , 1.375 g Na ₂ HPO ₄ , 8.8 g NaCl, R.O. H ₂ O up to 1 L
Cell permeabilization solution	Cell permeabilization	PBS with 0.1% Triton® X-100

Table 2.12 Antisera for immunofluorescence confocal microscopy

Antibody	Description	Dilution	Supplier
Vinculin	Mouse anti-vinculin, clone VIN-11-5, monoclonal	1:200 in Dako antibody diluent	Sigma-Aldrich, St. Louis, MO
Negative control mouse IgG1	Mouse anti- <i>Aspergillus niger</i> glucose oxidase, clone DAK-GO1, monoclonal	4 µg/ml in Dako antibody diluent	Dako Canada Inc., Burlington, ON

Table 2.13 Spectral properties of molecular probes and LSM 510 Duo Vario confocal microscope

Molecular Probe	Dilution	LSM Laser Lines for Excitation	LSM Emission Filters	Supplier
α SMA-cy3	1:100 in Dako antibody diluent	30 mW 514 nm Argon/2 Ion laser	BP 560-615 IR	Sigma-Aldrich, St. Louis, MO
Alexa Fluor 647	1:100 in Dako antibody diluent	5 mW 633 nm HeNe	LP 650	Life Technologies, Carlsbad, CA
Alexa Fluor 594	1:100 in Dako antibody diluent	30 mW 514 nm Argon/2 Ion laser	BP 560-615 IR	Life Technologies, Carlsbad, CA
Hoechst	1:10 000 in PBS	50 mW 405-50 nm Diode	BP 420-480	Life Technologies, Carlsbad, CA

2.2 Methods

2.2.1 Clinical specimen collection

Surgically resected normal skin, hypertrophic scar and keloid scar tissue samples were collected from patients in the clinics of the Roth|McFarlane Hand and Upper Limb Centre or in the operating rooms of St. Joseph's Hospital, London, Ontario. All subjects provided written informed consent and specimens were collected with the approval of Western University Research Ethics Board for Health Sciences Research involving Human Subjects (HSREB protocol # 08222E).

2.2.2 Primary cell culture

Primary cells were harvested from surgically resected hypertrophic scar, keloid scar and normal skin tissue as previously described (181). A total of eight patient-derived hypertrophic scar samples, three keloid scar samples and six normal skin samples were

used to derive primary fibroblasts for analyses in this thesis. In brief, tissue samples were finely minced, adhered to the bottom of 100 mm dishes and cultured in α MEM supplemented with 10% fetal bovine serum (FBS), 1x L-glutamine and 1x antibiotic-antimycotic solution at 37°C in 5% CO₂. Explant cultures (passage 0) were incubated for 2-4 weeks allowing for the migration, and subsequent proliferation, of fibroblasts from the tissue to the 100 mm dish. Upon reaching 50% confluency, primary cultures were sub-cultured using 0.05% Trypsin-EDTA. Primary fibroblast cultures at passage 1 were frozen down in freezing medium (Table 2.1) in Nalgene® cryogenic vials at -80°C overnight then stored in liquid nitrogen. All primary cell lines were used up and until a maximum of four passages, during which no changes in cell behavior or morphology attributable to serial passage were evident.

2.2.3 Preparation of rat tail type I collagen

Frozen rat tails were obtained from the laboratories of Drs. Ruud Veldhuizen and Ting-Yim Lee (Western University, London, ON). Frozen rat tails were thawed in 70% ethanol for one hour. Rat tails were skinned and collagen fibers were mechanically extracted from rat tail tendons. Collagen fibers were soaked in 70% ethanol for 30 minutes then placed under ultraviolet light overnight in a tissue culture cabinet. Under sterile conditions, collagen fibers were incubated in sterile 0.017M acetic acid with mechanical stirring for seven days at 4°C. Undissolved collagen fibers were removed from the solution by centrifugation at 18 000 x g at 4°C overnight. The supernatant was collected into sterile bottles and stored at 4°C. Collagen concentration was determined using the Sircol collagen quantification assay (Biocolor Ltd., Carrickfergus, UK) in accordance with the manufacturer's instructions.

2.2.4 WST-1 cell proliferation assay

The WST-1 proliferation assay was utilized to measure the proliferation of hypertrophic scar and normal skin fibroblasts grown in collagen cultures. Collagen lattices were cast in 96-well tissue culture trays. For each well, 48 μ l of type I rat tail collagen (final concentration of 1.8 mg/ml) was quickly mixed with 12 μ l of neutralization solution (3 parts Waymouth media: 2 parts 0.34 M NaOH), and 2 μ g/ml human recombinant periostin or vehicle (0.1% BSA-PBS). Collagen lattices were incubated at 37°C in 5%

CO₂ for 20 minutes to allow for collagen polymerization. 1×10^3 cells in 100 μ l of 2% FBS- α MEM \pm inhibitors (Table 2.2) were seeded onto the collagen lattices and incubated at 37°C in 5% CO₂. 10 μ l of WST-1 reagent was added at days 1, 3, 5 and 7 post seeding and incubated for 2 hours at 37°C to allow for the cleavage of tetrazolium salt to formazan by the succinate-tetrazolium reductase system. Equal volumes of media (90 μ l) were transferred to an additional 96-well tissue culture tray and absorbencies were measured at 450 and 650 nm (reference wavelength) using an iMARK Microplate Reader (Bio-Rad, Hercules, CA). Difference scores were calculated relative to day 1 absorbance readings.

2.2.5 Fibroblast Populated Collagen Lattices (FPCLs)

Collagen contraction assays were carried out using primary normal skin, hypertrophic scar and keloid scar fibroblasts based on Tomasek and Rayan (182). Collagen lattices were cast in 24-well tissue culture trays. For each well, 1×10^5 cells were quickly mixed with 400 μ l of type I rat tail collagen (final concentration of 1.8 mg/ml), 100 μ l of neutralization solution and 2 μ g/ml human recombinant periostin or vehicle. In a subset of experiments, normal skin fibroblasts were primed with 5 ng/ml recombinant TGF β -1 or vehicle (PBS with 1% BSA and 4 mM HCl) in 2% FBS- α MEM for 72 hours prior to sFPCL setup. Collagen lattices were incubated at 37°C in 5% CO₂ for 45 minutes to allow for collagen polymerization. Wells were then flooded with 1 ml of 2% FBS- α MEM. In a subset of experiments, wells were flooded with fibroblast-conditioned media (section 2.2.9.2). For stressed FPCLs (sFPCLs), collagen cultures were maintained for 72 hours. During this time, the primary fibroblasts in three-dimensional cultures respond to stress within the tethered, polymerized collagen lattice and differentiate into contractile myofibroblasts (183). After three days in culture, collagen lattices were simultaneously released from the wells using a metal spatula, thereby allowing the differentiated myofibroblasts to contract the untethered lattice. Floating lattices were digitally scanned within two minutes (designated time 0), 0.5, 2, 6, and 24 hours after release and the area of each lattice was determined using the freehand tool in ImageJ software (National Institutes of Health, Bethesda, MD). Sequential area calculations were normalized to the area of the well prior to release.

For relaxed FPCLs (rFPCLs), lattices were cultured for one hour prior to being mechanically released from the wells. Fibroblasts cultured in rFPCLs are not subjected to mechanical tension and do not differentiate into myofibroblasts. Therefore, rFPCLs undergo gradual lattice contraction over a 24 hour period due to fibroblast attachment, spreading and migration (183). Floating lattices for rFPCLs were digitally scanned at 24 hours after release.

2.2.6 Western immunoblotting

2.2.6.1 Protein extraction

For total protein extraction from fibroblasts cultured on collagen substrates, cultures were washed in PBS and incubated with 1 ml collagenase solution (final concentration of 0.25 mg/ml) for 30 minutes with gentle rocking at 37°C using a thermal rocker, in order to detach the fibroblasts from the collagen substrates. The collagenase solution was collected from each well and centrifuged at 600 x g for 4 minutes to pellet the cells. Cell pellets were washed with PBS and centrifuged at 16 000 x g for 1 minute. Cell pellets were resuspended in 100 µl of ice cold RIPA lysis buffer supplemented with proteinase inhibitor cocktail, 0.1M sodium fluoride (NaF), 10 mM phenylmethanesulfonyl fluoride (PMSF) and 10 mM sodium orthovanadate (Na₃VO₄). Cell pellets were incubated on ice for 30 minutes then subjected to needle aspiration. Cell lysates were centrifuged at 16 000 x g for 10 minutes and the supernatant was stored at -80°C.

For total protein extraction from sFPCLs, lattices were collected immediately prior to collagen lattice release (after 72 hours in culture), 24 and 48 hours after collagen lattice release and transferred to a 2 ml microcentrifuge tube containing 100 – 400 µl of ice cold RIPA lysis buffer supplemented with proteinase inhibitor, NaF, PMSF and Na₃VO₄. Collagen lattices were homogenized using an Ultra-Turrax T25 tissue homogenizer (IKA® Works Inc., Wilmington, NC) at 16 000 x g for 30 seconds. Cell extracts were incubated on ice for 30 minutes then subjected to needle aspiration. Cell extracts were centrifuged at 16 000 x g for 10 minutes to remove insoluble material and the supernatant was stored at -80°C.

2.2.6.2 Bicinchoninic acid (BCA) total protein assay

Bovine serum albumin (BSA) standards were prepared by serial dilution with RIPA lysis buffer to concentrations of 2000, 1000, 500, 250, 125, 62.5, 31.25 and 0 µg/ml. Total cell lysates were prepared in a 1/5 and 1/10 dilution in RIPA lysis buffer and 10 µl of each dilution and standard was added in triplicate to 96-well tissue culture trays. 200 µl of Pierce® BCA protein assay reagent A:B (49:1) was added to each well and samples were incubated for 30 minutes at 37°C in 5% CO₂. The colourimetric reaction was analyzed at 595 nm using an iMARK Microplate Reader. The data was used to construct a standard curve and protein concentrations were calculated from the obtained absorbance values to ensure equal loading into polyacrylamide gels. We were unable to perform BCA analyses on sFPCL lysates due to the high collagen concentration in the lysates and phenol red in the media. Therefore, 40 µl of total cell lysate was used for western immunoblotting and densitometry was performed to correct for unequal loading.

2.2.6.3 SDS-Polyacrylamide Gel Electrophoresis (SDS-PAGE)

8-10% polyacrylamide resolving gels were made with a 5% stacking gel and set up in the Bio-Rad Mini Protean III apparatus (Biorad, Hercules, CA). 8% polyacrylamide resolving gels were used for the analysis of αSMA, OB cadherin, periostin, integrins, β-catenin, FAK, Akt, ERK1/2 and GSK-3β. 10% polyacrylamide resolving gels were used for the analysis of myosin light chain and cofilin levels. Samples were diluted to load either 25 µg of total protein or 40 µl of sFPCL lysate per well and SDS gel-loading buffer (Table 2.3) was added to each sample at a 1:4 (v/v) ratio. Samples were boiled at 95°C for 5-10 minutes, placed on ice for 2 minutes and centrifuged at 16 000 x g for 1 minute. Samples were loaded into 1.5 mm wells and subjected to SDS-PAGE in 1x electrophoresis running buffer (Table 2.3) using a PowerPac 3000 (Bio-Rad, Hercules, CA) set to 80 V through the stacking gel and 120 V through the resolving gel.

2.2.6.4 Transfer, blocking, incubation, detection and densitometry

Proteins were transferred to polyvinylidene difluoride (PVDF) – plus, 0.45 micron transfer membranes in ice cold 1x electrophoresis transfer buffer (Table 2.3) on ice at 225 mA for two hours. The PVDF membranes were blocked for one hour in 5% non-fat milk (w/v) or 5% BSA (w/v) in TBS-0.1% Tween®20 (TBS/tween, Table 2.3) depending on

the primary antibody (Table 2.4). Membranes were washed with TBS/tween (3 x 5 minutes) and incubated with primary antibody overnight at 4°C with gentle rotation. Membranes were washed with TBS/tween (3 x 5 minutes) and probed with the corresponding horseradish peroxidase (HRP)–conjugated secondary antibody (Table 2.5) for 90 minutes at room temperature with gentle rotation. Membranes were washed with TBS/tween (3 x 5 minutes) and incubated with 1 ml Immobilon™ western chemiluminescent HRP substrate (1:1 ratio of luminal to HRP solution) and imaged using the ChemiGenius² Bio Imaging System (Syngene, Frederick, MD). Images were captured using Gene Snap (Syngene, Frederick, MD) and densitometry analysis was performed using the manual band quantification analysis function in Gene Tools (Syngene, Frederick, MD).

2.2.7 PCR

2.2.7.1 RNA extraction and cDNA synthesis

Cell pellets were collected from sFPCLs or two-dimensional collagen substrates using collagenase treatment (2.2.6.1). Cell pellets were lysed and total RNA was extracted using the RNeasy mini kit in accordance with the manufacturer's instructions. Total RNA was eluted in 50 µl of RNase-free water. Total RNA concentration and quality was assessed using the NanoDrop-1000 spectrophotometer (Thermo Scientific, Waltham, MA). 2 µg of high quality total RNA was reversed transcribed into cDNA first strand using the High-Capacity cDNA archive kit in accordance with the manufacturer's instructions.

2.2.7.2 Real time PCR

cDNA samples were diluted to a final concentration of 10 ng/µl in RNase/DNase free water and 20 ng of cDNA was loaded in triplicate into MicroAmp Optical 384-well reaction plates. TaqMan gene expression assays were used to measure *POSTN*, *CCND1*, *BAX* and *BCL2* expression in accordance with the manufacturer's instructions (Table 2.6 for primers). *POSTN* and *BAX* expression was measured relative to *GAPDH* endogenous control and *CCND1* and *BCL2* expression was measured relative to *ACTB* using the $\Delta\Delta C_t$ method (relative quantification, RQ) after confirmation of parallel PCR

amplification efficiencies using the 7900HT Sequence Detection System (Life Technologies, Carlsbad, CA). PCR reactions were carried out under the following conditions: Initial denaturation at 95°C for 5 minutes followed by cycles of denaturation (95°C for 15 seconds), primer annealing (60°C for 1 minute) and transcript extension (50°C for 2 minutes) for 40 cycles. The relative quantification for each gene normalized to vehicle controls was analyzed using RQ Manager 1.2.1 software (Life Technologies, Carlsbad, CA).

2.2.7.3 Reverse-transcription PCR

20 ng of cDNA was subjected to PCR analysis with Platinum®Taq DNA polymerase in accordance with the manufacturer's instructions. PCR reactions were carried out under the following conditions: initial denaturation at 95°C for 3 minutes, followed by cycles of denaturation (95°C for 30 seconds), primer annealing (58°C for 30 seconds) and transcript extension (72°C for 2 minutes) for 40 cycles, with a final extension at 72°C for 7 minutes. The primers (Forward 5'- ACAACGGGCAAATACTGGAA-3', Reverse 5'- AACTTCCTCACGGGTGTGTCA-3') were designed to have 100% sequence identity with four *POSTN* mRNA isoforms originally reported ((101), NCBI Reference Sequences: NM_006475.2, NM_001135934.1, NM_001135935.1 and NM_001135936.1). PCR products were visualized by agarose gel electrophoresis, amplicons were isolated using the QIAEX® II Gel extraction kit and sequenced at the Robarts Research Institute DNA sequencing facility (Western University, London, ON).

2.2.8 Flow Cytometry

Cell viability was assessed using the Guava ViaCount® assay that distinguishes between viable and non-viable cells based on the differential permeability of DNA-binding dyes in the ViaCount® reagent. Primary fibroblasts were cultured in sFPCLs treated with 2 µg/ml human recombinant periostin or vehicle for 72 hours. Cells were extracted from sFPCLs using collagenase (2.2.6.1). Cell pellets were resuspended in 1 ml of MCDB medium and cell number was assessed using a hemocytometer. Accurate cell counting on the Guava system occurs at a cell concentration of 1×10^4 - 5×10^5 cells/ml. Cell suspensions of appropriate concentrations were diluted to 300 µl in MCDB media and incubated with 100 µl of Guava ViaCount reagent for 5 minutes. Flow cytometry analysis

was performed using the Guava EasyCyte Mini (Millipore, Billerica, MA). Using a stained cell sample, threshold levels were set to separate nucleated cells from debris and viable cells from non-viable cells using CytoSoft 4.2.1 software (Millipore, Billerica, MA). Once threshold levels were set, samples were analyzed in triplicate for 1000 cellular events. Viability data was exported to FlowJo 7.6.5 (Tree Star Inc, Ashland, OR) and plotted with cell viability on the y-axis and forward scatter on the x-axis to separate collagen debris from the viable and non-viable cell populations. Manual gates were set and applied to all the samples within the experiment. Viability was assessed by calculating the percentage of viable versus non-viable cells from the total cell population.

2.2.9 Immunoprecipitation (IP)

2.2.9.1 Fixation

Primary hypertrophic scar fibroblasts were cultured on 100 mm tissue culture plates in 10% FBS- α MEM. When 85% confluency was achieved, fibroblasts were fixed with formaldehyde (final concentration of 1%) for 10 minutes at room temperature. 25 mM glycine solution (final concentration of 2.5 mM) was added to each plate and incubated for an additional five minutes at room temperature to quench the formaldehyde. Plates were washed with ice-cold PBS (5 x 1 minute), incubated with 100 μ l non-denaturing lysis buffer (Table 2.8) and cells were lysed using a cell scraper. Total protein extracts were collected in a 1.5 ml microcentrifuge tube, incubated on ice for 30 minutes and subjected to needle aspiration. Cell extracts were centrifuged at 16 000 x g for 10 minutes and the supernatant was stored at -80°C.

2.2.9.2 Generation of conditioned media

Primary hypertrophic scar or normal skin fibroblasts were cultured on 100 mm tissue culture plates in 10% FBS- α MEM until the cells achieved 80% confluency. Cells were washed overnight in serum free α MEM then cultured in 5 ml fresh serum-free α MEM for 96 hours. Conditioned media was collected, supplemented with proteinase inhibitor cocktail and stored at -80°C. For immunoprecipitation studies, fresh conditioned media was concentrated 50x using 10 kDa Amicon® Ultra centrifugal filters and the concentration was assessed by BCA assay (2.2.6.2).

2.2.9.3 Immunoprecipitation

1 mg of hypertrophic scar-conditioned media or total cell lysate (2.2.9.1), in a final volume of 1 ml, was incubated with 4 μg of periostin-specific antibody or IgG control (Table 2.7) overnight at 4°C with gentle rotation. Protein A/G magnetic beads were washed twice with wash buffer (175 μl and 1 ml for 1 minute each, Table 2.8), and incubated with the antigen/antibody mixture for 1 hour at room temperature with gentle rotation. Magnetic beads were washed with 500 μl wash buffer (3 x 5 minutes) and 500 μl purified water (1 x 2 minutes). Magnetic beads were resuspended in 80 μl lysis buffer (Table 2.8) and 20 μl SDS gel-loading buffer (Table 2.3) and boiled at 95°C for 5 minutes (conditioned media samples) or 70°C for 45 minutes to reverse formaldehyde crosslinks (total cell lysate samples). The supernatant was collected and 50 μl was loaded into 1.5 mm wells and subjected to SDS-PAGE. PVDF membranes were probed with antibodies against periostin and integrins α_V and α_5 (Table 2.4). 50 μg of total cell lysate or conditioned media (input samples) was analyzed to confirm the presence of periostin and integrins α_V and α_5 in the pre-immunoprecipitated sample.

2.2.9.4 Gel fixation and coomassie brilliant blue staining

Immunoprecipitated samples were subjected to SDS-PAGE and stained with coomassie brilliant blue for liquid chromatography tandem mass spectrometry analysis.

Polyacrylamide gels were fixed for 30 minutes at room temperature with gentle rocking in gel fixation solution (Table 2.8). Gels were stained with coomassie brilliant blue staining solution (Table 2.8) for 30 minutes at room temperature with gentle rocking. Gels were then destained in destaining solution (Table 2.8) for 2-3 hours at room temperature with gentle rocking. Destaining solution was replaced every 45 minutes. Gels were imaged using the ChemiGenius² Bio Imaging System and images were captured using Gene Snap. Gels were stored at 4°C in 5% acetic acid.

2.2.9.5 Spot picking, in-gel digestion and mass spectrometry

Differential protein bands in periostin immunoprecipitated samples relative to IgG controls were isolated using the Ettan spot picker (GE Healthcare, Little Chalfont, UK) at the Functional Proteomic Facility (FPF) at Western University (London, ON). Isolated samples were stored in R.O H₂O with 45% methanol and 5% acetic acid and submitted to

the FPF for in-gel digestion. In-gel digestion was performed using a MassPREP automated digester station (PerkinElmer, Waltham, MA). In brief, gel pieces were coomassie brilliant blue destained using 50 mM ammonium bicarbonate and 50% acetonitrile. Proteins were reduced using 10 mM DTT, followed by alkylation using 55 mM iodoacetamide and tryptic digestion. Peptides were extracted using a solution of 1% formic acid and 2% acetonitrile and lyophilized.

Lyophilized samples were submitted to the Biological Mass Spectrometry Laboratory (Western University, London, ON) for quadrupole time-of-flight (Q-TOF) liquid chromatography tandem mass spectrometry (LC-MS/MS) analysis. In brief, lyophilized fractions were reconstituted in 0.1% formic acid prior to injection. For gel-enhanced analysis, excised band samples were identified as having low, medium, or high complexity based on clear, light, or dark coomassie staining, respectively. Depending upon the anticipated complexity of the sample, $\sim 1/2$, $1/5$, or $1/8$ of each fraction was analyzed using a 60-, 90-, or 150-min LC method, respectively. Separation using LC (5–40% acetonitrile, 0.1% formic acid gradient) was performed on a NanoAcquity Ultra Performance Liquid Chromatography (UPLC, Waters Corporation, Milford, MA) with a 25 cm x 75 μm C₁₈ reverse phase column. Peptide ions were detected in data-dependent acquisition mode by tandem MS using a Q-ToF Ultima-Global mass spectrometer (Waters Corporation, Milford, MA). Raw data was refined, deNovo sequenced and searched using Peaks 6.0 (Bioinformatics Solutions Inc., Waterloo, ON) against NCBI nr – human database. Results were filtered using a false discovery rate of 1% and a minimum of two unique peptides were required for positive protein identification.

2.2.10 Nickel magnetic bead precipitation

Primary hypertrophic scar fibroblasts were cultured on 100 mm tissue culture plates in 10% FBS- α MEM until 80% confluency was achieved. Cultures were then treated with 2 $\mu\text{g}/\text{ml}$ human recombinant periostin or vehicle in 2% FBS- α MEM overnight. Samples were fixed and lysed as described 2.2.9.1. PureProteome™ Nickel Magnetic Beads (Millipore, Billerica, MA) were used to precipitate the histidine-tagged human recombinant periostin from total cell lysates. Nickel magnetic beads were placed in a magnetic stand to remove the storage buffer and washed for 1 minute with gentle rotation

with 500 μ l lysis buffer (Table 2.9). 1 mg of total cell lysate, in a final volume of 1 ml, was added to the magnetic beads and incubated at room temperature with gentle rotation for 2 hours. Magnetic beads were washed for 10 minutes with sterile water, 2.5 hours with wash buffer (Table 2.9), twice for 10 minutes with wash buffer then quickly in sterile water. Magnetic beads were incubated with 100 μ l elution buffer (Table 2.9) for 5 minutes at room temperature with gentle rotation. 25 μ l of SDS gel-loading buffer (Table 2.3) and 1 μ l proteinase inhibitor cocktail was added to the supernatant and samples were incubated at 70°C for 45 minutes to reverse the formaldehyde crosslinks. 50 μ l of the supernatant was loaded into 1.5 mm wells and subjected to SDS-PAGE. PVDF membranes were probed with antibodies against periostin and integrins α_v and α_5 (Table 2.4). 50 μ g of total cell lysate (input sample) was analyzed to confirm the presence of periostin and integrins α_v and α_5 in the pre-precipitated samples.

2.2.11 Loss-of-function studies

Adenoviral shRNA constructs were purchased from Vector Biolabs (Philadelphia, PA). Both *POSTN* shRNA and scrambled control vectors have an adenoviral-type 5 (dE1/E3) backbone, are regulated by the U6 promoter and co-express green fluorescent protein (GFP), allowing for visualization of transduction efficiency by epifluorescent microscopy. *POSTN* and scrambled shRNA sequences (Table 2.10) were analyzed by BLAST to confirm that the *POSTN* shRNA sequence was present in all *POSTN* variants and that the scrambled shRNA sequence was not directed against any known human target.

2.2.11.1 Amplification of adenoviral shRNA constructs

Adenoviral *POSTN* and scrambled shRNA vectors were amplified using HEK 293 cells (Gift from Dr. Lina Dagnino, Western University, London, ON). HEK 293 cells were cultured in 100 mm tissue culture plates to confluency in Dulbecco's modified Eagle's medium (DMEM) supplemented with 4% FBS. Adenovirus, at a multiplicity of infection (MOI) of 2, was added to fresh 4% FBS-DMEM and HEK 293 cells were incubated in this inoculum for 4-5 days. When 70% of the cells floated off the plate, cells were harvested by rinsing the plate with media. Cells were pelleted by centrifugation at 1300 x g for 5 minutes. The media was aspirated and cell pellets were resuspended in 1 ml sterile

10% glycerol-PBS. Cell pellets were subjected to four rounds of freeze/thaw cycles using liquid nitrogen and a warm water bath. Cell pellets were vortexed gently after each thaw. Cellular debris was removed from the samples by centrifugation at 16 000 x g for 10 minutes and the supernatant containing the virus was stored at -80°C.

2.2.11.2 GFP adenovirus titering

Primary hypertrophic scar fibroblasts were seeded in 10% FBS- α MEM in 24-well trays at a cell concentration of 100 000 cells/well and cultured overnight at 37°C in 5% CO₂. Viral dilutions of the amplified stocks were prepared by serially diluting virus in α MEM supplemented with 2% FBS. Viral dilutions were added to each well at 300 μ l/well in triplicate and incubated for 48 hours. After 48 hours, non-transduced cells were collected following trypsin digestion and counted using a hemocytometer to obtain a total cell count per well. The cells transduced with virus were fixed in 4% paraformaldehyde for 10 minutes at room temperature. Wells were washed with PBS (3 x 5 minutes) and stained with Hoescht for 5 minutes. Wells were then washed in PBS (2 x 5 minutes) and imaged using the Olympus IX81 deconvolution microscope (Olympus Corporation, Tokyo, Japan). Cell numbers per field were assessed by counting the number of Hoescht positive cells. The number of GFP positive-viral transduced cells were counted in the same field. The percentage of virus transduced cells was calculated in the lowest viral dilution where at least 70% of the cells were transduced. The percentage of viral transduced cells per field was multiplied by the total number of cells present in the well to determine the total number of cells transduced per well. Using the dilution factor and the number of transduced cells, the concentration of the virus was determined.

2.2.11.3 Multiplicity of infection (MOI) optimization studies

Primary hypertrophic scar fibroblasts were cultured on 100 mm tissue culture plates in 10% FBS- α MEM until the cells reached 60% confluence. The media was replaced with 2% FBS - α MEM containing adenoviral *POSTN* or scrambled shRNA constructs at an MOI of 0, 10, 25, 50 and 100. Cells were cultured for 72 hours at 37°C in 5% CO₂. After 72 hours, cell pellets were collected following digestion with trypsin (5 minutes at 37°C). Total protein and RNA was extracted from cells using methods described in 2.2.6 and 2.2.7. *POSTN* expression and periostin levels were assessed in *POSTN* shRNA treated

fibroblasts relative to scrambled shRNA controls using real time PCR and western immunoblotting, respectively.

2.2.11.4 Viral transduction

Primary fibroblasts were cultured in 10% FBS- α MEM on 100 mm tissue culture plates. When 60% confluency was achieved, fibroblasts were transduced with adenovirus constructs expressing shRNAs against *POSTN* or scrambled shRNA controls at an MOI of 25 in 2% FBS- α MEM. After 72 hours in culture, fibroblasts were assessed for GFP expression using an Olympus IX81 deconvolution microscope to determine transduction efficiency. If transduction efficiency was greater than 90%, the cells were collected by trypsin digestion and seeded into sFPCLs.

2.2.12 Immunofluorescence (IF) confocal microscopy

2.2.12.1 sFPCL setup for immunofluorescence confocal microscopy

Miniature collagen lattices were cast in 35 mm, poly-D-lysine coated glass bottom tissue culture plates with a No.1.5 cover slip with a glass diameter of 10 mm. For each glass bottom plate, 1×10^4 cells were quickly mixed with 40 μ l of type I rat tail collagen (final collagen concentration of 1.8 mg/ml), 10 μ l of neutralization solution and 2 μ g/ml human recombinant periostin or vehicle. Collagen lattices were incubated at 37°C in 5% CO₂ for 45 minutes to allow for collagen polymerization. Wells were then flooded with 1 ml 2% FBS- α MEM and incubated for 72 hours to achieve a stressed collagen matrix. After 72 hours, the media was aspirated and lattices were fixed with 4% paraformaldehyde for 10 minutes at room temperature. Plates were washed with PBS (3 x 5 minutes) and stored in 70% ethanol at 4°C.

2.2.12.2 Immunofluorescence staining with two primary antibodies from the same host species

Glass bottom plates were washed with IF-PBS (Table 2.11, 5 x 5 minutes) to remove the ethanol. Cell membranes were permeabilized (5 minutes, Table 2.11), washed with IF-PBS (3 x 5 minutes) and blocked with Background Sniper for 5-10 minutes. Incubation with Background Sniper for longer than 10 minutes resulted in loss of signal. Samples were washed briefly with IF-PBS and incubated with a primary vinculin antibody (Table

2.12) for 1 hour at room temperature in a covered humidity chamber. Samples were washed with IF-PBS (3 x 5 minutes) then incubated with an Alexa Fluor 647 conjugated secondary antibody (Table 2.13) for 1 hour at room temperature in a covered humidity chamber in the dark. Samples were washed with IF-PBS (3 x 5 minutes) then blocked with negative control mouse IgG1 (Table 2.12) for 45 minutes at room temperature in a covered humidity chamber in the dark. Samples were washed with IF-PBS (3 x 5 minutes) and incubated with a primary α SMA antibody conjugated to cy3 (Table 2.13) for 1 hour at room temperature in a covered humidity chamber in the dark. Samples were washed with IF-PBS (3 x 5 minutes), incubated with Hoechst (Table 2.13) for 5 minutes in the dark then washed with IF-PBS(2 x 5 minutes). Prolong Gold anti-fade reagent was added to the samples and a cover slip was applied over top. Samples were incubated overnight at 4° C then coverslips were sealed with nail polish. Samples were stored at 4°C in the dark.

2.2.12.3 Imaging and data analysis

Triple immunofluorescence-labelled cells were observed with a Zeiss LSM 510 Duo Vario confocal microscope (Zeiss Canada Inc., Toronto, ON) equipped with three lasers used simultaneously; an Argon/2 ion laser, a HeNe laser and a Diode laser (Table 2.13 for LSM laser lines for excitation and emission filters). All images were captured using a 40x/1.3 Oil Plan Apochromat objective lens. The pinhole was set to match 1 AU (airy unit) to ensure the best signal to noise ratio. Each channel was adjusted for gain and digital offset to achieve optimal fluorescent signal using Zen 2009 Software (Zeiss Canada Inc., Toronto, ON). Serial optical sections of individual cells were taken in a total depth of 3-6 μ m with an optimal z-step of 0.38 μ m determined by Zen 2009 Software. A minimum of 30 images from three different experiments (10 images per experiment) were captured per treatment. Images were exported as TIFFs using Zen Software and extended depth of field composite images of maximum intensity were generated for vinculin stained images using Image-Pro Plus 7.0 (Media Cybernetics, Inc., Rockville, MD). Length of focal adhesions (FA), determined by vinculin staining, was manually measured using the straight line tool in Image J. The length of vinculin-stained FAs were defined by their longest axis regardless of orientation. Total FA numbers, average FA

length and the classification of FAs were calculated using Excel. Focal adhesions were arbitrarily classified into three categories: immature FAs ($\leq 2 \mu\text{m}$), mature FAs (2-6 μm) and supermature FAs ($> 6 \mu\text{m}$, (184)).

2.2.13 Statistical analyses

Statistics were calculated using SPSS Statistics 17.0 software (IBM Corporation, Armonk, NY) and Microsoft Excel 2007 (Microsoft, Redmond, WA). All data sets consist of data obtained from a minimum of three patients from three independent experiments assessed in triplicate unless otherwise stated. ANOVA of repeated measures were used to assess significant treatment effects and significant treatment/time interactions to distinguish between overall treatment-induced effects from treatment-induced effects that become significant over time. When a significant treatment/time interaction was observed, simple main effects analyses were further performed to determine at which time point treatment had a significant effect. Significant treatment effects at individual time points were assessed by paired t-tests. Results were deemed significant when $p < 0.05$.

Chapter 3

3 *In vitro* analysis of the effects of periostin on fibroblast proliferation in hypertrophic scarring

3.1 Rationale

Excessive fibroblast proliferation is one of the hallmarks of “overhealing” conditions like hypertrophic scarring (55, 185, 186). Periostin has been demonstrated to induce proliferation in several cell types including human dermal fibroblasts (152), mouse embryonic fibroblasts (152), phenotypically normal palmar fascia fibroblasts from patients with Dupuytren’s disease (91), human periodontal ligament fibroblasts (178), mouse mesenchymal cells (179), colorectal cancer cells (180), human retinal pigment epithelial cells (187) and rat cardiomyocytes (132). Of these previous *in vitro* studies, only two groups (132, 187) have investigated the signalling pathways utilized by periostin to induce cellular proliferation. These studies have demonstrated that periostin-induced human retinal pigment epithelial cell and rat cardiomyocyte proliferation was dependent on phosphatidylinositol 3-kinases (PI3K)/Akt activation. However, there have been no studies in the literature investigating the effects of periostin on hypertrophic scar-derived fibroblast proliferation or the signalling intermediates activated by it, nor have these pathways been assessed in fibroblasts grown on physiologically relevant culture substrates. Since periostin has been demonstrated to induce proliferation in other cell types, it was hypothesized that periostin contributes to the excessive fibroblast proliferation characteristically observed in hypertrophic scarring.

The aim of this chapter is to describe the effects of periostin on hypertrophic scar (HTS)- and normal skin (NS)-derived fibroblast proliferation and to identify potential signalling pathways utilized by periostin to elicit these effects.

3.2 Assessment of *POSTN* expression and periostin levels in fibroblasts derived from hypertrophic scar tissue

Previous *in situ* hybridization studies performed in our laboratory demonstrated that *POSTN* expression was upregulated and persistent in keratinocytes in the basal stratum

and in dermal fibroblasts in hypertrophic scar tissue relative to normal scar tissue (96), consistent with a previous report (99). To confirm the increased expression of *POSTN* in primary HTS-derived fibroblasts relative to fibroblasts derived from NS, real time PCR for *POSTN* expression was performed as described in 2.2.7.2. *POSTN* expression was increased approximately six fold in primary fibroblasts derived from HTS tissue relative to NS tissue (Figure 3.1a, N=1 patient, n=1). These findings were consistent with our previous *in vivo* studies (96) and previously published data (99).

In parallel, western immunoblotting studies were performed to assess the levels of periostin in primary fibroblasts derived from HTS and NS tissue. Alternative splicing in the C-terminal region of *POSTN* results in periostin isoforms that range in size from 83-93 kDa (115). Western immunoblotting of total cell lysates with a periostin-specific antibody revealed two bands approximately 85 and 90 kDa in size. Densitometry analysis of both bands revealed that periostin levels were increased approximately five fold in primary fibroblasts derived from HTS tissue relative to NS tissue (Figure 3.1b, N=2 patient, n=1). These findings are consistent with previous immunohistochemistry studies performed by our group (95, 96) and others (97) that demonstrated that periostin was abnormally abundant in the dermis of hypertrophic and keloid scar tissue.

3.3 Identification of *POSTN* variants in fibroblasts derived from hypertrophic scar tissue

Up to eight human *POSTN* variants have been reported in various systems to date (101, 102, 116, 117, 188-190). To determine which *POSTN* variants were present in abnormal scar tissue, total RNA was extracted from HTS fibroblasts and amplified by reverse-transcription PCR. Forward and reverse primers designed to anneal to regions outside of the variable region in the C-terminal domain, as described in 2.2.7.3 (Figure 3.2a), revealed four amplicons (variants 1-4) representing four human *POSTN* variants originally reported by Horiuchi et al., (101) in human placental and osteosarcoma cDNA libraries (Figure 3.2b, N=2 patients, n=1). The predicted amplicon sizes were 1120 base pairs (bp) for variant 1, 946 bp for variant 2, 955 bp for variant 3 and 865 bp for variant 4. The identity of each *POSTN* variant was confirmed by DNA sequencing. Although not

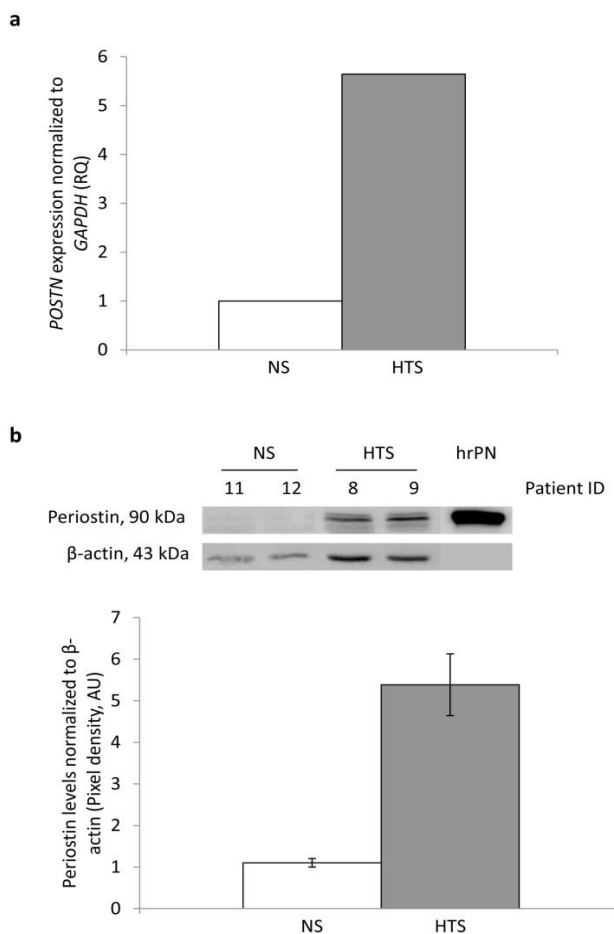


Figure 3.1 *POSTN* expression and periostin levels are abundant in primary fibroblasts derived from hypertrophic scar tissue. Primary hypertrophic scar (HTS)- and normal skin (NS)-derived fibroblasts were cultured on two-dimensional collagen substrates for 72 hours in 10% FBS- α MEM. (a) *POSTN* expression was assessed in total RNA by real time PCR as described in 2.2.7.2. As shown, *POSTN* expression was increased approximately five to six fold in HTS fibroblasts relative to NS fibroblasts. Expression data are normalized to NS (N=1 patient, n=1). (b) Periostin levels were assessed in total cell lysates by western immunoblotting and densitometry as described in 2.2.6. Periostin levels were increased five to six fold in HTS fibroblasts relative to NS fibroblasts. Values were normalized to NS patient 11 (N=2 patients, n=1). β -actin immunoreactivity was assessed to ensure equal protein loading. Human recombinant periostin (1 μ g/ml, hrPN) was used as a positive control. Data are represented by mean values and SEM. RQ= relative quantification, AU= arbitrary units.

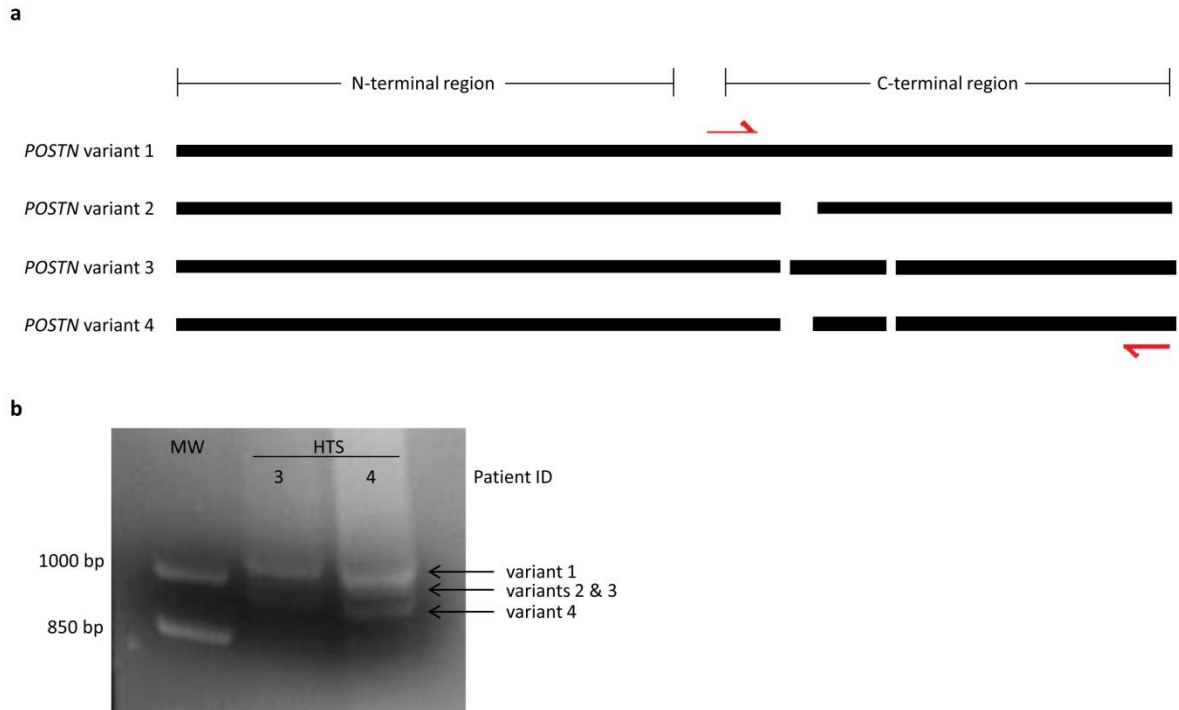


Figure 3.2 *POSTN* variant 1 is the most abundant transcript in hypertrophic scar fibroblasts. (a) Schematic representation of *POSTN* variants 1-4 and location of PCR primers within the cDNA (red arrows). Breaks in black bars represent deleted exon cassettes through alternative splicing. (b) Primary hypertrophic scar (HTS)-derived fibroblasts were cultured on two-dimensional collagen substrates for 72 hours in 10% FBS- α MEM. *POSTN* variants were assessed by reverse-transcription PCR of total RNA using primers designed to amplify the alternatively spliced C-terminal region. The identity of the largest MW amplicon was confirmed as isoform 1 by DNA sequencing (N=2 patients, n=1). MW= molecular weight ladder, bp= base pairs.

quantitative, these PCR analyses were performed using a single primer set and the relative intensity of each amplicon was predicted to approximate the amount of each variant in the sample. Based on this assumption, *POSTN* variant 1 was identified as the most abundant *POSTN* variant in hypertrophic scars. Western immunoblotting studies confirmed the most abundant periostin isoform in HTS cells was the same molecular weight as human recombinant periostin variant 1 (Figure 3.1b, N=2 patients, n=1).

3.4 Assessment of the basal proliferation rates of hypertrophic scar- and normal skin-derived fibroblasts in 2D collagen cultures

The “basal” (unstimulated) proliferation rates of primary fibroblasts derived from HTS and NS tissue were assessed on type I collagen substrates using the water soluble tetrazolium-1 (WST-1) proliferation assay as described in 2.2.4. Primary fibroblasts were seeded onto a thin two-dimensional (2D) type I collagen substrate in 2% FBS- α MEM and proliferation was assessed over a seven day period. As shown in Figure 3.3a, no significant differences between the basal proliferation rates of HTS and NS fibroblasts were observed over the course of the assay (N=3 patients, n=3).

3.5 Assessment of the effects of periostin on hypertrophic scar and normal skin fibroblast proliferation in 2D collagen cultures

To determine the effects of periostin on fibroblast proliferation, primary HTS and NS fibroblasts were seeded onto a type I collagen substrate containing 2 μ g/ml human recombinant periostin or vehicle (PBS with 0.1% BSA) and proliferation was assessed over a seven day period using the WST-1 proliferation assay (2.2.4). A significant interaction between periostin treatment and time was observed ($p < 0.05$) and the presence of periostin in the culture substrate enhanced HTS fibroblast proliferation over a seven day period relative to vehicle controls with significant differences evident at day five and seven (Figure 3.3b, $p < 0.05$, N=3 patients, n=3). In contrast, exogenous periostin treatment had no discernible effect on the proliferation of normal skin fibroblasts under identical culture conditions (Figure 3.3c, N=3 patients, n=3).

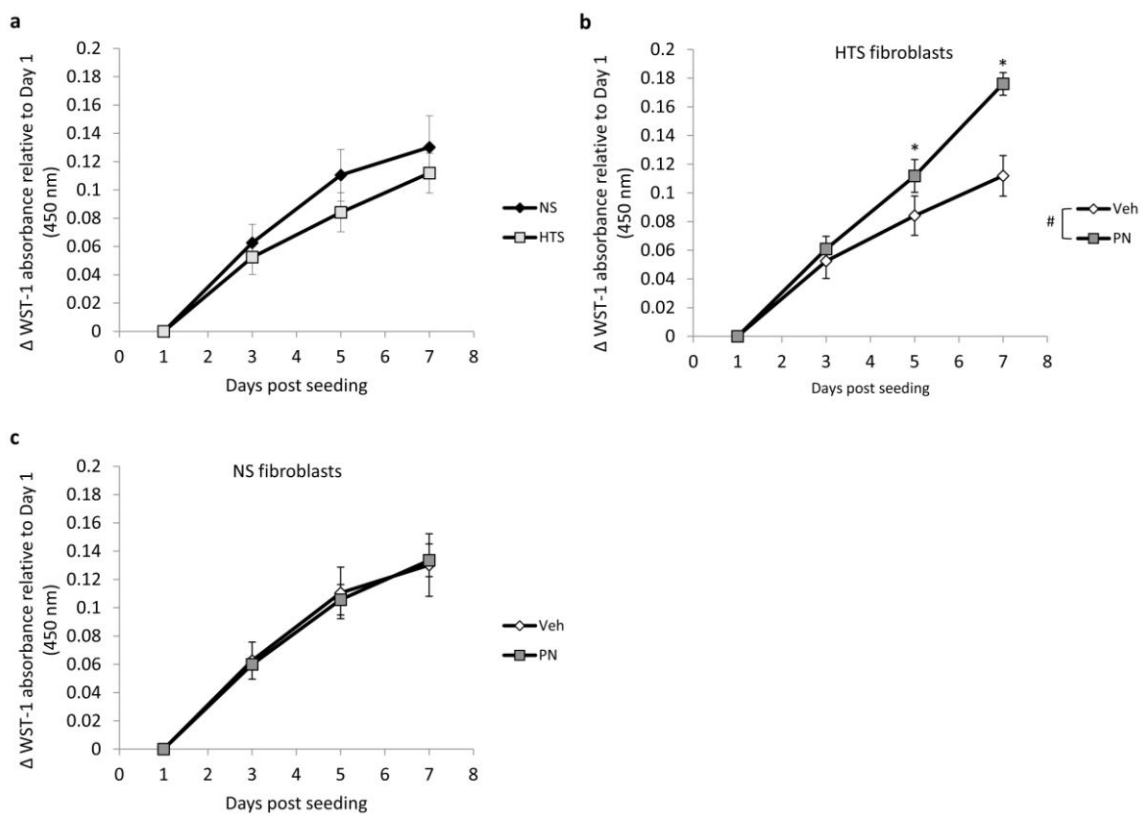


Figure 3.3 Periostin enhances the proliferation of hypertrophic scar-derived fibroblasts. Primary hypertrophic scar (HTS)- and normal skin (NS)-derived fibroblast proliferation was assessed using the WST-1 proliferation assay described in 2.2.4. Primary fibroblasts were seeded onto a two-dimensional type 1 collagen substrate containing periostin (PN, 2 μ g/ml) or vehicle (veh, 0.1% BSA in PBS) and proliferation was assessed over seven days. (a) No significant differences between the basal proliferation rates of HTS and NS fibroblasts were observed (N=3 patients each, n=3). (b) Incorporation of exogenous periostin into two-dimensional collagen lattices significantly enhanced HTS fibroblast proliferation relative to vehicle controls over a seven day period (N=3 patients, n=3). (c) Exogenous periostin treatment had no discernible effect on NS fibroblast proliferation under identical culture conditions (N=3 patients, n=3). Significant treatment/time interactions are denoted by # p <0.05 (ANOVA of repeated measures). Significant treatment effects at individual time points are denoted as * p <0.05 (simple main effects analyses). Data are presented by mean difference scores relative to day one absorbance readings and SEM.

3.6 Identification of the signalling pathway(s) utilized by periostin to induce hypertrophic scar fibroblast proliferation in 2D collagen cultures

A central aim of this chapter was to identify the signalling intermediates utilized by periostin to induce the proliferation of HTS fibroblasts. To achieve this, a series of pharmacological inhibitors were assessed. These inhibitors were targeted against signalling intermediates previously shown to be activated by periostin or other mitogens.

3.6.1 Assessment of PI3K inhibition effects on periostin-induced HTS fibroblast proliferation.

LY294002 is a small molecule inhibitor that competes with the ATP binding site in the catalytic domain of PI3K. To determine if periostin signalling required PI3K activity to enhance proliferation, LY294002 and periostin (2 µg/ml) were included in a subset of cultures of HTS fibroblasts and proliferation was assessed using WST-1 assays. 10 µM LY294002 was used in these experiments as this concentration has been demonstrated to inhibit human fibroblast proliferation in other systems (191-193). LY294002 has modest off-target effects at this concentration (194). As shown in Figure 3.4a, a significant interaction between LY294002 treatment and time was observed ($p < 0.05$) and PI3K inhibition attenuated periostin-induced HTS fibroblast proliferation over seven days relative to vehicle controls with significant differences evident at day three and seven ($p < 0.01$, $N=3$ patients, $n=3$). Similarly, a significant LY294002 treatment and time interaction was observed ($p < 0.05$) and LY294002 treatment was found to attenuate basal HTS fibroblast proliferation over the course of the assay relative to vehicle controls with significant effects observed at day five and seven (Figure 3.4b, $p < 0.05$, $N=3$ patients, $n=3$).

3.6.2 Assessment of Akt inhibition effects on periostin-induced HTS fibroblast proliferation

Akt inhibitor VIII is a small molecule inhibitor that binds to the pleckstrin homology domain of Akt and prevents activation by PI3K. To determine if periostin signalling required Akt activity to enhance HTS fibroblast proliferation, Akt inhibitor VIII and

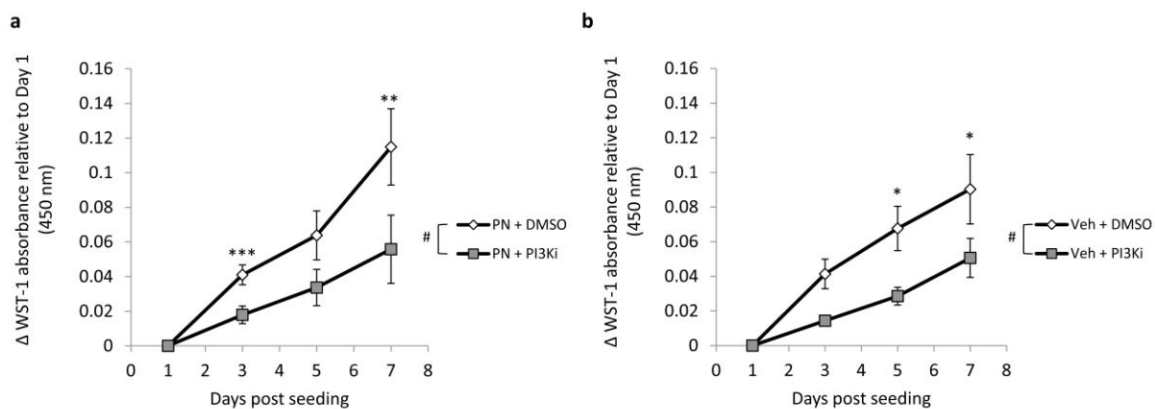


Figure 3.4 Inhibition of phosphatidylinositol 3-kinases attenuates periostin-induced and basal hypertrophic scar fibroblast proliferation. Primary hypertrophic scar (HTS)-derived fibroblasts were cultured onto two-dimensional collagen substrates containing periostin (PN, 2 $\mu\text{g/ml}$) or vehicle (veh). Culture medium was supplemented with 10 μM LY294002 (PI3Ki) or DMSO control and proliferation was assessed in WST-1 assays. As shown in (a), PI3K inhibition significantly attenuated PN-induced HTS fibroblast proliferation relative to vehicle controls (N=3 patients, n=3). (b) PI3K inhibition significantly attenuated basal proliferation over a seven day period relative to vehicle controls (N=3 patients, n=3). Significant treatment/time interactions are denoted by # $p < 0.05$ (ANOVA of repeated measures). Significant treatment effects at individual time points are denoted by * $p < 0.05$, ** $p < 0.01$ and *** $p < 0.001$ (simple main effects analyses). Data are presented by mean difference scores relative to day one absorbance readings and SEM.

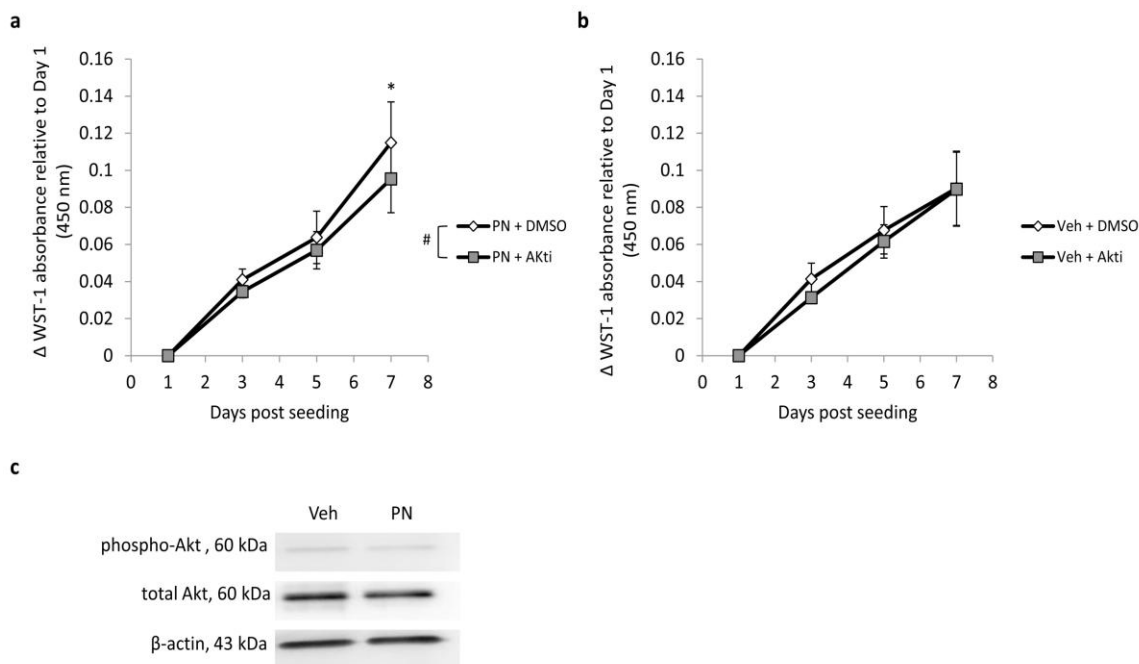


Figure 3.5 Inhibition of Akt attenuates periostin-induced hypertrophic scar

fibroblast proliferation. Primary hypertrophic scar (HTS)-derived fibroblasts were cultured on two-dimensional collagen substrates containing periostin (PN, 2 $\mu\text{g}/\text{ml}$) or vehicle (veh). Culture medium was supplemented with 0.5 μM Akt inhibitor VIII (Akti) or DMSO and proliferation was assessed in WST-1 assays. (a) Akt inhibition significantly attenuated PN-induced HTS fibroblast proliferation over seven days relative to vehicle controls (N=3 patients, n=3). (b) Akt inhibition had no discernible effects on basal HTS fibroblast proliferation over seven days relative to vehicle controls (N=3 patients, n=3). Significant treatment/time interactions are denoted by # $p < 0.05$ (ANOVA of repeated measures). Significant treatment effects at individual time points are denoted by * $p < 0.05$ (simple main effects analyses). Data are presented by mean difference scores relative to day one absorbance readings and SEM. (c) Primary HTS fibroblasts were cultured on two-dimensional collagen cultures for 72 hours, washed overnight in serum-free medium and treated with 2 $\mu\text{g}/\text{ml}$ PN or vehicle for 60 minutes in serum-free medium. Total cell lysates were assessed for phosphorylated (ser 473) and total Akt immunoreactivity by western immunoblotting as described in 2.2.6. Exogenous PN treatment had no effect on Akt activation (N=1 patient, n=3). β -actin immunoreactivity was assessed to ensure equal protein loading. Representative immunoblots are shown.

periostin (2 µg/ml) were included in a subset of cultures of HTS fibroblasts and proliferation was assessed using WST-1 assays. 0.5 µM Akt inhibitor VIII was used in these experiments based on previous studies investigating the effect of Akt inhibition on B-cell proliferation (195). At 1 µM, Akt inhibitor VIII does not significantly inhibit other kinases (194). A significant interaction between Akt inhibitor VIII treatment and time was observed ($p < 0.05$) and Akt inhibition attenuated periostin-induced HTS fibroblast proliferation over the course of the assay relative to vehicle controls with significant differences evident at day seven (Figure 3.5a, $p < 0.05$, N=3 patients, n=3). In contrast, Akt inhibition had no discernible effects on the proliferation of untreated HTS fibroblasts (Figure 3.5b, N=3 patients, n=3). In addition to WST-1 proliferation assays, western immunoblotting was performed to determine if exogenous periostin treatment induced the phosphorylation of Akt at serine 473. As shown in Figure 3.5c, addition of periostin had no discernible effects on the phosphorylation of serine 473 in HTS fibroblasts after treatment with periostin in media for 60 minutes relative to vehicle controls (N=1 patient, n=3).

3.6.3 Assessment of Glycogen synthase kinase - 3 beta (GSK-3β) inhibition effects on periostin-induced HTS fibroblast proliferation

GSK-3β inhibitor VIII is a small molecule inhibitor that competes with the ATP binding site in the catalytic domain of GSK-3β. To determine if periostin signalling required GSK-3β activity to promote HTS fibroblast proliferation, GSK-3β inhibitor VIII and periostin (2 µg/ml) were included in a subset of cultures of HTS fibroblasts and proliferation was assessed using WST-1 assays. 1 µM GSK-3β inhibitor VIII was used in these experiments as this concentration has been demonstrated to enhance prostate cancer cell proliferation (196). GSK-3β inhibitor VIII has no discernible off-target effects at concentrations up to 10 µM (194). GSK-3β inhibition had no discernible effects on periostin-induced or basal HTS fibroblasts proliferation relative to vehicle controls (Figure 3.6a and b, N=3 patients, n=3). In addition to WST-1 proliferation assays, western immunoblotting studies were performed to determine if exogenous periostin treatment increased β-catenin levels or the phosphorylation of GSK-3β at serine 9. As shown in Figure 3.6c, addition of periostin did not enhance β-catenin levels or induce

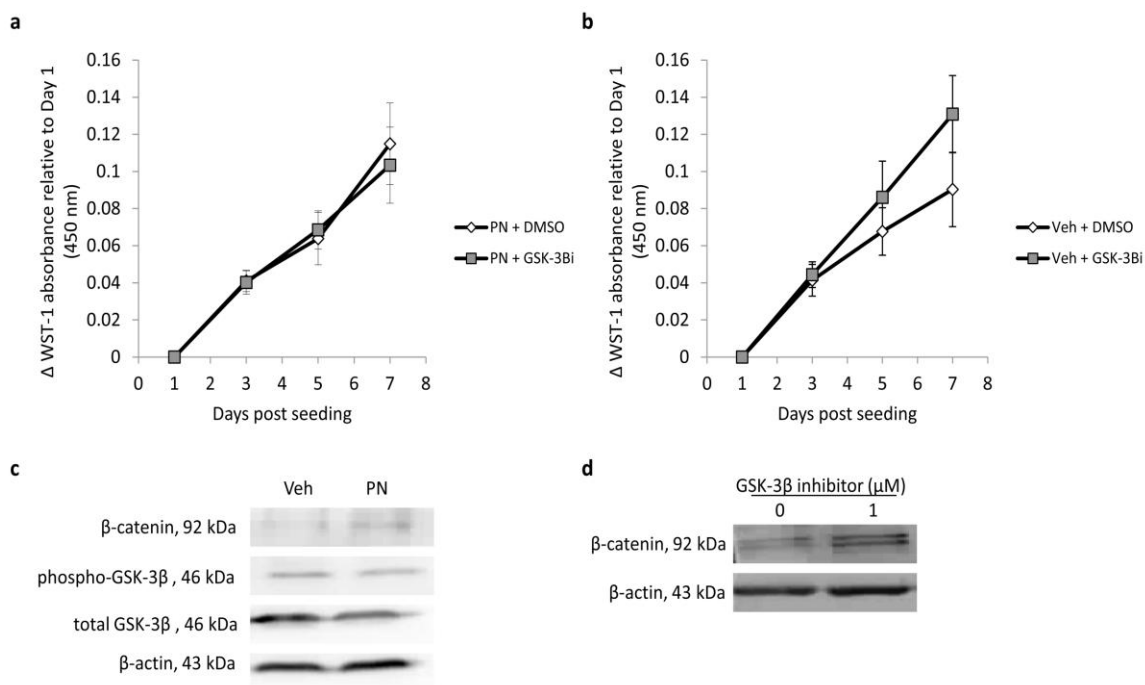


Figure 3.6 Glycogen synthase kinase-3 beta inhibition had no effect on hypertrophic scar fibroblast proliferation. Primary hypertrophic scar (HTS)-derived fibroblasts were cultured onto two-dimensional collagen substrates containing periostin (PN, 2 μ g/ml) or vehicle (veh). Culture medium was supplemented with 1 μ M GSK-3 β inhibitor VIII (GSK-3 β i) or DMSO and proliferation was assessed in WST-1 assays. GSK-3 β inhibition had no discernible effect on (a) PN-induced or (b) basal HTS fibroblast proliferation relative to vehicle controls (N=3 patients, n=3). Data are presented by mean difference scores relative to day one absorbance readings and SEM. (c) Primary HTS fibroblasts were cultured on two-dimensional collagen cultures for 72 hours, washed overnight in serum-free medium and treated with 2 μ g/ml PN or vehicle for 60 minutes in serum-free medium. Total cell lysates were extracted and assessed for β -catenin and total and phosphorylated (ser 9) GSK-3 β immunoreactivity by western immunoblotting as described in 2.2.6. Exogenous PN treatment did not affect β -catenin levels or induce GSK-3 β phosphorylation relative to vehicle controls (N=1 patient, n=3). (d) Positive control demonstrating that 1 μ M GSK-3 β inhibitor VIII was effective in inhibiting GSK-3 β activity by increasing β -catenin levels. β -actin immunoreactivity was assessed to ensure equal protein loading. Representation immunoblots are shown.

GSK-3 β phosphorylation at serine 9 in HTS fibroblasts after exposure to periostin in media for 60 minutes relative to vehicle controls (N=1 patient, n=3).

3.6.4 Assessment of Rho kinase (ROCK) inhibition effects on periostin-induced HTS fibroblast proliferation.

Y27632 is a small molecule inhibitor that competes with the ATP binding site in the catalytic domain of ROCK. To determine if periostin signalling required ROCK activity to enhance HTS fibroblast proliferation, Y27632 and periostin (2 μ g/ml) were included in a subset of cultures of HTS fibroblasts and proliferation was assessed using WST-1 assays. 10 μ M Y27632 was used in these experiments which has been demonstrated to inhibit NIH 3T3 and human gingival fibroblast proliferation (197, 198). Y27632 has modest off-target effects at this concentration (194). A significant interaction between Y27632 treatment and time was observed ($p < 0.05$) and ROCK inhibition significantly attenuated periostin-induced HTS fibroblast proliferation over seven days relative to vehicle controls with a strong trend ($p = 0.051$) towards decreased proliferation evident at day seven (Figure 3.7a, N=3 patients, n=3). In contrast, ROCK inhibition had no discernible effects on the basal proliferation of HTS fibroblasts cultured under identical conditions (Figure 3.7b, N=3 patients, n=3). In parallel, western immunoblotting was performed to determine if exogenous periostin treatment induced the phosphorylation of myosin light chain (MLC), an established downstream target of ROCK. MLC phosphorylation at serine 19 was not detected under these culture conditions (data not shown).

3.6.5 Extracellular signal-regulated kinase (ERK) inhibition effects on periostin-induced HTS fibroblast proliferation

ROCK has previously been shown to enhance proliferation through ERK (197-201). Therefore, the effects of ERK inhibition were assessed on periostin-induced HTS fibroblast proliferation. PD98059 is a small molecule inhibitor that prevents binding and activation of ERK1/2 by the ERK specific mitogen-activated protein kinase, MEK. To determine if periostin signalling required ERK1/2 activity to promote HTS fibroblast proliferation, PD98059 and periostin (2 μ g/ml) were included in a subset of cultures of

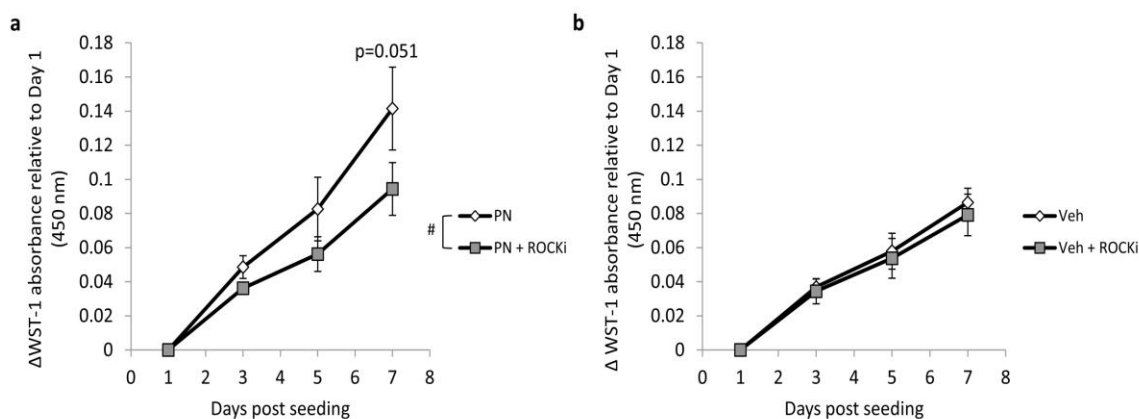


Figure 3.7 Rho kinase inhibition attenuates periostin-induced hypertrophic scar fibroblast proliferation. Primary hypertrophic scar (HTS)-derived fibroblasts were cultured onto two-dimensional collagen substrates containing periostin (PN, 2 $\mu\text{g/ml}$) or vehicle (veh). Culture medium was supplemented with 10 μM Y27632 (ROCKi) or vehicle and proliferation was assessed in WST-1 assays. (a) ROCK inhibition significantly attenuated PN-induced HTS fibroblast proliferation relative to vehicle controls over the course of the assay (N=3 patients, n=3). (b) In contrast, ROCK inhibition had no discernible effect on basal HTS fibroblast proliferation (N=3 patients, n=3). Significant treatment/time interactions are denoted by #p<0.05 (ANOVA of repeated measures). Data are presented by mean difference scores relative to day one absorbance readings and SEM.

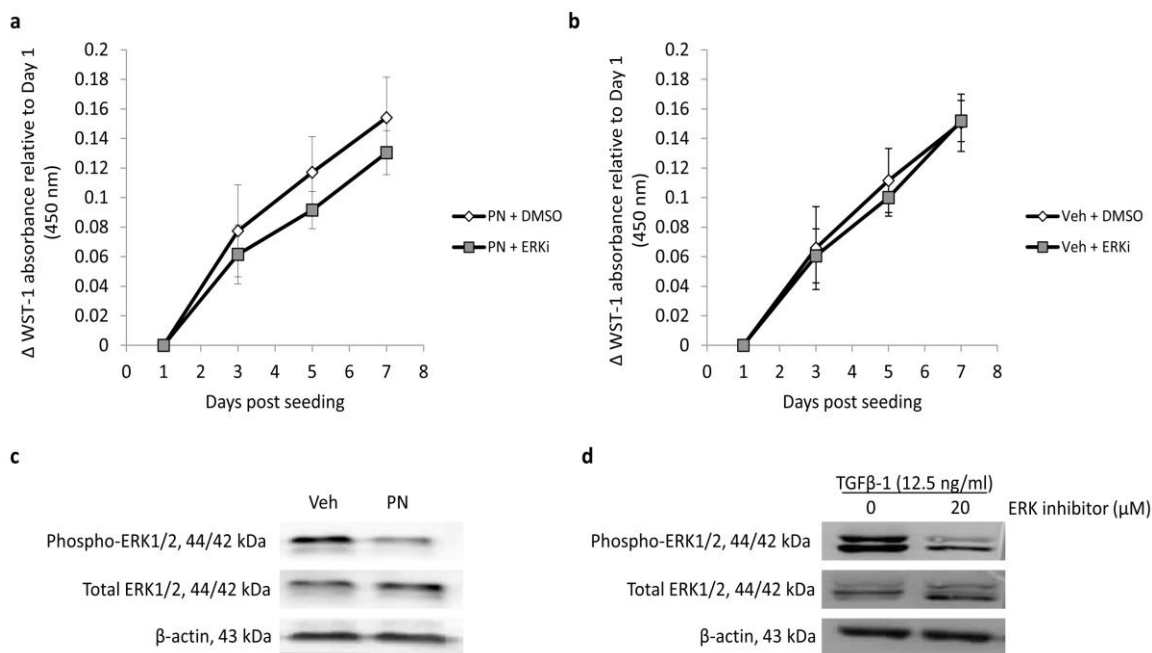


Figure 3.8 Extracellular signal-regulated kinase inhibition had no effect on basal or periostin-induced hypertrophic scar fibroblast proliferation. Primary hypertrophic scar (HTS)-derived fibroblasts were cultured on two-dimensional collagen substrates containing periostin (PN, 2 $\mu\text{g}/\text{ml}$) or vehicle (veh). Culture medium was supplemented with 20 μM PD98059 (ERKi) or DMSO and proliferation was assessed in WST-1 assays. ERK inhibition had no discernible effect on (a) PN-induced or (b) basal HTS fibroblast proliferation over the course of the assay relative to vehicle controls (N=3 patients, n=3). Data are presented by mean difference scores relative to day one absorbance readings and SEM. (c) Primary HTS fibroblasts were cultured on two-dimensional collagen cultures for 72 hours, washed overnight in serum-free medium and treated with 2 $\mu\text{g}/\text{ml}$ PN or vehicle for 60 minutes in serum-free medium. Total cell lysates were assessed for total and phosphorylated (thr 202/tyr 204, thr185/tyr187) ERK immunoreactivity by western immunoblotting as described in 2.2.6. Exogenous PN treatment did not enhance ERK phosphorylation relative to vehicle controls (N=1 patient, n=3). (d) Positive control demonstrating that 20 μM ERK inhibitor, PD98059, was effective at inhibiting TGF β -1-induced ERK1/2 phosphorylation. β -actin immunoreactivity was assessed to ensure equal protein loading. Representative immunoblots are shown.

HTS fibroblasts and proliferation was assessed using WST-1 assays. 20 μ M PD98059 was used in these experiments based on previous studies investigating the effects of ERK inhibition on human cardiac and dermal fibroblast proliferation (195). At 50 μ M, PD98059 has no discernible off-target effects (202). Inhibition of ERK activity had no discernible effects on periostin-induced or basal HTS fibroblast proliferation relative to vehicle controls (Figure 3.8a and b, N=3 patients, n=3). In parallel, western immunoblotting studies were performed to determine if exogenous periostin treatment induced the phosphorylation of ERK1/2. As shown in Figure 3.8c, periostin treatment did not increase ERK1/2 phosphorylation relative to vehicle controls after exposure to periostin in media for 60 minutes (N=1 patient, n=3).

3.7 Discussion

A central hypothesis of this thesis was that periostin contributes to excessive fibroblast proliferation in hypertrophic scarring. The *in vitro* studies presented in this chapter demonstrate that exogenous periostin treatment was able to enhance the proliferation of fibroblasts derived from abnormal scar tissue, supporting the central hypothesis. Periostin appears to elicit this effect in HTS fibroblasts through Akt and ROCK dependent pathways. In contrast, exogenous periostin had no discernible effects on the proliferation of NS fibroblasts cultured under identical conditions on type I collagen substrates.

One of the molecular features of hypertrophic scarring is the increased expression of *POSTN* and the abnormal abundance and persistence of its protein product, periostin. Real time PCR and western immunoblotting studies indicated that *POSTN* expression and periostin levels were increased in primary fibroblasts derived from HTS tissue relative to NS tissue in *in vitro* cultures. These data are consistent with previous *in vivo* studies performed by our laboratory (95, 96) and by other groups (97, 99) which demonstrated that *POSTN* expression is markedly increased in the basal epithelium and in dermal fibroblasts, and that periostin is abnormally abundant in the dermis of hypertrophic scar tissue relative to normal scar tissue. These findings indicate that *POSTN* expression and periostin levels in primary fibroblasts derived from NS and HTS tissues reflect the tissues from whence they were derived and these cells are therefore likely to be representative *in vitro* models of scarring.

As discussed in section 1.6.1, *POSTN* is alternatively spliced and up to eight human *POSTN* variants have been reported (101, 102, 116, 117, 188-190). The expression and function of these variants is currently unclear and the identity of specific *POSTN* variants expressed in hypertrophic scarring has not been previously reported. With reverse-transcription PCR, four amplicons were identified in total RNA extracted from HTS fibroblasts, and these amplicons corresponded to four of the *POSTN* variants previously identified (101). The largest and most abundant of these amplicons was identified as *POSTN* variant 1 by DNA sequencing. In addition, three additional splice variants (2, 3 and 4) were detected in HTS fibroblasts and sequenced. To our knowledge, this is the first study to identify different *POSTN* variants in hypertrophic scarring. Comparisons between the immunoreactivity of recombinant periostin and the endogenously produced periostin in human hypertrophic scar tissue lysates revealed that 2 µg/ml of recombinant periostin approximated the levels of periostin in hypertrophic scars *in vivo* (91, 96). Based on these findings, the effects of treating HTS and NS fibroblasts with recombinant periostin isoform 1 at 2 µg/ml were investigated in the remainder of the thesis.

A small number of *in vitro* studies have assessed the effects of periostin on proliferation in cells cultured on substrates that mimic the microenvironment (91, 203). However, the majority of *in vitro* studies (132, 152, 178-180, 187) have assessed periostin effects on proliferation in cells cultured on rigid tissue culture plastic. Tissue culture plastic provides an extremely stiff substrate that greatly exceeds the stiffness of the ECM of contracting or fibrotic tissues *in vivo* (169, 170) and invariably leads to robust myofibroblast differentiation in fibroblast cultures (31). Therefore, culturing primary fibroblasts on plastic substrates may provide misleading information derived from the differences in fibroblast and myofibroblast sensitivities to treatments. For this reason, the effects of periostin on HTS fibroblast proliferation was assessed on type I collagen substrates, the most abundant collagen in normal skin and mature scar tissue (8). As a matricellular protein, periostin serves as a link between cells and their collagenous ECM, and it can modify cellular behavior in response to external stimuli, including changes in ECM stiffness (90). Using collagen substrates, periostin can be incorporated into a collagenous ECM matrix to mimic its localization *in vivo* and provide a model system to assess the effects of ECM-associated periostin on HTS fibroblast proliferation under

physiological relevant conditions. Compliant 2D collagen gels have a Young's modulus of 300-400 Pa, which is equivalent to the ECM stiffness found in the provisional matrix *in vivo* (31, 173). Since fibroblasts are recruited to a similarly compliant provisional matrix during cutaneous wound healing (8), 2D collagen substrates provide a more physiologically representative *in vitro* model.

Fibroblast proliferation was assessed using the WST-1 proliferation assay, which measures cellular mitochondrial activity as an indicator of net cellular proliferation (the combined effects of growth and apoptosis). While this approach provides an indirect measure of proliferation, it is an optimal approach in this context because it avoids the need to disrupt cellular interactions with periostin embedded into the collagen substrate. Optimization studies in our laboratory have demonstrated a linear correlation between manual cell counts and WST-1 absorbance over a range of 0.03 to 0.4 absorbance units at 450 nm with every 0.038 nm correlating to approximately 1000 cells (data not shown). In addition, WST-1 absorbance values plateau in HTS fibroblasts cultured in the presence of mitomycin C, an established inhibitor of cellular proliferation (204), on 2D collagen substrates (data not shown). These findings indicate that this assay is a representative measure of cellular proliferation under these culture conditions.

Periostin has been demonstrated to induce the proliferation of various cell types in other culture systems (91, 132, 152, 178-180, 187). The data presented in this chapter indicates that exogenous ECM-associated periostin significantly enhances HTS fibroblast proliferation on 2D compliant collagen cultures. Based on these findings and the accumulation of periostin in the dermis of excisional mouse wounds as early as three days post wounding (98, 151), periostin may act as a growth factor during the initial stages of wound healing to increase fibroblast numbers at the wound site. Fibroblast proliferation in the provisional matrix and newly formed granulation tissue is vital for the regeneration of a functional dermis (8). Therefore, the persistent and abundant levels of periostin observed in the dermis of hypertrophic scars may continue to promote excessive fibroblast proliferation after wound closure. Excessive fibroblast proliferation at the wound site would be predicted to enhance the dermal density of the wound to abnormal

levels and promote excessive myofibroblast differentiation, thereby enhancing hypertrophic scar formation.

In contrast to HTS fibroblasts, exogenous periostin treatment had no effect on the proliferation of NS fibroblasts. The mechanisms that explain these differences in sensitivity to periostin between HTS and NS fibroblasts have yet to be elucidated. One possibility is that a combination of fibrosis-associated growth factors is required to “activate” NS fibroblasts to induce periostin sensitivity in these cells. This activation may include the expression of a receptor(s) or other interacting molecules not normally present in unwounded NS fibroblasts, or activation of a sequential or parallel pathway(s) required for periostin signalling. These possibilities are further addressed in Chapter 4.6. As NS fibroblasts appear relatively insensitive to ECM-associated periostin under these culture conditions, that may suggest that periostin promotes pathological, rather than normal, fibroblast proliferation. It remains unclear if periostin-induced fibroblast proliferation is a normal or abnormal component of cutaneous wound healing in humans, as normal scar tissue samples could not be obtained for primary cell derivation due to ethical constraints. Collectively, these studies indicate that periostin specifically enhances the growth of abnormal scar-derived fibroblasts cultured on 2D collagen substrates. Therefore, periostin may be an attractive therapeutic target for therapies designed to inhibit excessive fibroblast proliferation characteristically observed in hypertrophic scarring.

The second component of this chapter was to identify the signalling intermediates utilized by periostin to promote HTS fibroblast proliferation on 2D collagen cultures. As periostin has been demonstrated to signal through the PI3K/Akt pathway to elicit tumour growth (129-131) and proliferation of several cell types *in vitro* (132, 187), initial studies focused on these intermediates. PI3K inhibition was shown to significantly attenuate both basal and periostin-induced HTS fibroblast proliferation. These data were interpreted to indicate that PI3K inhibition attenuates multiple pathways involved in cellular proliferation and is therefore unlikely to be helpful for distinguishing the specific effects of periostin from other signalling pathways that also induce proliferation in a PI3K

dependent manner. Therefore, the effects of Akt inhibition, an established downstream target of PI3K (205), were assessed on periostin-induced HTS fibroblast proliferation.

Akt inhibition significantly attenuated periostin-induced HTS fibroblast proliferation while having no discernible effects on basal proliferation. These data are consistent with previous reports demonstrating that periostin promoted the proliferation of rat cardiomyocytes and retinal pigment epithelial cells through a PI3K/Akt dependent pathway (132, 187). Although significant, the effects of Akt inhibition on periostin-induced HTS fibroblast proliferation were quite modest and proliferation was attenuated by approximately 19% over seven days relative to vehicle controls. The modest cumulative reduction in proliferation across seven days led to the conclusion that Akt was not the major signalling pathway intermediate utilized for periostin-induced HTS fibroblast proliferation under these culture conditions.

While Akt inhibition significantly attenuated periostin-induced HTS fibroblast proliferation using WST-1 assays, no evidence of periostin-induced Akt activation was observed by western immunoblotting. These findings are inconsistent with previous reports demonstrating that periostin enhanced Akt activation in other systems (130, 152, 187). The contrasting findings between the WST-1 and western immunoblotting studies may be explained by the technical limitations of assessing matricellular interactions by western immunoblotting. Unlike the WST-1 assays, where periostin was incorporated into a collagen-rich matrix where it was constantly available to stimulate proliferation, it was necessary to add periostin directly to the culture medium to assay for rapid changes in Akt phosphorylation by western immunoblotting. Fibroblast attachment and spreading onto collagen substrates after seeding takes several hours. If periostin was incorporated into the collagen substrates prior to seeding, HTS fibroblasts would be exposed to periostin throughout the attachment and spreading process. Once these fibroblasts had achieved normal morphology, any effects of periostin on Akt activation may no longer be detectable, as Akt phosphorylation is typically rapid and transient. Therefore, periostin was added to the culture medium after the fibroblasts achieved normal morphology (130, 152, 187) in order to assess its effects on Akt activation. As it is a matricellular protein, periostin interacts with cells while attached to the surrounding ECM and modifies cellular

signalling and phenotype in response to changes in the microenvironment (90). It is plausible that soluble periostin (added to the culture medium) is functionally distinct from ECM-associated periostin and this may explain why no changes in kinase phosphorylation were detected.

To identify additional signalling pathway(s) utilized by periostin to induce HTS fibroblast proliferation, a series of pharmacological inhibitors targeted against GSK-3 β , ROCK and ERK1/2, each of which are established signalling intermediates in cellular proliferation (201, 206, 207), were assessed. These studies demonstrated that inhibition of GSK-3 β and ERK had no discernible effects on basal or periostin-induced HTS fibroblast proliferation in 2D collagen cultures, whereas ROCK inhibition significantly attenuated periostin-induced HTS fibroblast proliferation.

In addition to its well established roles in mediating stress fiber formation, focal adhesion formation and contraction of myofibroblasts (49-53, 208, 209), ROCK has also been shown to mediate proliferation in corneal epithelial cells (200, 210), neuroblastoma cells (211), hepatic stellate cells (201) and NIH 3T3 mouse fibroblasts (197). The ROCK specific inhibitor, Y27632, used for the studies in Chapter 3 had no effect on basal levels of proliferation relative to vehicle treated HTS fibroblasts, consistent with previous reports in corneal epithelial cells and neuroblastoma cells (210, 211). These data demonstrate that ROCK signalling is not essential for basal HTS fibroblast proliferation. However, ROCK inhibition significantly attenuated periostin-induced HTS fibroblast proliferation and this effect was more pronounced than that observed with Akt inhibition (37% decrease vs 19% decrease in proliferation over seven days). These data indicate that periostin also promotes HTS fibroblast proliferation in 2D collagen cultures through a ROCK dependent pathway. To our knowledge, this is the first study to identify ROCK as a signalling intermediate in periostin-induced proliferation in any model system.

Previous studies have demonstrated that ROCK induces the expression of cell cycle progression proteins, including cyclin D1, through a Ras/ERK mediated pathway (197-201). However, ERK inhibition had no discernible effect on periostin-induced HTS fibroblast proliferation. Parallel studies of *CCND1* expression, encoding cyclin D1, were

performed by culturing HTS fibroblasts in serum free media for 72 hours in order to synchronize the fibroblasts in G₀ prior to stimulation with serum and soluble periostin. No effects on *CCND1* expression were evident in periostin treated samples relative to serum controls after 3 hours (data not shown). As described for the western immunoblotting assays for Akt activity, periostin was not incorporated in the collagen substrates in these experiments, as it was necessary to synchronize the cells in G₀ prior to periostin stimulation. HTS fibroblasts secrete high levels of endogenous periostin, so it is very likely that these cells were exposed to periostin during the synchronization process prior to treatment, making these experiments difficult to interpret. It is currently unclear if soluble and ECM-associated periostin have differential effects on the behavior of HTS fibroblasts. Exposure to periostin during the synchronization process and treatment with soluble periostin may explain why *CCND1* expression was not altered in these experiments. The downstream mechanisms involved in ROCK-dependent periostin-induced HTS fibroblast proliferation will be a focus of future studies.

Previous studies have reported conflicting data in regards to the regulation of ROCK activity by PI3K activation (130, 212, 213), and this interaction may be dependent on particular cell type and/or specific treatment conditions (214). As PI3K inhibition significantly attenuated HTS fibroblast proliferation, it is conceivable that PI3K activation may be involved in periostin-induced ROCK activation in 2D collagen cultures. Future studies, outside the scope of this thesis, will investigate whether PI3K or a parallel pathway activates ROCK to promote periostin-induced HTS fibroblast proliferation in 2D collagen cultures.

In summary, periostin enhances HTS fibroblast proliferation in 2D collagen cultures that mimic the mechanical tension of the provisional matrix in the early stages of cutaneous wound healing *in vivo* (31, 173). As a hallmark of abnormal scarring, excessive fibroblast proliferation increases cell density and ECM deposition in the wound thereby increasing the number of cells available for myofibroblast differentiation and promoting abnormal dermal density. These studies demonstrate that periostin promotes HTS fibroblast proliferation through an Akt dependent pathway, consistent with previous reports (132, 187). Furthermore, periostin was shown for the first time to enhance HTS fibroblast

proliferation through a ROCK dependent pathway. As ROCK is better known as an essential component of myofibroblast differentiation and contraction (30), and since myofibroblasts are the cellular cause of excessive contraction and remodelling of the dermis during scar formation, the remainder of this thesis focuses on the roles of periostin on myofibroblast differentiation and persistence.

Chapter 4

4 *In vitro* analysis of the effects of periostin on myofibroblast differentiation and persistence in hypertrophic scarring

4.1 Rationale

The myofibroblast is a major cellular contributor in both normal cutaneous wound healing and abnormal scar formation (27, 28, 56-58). Myofibroblasts combine the contractile features of smooth muscle cells with the extensive ECM production of fibroblasts, thereby allowing them to deposit, contract and remodel granulation tissue (29, 31). In normal cutaneous wound healing, myofibroblast numbers increase during the proliferation phase and gradually undergo apoptosis in the remodelling phase. However, in abnormal scarring conditions, myofibroblast populations are maintained at high levels (56, 57, 92-94) due, at least in part, to a prolonged proliferation phase (59). An abnormal excess of myofibroblasts results in an “overhealing” phenomenon characterized by excessive collagen production and contracture of the ECM (56, 57, 92-94). The molecules that promote excessive myofibroblast differentiation and their persistence during hypertrophic scar formation are unclear.

Previous studies have demonstrated that periostin induces myofibroblast differentiation in animal models of normal cutaneous wound repair (133) and in primary human palmar fascia fibroblasts (91). In addition, changes in periostin levels over time have been demonstrated to parallel α SMA levels in murine models of cutaneous wound healing (98) suggesting a role for periostin in myofibroblast differentiation. These studies led to the hypothesis that periostin promotes excessive myofibroblast differentiation and persistence in hypertrophic scars.

4.2 Assessment of the basal contractility of hypertrophic scar- and normal skin-derived fibroblasts in stressed fibroblast populated collagen lattices (sFPCL)

The basal contractility of primary fibroblasts derived from HTS and NS tissue was assessed and compared using sFPCL contraction assays as described in 2.2.5. In brief, primary fibroblasts were seeded into 3D collagen lattices and maintained in culture for 72 hours in 2% FBS- α MEM to promote their tension-mediated differentiation into myofibroblasts, modelling their differentiation during wound closure *in vivo* (30, 183). After 72 hours, the collagen lattices were released from the surrounding well and lattice contraction was measured over a 24 hour period. As shown in Figure 4.1a, HTS fibroblasts were significantly more contractile than NS fibroblasts ($p < 0.01$) with significant increases in contraction observed immediately after release (designated as 0 hr), 6 hours and 24 hours after release ($p < 0.05$, $N=6$ patients, $n=3$). Similarly, fibroblasts derived from keloid scar (KS) tissue, an abnormal scarring condition with similarities to hypertrophic scarring including increased periostin levels (58, 59, 62, 97, 215), displayed a non-significant trend ($p=0.118$) towards increased contractility relative to NS fibroblasts (Figure 4.1b, $N=3$ patients, $n=3$).

4.3 Assessment of the effects of periostin on the contractility of HTS and NS fibroblasts in sFPCLs

To assess the effects of increased periostin levels in the dermis of hypertrophic scar tissue on collagen lattice contraction, primary fibroblasts were seeded in sFPCLs with 2 μ g/ml human recombinant periostin or vehicle incorporated into the collagen lattice. A significant interaction between periostin treatment and time was observed in HTS fibroblasts ($p < 0.01$) and periostin enhanced HTS fibroblast contractility over 24 hours relative to vehicle controls with significant differences evident at all time points assessed (Figure 4.2a, $p < 0.05$, $N=8$ patients, $n=3$). Periostin also significantly increased the contractility of KS fibroblasts above basal levels ($p < 0.05$) with significant differences evident at lattice release (Figure 4.2b, $p < 0.05$, $N=3$ patients, $n=3$). In contrast, a periostin-enriched matrix had no discernible effects on the contractility of NS fibroblasts relative to basal levels (Figure 4.2c, $N=6$ patients, $n=3$).

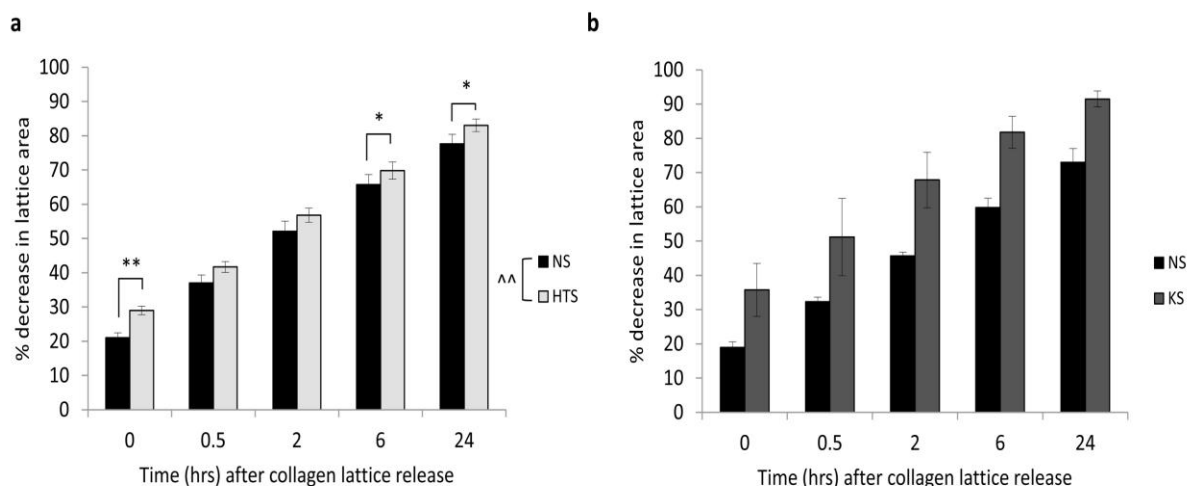


Figure 4.1 Hypertrophic scar-derived fibroblasts have enhanced contractility

relative to normal skin-derived fibroblasts. To assess the basal contractility of primary fibroblasts derived from hypertrophic scar (HTS), keloid scar (KS) and normal skin (NS) tissue, stressed fibroblast populated collagen lattices were used as described in 2.2.5. Primary fibroblasts were cultured within three-dimensional, tethered collagen lattices for 72 hours to induce myofibroblast differentiation. After 72 hours, collagen lattices were mechanically released from the surrounding wells allowing for myofibroblast-mediated contraction of the free floating collagen lattices. Area measurements were taken over a 24 hour period following release. (a) HTS fibroblasts significantly contracted collagen lattices to a greater extent than NS fibroblasts (N=6 patients, n=3). (b) A non-significant trend ($p=0.118$) towards enhanced collagen lattice contraction was observed in KS-derived fibroblasts relative to NS fibroblasts (N=3 patients, n=3). Significant overall treatment effects are denoted by $^{\wedge\wedge}p<0.01$ (ANOVA of repeated measures). Significant treatment effects at individual time points are denoted by $*p<0.05$ and $**p<0.01$ (t-tests). Data are presented by mean values and SEM.

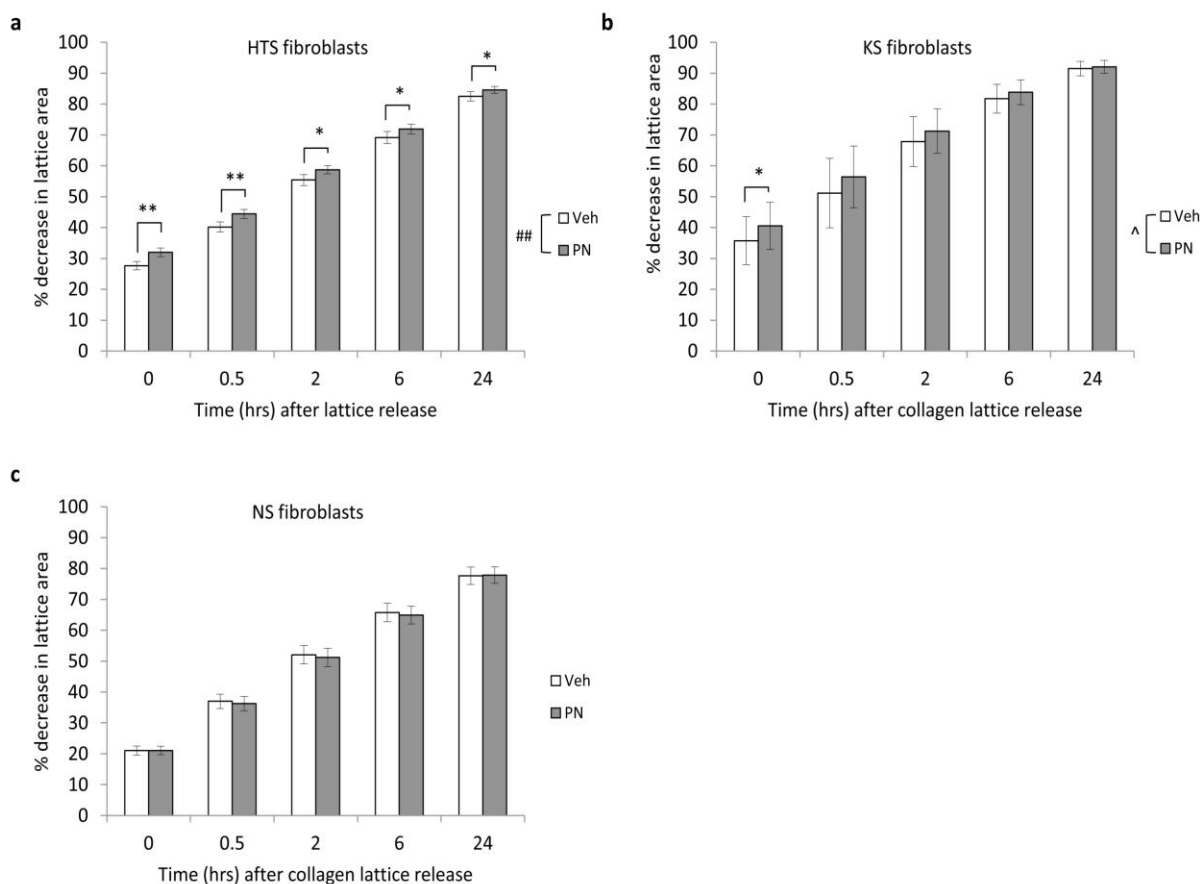


Figure 4.2 Periostin enhances collagen lattice contraction in abnormal scar-derived fibroblasts. To assess the effects of periostin (PN) on collagen lattice contraction, primary hypertrophic scar (HTS)-, keloid scar (KS)- and normal skin (NS)-derived fibroblasts were cultured in stressed fibroblast populated collagen lattices containing 2 $\mu\text{g/ml}$ PN or vehicle (veh, 0.1% BSA in PBS). (a) Exogenous PN treatment significantly enhanced HTS fibroblast collagen lattice contraction over 24 hours relative to vehicle controls (N=8 patients, n=3). (b) Exogenous PN treatment also significantly enhanced KS fibroblast collagen lattice contraction relative to vehicle controls (N=3 patients, n=3). (c) Exogenous PN treatment had no discernible effect on NS fibroblast collagen lattice contraction (N=6 patients, n=3). Significant overall treatment effects are denoted by $\wedge p < 0.05$ and significant treatment/time interactions are denoted by $\#\# p < 0.01$ (ANOVA of repeated measures). Significant treatment effects at individual time points are denoted by $* p < 0.05$ and $** p < 0.01$ (t-tests and simple main effects analyses). Data are presented by mean values and SEM.

4.4 Identification of the mechanisms utilized by periostin to enhance HTS fibroblast contractility

These findings suggested that, unlike NS fibroblasts, HTS fibroblasts were sensitive to periostin in their ECM and responded to its presence by increasing collagen lattice contraction. Periostin could potentially induce collagen lattice contraction through several mechanisms. These include increasing fibroblast proliferation and/or viability in the collagen lattice, increasing fibroblast migration and adhesion within the lattice, or by enhancing myofibroblast differentiation. Each of these mechanisms was assessed in turn to identify the molecular mechanism(s) utilized by periostin to induce collagen lattice contraction.

4.4.1 Assessment of the effects of periostin on cell viability in sFPCLs

To determine the effects of periostin on HTS fibroblast viability in sFPCLs, cell membrane permeability and *BCL2/BAX* mRNA ratio, independent markers of cell viability, were independently assessed using flow cytometry (2.2.8) and real time PCR (2.2.7), respectively. Exogenous periostin treatment had no discernible effect on HTS fibroblast membrane permeability in sFPCLs after 72 hours in culture (Figure 4.3a, N=4 patients, n=3) or *BCL2/BAX* ratio after 48 hours in sFPCL culture relative to vehicle controls (Figure 4.3b, N=3 patients, n=3). Similarly, exogenous periostin treatment had no discernible effect on the *BCL2/BAX* ratio in KS fibroblasts after 48 hours in sFPCL culture relative to vehicle controls (Figure 4.3c, N=3 patients, n=3).

4.4.2 Assessment of the effects of periostin on proliferation in sFPCLs

To determine if periostin induced HTS fibroblast proliferation in 3D cultures, *CCND1* expression was measured by real time PCR 48 hours after culture in a sFPCL, with or without periostin treatment. In contrast to periostin-induced HTS fibroblast proliferation in compliant 2D cultures over a seven day period, periostin had no effect on *CCND1* expression in HTS fibroblasts cultured under mechanical tension (Figure 4.4a, N=3 patients, n=3). Exogenous periostin treatment also had no discernible effect on *CCND1*

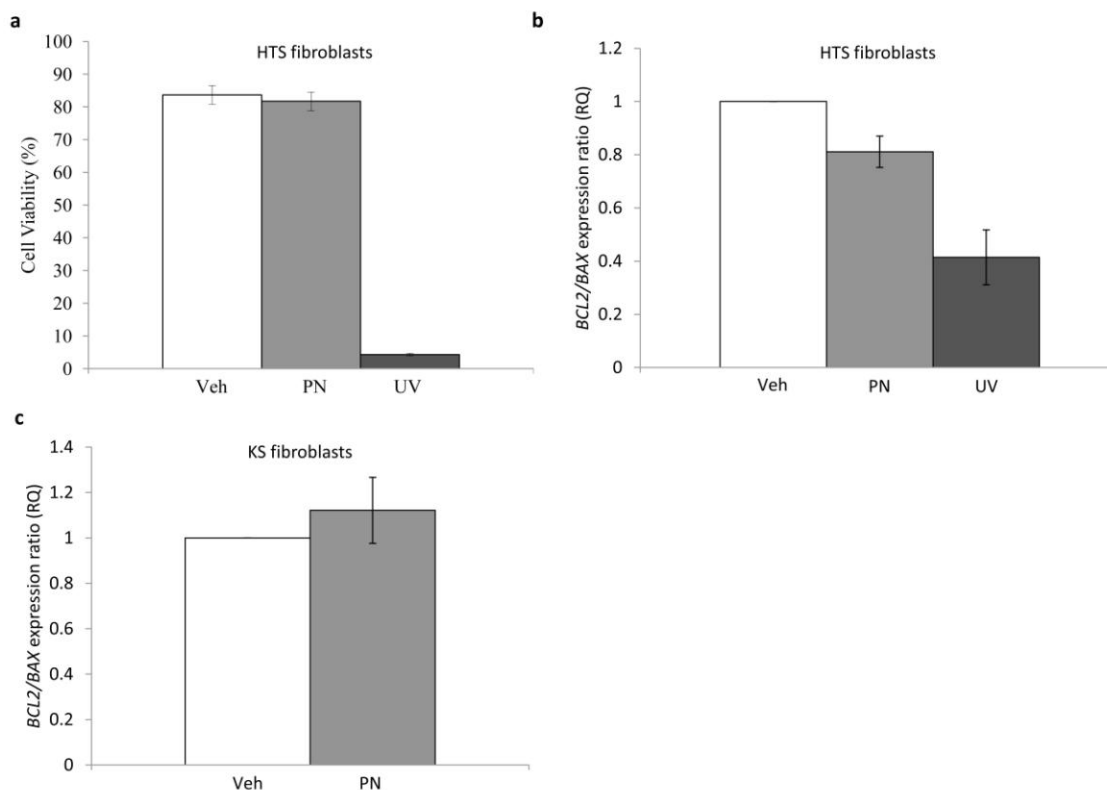


Figure 4.3 Periostin had no effect on hypertrophic scar fibroblast viability in

stressed fibroblast populated collagen lattices. Primary hypertrophic scar (HTS) and keloid scar (KS) fibroblasts were cultured in stressed fibroblast populated collagen lattices (sFPCLs) containing periostin (PN, 2 μ g/ml) or vehicle (veh). (a) The effects of PN on HTS fibroblast membrane permeability, an indicator of cellular viability, was assessed after 72 hours in sFPCL culture using flow cytometry as described in 2.2.8. PN had no discernible effect on HTS fibroblast viability relative to vehicle controls (N=4 patients, n=3). (b and c) The effects of PN on *BCL2/BAX* expression, a marker of apoptosis, were assessed in HTS and KS fibroblasts cultured in sFPCLs for 48 hours by real time PCR (2.2.7). PN had no effect on the *BCL2/BAX* ratio in (b) HTS or (c) KS fibroblasts relative to vehicle controls when cultured under mechanical tension. Values were normalized to vehicle controls (N=3 patients, n=3). Ultraviolet (UV) irradiation of HTS cells for 60 minutes was utilized as a positive control to induce cell death. Data are presented by mean values and SEM. RQ=relative quantification.

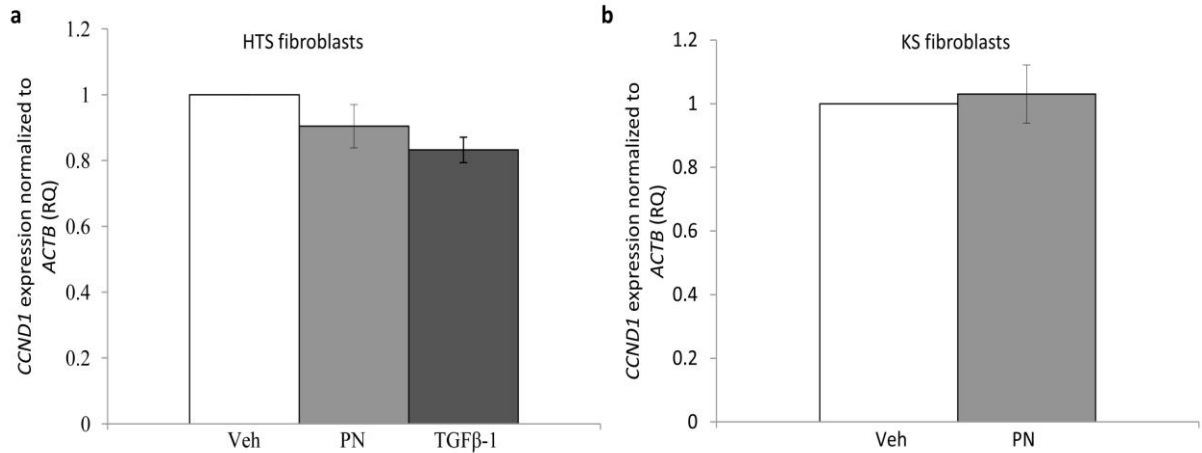


Figure 4.4 Periostin had no effect on hypertrophic scar fibroblast proliferation in stressed fibroblast populated collagen lattices. Primary hypertrophic scar (HTS) and keloid scar (KS) fibroblasts were cultured in stressed fibroblast populated collagen lattices (sFPCLs) containing periostin (PN, 2 μ g/ml) or vehicle (veh) for 48 hours. *CCND1* expression, a marker of proliferation, was assessed in total RNA by real time PCR as described in 2.2.7. Exogenous periostin treatment did not affect *CCND1* expression in (a) HTS or (b) KS fibroblasts cultured under mechanical tension relative to vehicle controls. Values were normalized to vehicle controls (N=3 patients, n=3). Transforming growth factor (TGF) β -1 (5 ng/ml) was utilized as a control to inhibit *CCND1* expression. Data are presented by mean values and SEM. RQ=relative quantification.

expression in KS fibroblasts cultured under identical conditions (Figure 4.4b, N=3 patients, n=3).

4.4.3 Assessment of the effects of periostin on adhesion and 3D migration in rFPCLs

Relaxed FPCLs (rFPCLs), described in 2.2.5, were utilized to assess the effects of periostin on HTS fibroblast adhesion and migration in 3D collagen cultures. Fibroblasts cultured in rFPCLs are not subjected to mechanical tension and do not undergo culture-induced myofibroblast differentiation (183). Instead, lattice contraction is induced by tractional forces generated by cellular adhesion to the collagen and migration within the lattice (183, 216, 217). Periostin treatment had no discernible effect on HTS or KS fibroblast contractility in rFPCLs (Figure 4.5a and b, N=3 patients, n=3).

4.4.4 Assessment of the effects of periostin on myofibroblast differentiation in sFPCLs

To determine if periostin-induced HTS fibroblast contraction of sFPCLs was the result of enhanced myofibroblast differentiation, cell lysates were derived from sFPCLs immediately prior to collagen lattice release (after 72 hours of culture in the restrained lattice). α SMA and OB cadherin levels, established markers of myofibroblast differentiation (30, 218), were assessed by western immunoblotting and densitometry. Exogenous periostin treatment significantly increased α SMA levels in HTS fibroblasts relative to vehicle controls under identical culture conditions (Figure 4.6a, $p < 0.05$, N=5 patients, n=3). A non-significant trend ($p = 0.066$) towards increased OB cadherin levels was observed in periostin treated HTS fibroblasts relative to vehicle controls (Figure 4.6b, N=5 patients, n=3). Periostin had no discernible effects on α SMA or OB cadherin levels in KS fibroblasts relative to vehicle controls (Figure 4.6c and d, N=3 patients, n=3).

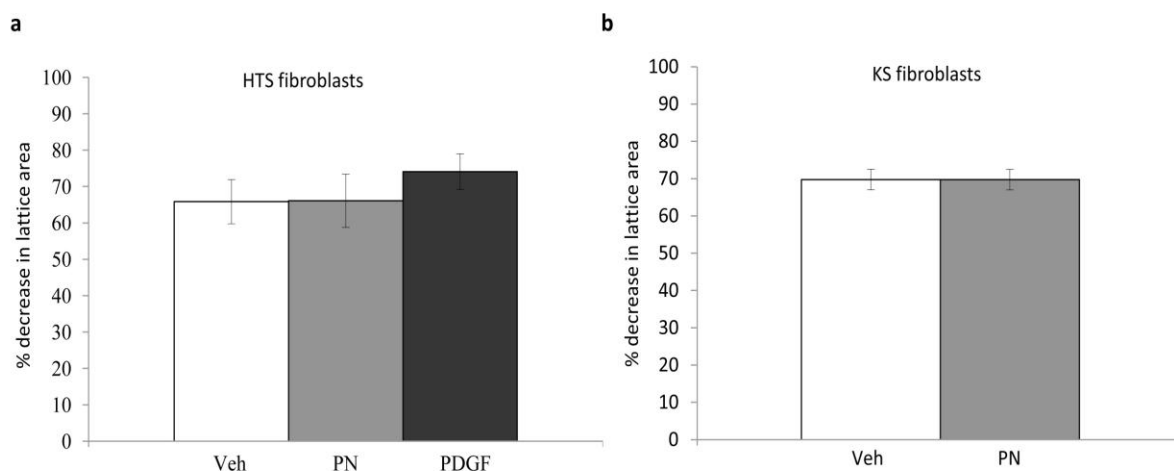


Figure 4.5 Periostin had no effect on hypertrophic scar fibroblast adhesion and migration in three dimensional collagen cultures. To assess the effects of exogenous periostin (PN) treatment on fibroblast adhesion and migration in three-dimensional (3D) collagen cultures, primary hypertrophic scar (HTS) and keloid scar (KS) fibroblasts were cultured in relaxed fibroblast populated collagen lattices containing PN (2 $\mu\text{g}/\text{ml}$) or vehicle (veh) as described in 2.2.5. Area measurements of the contracted collagen lattices were performed 24 hours after collagen lattice release. PN had no discernible effect on (a) HTS or (b) KS fibroblast migration in 3D collagen cultures (N=3 patients, n=3). Platelet-derived growth factor (PDGF) treatment (100 ng/ml) was utilized as a positive control to induce fibroblast migration based on previous studies (219). Data are presented by mean values and SEM.

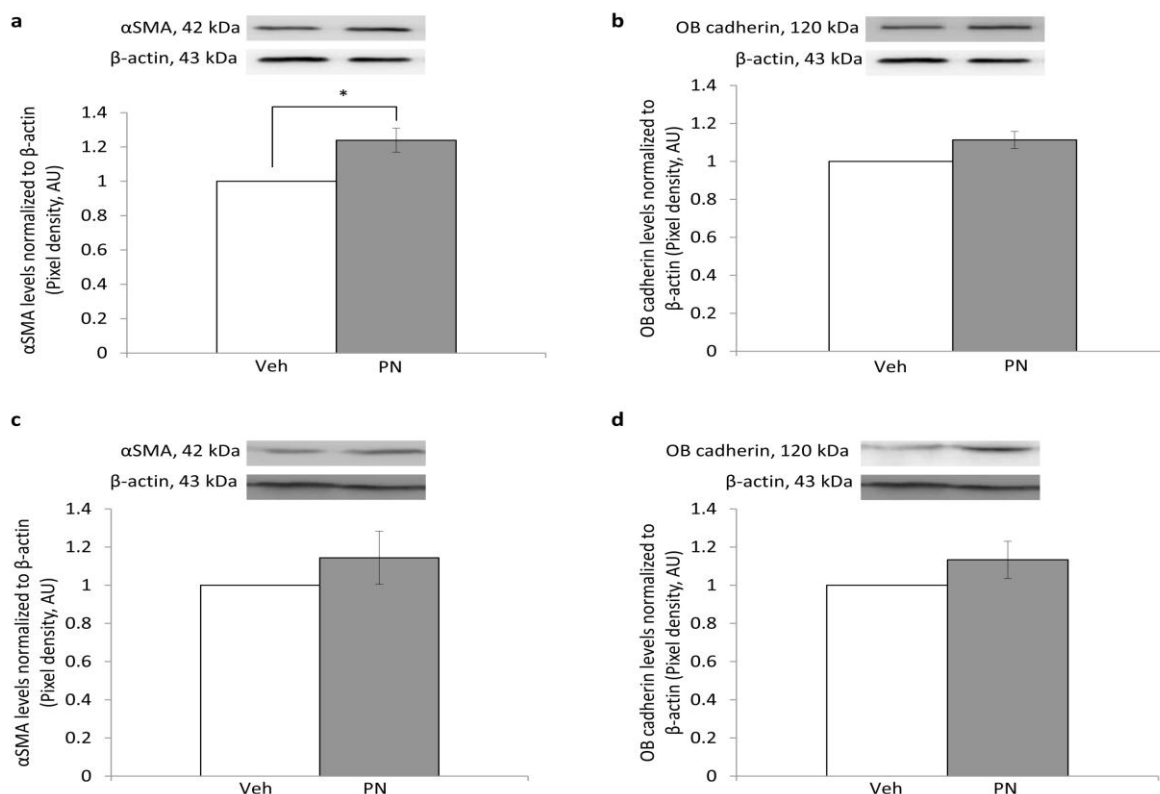


Figure 4.6 Periostin enhances myofibroblast differentiation in hypertrophic scar-derived fibroblasts. Primary hypertrophic scar (HTS) and keloid scar (KS) fibroblasts were cultured in stressed fibroblast populated collagen lattices containing periostin (PN, 2 μ g/ml) or vehicle (veh) for 72 hours as described in 2.2.5. Total cell lysates were assessed for alpha smooth muscle actin (α SMA) and OB cadherin immunoreactivity, markers of myofibroblast differentiation, by western immunoblotting and densitometry, as described in 2.2.6. (a) Exogenous PN treatment significantly increased α SMA levels in HTS fibroblasts cultured in sFPCLs relative to vehicle controls (N=5 patients, n=3). (b) A non-significant trend ($p=0.066$) towards increased OB cadherin levels were observed in HTS fibroblast cultured in sFPCLs embedded with PN relative to vehicle controls (N=5 patients, n=3 patients). Exogenous PN treatment had no discernible effects on (c) α SMA and (d) OB cadherin levels in KS fibroblasts relative to vehicle controls. Values were normalized to vehicle controls. β -actin immunoreactivity was assessed to ensure equal protein loading. Significant treatment effects are denoted by * $p < 0.05$ (t-tests). Data are presented by mean values and SEM. Representative immunoblots of the mean densitometry data are shown. AU=arbitrary units.

4.5 Assessment of the effects of periostin-depletion of HTS myofibroblast differentiation in sFPCLs

As shown in Figure 3.1b, HTS fibroblasts exhibit increased endogenous periostin levels relative to NS cells. The effects of exogenous periostin treatment on HTS fibroblasts described in the previous sections were therefore over and above the effects of endogenous periostin signalling. To obtain further support for the central hypothesis of this section, loss of function studies were performed in HTS fibroblasts by transducing them with an adenoviral vector containing a shRNA targeted against *POSTN*.

4.5.1 Assessment of *POSTN* expression and periostin levels in HTS fibroblasts following adenoviral transduction with shRNAs against *POSTN*

HTS fibroblasts were transduced with adenoviral vectors expressing either shRNAs against *POSTN* or scrambled control shRNAs. Transduction was at a multiplicity of infection (MOI) of 25 and the transduced fibroblasts were cultured on plastic tissue culture dishes for 72 hours in 2% FBS- α MEM. Transduction efficiency was then determined by assessing the percentage of cells expressing green fluorescent protein (GFP) by epifluorescence microscopy. As shown in Figure 4.7a and b, adenovirus transduction efficiency approximated 100% for all experiments assessed. Transduced HTS fibroblasts were then seeded into sFPCLs and *POSTN* and periostin levels were assessed after 72 hours in culture under 3D tension by real time PCR and western immunoblotting, respectively. As shown in Figure 4.7c and d, adenoviral transduction with shRNAs against *POSTN* significantly reduced *POSTN* expression by 92% and periostin levels by 60% relative to scrambled shRNA controls ($p < 0.001$, N=4 patients, n=3).

4.5.2 Assessment of the effects of periostin depletion on HTS myofibroblast differentiation in sFPCLs

To assess the effects of periostin depletion on HTS myofibroblast differentiation in sFPCLs, HTS fibroblasts were transduced with adenovirus expressing shRNAs against *POSTN* or scrambled control shRNAs for 72 hours in 2% FBS- α MEM prior to seeding in

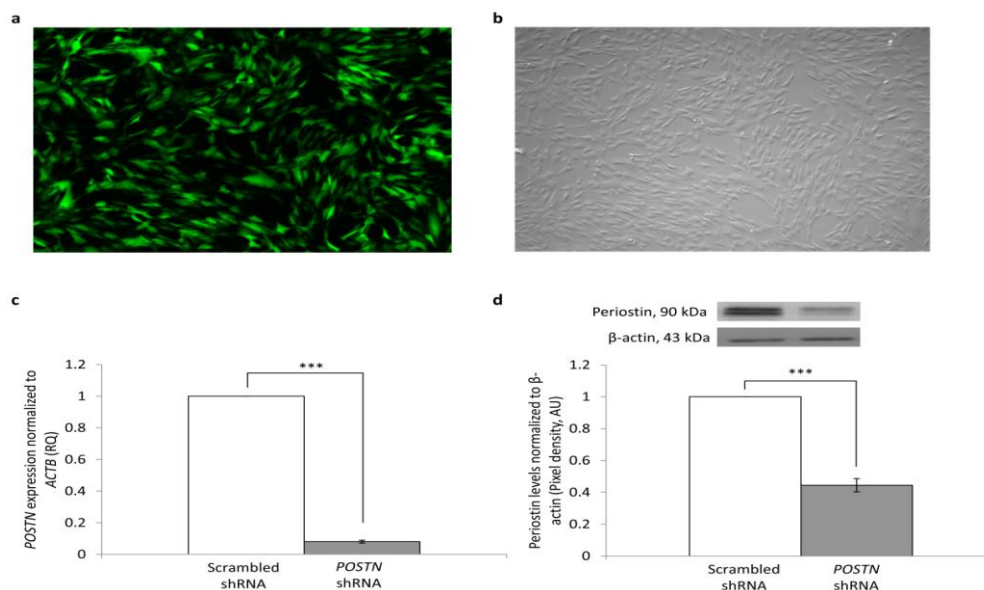


Figure 4.7 *POSTN* expression and periostin levels are significantly depleted in hypertrophic scar fibroblasts transduced with adenovirus expressing shRNAs against *POSTN*. Primary hypertrophic scar (HTS)-derived fibroblast were transduced with adenoviral vectors encoding shRNAs against *POSTN* or scrambled control shRNAs at a multiplicity of infection of 25. The adenoviral vector co-expresses green fluorescent protein, allowing transduction efficiency to be assessed by epifluorescence microscopy. (a) Comparisons of epifluorescence and (b) differential interference contrast microscopy indicate that transduction efficiency approximated 100% in all experiments. (c and d) Following adenoviral transduction, HTS fibroblasts were cultured in sFPCLs for 72 hours. (c) *POSTN* expression was assessed in total RNA by real time PCR as described in 2.2.7. Periostin depletion by shRNA treatment significantly decreased *POSTN* expression in HTS fibroblasts by 92% relative to scrambled controls (N=3 patients, n=3). (d) Total cell lysates were assessed for periostin immunoreactivity by western immunoblotting and densitometry as described in 2.2.6. Periostin depletion by shRNA treatment significantly decreased periostin levels by 60% relative to scrambled controls (N=4 patients, n=3). Values were normalized to scrambled shRNA controls. β -actin immunoreactivity was assessed to ensure equal protein loading. Significant treatment effects are denoted by *** $p < 0.001$ (t-tests). Data are presented by mean values and SEM. Representative immunoblots of the mean densitometry data are shown. RQ=relative quantification, AU=arbitrary units.

sFPCLs. No significant effects on the ability of HTS fibroblasts to contract sFPCLs were observed in periostin-depleted HTS or KS fibroblasts relative to scrambled controls (Figure 4.8a and b, N=3 patients, n=3 for each). Periostin depletion by shRNA treatment had no discernible effect on α SMA levels in HTS fibroblasts relative to scrambled shRNA controls (Figure 4.9a, N=4 patients, n=3). However, a significant decrease in α SMA levels was observed in periostin-depleted fibroblasts relative to scrambled shRNA controls in two of the four HTS patient fibroblast lines assessed ($p < 0.05$, Figure 4.9b). Periostin depletion by shRNA treatment had no effect on OB cadherin levels in HTS fibroblasts relative to scrambled shRNA controls (Figure 4.9c, N=4 patients, n=3). Additionally, periostin depletion by shRNA treatment had no significant effect on α SMA or OB cadherin levels in KS fibroblasts relative to scrambled shRNA controls (Figure 4.10a and b, N=3 patients, n=3).

4.6 Assessment of NS fibroblast responses to periostin

The contraction data presented in section 4.3 demonstrates that periostin induces collagen lattice contraction in HTS fibroblasts but not in NS fibroblasts. As NS fibroblasts are unlikely to be exposed to the growth factors and cytokines that promote abnormal wound healing, it was proposed that NS fibroblasts might need to be “activated” by fibrosis-associated factors before they can respond to periostin treatment. While not a major focus of this thesis, the following section describes pilot studies to identify some of the factors required for NS fibroblast “activation” in this model system.

4.6.1 Assessment of the effects of TGF β -1 priming on NS fibroblast contractility

During cutaneous wound healing, TGF β -1 is released following injury to the dermis and plays a critical role in many processes essential to normal wound repair (8, 13, 41, 174-177, 220). With relevance to the roles of periostin described in the previous sections, TGF β -1 signalling is required for myofibroblast differentiation (40, 41). Therefore, it was proposed that priming with TGF β -1 might be required to sensitize NS fibroblasts to the presence of periostin. To assess this, cultures were pretreated with 5 ng/ml human

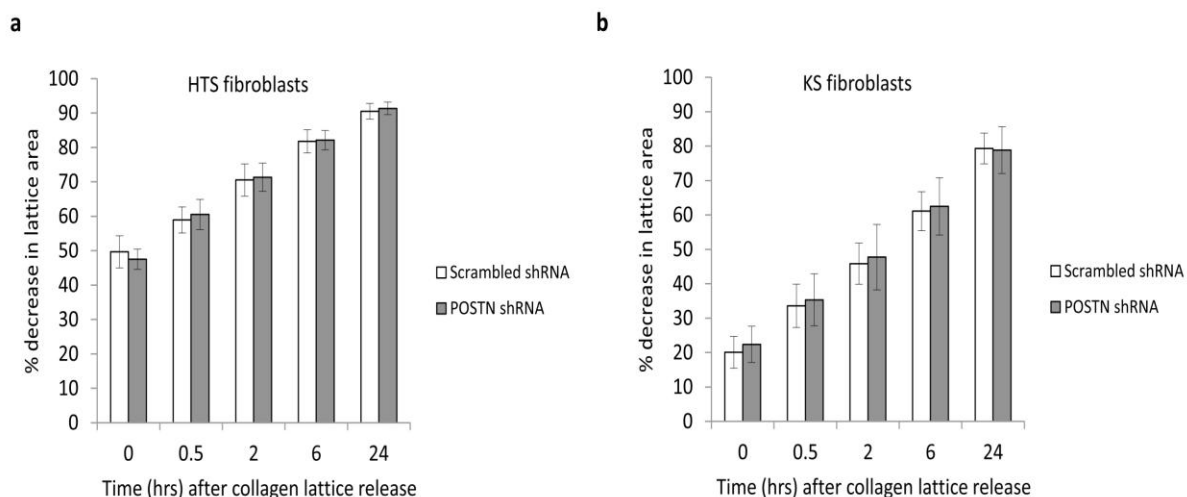


Figure 4.8 Periostin depletion had no effect on collagen lattice contraction in hypertrophic scar-derived fibroblasts. Primary hypertrophic scar (HTS) and keloid scar (KS)-derived fibroblasts were transduced with adenoviral vectors expressing shRNAs targeted against *POSTN* or scrambled control shRNAs for 72 hours on tissue culture plastic. To assess the effects of periostin depletion on collagen lattice contraction, shRNA treated HTS and KS fibroblasts were cultured in stressed fibroblast populated collagen lattices described in 2.2.5. Collagen lattice contraction was assessed over a 24 hour period. Periostin depletion by shRNA treatment had no effect on (a) HTS or (b) KS fibroblast collagen lattice contraction relative to scrambled shRNA controls (N=3 patients, n=3). Data are presented by mean values and SEM.

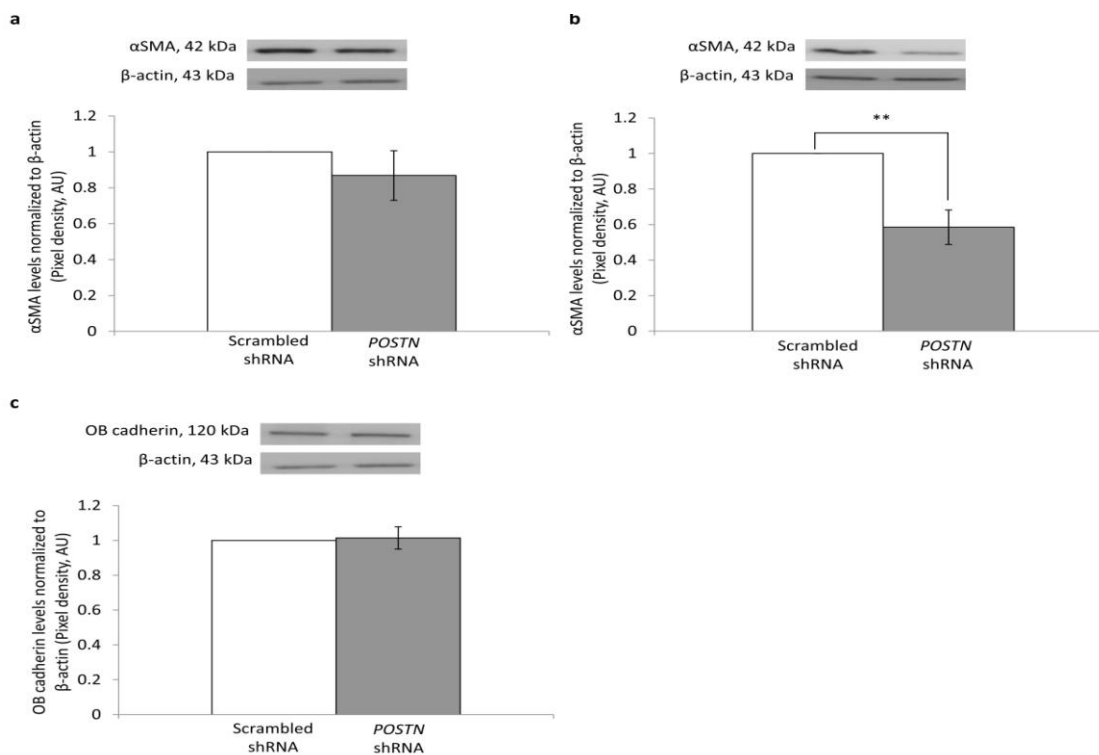


Figure 4.9 Periostin depletion significantly decreases α SMA levels in fibroblasts derived from a subset of HTS patients. Primary hypertrophic scar (HTS)-derived fibroblasts were transduced with adenoviral vectors expressing shRNAs targeted against *POSTN* or scrambled control shRNAs for 72 hours and then seeded into stressed fibroblast populated collagen lattices. Total cell lysates were assessed for alpha smooth muscle actin (α SMA) and OB cadherin immunoreactivity, by western immunoblotting and densitometry, immediately prior to collagen lattice release. (a) Periostin-depletion had no significant effects on α SMA levels in HTS fibroblasts assessed as a group (N=4 patients, n=3), (b) however, significant decreases in α SMA levels were observed following periostin depletion in a subset of individual patient-derived fibroblast cultures. Shown is a representative immunoblot and densitometry data for HTS patient #5. (c) No discernible effects on OB cadherin levels were observed in periostin-depleted HTS fibroblasts relative to scrambled shRNA controls (N=4 patients, n=3). Values were normalized to scrambled shRNA controls. β -actin immunoreactivity was assessed to ensure equal protein loading. Significant treatment effects are denoted by ** $p < 0.01$ (t-tests). Data are presented by mean values and SEM. Representative immunoblots of the mean densitometry data are shown. AU=arbitrary units.

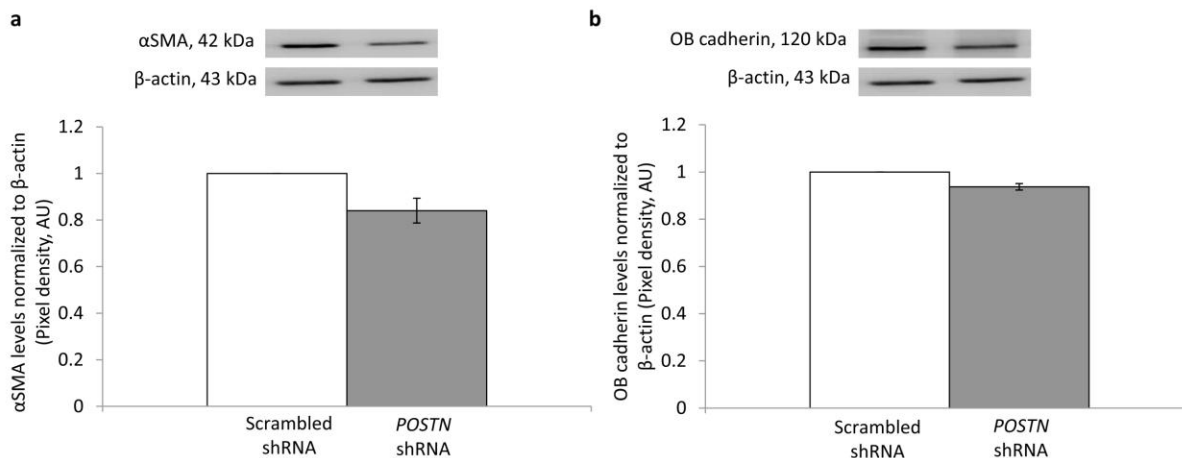


Figure 4.10 Periostin depletion had no significant effects on myofibroblast markers in keloid scar fibroblasts. Primary keloid scar (KS)-derived fibroblasts were transduced with adenoviral vectors expressing shRNAs targeted against *POSTN* or scrambled control shRNAs for 72 hours on tissue culture plastic then seeded into stressed fibroblast populated collagen lattices. Total cell lysates were assessed for alpha smooth muscle actin (α SMA) and OB cadherin immunoreactivity, by western immunoblotting and densitometry, immediately prior to collagen lattice release. Periostin-depletion had no significant effects on (a) α SMA or (b) OB cadherin levels in HTS fibroblasts relative to scrambled shRNA controls (N=3 patients, n=3). Values were normalized to scrambled shRNA controls. β -actin immunoreactivity was assessed to ensure equal protein loading. Data are presented by mean values and SEM. Representative immunoblots of the mean densitometry data are shown. AU=arbitrary units.

recombinant TGF β -1 for 72 hours prior to being seeded into sFPCLs. As shown in Figure 4.11a, a significant increase in sFPCL contraction was evident in TGF β -1 primed NS fibroblasts in collagen lattices containing periostin ($p < 0.05$) relative to TGF β -1 primed NS fibroblasts in the absence of periostin. This effect was only evident at release and no significant effects were observed at any time point assessed after release (N=3 patients, n=3).

4.6.2 Assessment of the effects of HTS-conditioned media on NS fibroblast contractility in sFPCLs

TGF β -1 is likely to be only one of many growth factors and cytokines secreted by HTS fibroblasts. To determine if additional fibrosis-associated signalling molecules were required to induce periostin sensitivity in NS fibroblasts, the effects of exposing NS fibroblasts to HTS fibroblast-conditioned culture media were assessed. HTS fibroblasts were grown to 80% confluency in serum-containing media, washed and cultured for 96 hours in serum free media, after which the conditioned media was collected. NS fibroblasts were then cultured in sFPCLs in the presence of HTS-conditioned media for 72 hours, with or without periostin addition to the collagen matrix. The addition of HTS-conditioned media had no effects on NS fibroblast contraction relative to fibroblasts cultured in the presence of NS-conditioned media (Figure 4.11b, N=1 patient, n=5). However, a significant periostin treatment and time interaction ($p < 0.01$) was observed and the presence of exogenous periostin significantly induced the contractility of NS fibroblasts cultured in HTS-conditioned media over 24 hours relative to vehicle controls. Significant increases in periostin-induced NS fibroblast contraction were observed at collagen lattice release, 0.5 and 2 hours after release (Figure 4.11c, $p < 0.05$, N=1 patient, n=5).

4.6.3 Identification of potential periostin interactors in HTS-conditioned media

A combination of periostin and HTS-conditioned media was found to significantly induce NS fibroblast contractility, whereas neither of these treatments alone had discernible effects on the ability of NS fibroblasts to contract collagen lattices. These data were interpreted to suggest that periostin needed to interact with one or more molecules in

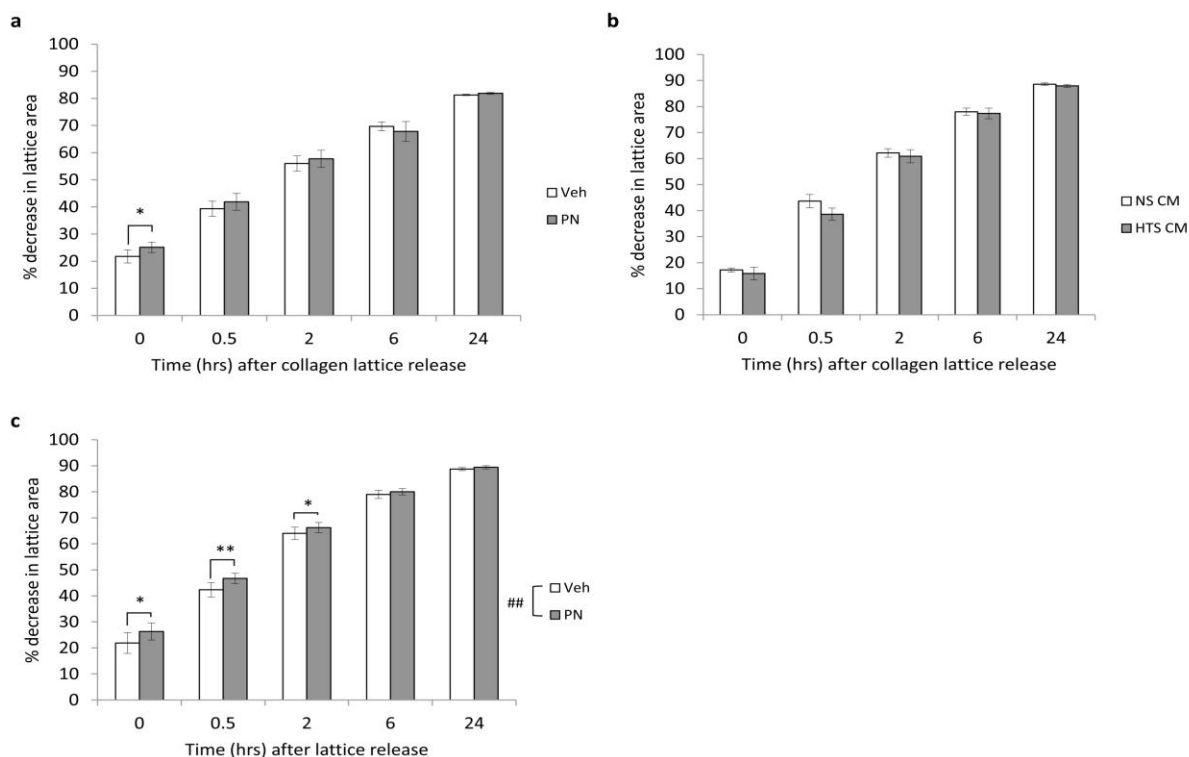


Figure 4.11 Fibrosis-associated growth factors are required to induce periostin sensitivity in normal skin fibroblasts. (a) Primary normal skin (NS) fibroblasts were cultured on tissue culture plastic for 72 hours in 10% FBS- α MEM supplemented with 5 ng/ml transforming growth factor (TGF) β -1. TGF β -1 primed NS fibroblasts were then seeded into stressed fibroblast populated collagen lattices (sFPCLs) containing 2 μ g/ml periostin (PN) or vehicle (veh) and cultured for 72 hours. Collagen lattice contraction was assessed over 24 hours. PN significantly enhanced TGF β -1-primed NS fibroblast contraction at collagen lattice release (N=3 patients, n=3). (b,c) Primary NS fibroblasts were seeded into sFPCLs embedded with PN or vehicle and cultured for 72 hours in hypertrophic scar (HTS)- or NS fibroblast-conditioned media (CM). (b) Culture in HTS CM had no effect on NS fibroblast collagen lattice contraction relative to NS fibroblasts cultured in NS CM (N=1 patient, n=3). (c) Exogenous periostin treatment significantly enhanced NS fibroblast contractility when cultured in HTS CM over 24 hours relative to vehicle controls (N=1 patient, n=5). Significant treatment/time interactions are denoted by ## p <0.01 (ANOVA of repeated measures). Significant treatment effects at individual time points are denoted by * p <0.05 and ** p <0.01 (t-tests and simple main effects analyses). Data are presented by mean values and SEM.

HTS fibroblast-conditioned media to enhance the contraction of NS fibroblasts. In order to identify potential periostin interactors, immunoprecipitation experiments were performed on HTS-conditioned media. In brief, HTS-conditioned media, in the absence of exogenous periostin, was concentrated 50 times and 1 mg of total protein was incubated with an antibody specific to periostin and precipitated with protein A/G magnetic beads. Eluted samples were separated using SDS-PAGE and analyzed by coomassie staining and western immunoblotting. Coomassie staining identified bands at approximately 85 and 90 kDa in periostin immunoprecipitated samples (Figure 4.12a) and western immunoblotting confirmed the identity of these bands as endogenous periostin (Figure 4.12b). Two additional bands were evident in the periostin immunoprecipitated samples that were absent or extremely faint in the IgG control lane (Figure 4.12a). These bands were excised and analyzed by liquid chromatography tandem mass spectrometry (LC-MS/MS). They were identified as keratin-14 (user contamination) and fragments of IgG and periostin. Optimization experiments utilizing a variety of protocol modifications failed to identify potential periostin interactors in HTS-conditioned media.

4.7 Assessment of the effects of periostin on HTS myofibroblast persistence in sFPCLs

Normally, as cutaneous wounds heal and ECM stress is relieved, the myofibroblasts that promote wound closure undergo apoptosis (8, 12). However, in abnormal scarring, myofibroblasts fail to undergo apoptosis and persist, resulting in excessive collagen production and contracture of the ECM (56, 57, 92-94) that promotes hypertrophic scar formation. When sFPCLs are released, a rapid contraction of the collagen lattices decreases the tension in the ECM. This release in ECM tension correlates with disassembly of stress fibers in myofibroblasts (47). To determine if periostin promotes myofibroblast persistence in HTS fibroblasts, α SMA levels were assessed in sFPCL cultures immediately prior to release (under mechanical tension for 72 hours) and up to 48 hours after collagen lattice release (in the presence of decreased ECM tension) by western immunoblotting and densitometry. HTS fibroblasts with high levels of

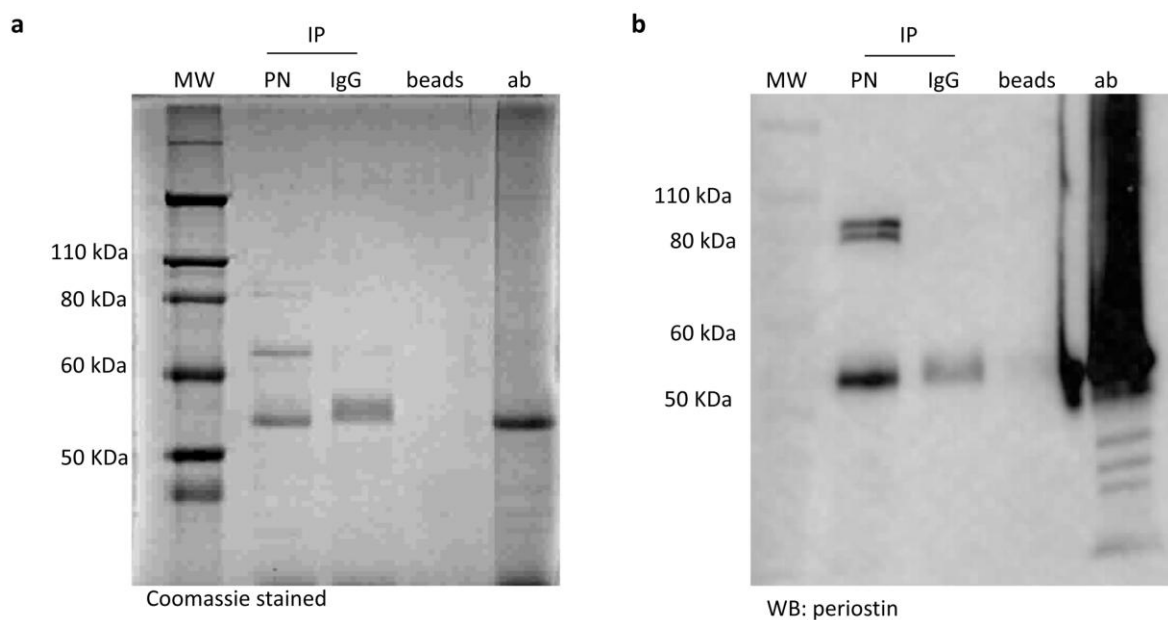


Figure 4.12 Identification of potential periostin interactors in hypertrophic scar-conditioned media. Hypertrophic scar (HTS) conditioned media was generated (2.2.9.2) and concentrated 50 times. 1 mg of total protein was incubated with a periostin (PN)-specific antibody and immunoprecipitated (IP) with protein A/G magnetic beads as described in 2.2.9.3. IP samples were separated using SDS-PAGE and samples were analyzed by (a) coomassie staining (2.2.9.4) and (b) western immunoblotting (2.2.6). (a) Coomassie staining identified 4 bands at molecular weights of 90 kDa, 85 kDa, 65 kDa and 60 kDa that were absent or extremely faint in IgG control samples. The 65 and 60 kDa bands were identified as keratin-14 and fragments of IgG and PN by liquid chromatography tandem mass spectrometry (not shown). (b) The 90 and 85 kDa bands were identified as endogenous PN by western immunoblotting with a PN-specific antibody. Protein A/G magnetic beads (beads) and PN-specific antibody (ab) were used as controls. Bands at 55 kDa in both images correlate to the size of IgG heavy chain. Representative images are shown. MW= molecular weight ladder, WB= western immunoblot.

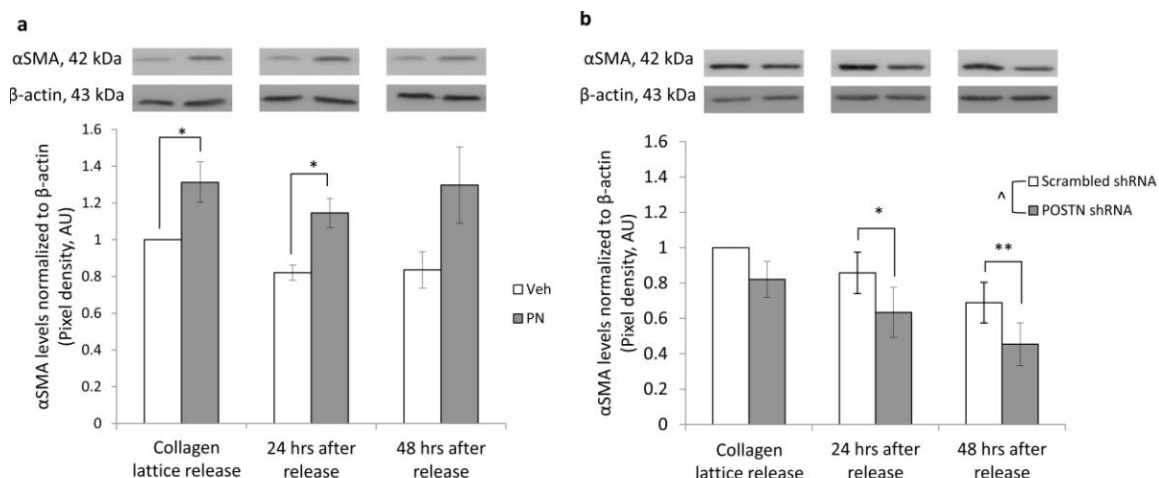


Figure 4.13 Periostin maintains myofibroblasts in a differentiated state under conditions of decreasing ECM tension. Primary hypertrophic scar (HTS) fibroblasts were cultured in stressed fibroblast populated collagen lattices (sFPCLs) and total cell lysates were derived immediately prior to collagen lattice release (after 72 hours of culture), 24 and 48 hours after collagen lattice release. The effects of periostin (PN) addition or depletion on alpha smooth muscle actin (α SMA) levels were assessed by western immunoblotting and densitometry. (a) HTS fibroblasts maintained α SMA levels following collagen lattice release in the presence of endogenous PN. α SMA levels were significantly increased in PN treated HTS fibroblasts relative to vehicle controls and α SMA levels were maintained for at least 48 hours after lattice release. Values were normalized to vehicle controls immediately prior to lattice release (N=5 patients, n=3). (b) Periostin depletion by shRNA treatment resulted in a significant and ongoing decrease in α SMA levels in HTS fibroblasts following collagen lattice release relative to scrambled shRNA controls. Values were normalized to scrambled controls immediately prior to lattice release (N=4 patients, n=3). β -actin immunoreactivity was assessed to ensure equal protein loading. Significant overall treatment effects are denoted by $^{\wedge}p<0.05$ (ANOVA of repeated measures). Significant treatment effects at individual time points are denoted by $*p<0.05$ and $**p<0.01$ (t-tests). Data are presented as mean values and SEM. Representative immunoblots of the mean densitometry data are shown. AU=arbitrary units.

endogenous periostin expression (vehicle treated fibroblasts) maintained α SMA levels following collagen lattice release. HTS fibroblasts treated with exogenous periostin had significantly higher α SMA levels ($p < 0.05$) relative to vehicle treated fibroblasts cultured under mechanical tension and were able to maintain these high levels of α SMA following the release of ECM tension (Figure 4.13a, N=5 patients, n= 3). In contrast, periostin-depleted HTS fibroblasts had significantly decreased α SMA levels ($p < 0.05$) relative to scrambled shRNA controls with significant decreases observed at 24 and 48 hours after collagen lattice release (Figure 4.13b, $p < 0.05$, N=4 patients, n=3).

4.8 Discussion

In order to assess periostin effects on myofibroblast differentiation and persistence, it was necessary to perform studies in a model system that mimicked *in vivo* conditions of 3D stress in a collagen-enriched environment. The stressed fibroblast populated collagen lattice (sFPCL) assay was chosen on this basis. When initially seeded into sFPCL, the fibroblasts experience an ECM environment similar to that of the provisional matrix *in vivo* (31, 173). During ECM remodelling, tractional forces generated by migrating fibroblasts increase the mechanical tension of the ECM thereby inducing proto-myofibroblast and myofibroblast differentiation (30, 156). This mechanical tension is sustained until the collagen lattice is released from its points of attachment (30). Upon release, myofibroblast-mediated contraction rapidly contracts the collagen lattice.

To investigate periostin effects on myofibroblast differentiation in HTS fibroblasts, three markers of myofibroblast differentiation were assessed: contractility, α SMA and OB cadherin levels. The neo-expression of α SMA in their stress fibres is a distinguishing feature of myofibroblasts and facilitates their hyper-contractile phenotype (30).

Incorporation of α SMA into stress fibers is specific to differentiated myofibroblasts, as the stress fibers in proto-myofibroblast are composed solely of β - and γ -actins (38, 39). OB cadherin, a membrane protein involved in adherens junctions (221), also enhances collagen lattice contraction by myofibroblasts (218) and its expression is reported to be upregulated in differentiated myofibroblasts relative to proto-myofibroblasts (218).

The findings reported in this chapter indicate that periostin enhances myofibroblast differentiation in human dermal fibroblasts derived from hypertrophic scar tissue. The evidence supporting this conclusion includes significant increases in HTS fibroblast contractility and α SMA levels in the presence of exogenous periostin. In addition, a non-significant trend towards increased OB cadherin levels in periostin treated HTS fibroblasts was noted. The absence of any discernible effects of periostin treatment on fibroblast proliferation, viability, adhesion or migration in 3D cultures suggests that they are unlikely to explain periostin-induced HTS collagen lattice contraction. Furthermore, periostin significantly enhanced KS fibroblast contractility above highly contractile basal levels. These data suggest that periostin effects on myofibroblast differentiation may not be specific to HTS fibroblasts but may be a common feature of fibrotic conditions of the skin. Periostin also induces myofibroblast differentiation of fibroblasts derived from Dupuytren's disease, a fibrosis of the palmar fascia with similarities to scarring (91), suggesting that these findings may be extendible to other tissues.

Since HTS fibroblasts express increased endogenous levels of periostin relative to NS cells and as exogenous periostin addition promoted increased myofibroblast differentiation in HTS-derived fibroblast, loss of function studies were performed to confirm these findings. Adenoviral transduction was chosen as an optimal method for shRNA delivery for several reasons. Transient transfection efficiency is typically low in primary fibroblasts and selection for stable transfection is impractical in primary fibroblasts that lose their *in vivo* characteristics after a limited number of passages. Previous studies in our laboratory have demonstrated that, unlike transient transfection, viral transduction efficiency approximates 100% in primary fibroblasts under optimal conditions. An adenoviral transduction system was used in preference to a lentiviral system because adenovirus remains episomal and does not integrate into the host genome, thereby limiting the potential for non-specific disruption of gene expression caused by viral DNA integration into the genome.

In contrast to the gain-of-function studies where exogenous periostin significantly enhanced HTS myofibroblast differentiation, no significant effects of periostin depletion on myofibroblast differentiation were evident in the loss-of-function studies. As markers

of myofibroblast differentiation, a significant decrease in collagen lattice contraction, α SMA or OB cadherin levels would have provided independent support for the gain-of-function studies. The lack of significant findings in these loss-of-function studies may be explained in part by inter-patient variability. Factors including age, gender and race may affect the sensitivity of periostin depletion between individual patients and make it difficult to identify consistent effects. Future analyses of additional patients may be required to overcome inter-patient variability and allow us to identify consistent effects in all, or even a majority of, patients assessed. It is also a possibility that a 60% reduction in endogenous periostin levels in HTS fibroblasts following *POSTN* shRNA treatment was insufficient to induce detectable effects on contraction and myofibroblast differentiation. Periostin is proposed to be a very stable protein with a long half-life that is difficult to deplete under conditions of high ECM tension (222). Therefore, depletion of intracellular periostin in HTS fibroblasts may not correlate with depletion of secreted and potentially very stable ECM-associated periostin. Another possibility is that, while periostin can modestly enhance myofibroblast differentiation above basal levels, its primary role is to maintain, rather than induce, myofibroblast differentiation. Therefore, increased matrix tension, such as that experienced by fibroblasts cultured in sFPCLs, may be sufficient to induce HTS myofibroblast differentiation and periostin may play a modestly stimulatory, but dispensable, role in this process.

Interestingly, no evidence of periostin-induced myofibroblast contraction was observed in NS fibroblast cultured in sFPCLs. These findings suggest that periostin induces pathological, rather than normal, collagen lattice contraction, as the effects were specific to fibroblasts derived from abnormal scar tissue. It remains unclear if periostin-induced contraction is a component of normal cutaneous wound healing, as, due to ethical constraints, we were unable to obtain samples of normal human scar tissue from which to derive primary fibroblasts. The mechanisms that explain the differences in sensitivity to periostin between HTS and NS fibroblasts are currently unclear. It is feasible that NS fibroblasts may need to be “activated” in order to respond to periostin. This activation could include induction or activation of a receptor(s) not normally present in unwounded NS fibroblasts or exposure to fibrosis-associated growth factors and cytokines required for periostin signalling.

Preliminary western immunoblotting studies demonstrated that both HTS and NS fibroblasts express integrins α_V , β_3 and β_5 subunits (data not shown) through which periostin has been shown to signal in other systems (127-129, 131-134). Although HTS and NS fibroblasts had similar expression profiles of individual integrin subunits, it is unclear if HTS and NS fibroblasts express different integrin heterodimers and the activation state of these dimers.

The hypothesis that exposure to fibrosis-associated growth factors and cytokines are required to activate and induce periostin sensitivity in NS fibroblasts was also tested. During cutaneous wound healing, TGF β -1 is released following injury to the dermis and plays a critical role in many processes essential to normal wound repair, including myofibroblast differentiation (8, 13, 40, 41, 174-177, 220). Therefore, TGF β -1 signalling may be required to activate NS fibroblasts and induce periostin sensitivity in these cells. These studies indicated that priming NS fibroblasts with recombinant TGF β -1 was only partially effective in inducing NS fibroblast sensitivity to periostin. It is likely that a combination of fibrosis-associated growth factors that are expressed at high levels by HTS fibroblasts (for example, CCN2 (223)), might be required to induce periostin sensitivity in NS fibroblasts.

Since a large number of growth factors are secreted by fibroblasts during cutaneous wound healing (8), it is feasible that HTS fibroblasts might secrete factors that can activate NS fibroblasts. The data presented in this chapter supports this notion as periostin significantly enhanced NS fibroblast contractility when cultured in HTS-conditioned media. As HTS-conditioned media had no discernible effect on NS fibroblast contractility in the absence of exogenous periostin, these data imply that periostin is interacting with a component in the conditioned media to enhance contraction of NS fibroblasts. Despite multiple optimization experiments, no periostin interacting molecules that were specific to HTS-conditioned media were identified by immunoprecipitation analyses. Future studies, beyond the scope of this thesis, will be required to identify the elusive molecular interactions that induce periostin sensitivity in NS fibroblasts.

The second component of this aim was to assess periostin effects on myofibroblast persistence. Normally, as cutaneous wounds heal and ECM stress is relieved, the myofibroblasts that promote wound closure undergo apoptosis (8, 12). However, in abnormal scarring conditions, myofibroblasts fail to undergo apoptosis and persist, and continue to remodel the ECM and increase dermal density to abnormal levels. Many factors, most notably TGF β -1 (41), have been demonstrated to induce myofibroblast differentiation in combination with increased ECM tension (30, 38, 42). However, much less is known about the factors that maintain myofibroblasts in a differentiated state in hypertrophic scars that persist for month or years. Since periostin promotes myofibroblast differentiation in HTS fibroblasts and is abundant and persistent in the dermis of hypertrophic scars, it was hypothesized that periostin promotes myofibroblast persistence in hypertrophic scarring.

To test this hypothesis, α SMA levels in HTS fibroblasts in sFPCLs cultured under mechanical tension (pre-release) and up to 48 hours after collagen lattice release were assessed. This model was designed to mimic the loss of ECM stress that induces apoptosis in normal scar myofibroblasts (8, 12). While the rapid loss of ECM tension induced by collagen lattice release in sFPCLs is much more abrupt than the physiological process it is designed to mimic (183), it does provide a reproducible assay system for myofibroblast persistence under rapidly diminishing ECM tension. These studies demonstrate that HTS fibroblasts are able to maintain α SMA levels at constant levels under conditions of decreasing ECM tension in the presence of endogenous periostin and that these levels are significantly increased and maintained by the addition of exogenous periostin. In contrast, α SMA levels were significantly decreased in periostin-depleted HTS fibroblasts under conditions of decreasing ECM tension relative to scrambled controls. It is unclear if this loss in α SMA levels following collagen lattice release was due to the onset of myofibroblast apoptosis, myofibroblasts dedifferentiation or a combination of both. These findings support the hypothesis that periostin maintains myofibroblast differentiation in HTS fibroblasts under conditions of decreasing ECM tension.

In summary, these studies demonstrated that periostin induces HTS fibroblast contraction and differentiation in 3D collagen lattices, a model that mimics the mechanical tension of granulation tissue during cutaneous wound healing. In addition, periostin maintained α SMA levels, a marker of myofibroblast differentiation, in sFPCL cultures exposed to reduced ECM tension, mimicking wound remodelling after closure. Together these data demonstrate novel roles for periostin in inducing and maintaining myofibroblast differentiation and persistence in HTS fibroblasts.

Chapter 5

5 *In vitro* analysis of the mechanisms utilized by periostin to induce myofibroblast differentiation and persistence in hypertrophic scarring

5.1 Rationale

Periostin was shown to induce dermal fibroblasts derived from hypertrophic scar tissue to express α smooth muscle actin (α SMA) and differentiate into myofibroblasts in Chapter 4. However, the signalling pathway(s) and mechanisms activated by periostin to induce and/or maintain myofibroblast differentiation had not been elucidated. Therefore, the focus of Chapter 5 is to identify these pathway(s). Periostin has been previously reported to signal through integrins in other cell types (127-134), and integrins have well-established roles in mediating signalling events that increase cellular attachment and contraction of the ECM (46). The integrin-associated complexes that form between cells and the matrix are known as focal adhesions (30, 46, 156). Previous studies have shown that α SMA is only incorporated into the stress fibers of these cells when the mechanical tension in the surrounding ECM is sufficient to induce the “maturation” of focal adhesions (FAs) into “supermature” focal adhesions (suFAs, (30, 43)). As periostin induces α SMA production and HTS myofibroblast contractility, the hypothesis for this chapter was that periostin signals through integrins in HTS fibroblasts, activates integrin-associated signalling pathways, enhances the formation of suFAs between HTS fibroblasts and the surrounding collagen matrix and promotes the incorporation of α SMA into stress fibres. This hypothesis is illustrated in Figure 5.1.

5.2 Immunoprecipitation analyses of receptor interactions with periostin in HTS fibroblasts.

To determine if periostin interacts with integrins in HTS fibroblasts, immunoprecipitation analyses with a periostin-specific antibody were performed on total cell lysates derived from HTS fibroblasts cultured on plastic as described in 2.2.9. Using this approach, periostin immunoreactivity was evident in samples immunoprecipitated with a periostin-

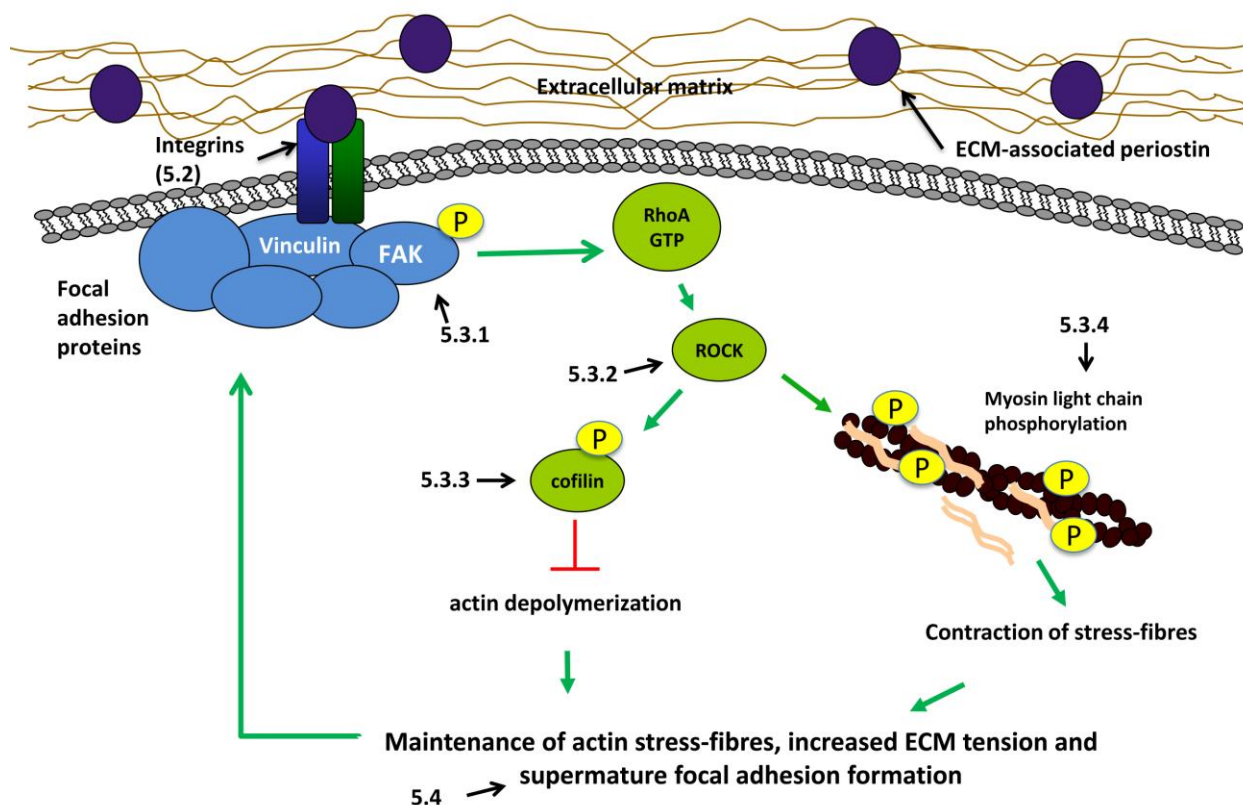


Figure 5.1 Schematic representation of the proposed signalling pathway utilized by periostin to induce myofibroblast differentiation and persistence. The central hypothesis of Chapter 5 is that ECM-associated periostin signals through integrins (Chapter 5.2) in HTS fibroblasts to activate focal adhesion kinase (FAK, Chapter 5.3.1), a tyrosine kinase that localizes to focal adhesion complexes. FAK activation promotes myofibroblast differentiation and focal adhesion formation through RhoA-GTP and ROCK (Chapter 5.3.2) and its downstream effectors cofilin (Chapter 5.3.3) and myosin light chain (MLC, Chapter 5.3.4). Cofilin inhibition and MLC-mediated stress fiber contraction promotes stress fiber maintenance, increased ECM tension and integrin clustering resulting in the formation of supermature focal adhesions (suFA, Chapter 5.4), a prerequisite for α SMA incorporation into stress fibers of differentiated myofibroblasts.

specific antibody and absent in samples immunoprecipitated with a non-specific IgG control, demonstrating the specificity of the antibodies for periostin. Western immunoblotting analyses revealed interactions between periostin and integrins α_v and α_5 however, these interactions were also consistently evident in samples immunoprecipitated with a non-specific IgG control. These data indicated that these interactions were not specific to periostin. Several modifications of standard immunoprecipitation protocols were trialed including the use of nickel (Ni) coated magnetic beads that bind specifically to histidine-tagged human recombinant periostin, shorter incubation times and more stringent washing conditions (described in detail in 2.2.10) to enhance the specificity of interactions between periostin and integrin subunits. The approach of using Ni coated magnetic bead to specifically isolate recombinant periostin from total cell lysates of HTS fibroblasts exposed to treatment was successful (Figure 5.2a). However, interactions between periostin and integrins α_v and α_5 were evident in HTS cell lysates in both the presence and absence of recombinant periostin treatment, indicating a high background level of non-specific interactions (Figures 5.2b and c). In addition to western immunoblotting analyses, immunoprecipitated samples were stained with coomassie to identify bands of unique molecular weight in comparisons between treated and untreated samples, potentially indicating novel periostin interactors. Despite substantial method optimization and multiple mass spectrometry analyses, no novel periostin interactors were identified using this approach (data not shown). Therefore, this research effort was refocused onto the identification of integrin-associated signalling intermediates that were modified by periostin during myofibroblast differentiation.

5.3 Assessment of the effects of periostin on integrin-associated signalling molecules in HTS-derived fibroblasts

The integrin-associated complexes that form between cells and the ECM are known as focal adhesions (30, 46, 156). Focal adhesion kinase (FAK) is a tyrosine phosphorylated protein that localizes to focal adhesions (224, 225) and its activation is required for adhesion-mediated myofibroblast differentiation (226) and suFA formation (43). FAK

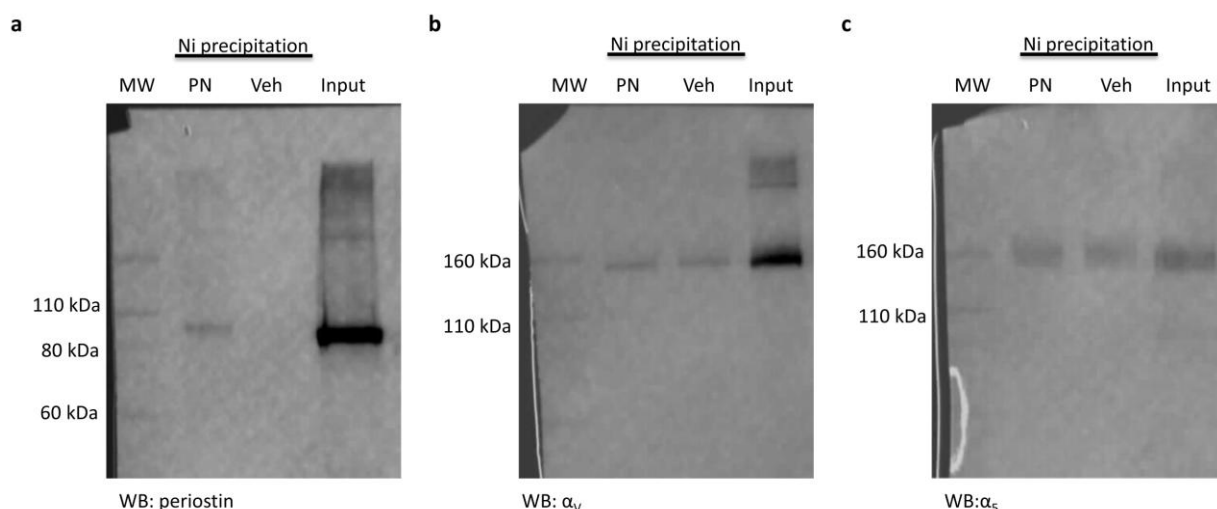


Figure 5.2 Immunoprecipitation analyses of receptor interactions with periostin in HTS fibroblasts. Primary hypertrophic scar (HTS) fibroblasts were cultured to 85% confluency on tissue culture plastic trays and treated with 2 $\mu\text{g/ml}$ periostin (PN) or vehicle (veh) in 2% FBS- αMEM overnight prior to formaldehyde fixation. 1 mg of total cell lysate was precipitated using nickel (Ni) coated magnetic beads to bind histidine-tagged human recombinant periostin as described in 2.2.10. Eluted precipitation complexes were subjected to SDS-PAGE and assessed for periostin, α_v and α_5 integrin immunoreactivity by western immunoblotting as described in 2.2.6. (a) Ni coated magnetic beads specifically precipitated recombinant periostin as demonstrated by the presence of a band at 90 kDa that is absent in the vehicle control lane. (b and c) Ni coated magnetic beads non-specifically precipitated integrins α_v and α_5 as demonstrated by the presence of bands at (b) 140 kDa and (c) 150 kDa in both the periostin and vehicle treated samples. Representative immunoblots are shown. MW= molecular weight, WB=western immunoblot.

can promote myofibroblast differentiation and focal adhesion formation by modifying Rho Kinase (ROCK) activity and the activities of its downstream targets. These targets include cofilin and myosin light chain (MLC), which regulate stress fiber stabilization and stress fiber-mediated contraction, respectively. Therefore, it was hypothesized that periostin promotes myofibroblast differentiation and persistence through a FAK-ROCK dependent signalling pathway.

5.3.1 Assessment of the effects of periostin on FAK activation in HTS fibroblasts cultured in sFPCLs

To assess the contribution of FAK activation in periostin-induced HTS myofibroblast differentiation and persistence, phosphorylated FAK levels were assessed in sFPCL lysates immediately prior to release and up to 48 hours after release by western immunoblotting and densitometry. A significant interaction between periostin treatment and time was observed ($p < 0.01$) and exogenous periostin treatment enhanced FAK phosphorylation following collagen lattice release relative to vehicle controls with a significant increase in FAK phosphorylation evident at 48 hours after lattice release (Figure 5.3a, $p < 0.05$, $N=3$ patients, $n=3$). A significant overall treatment effect was also evident in periostin-depleted HTS fibroblasts ($p < 0.05$) with periostin-depleted HTS fibroblasts displaying increased levels of phosphorylated FAK relative to scrambled shRNA controls. Significant increases in FAK phosphorylation were evident in periostin-depleted HTS fibroblasts immediately prior to collagen lattice release and at 48 hours after release (Figure 5.3b, $p < 0.05$, $N=3$ patients, $n=3$). Periostin addition or depletion had no discernible effects on total FAK levels (data not shown, $N=3$ patients, $n=3$).

5.3.2 Assessment of the effects of ROCK inhibition on periostin-induced HTS myofibroblast differentiation

ROCK plays a central and essential role in activating and maintaining myofibroblast differentiation and contractility (30, 43, 51-53). To confirm that periostin signalling required ROCK activity to induce HTS myofibroblast-mediated collagen lattice contraction, a ROCK specific inhibitor, Y27632, was included in a subset of sFPCL cultures of HTS fibroblasts, with or without exogenous periostin treatment, and collagen

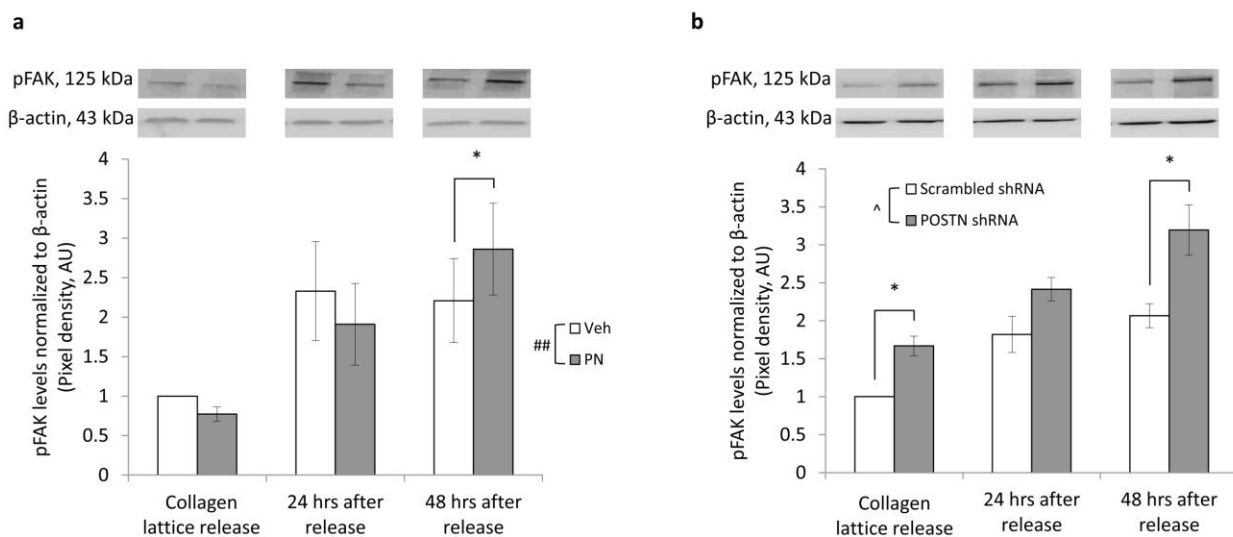


Figure 5.3 Periostin enhances focal adhesion kinase phosphorylation. Primary hypertrophic scar (HTS) fibroblasts were cultured in stressed fibroblast populated collagen lattices (sFPCLs) as described in 2.2.5 and total cell lysates were derived immediately prior to sFPCL release (72 hours after polymerization), 24 and 48 hours after release. Levels of phosphorylated focal adhesion kinase (pFAK, tyr397) were assessed in HTS lysates by western immunoblotting and densitometry as described in 2.2.6. (a) Periostin significantly enhanced FAK phosphorylation in HTS fibroblasts cultured in conditions of decreasing ECM tension relative to vehicle controls. Values were normalized to vehicle controls immediately prior to lattice release (N=3 patients, n=3). (b) Periostin depletion by shRNA treatment significantly increased FAK phosphorylation in HTS fibroblasts in a model of decreasing ECM tension relative to scrambled shRNA controls. Values were normalized to scrambled shRNA controls immediately prior to lattice release (N=3 patients, n=3). β -actin immunoreactivity was assessed to ensure equal protein loading. Significant overall treatment effects are denoted by $^{\wedge}p < 0.05$ and significant treatment/time interactions are denoted by $##p < 0.01$ (ANOVA of repeated measures). Significant treatment effects at individual time points are denoted as $*p < 0.05$ (t-tests and simple main effect analyses). Data are presented by mean values and SEM. Representative immunoblots of the mean densitometry data are shown. AU=arbitrary units.

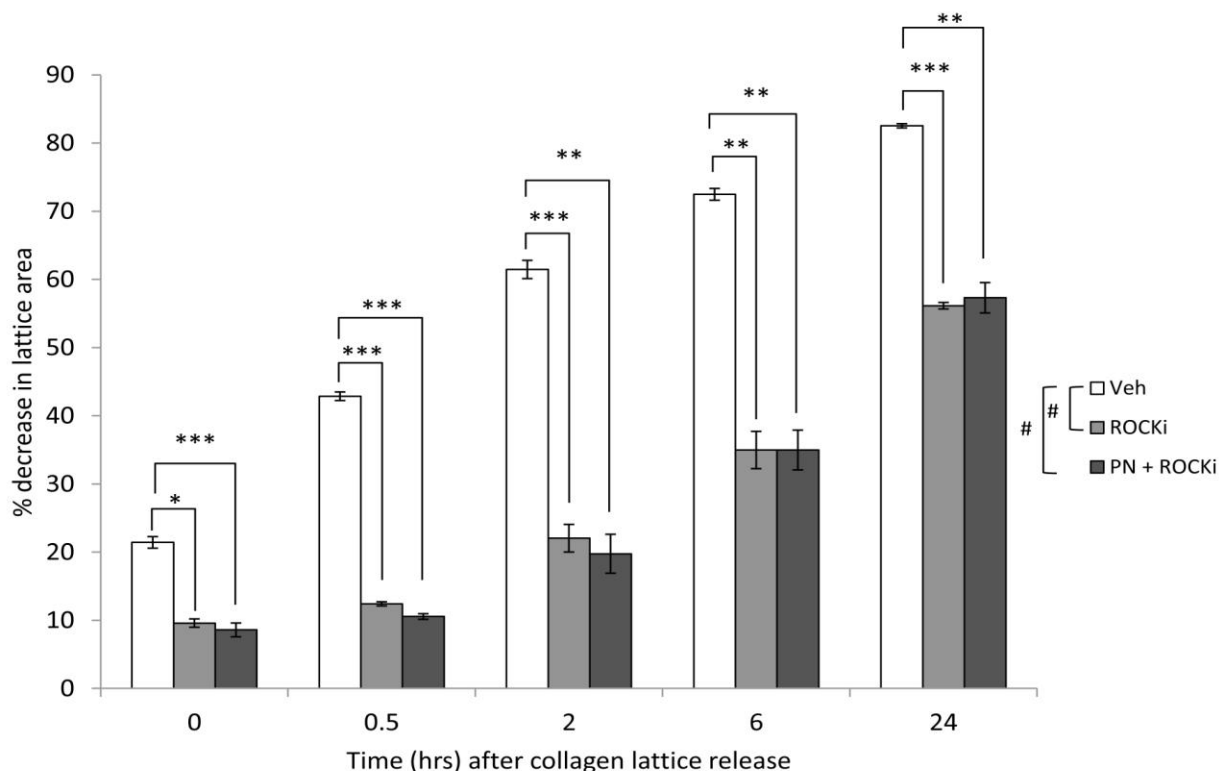


Figure 5.4 Rho kinase inhibition significantly attenuates hypertrophic scar fibroblast contraction of stressed fibroblast populated collagen lattices. To assess the effects of Rho kinase (ROCK) inhibition of hypertrophic scar (HTS) fibroblast contractility, primary HTS fibroblasts were seeded in stressed fibroblast populated collagen lattices containing periostin (PN) or vehicle (veh) as described in 2.2.5 and cultured in 2% FBS- α MEM supplemented with 10 μ M ROCK inhibitor, Y27632 (ROCKi), or vehicle control (water) for 72 hours. Collagen lattice contraction was assessed over 24 hours. ROCK inhibition significantly attenuated basal HTS fibroblast collagen lattice contraction at all time points assessed. The addition of exogenous PN was unable to rescue HTS fibroblast contraction in the presence of Y27632 (N=1 patient, n=3). Significant treatment/time interactions are denoted by # p <0.05 (ANOVA of repeated measures). Significant treatment effects at individual time points are denoted by * p <0.05, ** p <0.01, *** p <0.001 (simple main effect analyses). Data are presented by mean values and SEM.

lattice contraction was assessed over 24 hours. A significant interaction between Y27632 treatment and time was observed ($p < 0.01$) and ROCK inhibition strongly attenuated HTS fibroblast contractility relative to vehicle controls with significant differences observed at all time points assessed ($p < 0.05$). The addition of exogenous periostin did not rescue HTS fibroblast contraction in the presence of Y27632 (Figure 5.4, N=1 patient, n=3).

5.3.3 Assessment of the effects of periostin on cofilin activation in HTS fibroblasts cultured in sFPCLs

Cofilin is an actin-binding protein that is a downstream target of ROCK and promotes actin stress fiber depolymerization (227). ROCK activation leads to the phosphorylation and inhibition of cofilin activity, thereby preventing actin depolymerization (228). To assess the contribution of cofilin in periostin-induced HTS myofibroblast differentiation, phosphorylated cofilin levels were assessed in sFPCL lysates immediately prior to release and up to 48 hours after release by western immunoblotting and densitometry.

Exogenous periostin treatment had no significant effect on cofilin phosphorylation relative to vehicle controls when HTS fibroblasts were assessed as a group (Figure 5.5a, N=3 patients, n=3). However, it was noted that periostin significantly increased cofilin phosphorylation at individual time points in two of the three individual patients assessed (Figure 5.5b, $p < 0.05$).

Periostin depletion by shRNA treatment had no significant effects on cofilin phosphorylation in HTS fibroblasts when assessed as a group (Figure 5.5c, N=3 patients, n=3). However, a significant treatment effect was observed ($p < 0.05$) in one of the three patient-derived fibroblast lines assessed and phosphorylated cofilin levels were found to be significantly decreased in periostin-depleted HTS myofibroblasts relative to scrambled shRNA controls. In addition, phosphorylated cofilin levels were found to be significantly decreased at individual time points in the other two patient-derived fibroblast lines assessed (Figure 5d, $p < 0.05$). Periostin addition or depletion had no discernible effects on total cofilin levels (data not shown, N=3 patients, n=3).

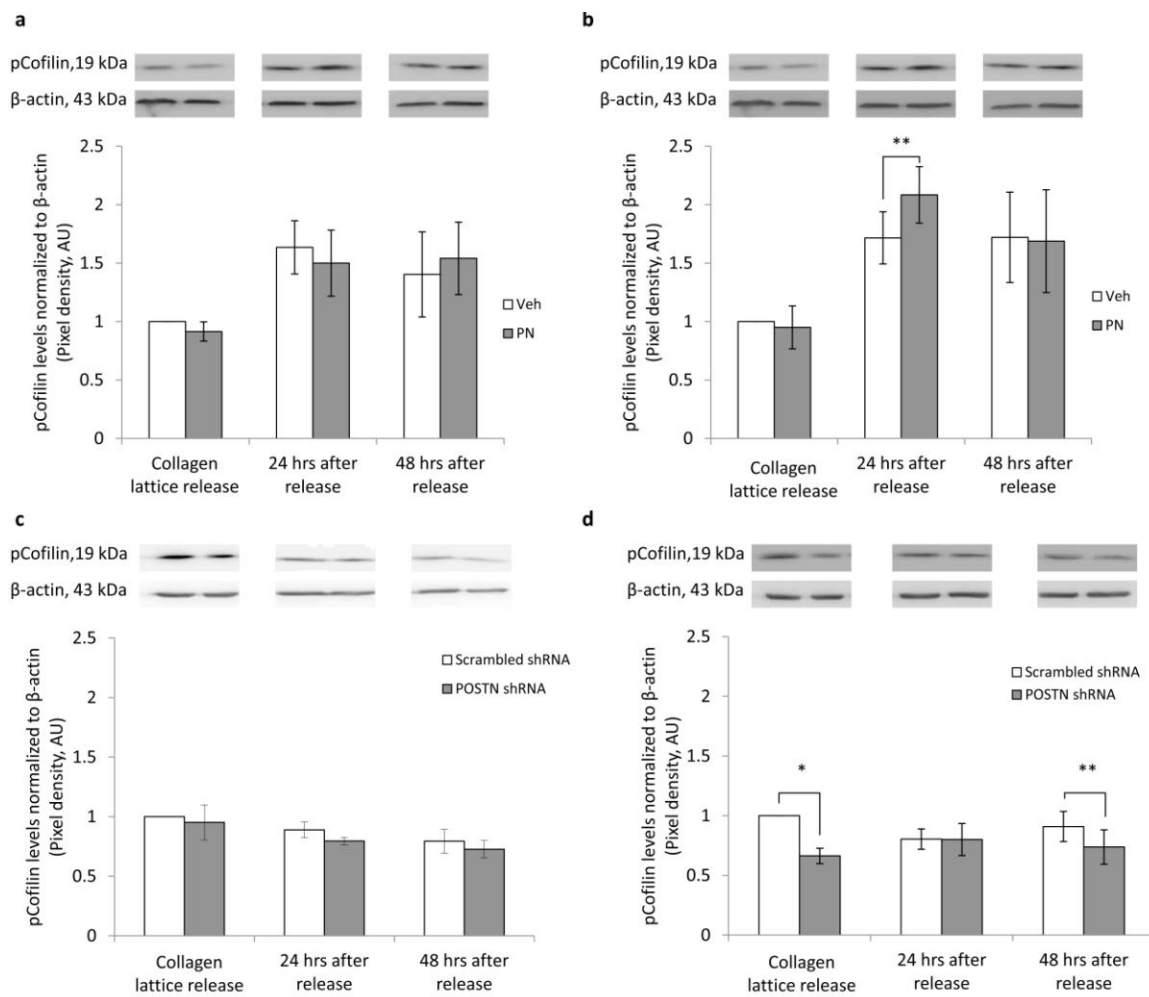


Figure 5.5 Periostin enhances cofilin phosphorylation in conditions of decreasing ECM tension in a subset of patients. Primary hypertrophic scar (HTS) fibroblasts were cultured in stressed fibroblast populated collagen lattices (sFPCLs) and total cell lysates were derived immediately prior to sFPCL release (72 hours after polymerization), 24 and 48 hrs after release. Levels of phosphorylated cofilin (pCofilin, ser3) were assessed in HTS lysates by western immunoblotting and densitometry. (a) Periostin had no discernible effect on cofilin phosphorylation relative to vehicle controls when assessed as a group (N=3 patients, n=3 patient). (b) However, periostin significantly enhanced cofilin phosphorylation relative to vehicle controls in a subset of individual patients. Shown is a representative immunoblot and densitometry data for HTS patient #5. Values were normalized to vehicle controls immediately prior to lattice release. (c) Periostin depletion by shRNA treatment had no significant effects on cofilin phosphorylation relative to scrambled shRNA controls when assessed as a group (N=3 patients, n=3). (d) In contrast, periostin depletion by shRNA treatment significantly decreased cofilin phosphorylation relative to scrambled shRNA controls in a subset of individual patients. Shown is a representative immunoblot and densitometry data for HTS patient #5. Values were normalized to scrambled shRNA controls immediately prior to lattice release. β -actin immunoreactivity was assessed to ensure equal protein loading. Significant treatment effects at individual time points are denoted by * $p < 0.05$ (t-tests). Data are presented by mean values and SEM. Representative immunoblots of the mean densitometry data are shown. AU=arbitrary units.

5.3.4 Assessment of the effects of periostin on MLC activation in HTS fibroblasts cultured in sFPCLs

The contractile forces induced by myofibroblasts on their ECM are generated by contractile stress fibres composed of actin bundles, non-muscle myosin, and actin-binding proteins and is regulated by the activity (phosphorylation) of MLC (30, 45-47). To assess the contribution of MLC in periostin-induced HTS myofibroblast differentiation, phosphorylated MLC levels were assessed in sFPCL lysates immediately prior to release and up to 48 hours after release by western immunoblotting and densitometry. Exogenous periostin addition to sFPCL cultures had no significant effect on MLC phosphorylation in HTS fibroblasts cultured under mechanical tension or following the release of tension relative to vehicle controls (Figure 5.6a, N=3 patients, n=3). No significant changes in MLC phosphorylation were observed in periostin-depleted HTS fibroblasts relative to scrambled shRNA controls cultured under mechanical tension and following the release of tension (Figure 5.6b, N=3 patients, n=3). However, a significant treatment effect was observed ($p < 0.05$) in one of three patient-derived fibroblast lines assessed with phosphorylated MLC levels being significantly lower in periostin-depleted HTS fibroblasts relative to vehicle controls (Figure 5.6c). Periostin addition or depletion had no discernible effects on total MLC levels (data not shown, N=3 patients, n=3).

As described earlier in this chapter, FAK activity enhances suFA formation and myofibroblast differentiation through the activation of ROCK and its downstream targets cofilin and MLC. ROCK-mediated cofilin inhibition prevents stress fiber depolymerization, whereas MLC activation leads to myofibroblast contraction that increases the mechanical tension in the ECM and induces integrin clustering resulting in the formation of larger focal adhesion complexes. Although no consistent effects of periostin on cofilin inhibition and MLC activation could be discerned in HTS fibroblasts when assessed as a group, the significant effects noted in individual fibroblast lines were invariably consistent with periostin promoting suFA formation during myofibroblast differentiation. Therefore, the potential for periostin to enhance suFA formation was assessed in HTS fibroblasts as a group.

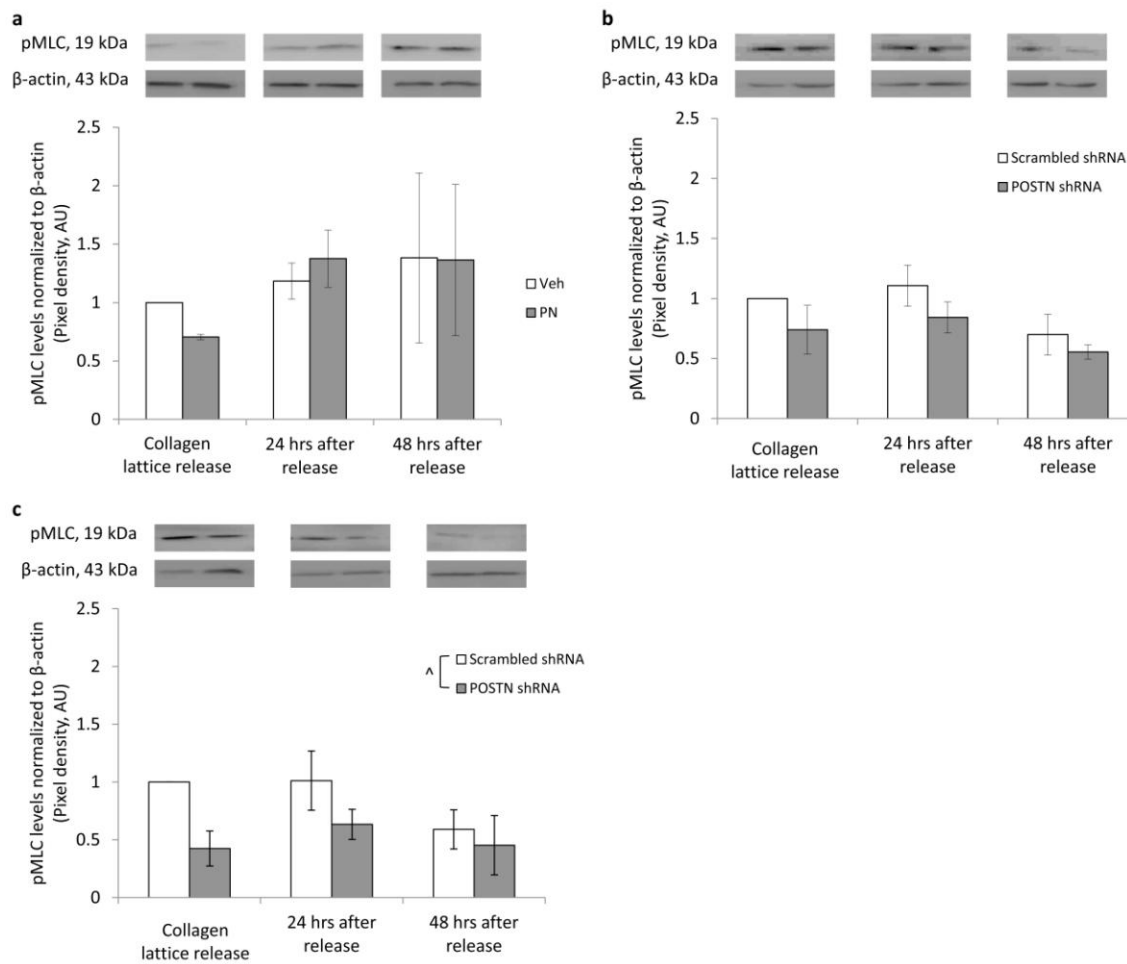


Figure 5.6 Periostin depletion reduces myosin light chain phosphorylation in HTS myofibroblasts cultured in sFPCLs in a subset of individuals. Primary hypertrophic scar (HTS) fibroblasts were cultured in stressed fibroblast populated collagen lattices (sFPCLs) and total cell lysates were derived immediately prior to sFPCL release (72 hours after polymerization), 24 and 48 hours after release. Levels of phosphorylated myosin light chain (pMLC, ser19) were assessed in HTS lysates by western immunoblotting and densitometry. (a) Periostin had no significant effect on MLC phosphorylation in HTS fibroblasts cultured in sFPCLs relative to vehicle controls. Values were normalized to vehicle controls immediately prior to collagen lattice release (N=3 patients, n=3). (b) Periostin depletion by shRNA treatment had no significant effects on MLC phosphorylation in HTS fibroblasts relative to scrambled shRNA controls when assessed as a group (N=3 patients, n=3). (c) While periostin treatment did not significantly affect MLC phosphorylation at any specific time point, an overall treatment effect indicating a significant decrease in MLC phosphorylation in periostin-depleted HTS fibroblasts relative to scrambled shRNA controls was detected in a subset of individual patients. Shown is a representative immunoblot and densitometry data for HTS patient #9. Values were normalized to scrambled shRNA controls immediately prior to collagen lattice release. β -actin immunoreactivity was assessed to ensure equal protein loading. Significant overall treatment effects are denoted by $^*p < 0.05$ (ANOVA of repeated measures). Data are presented by mean values and SEM. Representative immunoblots of the mean densitometry data are shown. AU=arbitrary units.

5.4 Supermature focal adhesions

Focal adhesions are integrin-associated complexes that facilitate communication between cells and their surrounding ECM (30, 46, 156). Fibroblasts typically exhibit a mixture of immature and mature focal adhesions (FAs, (229)) and, when they differentiate into myofibroblasts, the formation of suFAs corresponds with the incorporation of α SMA into stress fibres (43, 184, 230). suFAs can be identified by the coexpression of α SMA with other proteins normally found in FAs including ED-A fibronectin, vinculin, paxillin and tensin (230). suFAs can also be distinguished by size, where suFAs are defined as FAs that are greater than 6 μ m in length, mature focal adhesions are typically between 2 and 6 μ m in length, and immature FAs are typically less than 2 μ m in length (43, 184, 230, 231). The incorporation of α SMA in suFAs is essential to allow myofibroblasts to exert a greater (typically 2 to 4-fold) higher contractile force on the surrounding ECM thereby enhancing ECM tension and maintaining the myofibroblast phenotype (30, 43).

5.4.1 Assessment of the effects of periostin on the formation of supermature focal adhesions

To determine if periostin enhances suFA formation, a novel approach was developed to measure focal adhesion length in sFPCLs by immunofluorescence confocal microscopy based on modifications of protocols described in previous studies (184, 232). In brief, “mini” sFPCL cultures were designed to be thin enough to allow confocal microscopy of the cells within a three-dimensional matrix and while under mechanical tension. These cultures of HTS fibroblasts were prepared in the presence or absence of matrix-associated periostin and, after a 72 hour incubation to induce myofibroblast differentiation, the mini sFPCLs were co-stained with α SMA to confirm myofibroblast differentiation, and vinculin, a focal adhesion protein found in all three focal adhesion classes (Figure 5.7, (184)). Focal adhesion length was measured in serial optical sections of individual cells cultured under 3D matrix tension in collagen using Image-Pro Plus 7.0 and the straight-line tool in Image J as described in 2.2.12.3. The total number of focal adhesions, their average length and their classification as immature ($\leq 2 \mu$ m), mature (2-6 μ m) and supermature ($\geq 6 \mu$ m) FAs were determined in 30 cells per treatment in HTS fibroblasts derived from three patients.

As shown in Figure 5.8a, periostin treatment had no significant effects on the total number of focal adhesions present in HTS fibroblasts cultured in sFPCLs relative to vehicle controls (53.5 FAs \pm 10.8 vs 47 FAs \pm 9.9, N=3 patients, n=30 cells per treatment). However, the average length of FAs were significantly increased in periostin treated HTS fibroblasts (4.55 μ m \pm 0.26 in length) compared to vehicle treated controls (4.02 μ m \pm 0.24 in length, Figure 5.8b, N=3 patients, n=30 cells per treatment). Vehicle treated HTS fibroblasts contained significantly more immature FAs (10.00 % \pm 1.63 vs 7.04 % \pm 1.61) and mature FAs (76.95 % \pm 1.32 vs 72.91% \pm 1.28) than periostin treated fibroblasts. Conversely, periostin treated HTS fibroblasts contained a significantly higher percentage of suFAs than vehicle treated cells (20.04 % \pm 2.53 vs 13.12 % \pm 2.58) cultured under identical conditions (Figure 5.8c, N=3 patients, n=30 cells per treatment).

5.5 Discussion

The objectives of this chapter were to identify the signalling pathways utilized by periostin to induce myofibroblast differentiation in hypertrophic scarring and to identify the structural consequences of activating this pathway. The *in vitro* studies presented here demonstrate that periostin promotes/maintains myofibroblast differentiation through the formation of supermature focal adhesions by activating FAK-ROCK mediated pathway(s).

The first objective of this chapter was to identify the receptor(s) utilized by periostin to induce myofibroblast differentiation. Changes in mechanical tension within the ECM are transmitted between the ECM and cells through integrin-adhesion complexes (46). Since periostin has been reported to signal through integrins in other systems (127-134), it was hypothesized that periostin promotes myofibroblast differentiation and persistence through an integrin-mediated pathway. Immunoprecipitation experiments were performed to address this question. When performing immunoprecipitation experiments for receptors, disruption of the cell membrane with harsh detergents, denaturing buffers or mechanical lysing can lead to receptor deactivation and loss of receptor-ligand interaction, especially if the interaction is weak. To account for this, immunoprecipitation experiments were performed in non-denaturing lysis buffers with gentle detergents and a

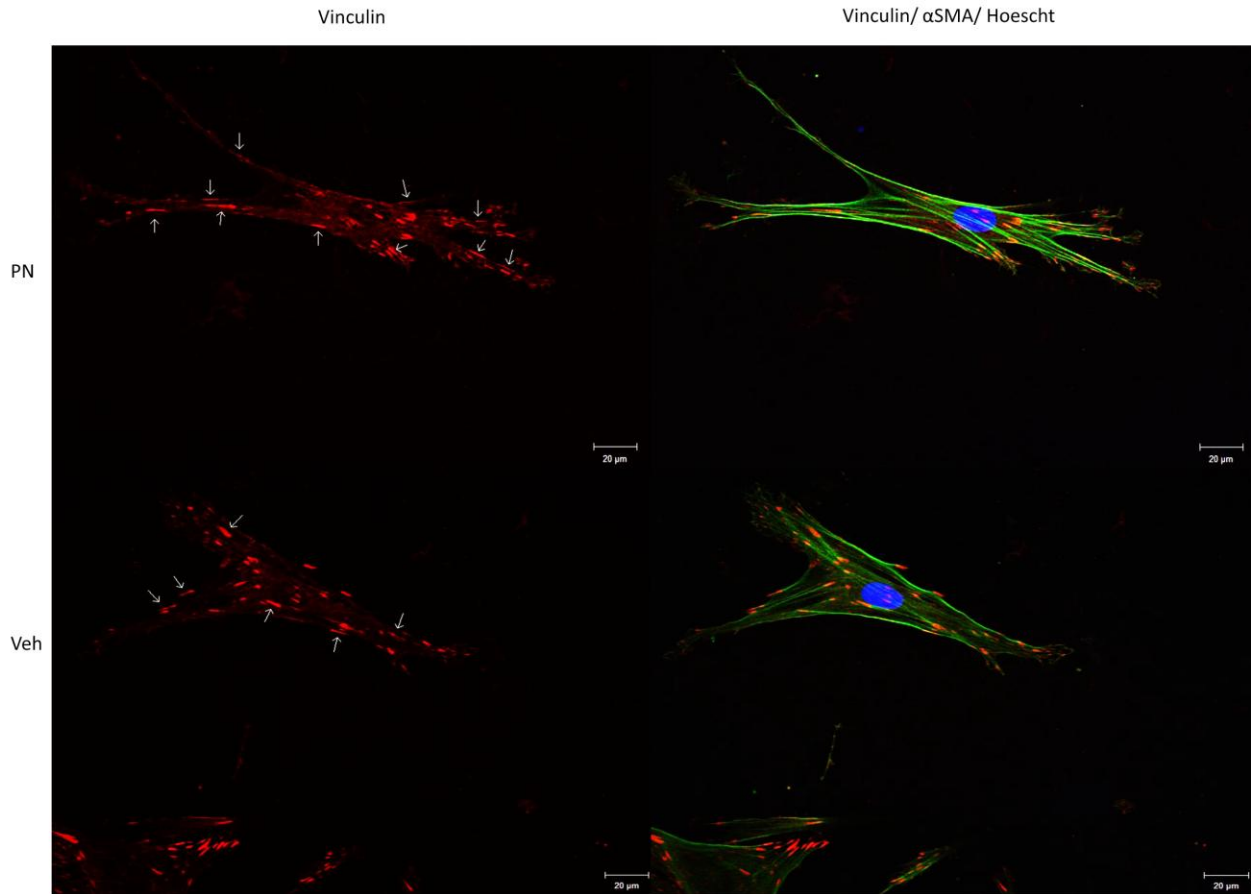


Figure 5.7 Periostin enhances supermature focal adhesion formation in hypertrophic scar-derived fibroblasts. (a) Primary hypertrophic scar (HTS) fibroblasts were cultured in “mini” stressed fibroblast populated collagen lattices (sFPCLs) for 72 hours in the presence or absence of periostin (PN, 2 $\mu\text{g}/\text{ml}$) as described in 2.2.12.1. Lattices were fixed and assessed for vinculin immunoreactivity (red), alpha smooth muscle actin (αSMA) immunoreactivity (green), co-stained with Hoescht (blue) to identify nuclei and imaged using immunofluorescence confocal microscopy as described in 2.2.12.2. Focal adhesion length was measured as described in 2.2.12.3 and supermature focal adhesions ($<6 \mu\text{m}$ in length) are indicated by arrows. Representative photographs are shown. Scale bar = 20 μm .

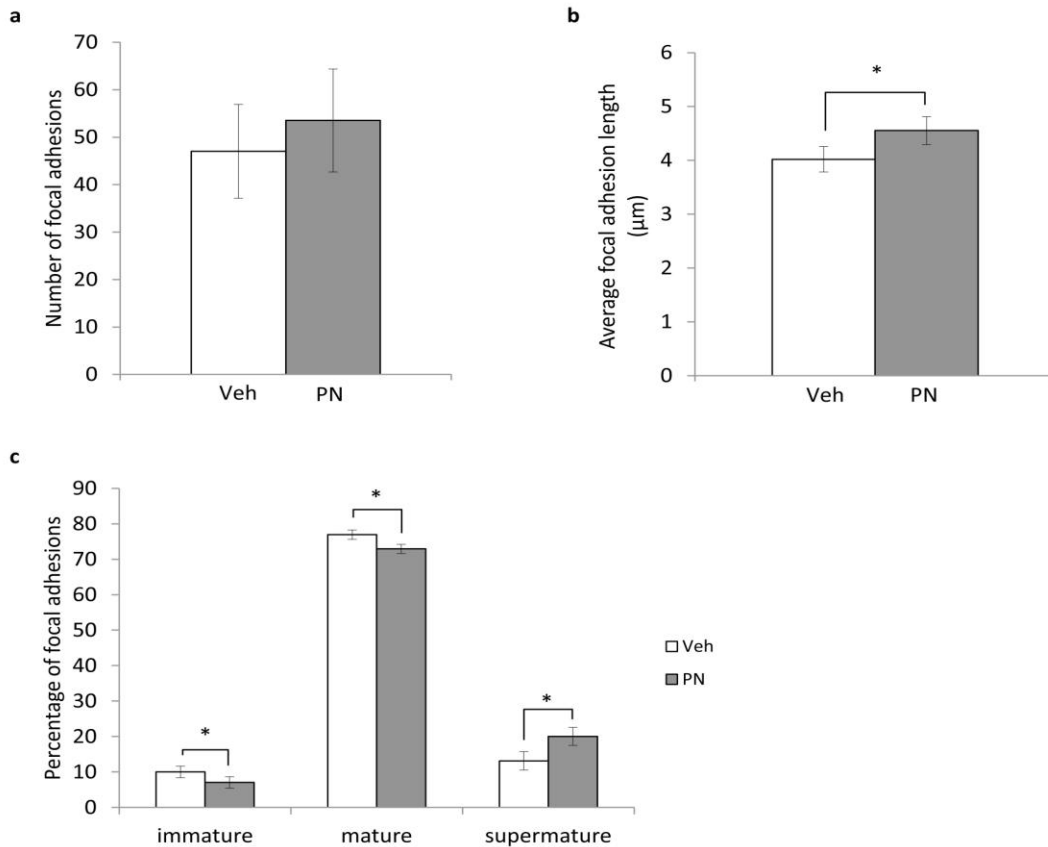


Figure 5.8 Periostin enhances focal adhesion length and supermature focal adhesion formation in hypertrophic scar-derived fibroblasts. Primary hypertrophic scar (HTS)-derived fibroblasts were cultured in mini stressed fibroblast populated collagen lattices for 72 hours and focal adhesion numbers and length were assessed by immunofluorescence confocal microscopy as described in 2.2.12. (a) Exogenous PN treatment had no discernible effects on the total number of focal adhesions present in HTS fibroblasts cultured under mechanical tension (N=3 patients, n=30 cells per treatment). (b) The average focal adhesion length was significantly greater in PN treated HTS fibroblasts relative to vehicle (veh) controls (N=3 patients, n=30 cells per treatment). (c) Vehicle treated HTS fibroblasts had significantly more immature and mature focal adhesions relative to PN treated fibroblasts. However, PN treated HTS fibroblasts had significantly more supermature focal adhesions relative to vehicle treated cells under these culture conditions (N=3 patients, n=30 cells per treatment). Significant treatment effects are denoted by * $p < 0.05$ (t-tests). Data are presented by mean values and SEM.

subset of samples were formaldehyde fixed prior to lysis to stabilize potential interactions (233, 234). Optimization studies demonstrated that formaldehyde fixation prior to cell lysis had no discernible negative effects on the ability of the periostin antibody or nickel coated magnetic beads to bind periostin in the samples (data not shown).

Multiple assay conditions were tested to optimize the detection of direct interactions between periostin and integrins. Initial immunoprecipitation studies were performed in sFPCLs to model 3D interactions *in vivo*, however neither endogenous nor recombinant periostin could be detected in the subsequent immunoprecipitation analyses. While the technical roadblocks that prevented periostin detection in these assays remains unclear, one possibility was that the abundance of collagen caused non-specific antibody binding and/or interfered with antibody-epitope binding. Therefore, despite being potentially less physiologically relevant, subsequent immunoprecipitation experiments were performed on HTS fibroblasts cultured on plastic dishes in the absence of a collagen substrate. While periostin and integrin subunits were consistently co-immunoprecipitated in these analyses, apparently non-specific, yet consistent, integrin binding was also observed in samples immunoprecipitated with non-antigen specific IgG controls, making it impossible to demonstrate that these interactions were specific to periostin. Optimization studies were undertaken with the aim of reducing non-specific integrin binding in the IgG immunoprecipitated samples. These included 1) the use of different IgG controls from different suppliers, 2) the use of Ni coated magnetic beads to bind histidine tags at the amino terminus of the recombinant periostin, 3) various combinations of incubation times and 4) more stringent binding and washing conditions. None of these modifications proved to be effective for reducing non-specific binding between these integrin subunits and IgG controls.

To our knowledge, there are currently no examples of immunoprecipitation experiments demonstrating interactions between periostin and integrins in the literature. Previous studies investigating periostin interactions with integrins have utilized blocking antibodies that are targeted against specific integrins in functional assays (128, 131, 134). Experiments designed to assess these interactions with HTS fibroblasts in sFPCLs using blocking antibodies against integrin $\alpha_v\beta_3$ and β_1 induced very modest decreases in lattice

contractility that were indistinguishable to the effects induced by non-specific IgG controls (data not shown). Co-localization experiments for periostin and integrins were also performed using immunofluorescence confocal microscopy. However, HTS fibroblasts that were fixed and probed with a fluorescently labeled periostin antibody exhibited abundant and saturated staining throughout the collagen matrix, making it impractical to use this approach to identify specific areas of co-localization with integrins in these cultures (data not shown).

In the event that periostin might interact with and signal through molecules other than integrins, multiple immunoprecipitation experiments were performed using a periostin-specific antibody and coomassie staining to detect differential banding patterns between periostin and IgG immunoprecipitated samples. No differential banding patterns were observed in these assays. Coomassie staining is insensitive relative to some other protein stains, such as silver nitrate, however these stains were incompatible with subsequent mass spectrometry analyses. In summary, no specific interactions between periostin and integrins or other molecules could be demonstrated. The development of substantially more sensitive and specific methodologies will be required for future studies assessing protein interactions with periostin in more physiologically relevant, 3D collagen matrices.

The second objective of this chapter was to identify the signalling pathway(s) utilized by periostin to induce myofibroblast differentiation and persistence. The ROCK signalling pathway was an obvious focus for these studies, as ROCK activation plays a central and essential role in activating and maintaining myofibroblast differentiation and contractility (30, 51-53). ROCK inhibition was shown to significantly attenuate basal HTS fibroblast contractility, and this effect could not be rescued by exogenous periostin treatment. Inhibiting such a central and essential regulator of myofibroblast differentiation and contraction is unlikely to be helpful for distinguishing the specific effects of periostin from multiple signalling pathways that also induce differentiation and contraction in a ROCK dependent manner. Therefore, gain- and loss-of-function studies were performed to assess the effects of periostin addition or depletion on upstream and downstream effectors of ROCK-mediated myofibroblast differentiation and contraction.

Integrin-associated complexes known as focal adhesions (30, 46, 156) mediate communication between cells and the ECM. These complexes transmit external signals from the microenvironment to modulate cellular phenotypes (235). Focal adhesion kinase (FAK) has been shown to localize to focal adhesions (224, 225), regulate ROCK-dependent stress fiber formation and maintenance (236), promote suFAs formation (43) and to be involved in adhesion-mediated myofibroblast differentiation (226). Since periostin has been shown to enhance FAK phosphorylation in other systems (130, 133, 134, 187, 237, 238), it was hypothesized that periostin promotes HTS myofibroblast differentiation and maintenance through a FAK-ROCK dependent signalling pathway.

The findings presented in this chapter demonstrate that, when cultured under isometric tension, periostin had no significant additive effects on FAK phosphorylation in HTS fibroblasts. However, after the release of isometric tension, a significant increase in FAK phosphorylation was observed in periostin treated HTS fibroblasts for up to 48 hours relative to vehicle controls. While these results are not informative regarding FAK activation during myofibroblast differentiation, these data suggest that periostin enhances FAK activation in HTS fibroblasts under conditions of decreasing mechanical tension. Surprisingly, phosphorylated FAK levels were also significantly increased in periostin-depleted HTS fibroblasts 48 hours after collagen lattice release relative to vector transduced controls. These findings may be explained in the context of previous studies demonstrating that FAK signalling can both promote and inhibit ROCK activation and stress fiber maintenance (236, 239-241).

FAK signalling can promote stress fiber formation and contraction through the phosphorylation and activation of p190 RhoGEF (236, 241). p190 RhoGEF is a Rho specific guanine nucleotide exchange factor (GEF) that activates RhoA by promoting the dissociation of guanosine-5'-diphosphate (GDP) and the binding of GTP to RhoA (242, 243). RhoA-GTP binding to ROCK induces a conformational change in ROCK that activates the protein (244, 245). FAK signalling can also promote the phosphorylation and activation of p190 RhoGAP, a GTPase activating protein (GAP), which inhibits RhoA activity by promoting binding of GDP to RhoA (236, 246). Inhibition of RhoA prevents downstream activation of signalling intermediates involved in stress fiber

maintenance and contraction. It is possible that, following the release of mechanical tension in sFPCLs, periostin signalling is able to maintain positive FAK-ROCK activation and thereby promote myofibroblast persistence.

This hypothesis could be tested by assessing the effects of periostin on the activity of RhoA and ROCK. The RhoA activity assays currently available utilize the Rho binding domain of the Rho effector protein, Rhotekin, to specifically bind RhoA-GTP. However, these analyses require the precipitation of Rhotekin-RhoA-GTP complexes using glutathione affinity beads. Unfortunately, the amount of total cell lysate required for this assay would be unattainable in practice for 3D collagen cultures. As ROCK is activated by a conformational change induced by RhoA-GTP binding, its activity cannot be assessed using western immunoblotting. Therefore, to gain additional insights into periostin effects on ROCK activation, the activation of downstream ROCK targets were assessed using gain- and loss-of-function studies.

ROCK activation can promote stress fiber maintenance, focal adhesion formation and myofibroblast differentiation through two divergent pathways. Cofilin, a downstream target of ROCK, is an actin-binding protein that promotes actin stress fiber depolymerization (227). ROCK-mediated cofilin phosphorylation inhibits cofilin activity and actin depolymerization, thereby promoting stress fiber maintenance (228). ROCK activation also induces myofibroblast-mediated contraction through phosphorylation and activation of the regulatory MLC (51-53). In combination, these signalling events promote the formation and maintenance of stress fibers and increase ECM tension through myofibroblast contraction, resulting in integrin clustering, the formation of suFA complexes and myofibroblast differentiation and/or persistence (247).

No significant changes in the phosphorylation states of cofilin or MLC were consistently detected in HTS myofibroblasts cultured under isometric tension or following the release of tension irrespective of treatment. It is likely that the lack of significant findings in these studies can be explained by inter-patient variability. Gender, age, scar location, scar maturity and additional co-morbidities may influence periostin sensitivity between individual patients and this variability can make it difficult to detect significant

differences when patients are assessed as a group. This was evident in several of these studies as statistically significant treatment effects were observed in a subset of individual patients but significance was lost when the patients were assessed as a group. Future analyses of much larger numbers of patient-derived fibroblast lines may be required to overcome this inter-patient variability, and sub-group analyses of those that yield significant results may shed new light on the source(s) of variability. These findings also illustrate the importance of assessing treatment effects in primary fibroblast lines derived from multiple patients, as such variability might not be observed in an immortalized cell line derived from a single patient.

Although inconclusive, these studies did not rule out the possibility that periostin signalled through these intermediates to enhance suFA formation, myofibroblast differentiation and/or persistence. Therefore, independent analyses of suFA formation were performed. As described previously in this chapter, α SMA is only incorporated into stress fibers of myofibroblasts when the mechanical tension in the ECM passes a critical threshold that allows for the formation of suFAs (30). The formation of suFAs and the *de novo* expression and incorporation of α SMA into stress fibers allows myofibroblasts to exert much greater contractile forces on the ECM (43), thereby contributing to the abnormal dermal density that characterizes scar formation. As periostin promotes myofibroblast differentiation and persistence in hypertrophic scarring (Chapter 4.4 and 4.7), potentially by activating focal adhesion signalling molecules (Chapter 5.3), it was hypothesized that exogenous periostin treatment would enhance the formation of suFAs.

To assess suFA formation, two markers of suFAs, α SMA and vinculin, were assessed by immunofluorescence confocal microscopy. The combination of α SMA and vinculin was optimal for confirming the differentiated state of the myofibroblasts while simultaneously visualizing all three FA classes (184). The length of each FA was assessed along its longest axis regardless of orientation as described in previous studies (184). Using this approach, periostin treated HTS fibroblasts cultured under mechanical tension were shown to exhibit significantly larger focal adhesions and a higher percentage of suFAs (> 6 μ m in length) per cell relative to vehicle controls. A feedback mechanism between enhanced suFA formation and increased ECM tension above threshold levels promotes

myofibroblast differentiation and persistence (43, 44) leading to the excessive deposition and contracture of the ECM characteristically seen in hypertrophic scarring. These data suggest that periostin signalling may promote and maintain suFA formation and myofibroblast differentiation in patients prone to hypertrophic scarring.

In summary, periostin was shown to promote myofibroblast differentiation by enhancing suFA formation in HTS myofibroblasts. Although the receptor(s) utilized by periostin to induce suFA formation are yet to be identified, these findings are consistent with periostin enhancing myofibroblast differentiation and persistence in hypertrophic scarring through a FAK-ROCK dependent pathway. This is the first study to link periostin activation of these signalling pathways to suFA formation in hypertrophic scarring. As hypertrophic scarring and related benign fibrotic conditions are characterized by enhanced myofibroblast differentiation and the persistence of these highly contractile cells within the dermis, periostin may have potential as a therapeutic target for novel therapies designed to induce myofibroblast de-differentiation and/or apoptosis and, thereby, enhance hypertrophic scar resolution.

Chapter 6

6 Conclusion

Hundreds of millions of patients in developed countries develop scars each year following surgical procedures, with the incidence rate for hypertrophic scar formation varying between 40-70% in many centers (66, 67, 248). Hypertrophic scars and other abnormal scarring conditions are the result of aberrant wound healing after an insult to the deep dermis. Scarring imposes morbidity that is difficult to quantify, but includes pain and loss of mobility, especially if the scar is associated with a joint (60). As well as imposing a financial burden, scars are often disfiguring and can adversely affect a patient's quality of life, both physically and psychologically (60, 61). Unfortunately, there are few, if any, truly effective treatment options for abnormal scarring conditions (58, 60). Prevention of hypertrophic scarring is also difficult, as abnormal skin remodelling may not become evident until 4-8 weeks after wound closure (59). Current treatment strategies have therefore focused on improving hypertrophic and keloid scar resolution, rather than on prevention.

The findings presented in this thesis suggest that increased and persistent levels of periostin in the dermis of human hypertrophic scar tissue contribute to excessive fibroblast proliferation and myofibroblast differentiation and persistence (Figure 6.1). Periostin depletion in the dermis of hypertrophic scars may therefore have utility as a therapeutic target for novel therapies designed to improve scar resolution by attenuating fibroblast proliferation and promoting myofibroblast apoptosis and/or dedifferentiation. In addition to hypertrophic scars, periostin is abnormally abundant in keloid scars and periostin may play a similar role in promoting and maintaining myofibroblast differentiation of keloid scar-derived fibroblasts. These data suggest that the effects of periostin described in this thesis may not be specific to HTS but may be a common feature of other benign fibroses. This concept is supported by findings that periostin promotes myofibroblast differentiation of primary fibroblasts derived from Dupuytren's Disease, a benign fibrosis of the palmar fascia (91). Therefore, periostin may not only be

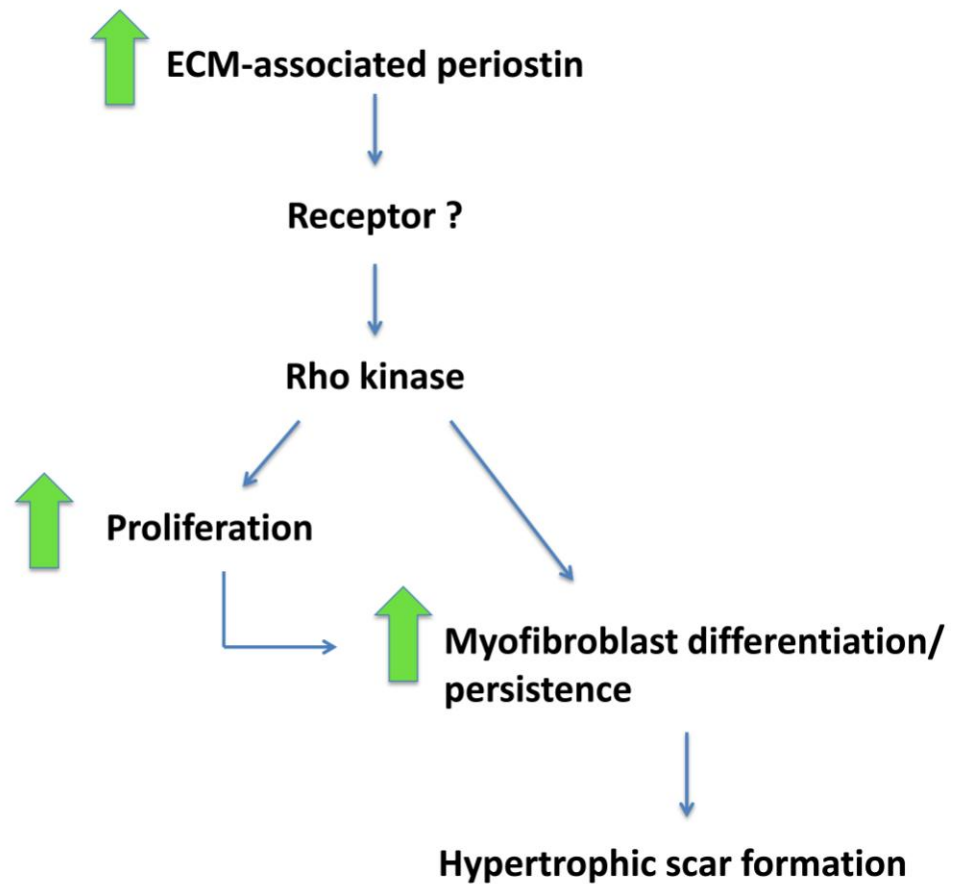


Figure 6.1 Schematic representation of the roles of periostin in hypertrophic scarring. Increased and persistent levels of ECM-associated periostin in the dermis of hypertrophic scar tissue contribute to hypertrophic scar formation by enhancing fibroblast proliferation and myofibroblast differentiation and persistence through a Rho kinase mediated pathway. Enhanced fibroblast proliferation and myofibroblast differentiation leads to excessive ECM deposition and remodelling leading to the formation of raised, dense collagenous scars.

an attractive therapeutic target to improve abnormal scar resolution but may have utility as a more universal target for treating a variety of benign fibrotic conditions.

Non-healing chronic wounds are a less obvious but potentially relevant application of these findings. Chronic non-healing wounds do not progress beyond the inflammatory phase of wound healing (54), display decreased growth factor activity and increased fibroblast senescence relative to normal healing wounds (249). The prevalence of non-healing wounds within the Canadian healthcare system is approximately 35% (250) and may result in amputation of the affected limb due to lack of effective treatment options (251). Since periostin expression is decreased in chronic non-healing wounds (97), exogenous periostin treatment may stimulate fibroblast proliferation and myofibroblast-mediated ECM deposition and remodelling resulting in wound closure.

In order to assess the role(s) of periostin in normal and abnormal cutaneous wound repair, an appropriate model system was required. Unfortunately, there is a lack of representative and physiological relevant *in vivo* animal models of hypertrophic scarring (59).

Hypertrophic or any other forms of fibrotic dermal scarring do not normally occur in mice (163) as they can regenerate dermal wounds very efficiently (160). While several scarring-prone mouse models have been developed after genetic modifications or chemical treatments (165, 252), the physiological relevance of these models are unclear. There are significant anatomical differences between the inter-follicular area (161), epidermal thickness and turnover rate (159) and dermal thickness (160) of mouse and human skin, limiting our ability to translate findings between these species (253, 254). More recently, the red duroc pig has been utilized as a model for human cutaneous wound healing. Swine have a similar dermal and epidermal architecture (255-257) and heal wounds by re-epithelialization in a similar manner to humans (258). In contrast to mouse models, red duroc pigs readily form raised collagenous scars that are similar to hypertrophic scars following insult to the deep dermis (255, 259). Nonetheless, the clinical relevance of these extremely expensive models (257) remains unclear. Very little is known about the complex array of single nucleotide polymorphisms or other genetic or epigenetic changes that predispose some patients to scarring, and these details will need to be elucidated before any truly representative animal models can be developed. As it is

not ethically feasible to perform scarring experiments on humans, it can be argued that the best available models of hypertrophic scarring are the tissues or tissue-derived cells derived from surgical scar resection. In this thesis, primary human dermal fibroblasts derived from hypertrophic scar, keloid scar and normal skin from multiple patients were chosen to assess periostin effects in *in vitro* models.

While the clinical relevance of analyzing primary dermal fibroblasts obtained from normal and abnormal human tissue is obvious, these cells have inherent characteristics that can make them challenging to interpret. Scars are generally resected months or years after their initial formation, making it difficult or impossible to identify the earliest signalling events that promote abnormal scar formation (59). The major challenge, however, is inter-patient variability. Differences in gender, race, age, scar location, and other co-morbidities may affect the sensitivity of individual patient-derived fibroblasts to treatment and can make it extremely difficult to identify consistent effects on fibroblast proliferation and/or myofibroblast differentiation in all, or even the majority, of patients. This was evident in several studies presented in this thesis, as significant treatment effects were evident in a subset of patients but absent in others. Additionally, variation can arise from selection between passages, as the fibroblasts derived from patient tissues are a heterogeneous population of cells. Therefore, there is the potential to select for different subsets of fibroblasts that have differing tolerances to *in vitro* culture with each passage. With inter-patient and inter-passage variability, it can be difficult to identify statistically significant effects when assessing the mean data derived from a mixed population. Thus, several trends have been identified in this thesis that may or may not represent real effects in a subset of patient-derived fibroblasts. Assessment of very large numbers of patients may be required to identify the source of this inter-patient variability and yield significant findings within pre-identified sub groups of patients. However, such variability may also be impossible to avoid in practice due to the very large number of variables between individuals.

Another limitation of using primary cells is their limited replicative potential compared to immortalized cell lines. The pilot studies that led to this project in our laboratory demonstrated that HTS fibroblasts lose their initial characteristics after approximately

four passages. Due to their short “shelf life,” it is difficult to genetically modify primary fibroblasts by conventional transfection techniques and obtain meaningful results in four passages or less. It could be argued that an immortalized human HTS fibroblast cell line, which currently does not exist to our knowledge, would be beneficial in reducing experimental variability in these assays and in identifying and characterizing periostin-induced specific signalling pathways in more detail. However, the “trade off” with such a cell line is that it would be even more difficult to translate the findings in these immortalized cells to a clinical setting. A single cell line could only provide a detailed assessment of periostin effects in a single patient that may, or may not, be representative of the broad and variable population of individuals affected by abnormal scarring. Thus, despite their inherent limitations, this thesis focused on *in vitro* analyses of primary fibroblasts derived from surgically resected scar tissue of multiple patients, and on identifying and characterizing the signalling pathways that were activated by periostin in most or all of these patients. With further development, the approach of using primary cell “banks” derived directly from patients may have great potential for providing clinically relevant information about the cellular processes that cause the abnormal persistence of scars.

The molecular focus of this thesis was periostin, a TGF β -1-inducible secreted ECM protein (101) that is transiently expressed during normal cutaneous wound repair (98, 151, 152), and is abnormally abundant and persistent in abnormal scars and other benign fibroses (91, 97-99, 148, 150, 179, 260-263). This protein is often described as a “matricellular” molecule, a term originally coined by Bornstein (90, 124) to describe extracellular proteins that do not contribute directly to the structure of the ECM but instead serve to modulate cell-matrix interactions and cell function. Periostin has been demonstrated to enhance fibroblast proliferation and myofibroblast differentiation in other models of variable physiological relevance to humans (91, 132, 133, 152, 178-180). To assess the functional consequences of enhancing or depleting any matricellular protein, it is essential that an appropriate 3D cell culture system be in place to assess signalling effects from the ECM that may or may not occur in the absence of a physiologically relevant ECM as a culture substrate. Previous studies have demonstrated that culturing fibroblasts on rigid tissue culture plastic dishes results in spontaneous

proto- and myofibroblast differentiation (31) and that substrate-induced effects can overshadow treatment effects on cellular phenotypes (133). Our laboratory is one of many that have shown that variations in substrate stiffness can modify gene expression and protein levels in primary human fibroblasts (171). Others have shown that, when cultured on tissue culture plastic, cells can adopt very different structures to *in vivo* and fail to respond to appropriate stimuli. However, if the same cells are cultured on substrates that mimic the *in vivo* microenvironment, they adopt *in vivo*-like structures and function (264-266). The effectiveness of therapeutic treatments has also been shown to differ between cells cultured on plastic and on *in vivo*-like matrices (267-269). Taken together, these studies highlight the importance of the microenvironment in regulating cellular phenotype in *in vitro* cultures, particularly in the context of matricellular signalling.

For these reasons, the primary human fibroblasts examined in this thesis were cultured on two- and three-dimensional type I collagen substrates, the most abundant collagen in the skin and mature scars (8), to more closely mimic the microenvironment and substrate stiffness experienced by these fibroblasts *in vivo*. Although the dermal ECM is much more complex than polymerized type I collagen, the use of collagen substrates allows for the incorporation of periostin within a collagenous ECM matrix, mimicking its localization *in vivo*, and provides a simple and reproducible physiological relevant *in vitro* culture system for assessing the effects of periostin on hypertrophic scar formation. To gain additional insight into the roles of periostin in promoting abnormal scar formation, future *in vitro* studies should focus on culturing fibroblasts directly on decellularized hypertrophic scar and normal skin tissue to achieve even better models of the microenvironments in normal and abnormal conditions. Alternatively, much more complex mixtures of purified collagens and other ECM molecules, or co-culture experiments with other cell types involved in cutaneous wound repair such as keratinocytes, may be used for *in vitro* analyses to enhance the physiological relevance of the cellular environment.

Despite the methodological challenges in achieving such complex culture systems, there is a clear and urgent need for better *in vitro* models that are physiologically relevant to

humans and representative of a genetically diverse population. Recent high profile reports (270) have described how the majority of peer reviewed medical research publications describing novel drug targets and similar findings cannot be independently reproduced. Amongst many other contributing factors, a lack of physiologically relevant and representative models is likely to have contributed significantly to this problem. We should not be surprised that novel drug targets identified in immortalized human cells derived from a single individual, and then “verified” in animal models with significant physiological differences to humans and with much less individual variability, fail to progress in clinical trials on human populations.

The identification of molecules that promote aberrant wound healing signals will improve our current understanding of the processes involved in abnormal scar formation. The findings presented in this thesis indicate that periostin enhances fibroblast proliferation in compliant collagen cultures, a model designed to mimic the low mechanical tension of the provisional matrix in the early stages of wound healing, through an Akt and ROCK dependent pathway. When subjected to isometric tension in sFPCLs, a model that mimics aspects of wound closure *in vivo*, periostin induces myofibroblast differentiation, as evidenced by an increase in α SMA levels, collagen lattice contraction and supermature focal adhesion formation. Additionally, periostin signalling maintained α SMA levels in myofibroblasts in an environment of decreasing ECM stress, indicating a role for periostin in myofibroblast persistence, potentially through a FAK-ROCK dependent pathway. Since periostin had no discernible effects on NS-derived fibroblast proliferation or differentiation, these data support the central hypothesis that periostin promotes pathological effects leading to abnormal scar formation.

The function of an organ, including the skin, is dependent on the numerous cell types that make up the organ and the organization of the surrounding extracellular matrix (235). Interactions between the cells and the surrounding ECM through integrins and cell-cell interactions through adherens junctions determine the gene expression and phenotype of the resident cells without altering the genotype (235, 271). Therefore, the microenvironment provides necessary signalling to maintain tissue homeostasis and suppress malignant or abnormal phenotypes. However, aberrant signalling from the

microenvironment can lead to loss of tissue homeostasis and promote abnormal or malignant behaviours in the resident cells (271).

Wounding events have been shown to be an effective stimulus for promoting malignancy (272). Stromal fibroblasts are responsible for the production, deposition and remodelling of the ECM (271) and increased stromal density (changing tissue microenvironment) has been correlated with an increase risk of cancer progression (273, 274). Increased myofibroblast differentiation within the stroma has been correlated with increased risk of cancer development and the induction of an inflammatory response by an established tumour can further promote a fibrotic stroma (271). Studies in mouse models of epithelial cancer progression have demonstrated that increased stromal density enhanced epithelial cell proliferation, tumourgenesis, tumour growth, migration and invasion (275-277), some of which may be induced by FAK and Rho signalling within epithelial cells (278-280).

These finding may be relevant to this thesis because, in addition to being an upregulated component of benign fibroses, periostin expression is also increased in malignant diseases. Periostin is upregulated in a variety of tumours and associated stroma and its increased expression is correlated with malignancy (108, 128, 129, 141, 180, 281). Periostin can interact with several integrins to induce tumour cell migration, growth, EMT and survival (128-131, 142). Over expression of periostin in colon cancer cells increased the size and number of metastatic colonies at secondary sites (129). A recent study by Malanchi et al., (281) demonstrated that metastatic colonies required periostin expression by stromal fibroblasts in order to successfully colonize at those locations. As periostin enhanced fibroblast proliferation and myofibroblast differentiation in fibroblasts derived from hypertrophic scar tissue, the findings in this thesis may enhance our understanding of periostin's roles in tissue remodelling in metastatic conditions. Increased levels of periostin in the stroma of metastatic diseases may promote excessive fibroblast proliferation and myofibroblast differentiation, causing abnormal stromal density and enhanced tumour formation, growth and invasion. A normal microenvironment can induce some malignant cells to regain a normal phenotype *in vitro* (235, 282) stressing the importance of the microenvironment in tissue homeostasis and

disease progression. Therefore, periostin depletion in the stroma surrounding malignant cells may be an attractive therapeutic target for novel therapies designed to reduce stromal density.

It has become increasingly evident that achieving normal tissue homeostasis is the ultimate treatment outcome and that targeting the microenvironment may have profound clinical benefits (271). The findings presented in this thesis demonstrate that increased levels of periostin in the wound microenvironment of hypertrophic scar tissue results in excessive fibroblast proliferation and myofibroblast differentiation. Even in conditions of decreasing ECM tension, abundant and persistent levels of periostin in the microenvironment “shield” HTS myofibroblasts from the mechanotransduction signalling events associated with changes in ECM tension, thereby allowing these cells to maintain a differentiated state. Identification of the molecular components and mechanisms involved in periostin regulation and degradation may have profound clinical benefits for improving scar resolution in patients affected by abnormal scarring.

Periostin levels are increased and persistent in the ECM of benign fibrotic conditions such as hypertrophic scarring. It is plausible that the pathways that normally regulate periostin levels in the ECM are atypical in these conditions and that their identification may reveal attractive therapeutic agents for depleting periostin levels in the microenvironment of hypertrophic scar tissue. Periostin expression is reported to be regulated by a number of factors essential for normal cutaneous wound healing such as TGF β -1, platelet derived growth factor, interleukins, fibroblast growth factor and mechanical tension (101, 103, 104, 283) and these would be difficult to target in a clinical setting. The factors that regulate periostin depletion in normal cutaneous wound healing are unclear. As periostin is proposed to be a very stable protein with a long half-life, and to be difficult to deplete under conditions of high ECM tension (222), active degradation of periostin in the dermis may be responsible for decreased periostin levels in the dermis during the remodelling phase of normal cutaneous wound healing.

Unfortunately, nothing is known about periostin degradation. Previous studies have shown that matricellular proteins thrombospondin-1, SPARC and CCN1 are targets of

several proteases including plasmin, MMP-1 and MMP-9 (284-286). As levels of plasmin, MMP-1 and MMP-9 are decreased in hypertrophic and keloid scarring (287-289), these or similar proteases may have roles in the degradation of the matricellular protein periostin in hypertrophic scarring. This hypothesis should be assessed initially in a cell free system to determine if individual proteases degrade periostin in solution, and then verified in 3D restrained collagen *in vitro* model systems like those described in this thesis. If periostin levels were significantly reduced following protease treatment relative to controls, addition of these proteases to sFPCL cultures should inhibit periostin-induced HTS myofibroblast differentiation and promote myofibroblast apoptosis and/or dedifferentiation in conditions of decreasing ECM tension.

Another intriguing possibility is that dermal periostin levels may be regulated by receptor-mediated endocytosis and lysosomal degradation. The matricellular protein SPARC has been shown to be regulated by interacting with stabilin-1 (290), a scavenger receptor involved in receptor-mediated endocytosis expressed in macrophages and endothelial cells (291). Periostin and stabilin-1 both belong to the fasciclin family of proteins characterized by the presence of FAS-1 domains involved in cell adhesion and protein-protein interactions (108). Therefore, it is possible that interactions between periostin and stabilin-1 may regulate periostin levels in normal and abnormal wound healing.

Identification of proteases and/or mechanisms involved in periostin degradation may have profound benefits as therapeutic treatments designed promote myofibroblast apoptosis and reduce dermal density in patients affected by hypertrophic scarring. Conversion of the disease microenvironment to a more homeostatic state should improve scar resolution and eliminate the need for costly surgical and therapeutic interventions. It is hoped that these studies will encourage research in the area of periostin regulation in excessive cutaneous wound repair with the goal of uncovering new therapeutic approaches for disease resolution.

References

1. Kanitakis, J. (2002) Anatomy, histology and immunohistochemistry of normal human skin, *Eur J Dermatol* 12, 390-399; quiz 400-391.
2. McLafferty, E., Hendry, C., and Alistair, F. (2012) The integumentary system: anatomy, physiology and function of skin, *Nurs Stand* 27, 35-42.
3. Martin, P. (1997) Wound healing--aiming for perfect skin regeneration, *Science* 276, 75-81.
4. Proksch, E., Brandner, J. M., and Jensen, J. M. (2008) The skin: an indispensable barrier, *Exp Dermatol* 17, 1063-1072.
5. Hwa, C., Bauer, E. A., and Cohen, D. E. (2011) Skin biology, *Dermatol Ther* 24, 464-470.
6. Smith, K. L., and Dean, S. J. (1998) Tissue repair of the epidermis and dermis, *J Hand Ther* 11, 95-104.
7. McAnulty, R. J. (2007) Fibroblasts and myofibroblasts: their source, function and role in disease, *Int J Biochem Cell Biol* 39, 666-671.
8. Baum, C. L., and Arpey, C. J. (2005) Normal cutaneous wound healing: clinical correlation with cellular and molecular events, *Dermatol Surg* 31, 674-686; discussion 686.
9. Robson, M. C., Steed, D. L., and Franz, M. G. (2001) Wound healing: biologic features and approaches to maximize healing trajectories, *Curr Probl Surg* 38, 72-140.
10. Reinke, J. M., and Sorg, H. (2012) Wound repair and regeneration, *Eur Surg Res* 49, 35-43.
11. Alonso, J. E., Lee, J., Burgess, A. R., and Browner, B. D. (1996) The management of complex orthopedic injuries, *Surg Clin North Am* 76, 879-903.
12. Velnar, T., Bailey, T., and Smrkolj, V. (2009) The wound healing process: an overview of the cellular and molecular mechanisms, *J Int Med Res* 37, 1528-1542.
13. Werner, S., and Grose, R. (2003) Regulation of wound healing by growth factors and cytokines, *Physiol Rev* 83, 835-870.
14. Szpaderska, A. M., Egozi, E. I., Gamelli, R. L., and DiPietro, L. A. (2003) The effect of thrombocytopenia on dermal wound healing, *J Invest Dermatol* 120, 1130-1137.

15. Becker, B. F., Heindl, B., Kupatt, C., and Zahler, S. (2000) Endothelial function and hemostasis, *Z Kardiol* 89, 160-167.
16. Lawrence, W. T. (1998) Physiology of the acute wound, *Clin Plast Surg* 25, 321-340.
17. Wahl, S. M., Hunt, D. A., Wakefield, L. M., McCartney-Francis, N., Wahl, L. M., Roberts, A. B., and Sporn, M. B. (1987) Transforming growth factor type beta induces monocyte chemotaxis and growth factor production, *Proc Natl Acad Sci U S A* 84, 5788-5792.
18. Singer, A. J., and Clark, R. A. (1999) Cutaneous wound healing, *N Engl J Med* 341, 738-746.
19. Steed, D. L. (1997) The role of growth factors in wound healing, *Surg Clin North Am* 77, 575-586.
20. Koh, T. J., and DiPietro, L. A. (2011) Inflammation and wound healing: the role of the macrophage, *Expert Rev Mol Med* 13, e23.
21. DiPietro, L. A., and Polverini, P. J. (1993) Role of the macrophage in the positive and negative regulation of wound neovascularization, *Behring Inst Mitt*, 238-247.
22. Sakai, T., Johnson, K. J., Murozono, M., Sakai, K., Magnuson, M. A., Wieloch, T., Cronberg, T., Isshiki, A., Erickson, H. P., and Fassler, R. (2001) Plasma fibronectin supports neuronal survival and reduces brain injury following transient focal cerebral ischemia but is not essential for skin-wound healing and hemostasis, *Nat Med* 7, 324-330.
23. Postlethwaite, A. E., Keski-Oja, J., Balian, G., and Kang, A. H. (1981) Induction of fibroblast chemotaxis by fibronectin. Localization of the chemotactic region to a 140,000-molecular weight non-gelatin-binding fragment, *J Exp Med* 153, 494-499.
24. Eckes, B., Nischt, R., and Krieg, T. (2010) Cell-matrix interactions in dermal repair and scarring, *Fibrogenesis Tissue Repair* 3, 4.
25. Barker, T. H. (2011) The role of ECM proteins and protein fragments in guiding cell behavior in regenerative medicine, *Biomaterials* 32, 4211-4214.
26. Li, J., Zhang, Y. P., and Kirsner, R. S. (2003) Angiogenesis in wound repair: angiogenic growth factors and the extracellular matrix, *Microsc Res Tech* 60, 107-114.
27. Hinz, B., Phan, S. H., Thannickal, V. J., Prunotto, M., Desmouliere, A., Varga, J., De Wever, O., Mareel, M., and Gabbiani, G. (2012) Recent developments in myofibroblast biology: paradigms for connective tissue remodeling, *Am J Pathol* 180, 1340-1355.

28. Wynn, T. A. (2008) Cellular and molecular mechanisms of fibrosis, *J Pathol* 214, 199-210.
29. Gabbiani, G., Ryan, G. B., and Majne, G. (1971) Presence of modified fibroblasts in granulation tissue and their possible role in wound contraction, *Experientia* 27, 549-550.
30. Tomasek, J. J., Gabbiani, G., Hinz, B., Chaponnier, C., and Brown, R. A. (2002) Myofibroblasts and mechano-regulation of connective tissue remodelling, *Nat Rev Mol Cell Biol* 3, 349-363.
31. Hinz, B. (2010) The myofibroblast: paradigm for a mechanically active cell, *J Biomech* 43, 146-155.
32. Hinz, B. (2007) Formation and function of the myofibroblast during tissue repair, *J Invest Dermatol* 127, 526-537.
33. Hao, H., Gabbiani, G., Camenzind, E., Bacchetta, M., Virmani, R., and Bochaton-Piallat, M. L. (2006) Phenotypic modulation of intima and media smooth muscle cells in fatal cases of coronary artery lesion, *Arterioscler Thromb Vasc Biol* 26, 326-332.
34. Abe, R., Donnelly, S. C., Peng, T., Bucala, R., and Metz, C. N. (2001) Peripheral blood fibrocytes: differentiation pathway and migration to wound sites, *J Immunol* 166, 7556-7562.
35. Zeisberg, M., and Kalluri, R. (2004) The role of epithelial-to-mesenchymal transition in renal fibrosis, *J Mol Med (Berl)* 82, 175-181.
36. Kim, K. K., Kugler, M. C., Wolters, P. J., Robillard, L., Galvez, M. G., Brumwell, A. N., Sheppard, D., and Chapman, H. A. (2006) Alveolar epithelial cell mesenchymal transition develops in vivo during pulmonary fibrosis and is regulated by the extracellular matrix, *Proc Natl Acad Sci U S A* 103, 13180-13185.
37. Hinz, B., Phan, S. H., Thannickal, V. J., Galli, A., Bochaton-Piallat, M. L., and Gabbiani, G. (2007) The myofibroblast: one function, multiple origins, *Am J Pathol* 170, 1807-1816.
38. Hinz, B., Mastrangelo, D., Iselin, C. E., Chaponnier, C., and Gabbiani, G. (2001) Mechanical tension controls granulation tissue contractile activity and myofibroblast differentiation, *Am J Pathol* 159, 1009-1020.
39. Serini, G., Bochaton-Piallat, M. L., Ropraz, P., Geinoz, A., Borsi, L., Zardi, L., and Gabbiani, G. (1998) The fibronectin domain ED-A is crucial for myofibroblastic phenotype induction by transforming growth factor-beta1, *J Cell Biol* 142, 873-881.

40. Malmstrom, J., Lindberg, H., Lindberg, C., Bratt, C., Wieslander, E., Delander, E. L., Sarnstrand, B., Burns, J. S., Mose-Larsen, P., Fey, S., and Marko-Varga, G. (2004) Transforming growth factor-beta 1 specifically induce proteins involved in the myofibroblast contractile apparatus, *Mol Cell Proteomics* 3, 466-477.
41. Desmouliere, A., Geinoz, A., Gabbiani, F., and Gabbiani, G. (1993) Transforming growth factor-beta 1 induces alpha-smooth muscle actin expression in granulation tissue myofibroblasts and in quiescent and growing cultured fibroblasts, *J Cell Biol* 122, 103-111.
42. Wipff, P. J., Rifkin, D. B., Meister, J. J., and Hinz, B. (2007) Myofibroblast contraction activates latent TGF-beta1 from the extracellular matrix, *J Cell Biol* 179, 1311-1323.
43. Hinz, B. (2006) Masters and servants of the force: the role of matrix adhesions in myofibroblast force perception and transmission, *Eur J Cell Biol* 85, 175-181.
44. Goffin, J. M., Pittet, P., Csucs, G., Lussi, J. W., Meister, J. J., and Hinz, B. (2006) Focal adhesion size controls tension-dependent recruitment of alpha-smooth muscle actin to stress fibers, *J Cell Biol* 172, 259-268.
45. Serini, G., and Gabbiani, G. (1999) Mechanisms of myofibroblast activity and phenotypic modulation, *Exp Cell Res* 250, 273-283.
46. Burridge, K., and Chrzanowska-Wodnicka, M. (1996) Focal adhesions, contractility, and signaling, *Annu Rev Cell Dev Biol* 12, 463-518.
47. Tomasek, J. J., Haaksma, C. J., Eddy, R. J., and Vaughan, M. B. (1992) Fibroblast contraction occurs on release of tension in attached collagen lattices: dependency on an organized actin cytoskeleton and serum, *Anat Rec* 232, 359-368.
48. Katoh, K., Kano, Y., Masuda, M., Onishi, H., and Fujiwara, K. (1998) Isolation and contraction of the stress fiber, *Mol Biol Cell* 9, 1919-1938.
49. Leung, T., Manser, E., Tan, L., and Lim, L. (1995) A novel serine/threonine kinase binding the Ras-related RhoA GTPase which translocates the kinase to peripheral membranes, *J Biol Chem* 270, 29051-29054.
50. Ishizaki, T., Maekawa, M., Fujisawa, K., Okawa, K., Iwamatsu, A., Fujita, A., Watanabe, N., Saito, Y., Kakizuka, A., Morii, N., and Narumiya, S. (1996) The small GTP-binding protein Rho binds to and activates a 160 kDa Ser/Thr protein kinase homologous to myotonic dystrophy kinase, *EMBO J* 15, 1885-1893.
51. Amano, M., Ito, M., Kimura, K., Fukata, Y., Chihara, K., Nakano, T., Matsuura, Y., and Kaibuchi, K. (1996) Phosphorylation and activation of myosin by Rho-associated kinase (Rho-kinase), *J Biol Chem* 271, 20246-20249.

52. Kimura, K., Ito, M., Amano, M., Chihara, K., Fukata, Y., Nakafuku, M., Yamamori, B., Feng, J., Nakano, T., Okawa, K., Iwamatsu, A., and Kaibuchi, K. (1996) Regulation of myosin phosphatase by Rho and Rho-associated kinase (Rho-kinase), *Science* 273, 245-248.
53. Kawano, Y., Fukata, Y., Oshiro, N., Amano, M., Nakamura, T., Ito, M., Matsumura, F., Inagaki, M., and Kaibuchi, K. (1999) Phosphorylation of myosin-binding subunit (MBS) of myosin phosphatase by Rho-kinase in vivo, *J Cell Biol* 147, 1023-1038.
54. Guo, S., and Dipietro, L. A. (2010) Factors affecting wound healing, *J Dent Res* 89, 219-229.
55. Tredget, E. E., Nedelec, B., Scott, P. G., and Ghahary, A. (1997) Hypertrophic scars, keloids, and contractures. The cellular and molecular basis for therapy, *Surg Clin North Am* 77, 701-730.
56. Moulin, V., Larochelle, S., Langlois, C., Thibault, I., Lopez-Valle, C. A., and Roy, M. (2004) Normal skin wound and hypertrophic scar myofibroblasts have differential responses to apoptotic inductors, *J Cell Physiol* 198, 350-358.
57. Desmouliere, A. (1995) Factors influencing myofibroblast differentiation during wound healing and fibrosis, *Cell Biol Int* 19, 471-476.
58. Wolfram, D., Tzankov, A., Pulzl, P., and Piza-Katzer, H. (2009) Hypertrophic scars and keloids--a review of their pathophysiology, risk factors, and therapeutic management, *Dermatol Surg* 35, 171-181.
59. Gauglitz, G. G., Korting, H. C., Pavicic, T., Ruzicka, T., and Jeschke, M. G. (2011) Hypertrophic scarring and keloids: pathomechanisms and current and emerging treatment strategies, *Mol Med* 17, 113-125.
60. Leventhal, D., Furr, M., and Reiter, D. (2006) Treatment of keloids and hypertrophic scars: a meta-analysis and review of the literature, *Arch Facial Plast Surg* 8, 362-368.
61. Bock, O., Schmid-Ott, G., Malewski, P., and Mrowietz, U. (2006) Quality of life of patients with keloid and hypertrophic scarring, *Arch Dermatol Res* 297, 433-438.
62. Kose, O., and Waseem, A. (2008) Keloids and hypertrophic scars: are they two different sides of the same coin?, *Dermatol Surg* 34, 336-346.
63. Tanaka, A., Hatoko, M., Tada, H., Iioka, H., Niitsuma, K., and Miyagawa, S. (2004) Expression of p53 family in scars, *J Dermatol Sci* 34, 17-24.

64. Moustafa, M. F., Abdel-Fattah, M. A., and Abdel-Fattah, D. C. (1975) Presumptive evidence of the effect of pregnancy estrogens on keloid growth. Case report, *Plast Reconstr Surg* 56, 450-453.
65. Schierle, H. P., Scholz, D., and Lemperle, G. (1997) Elevated levels of testosterone receptors in keloid tissue: an experimental investigation, *Plast Reconstr Surg* 100, 390-395; discussion 396.
66. Deitch, E. A., Wheelahan, T. M., Rose, M. P., Clothier, J., and Cotter, J. (1983) Hypertrophic burn scars: analysis of variables, *J Trauma* 23, 895-898.
67. Lewis, W. H., and Sun, K. K. (1990) Hypertrophic scar: a genetic hypothesis, *Burns* 16, 176-178.
68. Juckett, G., and Hartman-Adams, H. (2009) Management of keloids and hypertrophic scars, *Am Fam Physician* 80, 253-260.
69. Bayat, A., Arscott, G., Ollier, W. E., McGrouther, D. A., and Ferguson, M. W. (2005) Keloid disease: clinical relevance of single versus multiple site scars, *Br J Plast Surg* 58, 28-37.
70. Gauglitz, G. G. (2013) Management of keloids and hypertrophic scars: current and emerging options, *Clin Cosmet Investig Dermatol* 6, 103-114.
71. Bock, O., Yu, H., Zitron, S., Bayat, A., Ferguson, M. W., and Mrowietz, U. (2005) Studies of transforming growth factors beta 1-3 and their receptors I and II in fibroblast of keloids and hypertrophic scars, *Acta Derm Venereol* 85, 216-220.
72. Shah, M., Foreman, D. M., and Ferguson, M. W. (1995) Neutralisation of TGF-beta 1 and TGF-beta 2 or exogenous addition of TGF-beta 3 to cutaneous rat wounds reduces scarring, *J Cell Sci* 108 (Pt 3), 985-1002.
73. Soo, C., Beanes, S. R., Hu, F. Y., Zhang, X., Dang, C., Chang, G., Wang, Y., Nishimura, I., Freymiller, E., Longaker, M. T., Lorenz, H. P., and Ting, K. (2003) Ontogenetic transition in fetal wound transforming growth factor-beta regulation correlates with collagen organization, *Am J Pathol* 163, 2459-2476.
74. Ferguson, M. W., Duncan, J., Bond, J., Bush, J., Durani, P., So, K., Taylor, L., Chantrey, J., Mason, T., James, G., Lavery, H., Ocleston, N. L., Sattar, A., Ludlow, A., and O'Kane, S. (2009) Prophylactic administration of avotermin for improvement of skin scarring: three double-blind, placebo-controlled, phase I/II studies, *Lancet* 373, 1264-1274.
75. Grotendorst, G. R., Rahmanie, H., and Duncan, M. R. (2004) Combinatorial signaling pathways determine fibroblast proliferation and myofibroblast differentiation, *FASEB J* 18, 469-479.

76. Roberts, A. B., and Sporn, M. B. (1993) Physiological actions and clinical applications of transforming growth factor-beta (TGF-beta), *Growth Factors* 8, 1-9.
77. Brown, R. L., Ormsby, I., Doetschman, T. C., and Greenhalgh, D. G. (1995) Wound healing in the transforming growth factor-beta-deficient mouse, *Wound Repair Regen* 3, 25-36.
78. Kulkarni, A. B., Huh, C. G., Becker, D., Geiser, A., Lyght, M., Flanders, K. C., Roberts, A. B., Sporn, M. B., Ward, J. M., and Karlsson, S. (1993) Transforming growth factor beta 1 null mutation in mice causes excessive inflammatory response and early death, *Proc Natl Acad Sci U S A* 90, 770-774.
79. Martinez-Ferrer, M., Afshar-Sherif, A. R., Uwamariya, C., de Crombrughe, B., Davidson, J. M., and Bhowmick, N. A. (2010) Dermal transforming growth factor-beta responsiveness mediates wound contraction and epithelial closure, *Am J Pathol* 176, 98-107.
80. Ashcroft, G. S., Yang, X., Glick, A. B., Weinstein, M., Letterio, J. L., Mizel, D. E., Anzano, M., Greenwell-Wild, T., Wahl, S. M., Deng, C., and Roberts, A. B. (1999) Mice lacking Smad3 show accelerated wound healing and an impaired local inflammatory response, *Nat Cell Biol* 1, 260-266.
81. Crowe, M. J., Doetschman, T., and Greenhalgh, D. G. (2000) Delayed wound healing in immunodeficient TGF-beta 1 knockout mice, *J Invest Dermatol* 115, 3-11.
82. Denton, C. P., Khan, K., Hoyles, R. K., Shiwen, X., Leoni, P., Chen, Y., Eastwood, M., and Abraham, D. J. (2009) Inducible lineage-specific deletion of TbetaRII in fibroblasts defines a pivotal regulatory role during adult skin wound healing, *J Invest Dermatol* 129, 194-204.
83. Bielefeld, K. A., Amini-Nik, S., and Alman, B. A. (2013) Cutaneous wound healing: recruiting developmental pathways for regeneration, *Cell Mol Life Sci* 70, 2059-2081.
84. Pietenpol, J. A., Holt, J. T., Stein, R. W., and Moses, H. L. (1990) Transforming growth factor beta 1 suppression of c-myc gene transcription: role in inhibition of keratinocyte proliferation, *Proc Natl Acad Sci U S A* 87, 3758-3762.
85. Wipff, P. J., and Hinz, B. (2008) Integrins and the activation of latent transforming growth factor beta 1 - an intimate relationship, *Eur J Cell Biol* 87, 601-615.
86. Annes, J. P., Chen, Y., Munger, J. S., and Rifkin, D. B. (2004) Integrin alphaVbeta6-mediated activation of latent TGF-beta requires the latent TGF-beta binding protein-1, *J Cell Biol* 165, 723-734.

87. Jenkins, G. (2008) The role of proteases in transforming growth factor-beta activation, *Int J Biochem Cell Biol* 40, 1068-1078.
88. Sheppard, D. (2005) Integrin-mediated activation of latent transforming growth factor beta, *Cancer Metastasis Rev* 24, 395-402.
89. Stamenkovic, I. (2003) Extracellular matrix remodelling: the role of matrix metalloproteinases, *J Pathol* 200, 448-464.
90. Bornstein, P. (1995) Diversity of function is inherent in matricellular proteins: an appraisal of thrombospondin 1, *J Cell Biol* 130, 503-506.
91. Vi, L., Feng, L., Zhu, R. D., Wu, Y., Satish, L., Gan, B. S., and O'Gorman, D. B. (2009) Periostin differentially induces proliferation, contraction and apoptosis of primary Dupuytren's disease and adjacent palmar fascia cells, *Exp Cell Res* 315, 3574-3586.
92. Shi-Wen, X., Chen, Y., Denton, C. P., Eastwood, M., Renzoni, E. A., Bou-Gharios, G., Pearson, J. D., Dashwood, M., du Bois, R. M., Black, C. M., Leask, A., and Abraham, D. J. (2004) Endothelin-1 promotes myofibroblast induction through the ETA receptor via a rac/phosphoinositide 3-kinase/Akt-dependent pathway and is essential for the enhanced contractile phenotype of fibrotic fibroblasts, *Mol Biol Cell* 15, 2707-2719.
93. Wynes, M. W., Frankel, S. K., and Riches, D. W. (2004) IL-4-induced macrophage-derived IGF-I protects myofibroblasts from apoptosis following growth factor withdrawal, *J Leukoc Biol* 76, 1019-1027.
94. Horowitz, J. C., Rogers, D. S., Sharma, V., Vittal, R., White, E. S., Cui, Z., and Thannickal, V. J. (2007) Combinatorial activation of FAK and AKT by transforming growth factor-beta1 confers an anoikis-resistant phenotype to myofibroblasts, *Cell Signal* 19, 761-771.
95. Crawford J, N. K., Gan BS and O'Gorman D. (2014) *Periostin promotes and maintains the differentiation of myofibroblasts in hypertrophic scars.* , *Manuscript submitted for publication.*
96. Crawford J, N. K., Gan BS and O'Gorman D. (2014) *Matrix associated periostin induces hypertrophic scar fibroblast proliferation through a rho kinase dependent pathway.*, *Manuscript in preparation.*
97. Zhou, H. M., Wang, J., Elliott, C., Wen, W., Hamilton, D. W., and Conway, S. J. (2010) Spatiotemporal expression of periostin during skin development and incisional wound healing: lessons for human fibrotic scar formation, *J Cell Commun Signal* 4, 99-107.

98. Jackson-Boeters, L., Wen, W., and Hamilton, D. W. (2009) Periostin localizes to cells in normal skin, but is associated with the extracellular matrix during wound repair, *J Cell Commun Signal* 3, 125-133.
99. Song, Z. H., and Qin, Z. L. (2008) [Expression of periostin and the effect of hydrocortisone on it in human fibroblasts of scar], *Beijing Da Xue Xue Bao* 40, 301-305.
100. Takeshita, S., Kikuno, R., Tezuka, K., and Amann, E. (1993) Osteoblast-specific factor 2: cloning of a putative bone adhesion protein with homology with the insect protein fasciclin I, *Biochem J* 294 (Pt 1), 271-278.
101. Horiuchi, K., Amizuka, N., Takeshita, S., Takamatsu, H., Katsuura, M., Ozawa, H., Toyama, Y., Bonewald, L. F., and Kudo, A. (1999) Identification and characterization of a novel protein, periostin, with restricted expression to periosteum and periodontal ligament and increased expression by transforming growth factor beta, *J Bone Miner Res* 14, 1239-1249.
102. Hoersch, S., and Andrade-Navarro, M. A. (2010) Periostin shows increased evolutionary plasticity in its alternatively spliced region, *BMC Evol Biol* 10, 30.
103. Li, G., Oparil, S., Sanders, J. M., Zhang, L., Dai, M., Chen, L. B., Conway, S. J., McNamara, C. A., and Sarembock, I. J. (2006) Phosphatidylinositol-3-kinase signaling mediates vascular smooth muscle cell expression of periostin in vivo and in vitro, *Atherosclerosis* 188, 292-300.
104. Takayama, G., Arima, K., Kanaji, T., Toda, S., Tanaka, H., Shoji, S., McKenzie, A. N., Nagai, H., Hotokebuchi, T., and Izuhara, K. (2006) Periostin: a novel component of subepithelial fibrosis of bronchial asthma downstream of IL-4 and IL-13 signals, *J Allergy Clin Immunol* 118, 98-104.
105. Callebaut, I., Mignotte, V., Souchet, M., and Mornon, J. P. (2003) EMI domains are widespread and reveal the probable orthologs of the *Caenorhabditis elegans* CED-1 protein, *Biochem Biophys Res Commun* 300, 619-623.
106. Norris, R. A., Damon, B., Mironov, V., Kasyanov, V., Ramamurthi, A., Moreno-Rodriguez, R., Trusk, T., Potts, J. D., Goodwin, R. L., Davis, J., Hoffman, S., Wen, X., Sugi, Y., Kern, C. B., Mjaatvedt, C. H., Turner, D. K., Oka, T., Conway, S. J., Molkentin, J. D., Forgacs, G., and Markwald, R. R. (2007) Periostin regulates collagen fibrillogenesis and the biomechanical properties of connective tissues, *J Cell Biochem* 101, 695-711.
107. Zinn, K., McAllister, L., and Goodman, C. S. (1988) Sequence analysis and neuronal expression of fasciclin I in grasshopper and *Drosophila*, *Cell* 53, 577-587.
108. Ruan, K., Bao, S., and Ouyang, G. (2009) The multifaceted role of periostin in tumorigenesis, *Cell Mol Life Sci* 66, 2219-2230.

109. Coutu, D. L., Wu, J. H., Monette, A., Rivard, G. E., Blostein, M. D., and Galipeau, J. (2008) Periostin, a member of a novel family of vitamin K-dependent proteins, is expressed by mesenchymal stromal cells, *J Biol Chem* 283, 17991-18001.
110. Maruhashi, T., Kii, I., Saito, M., and Kudo, A. (2010) Interaction between periostin and BMP-1 promotes proteolytic activation of lysyl oxidase, *J Biol Chem* 285, 13294-13303.
111. Kii, I., Nishiyama, T., Li, M., Matsumoto, K., Saito, M., Amizuka, N., and Kudo, A. (2010) Incorporation of tenascin-C into the extracellular matrix by periostin underlies an extracellular meshwork architecture, *J Biol Chem* 285, 2028-2039.
112. Kim, J. E., Kim, S. J., Lee, B. H., Park, R. W., Kim, K. S., and Kim, I. S. (2000) Identification of motifs for cell adhesion within the repeated domains of transforming growth factor-beta-induced gene, betaig-h3, *J Biol Chem* 275, 30907-30915.
113. Park, S. J., Park, S., Ahn, H. C., Kim, I. S., and Lee, B. J. (2004) Conformational resemblance between the structures of integrin-activating pentapeptides derived from betaig-h3 and RGD peptide analogues in a membrane environment, *Peptides* 25, 199-205.
114. Litvin, J., Selim, A. H., Montgomery, M. O., Lehmann, K., Rico, M. C., Devlin, H., Bednarik, D. P., and Safadi, F. F. (2004) Expression and function of periostin-isoforms in bone, *J Cell Biochem* 92, 1044-1061.
115. Morra, L., and Moch, H. (2011) Periostin expression and epithelial-mesenchymal transition in cancer: a review and an update, *Virchows Arch* 459, 465-475.
116. Bai, Y., Nakamura, M., Zhou, G., Li, Y., Liu, Z., Ozaki, T., Mori, I., and Kakudo, K. (2010) Novel isoforms of periostin expressed in the human thyroid, *Jpn Clin Med* 1, 13-20.
117. Morra, L., Rechsteiner, M., Casagrande, S., von Teichman, A., Schraml, P., Moch, H., and Soltermann, A. (2012) Characterization of periostin isoform pattern in non-small cell lung cancer, *Lung Cancer* 76, 183-190.
118. Kruzynska-Frejtag, A., Wang, J., Maeda, M., Rogers, R., Krug, E., Hoffman, S., Markwald, R. R., and Conway, S. J. (2004) Periostin is expressed within the developing teeth at the sites of epithelial-mesenchymal interaction, *Dev Dyn* 229, 857-868.
119. Zhu, S., Barbe, M. F., Amin, N., Rani, S., Popoff, S. N., Safadi, F. F., and Litvin, J. (2008) Immunolocalization of Periostin-like factor and Periostin during embryogenesis, *J Histochem Cytochem* 56, 329-345.

120. Shimazaki, M., Nakamura, K., Kii, I., Kashima, T., Amizuka, N., Li, M., Saito, M., Fukuda, K., Nishiyama, T., Kitajima, S., Saga, Y., Fukayama, M., Sata, M., and Kudo, A. (2008) Periostin is essential for cardiac healing after acute myocardial infarction, *J Exp Med* 205, 295-303.
121. Merle, B., and Garnero, P. (2012) The multiple facets of periostin in bone metabolism, *Osteoporos Int* 23, 1199-1212.
122. Schwarz-Linek, U., Werner, J. M., Pickford, A. R., Gurusiddappa, S., Kim, J. H., Pilka, E. S., Briggs, J. A., Gough, T. S., Hook, M., Campbell, I. D., and Potts, J. R. (2003) Pathogenic bacteria attach to human fibronectin through a tandem beta-zipper, *Nature* 423, 177-181.
123. Norris, R. A., Borg, T. K., Butcher, J. T., Baudino, T. A., Banerjee, I., and Markwald, R. R. (2008) Neonatal and adult cardiovascular pathophysiological remodeling and repair: developmental role of periostin, *Ann N Y Acad Sci* 1123, 30-40.
124. Bornstein, P., and Sage, E. H. (2002) Matricellular proteins: extracellular modulators of cell function, *Curr Opin Cell Biol* 14, 608-616.
125. Frangogiannis, N. G. (2012) Matricellular proteins in cardiac adaptation and disease, *Physiol Rev* 92, 635-688.
126. Murphy-Ullrich, J. E. (2001) The de-adhesive activity of matricellular proteins: is intermediate cell adhesion an adaptive state?, *J Clin Invest* 107, 785-790.
127. Kudo, A. (2011) Periostin in fibrillogenesis for tissue regeneration: periostin actions inside and outside the cell, *Cell Mol Life Sci* 68, 3201-3207.
128. Gillan, L., Matei, D., Fishman, D. A., Gerbin, C. S., Karlan, B. Y., and Chang, D. D. (2002) Periostin secreted by epithelial ovarian carcinoma is a ligand for alpha(V)beta(3) and alpha(V)beta(5) integrins and promotes cell motility, *Cancer Res* 62, 5358-5364.
129. Bao, S., Ouyang, G., Bai, X., Huang, Z., Ma, C., Liu, M., Shao, R., Anderson, R. M., Rich, J. N., and Wang, X. F. (2004) Periostin potently promotes metastatic growth of colon cancer by augmenting cell survival via the Akt/PKB pathway, *Cancer Cell* 5, 329-339.
130. Baril, P., Gangeswaran, R., Mahon, P. C., Caulee, K., Kocher, H. M., Harada, T., Zhu, M., Kalthoff, H., Crnogorac-Jurcevic, T., and Lemoine, N. R. (2007) Periostin promotes invasiveness and resistance of pancreatic cancer cells to hypoxia-induced cell death: role of the beta4 integrin and the PI3k pathway, *Oncogene* 26, 2082-2094.

131. Butcher, J. T., Norris, R. A., Hoffman, S., Mjaatvedt, C. H., and Markwald, R. R. (2007) Periostin promotes atrioventricular mesenchyme matrix invasion and remodeling mediated by integrin signaling through Rho/PI 3-kinase, *Dev Biol* 302, 256-266.
132. Kuhn, B., del Monte, F., Hajjar, R. J., Chang, Y. S., Lebeche, D., Arab, S., and Keating, M. T. (2007) Periostin induces proliferation of differentiated cardiomyocytes and promotes cardiac repair, *Nat Med* 13, 962-969.
133. Elliott, C. G., Wang, J., Guo, X., Xu, S. W., Eastwood, M., Guan, J., Leask, A., Conway, S. J., and Hamilton, D. W. (2012) Periostin modulates myofibroblast differentiation during full-thickness cutaneous wound repair, *J Cell Sci* 125, 121-132.
134. Li, G., Jin, R., Norris, R. A., Zhang, L., Yu, S., Wu, F., Markwald, R. R., Nanda, A., Conway, S. J., Smyth, S. S., and Granger, D. N. (2010) Periostin mediates vascular smooth muscle cell migration through the integrins α v β 3 and α v β 5 and focal adhesion kinase (FAK) pathway, *Atherosclerosis* 208, 358-365.
135. Utispan, K., Sonongbua, J., Thuwajit, P., Chau-In, S., Pairojkul, C., Wongkham, S., and Thuwajit, C. (2012) Periostin activates integrin α 5 β 1 through a PI3K/AKTdependent pathway in invasion of cholangiocarcinoma, *Int J Oncol* 41, 1110-1118.
136. Lafrenie, R. M., and Yamada, K. M. (1996) Integrin-dependent signal transduction, *J Cell Biochem* 61, 543-553.
137. Hynes, R. O. (1992) Integrins: versatility, modulation, and signaling in cell adhesion, *Cell* 69, 11-25.
138. Chang, Y., Lee, T. C., Li, J. C., Lai, T. L., Chua, H. H., Chen, C. L., Doong, S. L., Chou, C. K., Sheen, T. S., and Tsai, C. H. (2005) Differential expression of osteoblast-specific factor 2 and polymeric immunoglobulin receptor genes in nasopharyngeal carcinoma, *Head Neck* 27, 873-882.
139. Grigoriadis, A., Mackay, A., Reis-Filho, J. S., Steele, D., Iseli, C., Stevenson, B. J., Jongeneel, C. V., Valgeirsson, H., Fenwick, K., Iravani, M., Leao, M., Simpson, A. J., Strausberg, R. L., Jat, P. S., Ashworth, A., Neville, A. M., and O'Hare, M. J. (2006) Establishment of the epithelial-specific transcriptome of normal and malignant human breast cells based on MPSS and array expression data, *Breast Cancer Res* 8, R56.
140. Kudo, Y., Ogawa, I., Kitajima, S., Kitagawa, M., Kawai, H., Gaffney, P. M., Miyauchi, M., and Takata, T. (2006) Periostin promotes invasion and anchorage-independent growth in the metastatic process of head and neck cancer, *Cancer Res* 66, 6928-6935.

141. Sasaki, H., Dai, M., Auclair, D., Fukai, I., Kiriya, M., Yamakawa, Y., Fujii, Y., and Chen, L. B. (2001) Serum level of the periostin, a homologue of an insect cell adhesion molecule, as a prognostic marker in nonsmall cell lung carcinomas, *Cancer* 92, 843-848.
142. Yan, W., and Shao, R. (2006) Transduction of a mesenchyme-specific gene periostin into 293T cells induces cell invasive activity through epithelial-mesenchymal transformation, *J Biol Chem* 281, 19700-19708.
143. Tanabe, H., Takayama, I., Nishiyama, T., Shimazaki, M., Kii, I., Li, M., Amizuka, N., Katsube, K., and Kudo, A. (2010) Periostin associates with Notch1 precursor to maintain Notch1 expression under a stress condition in mouse cells, *PLoS One* 5, e12234.
144. Tkatchenko, T. V., Moreno-Rodriguez, R. A., Conway, S. J., Molkenin, J. D., Markwald, R. R., and Tkatchenko, A. V. (2009) Lack of periostin leads to suppression of Notch1 signaling and calcific aortic valve disease, *Physiol Genomics* 39, 160-168.
145. Canalis, E., Economides, A. N., and Gazzerro, E. (2003) Bone morphogenetic proteins, their antagonists, and the skeleton, *Endocr Rev* 24, 218-235.
146. Kruzynska-Frejtag, A., Machnicki, M., Rogers, R., Markwald, R. R., and Conway, S. J. (2001) Periostin (an osteoblast-specific factor) is expressed within the embryonic mouse heart during valve formation, *Mech Dev* 103, 183-188.
147. Norris, R. A., Kern, C. B., Wessels, A., Moralez, E. I., Markwald, R. R., and Mjaatvedt, C. H. (2004) Identification and detection of the periostin gene in cardiac development, *Anat Rec A Discov Mol Cell Evol Biol* 281, 1227-1233.
148. Stansfield, W. E., Andersen, N. M., Tang, R. H., and Selzman, C. H. (2009) Periostin is a novel factor in cardiac remodeling after experimental and clinical unloading of the failing heart, *Ann Thorac Surg* 88, 1916-1921.
149. Hakuno, D., Kimura, N., Yoshioka, M., Mukai, M., Kimura, T., Okada, Y., Yozu, R., Shukunami, C., Hiraki, Y., Kudo, A., Ogawa, S., and Fukuda, K. (2010) Periostin advances atherosclerotic and rheumatic cardiac valve degeneration by inducing angiogenesis and MMP production in humans and rodents, *J Clin Invest* 120, 2292-2306.
150. Oka, T., Xu, J., Kaiser, R. A., Melendez, J., Hambleton, M., Sargent, M. A., Lorts, A., Brunskill, E. W., Dorn, G. W., 2nd, Conway, S. J., Aronow, B. J., Robbins, J., and Molkenin, J. D. (2007) Genetic manipulation of periostin expression reveals a role in cardiac hypertrophy and ventricular remodeling, *Circ Res* 101, 313-321.

151. Nishiyama, T., Kii, I., Kashima, T. G., Kikuchi, Y., Ohazama, A., Shimazaki, M., Fukayama, M., and Kudo, A. (2011) Delayed re-epithelialization in periostin-deficient mice during cutaneous wound healing, *PLoS One* 6, e18410.
152. Ontsuka, K., Kotobuki, Y., Shiraishi, H., Serada, S., Ohta, S., Tanemura, A., Yang, L., Fujimoto, M., Arima, K., Suzuki, S., Murota, H., Toda, S., Kudo, A., Conway, S. J., Narisawa, Y., Katayama, I., Izuhara, K., and Naka, T. (2012) Periostin, a matricellular protein, accelerates cutaneous wound repair by activating dermal fibroblasts, *Exp Dermatol* 21, 331-336.
153. Rios, H., Koushik, S. V., Wang, H., Wang, J., Zhou, H. M., Lindsley, A., Rogers, R., Chen, Z., Maeda, M., Kruzynska-Frejtag, A., Feng, J. Q., and Conway, S. J. (2005) periostin null mice exhibit dwarfism, incisor enamel defects, and an early-onset periodontal disease-like phenotype, *Mol Cell Biol* 25, 11131-11144.
154. Snider, P., Hinton, R. B., Moreno-Rodriguez, R. A., Wang, J., Rogers, R., Lindsley, A., Li, F., Ingram, D. A., Menick, D., Field, L., Firulli, A. B., Molkentin, J. D., Markwald, R., and Conway, S. J. (2008) Periostin is required for maturation and extracellular matrix stabilization of noncardiomyocyte lineages of the heart, *Circ Res* 102, 752-760.
155. Bonnet, N., Standley, K. N., Bianchi, E. N., Stadelmann, V., Foti, M., Conway, S. J., and Ferrari, S. L. (2009) The matricellular protein periostin is required for sost inhibition and the anabolic response to mechanical loading and physical activity, *J Biol Chem* 284, 35939-35950.
156. Grinnell, F. (1994) Fibroblasts, myofibroblasts, and wound contraction, *J Cell Biol* 124, 401-404.
157. Elliott, C. G., Kim, S. S., and Hamilton, D. W. (2012) Functional significance of periostin in excisional skin repair: is the devil in the detail?, *Cell Adh Migr* 6, 319-326.
158. Wong, V. W., Sorkin, M., Glotzbach, J. P., Longaker, M. T., and Gurtner, G. C. (2011) Surgical approaches to create murine models of human wound healing, *J Biomed Biotechnol* 2011, 969618.
159. Berking, C., Takemoto, R., Binder, R. L., Hartman, S. M., Ruitter, D. J., Gallagher, P. M., Lessin, S. R., and Herlyn, M. (2002) Photocarcinogenesis in human adult skin grafts, *Carcinogenesis* 23, 181-187.
160. Khavari, P. A. (2006) Modelling cancer in human skin tissue, *Nat Rev Cancer* 6, 270-280.
161. Schon, M. P., Blume-Peytavi, U., Schon, M., and Orfanos, C. E. (1995) The human hair follicle: glycoprotein-related antigenic profile of distinct keratinocyte populations in vivo and their alterations in vitro, *Arch Dermatol Res* 287, 591-598.

162. Lindblad, W. J. (2008) Considerations for selecting the correct animal model for dermal wound-healing studies, *J Biomater Sci Polym Ed* 19, 1087-1096.
163. Nedelec, B., Ghahary, A., Scott, P. G., and Tredget, E. E. (2000) Control of wound contraction. Basic and clinical features, *Hand Clin* 16, 289-302.
164. Cameron, A. M., Adams, D. H., Greenwood, J. E., Anderson, P. J., and Cowin, A. J. (2014) A novel murine model of hypertrophic scarring using subcutaneous infusion of bleomycin, *Plast Reconstr Surg* 133, 69-78.
165. Liu, S., Parapuram, S. K., and Leask, A. (2013) Fibrosis caused by loss of PTEN expression in mouse fibroblasts is crucially dependent on CCN2, *Arthritis Rheum* 65, 2940-2944.
166. Liu, S., Shi-wen, X., Abraham, D. J., and Leask, A. (2011) CCN2 is required for bleomycin-induced skin fibrosis in mice, *Arthritis Rheum* 63, 239-246.
167. Zhu, K. Q., Engrav, L. H., Gibran, N. S., Cole, J. K., Matsumura, H., Piepkorn, M., Isik, F. F., Carrougher, G. J., Muangman, P. M., Yunusov, M. Y., and Yang, T. M. (2003) The female, red Duroc pig as an animal model of hypertrophic scarring and the potential role of the cones of skin, *Burns* 29, 649-664.
168. Yeung, T., Georges, P. C., Flanagan, L. A., Marg, B., Ortiz, M., Funaki, M., Zahir, N., Ming, W., Weaver, V., and Janmey, P. A. (2005) Effects of substrate stiffness on cell morphology, cytoskeletal structure, and adhesion, *Cell Motil Cytoskeleton* 60, 24-34.
169. Hinz, B. (2009) Tissue stiffness, latent TGF-beta1 activation, and mechanical signal transduction: implications for the pathogenesis and treatment of fibrosis, *Curr Rheumatol Rep* 11, 120-126.
170. Callister W. D., R. D. G. (2000) *Fundamentals of Materials Science and Engineering: an Interactive E-Text*, Fifth Edition ed., John Wiley and Sons, Inc., New Jersey.
171. Vi, L., Njarlangattil, A., Wu, Y., Gan, B. S., and O'Gorman, D. B. (2009) Type-1 Collagen differentially alters beta-catenin accumulation in primary Dupuytren's Disease cord and adjacent palmar fascia cells, *BMC Musculoskelet Disord* 10, 72.
172. Grinnell, F. (2003) Fibroblast biology in three-dimensional collagen matrices, *Trends Cell Biol* 13, 264-269.
173. Marenzana, M., Wilson-Jones, N., Mudera, V., and Brown, R. A. (2006) The origins and regulation of tissue tension: identification of collagen tension-fixation process in vitro, *Exp Cell Res* 312, 423-433.

174. Varga, J., Rosenbloom, J., and Jimenez, S. A. (1987) Transforming growth factor beta (TGF beta) causes a persistent increase in steady-state amounts of type I and type III collagen and fibronectin mRNAs in normal human dermal fibroblasts, *Biochem J* 247, 597-604.
175. Schreier, T., Degen, E., and Baschong, W. (1993) Fibroblast migration and proliferation during in vitro wound healing. A quantitative comparison between various growth factors and a low molecular weight blood dialysate used in the clinic to normalize impaired wound healing, *Res Exp Med (Berl)* 193, 195-205.
176. Hocevar, B. A., Brown, T. L., and Howe, P. H. (1999) TGF-beta induces fibronectin synthesis through a c-Jun N-terminal kinase-dependent, Smad4-independent pathway, *EMBO J* 18, 1345-1356.
177. Yang, C. C., Lin, S. D., and Yu, H. S. (1997) Effect of growth factors on dermal fibroblast contraction in normal skin and hypertrophic scar, *J Dermatol Sci* 14, 162-169.
178. Padial-Molina, M., Volk, S. L., and Rios, H. F. (2013) Periostin increases migration and proliferation of human periodontal ligament fibroblasts challenged by tumor necrosis factor -alpha and Porphyromonas gingivalis lipopolysaccharides, *J Periodontal Res.*
179. Naik, P. K., Bozyk, P. D., Bentley, J. K., Popova, A. P., Birch, C. M., Wilke, C. A., Fry, C. D., White, E. S., Sisson, T. H., Tayob, N., Carnemolla, B., Orecchia, P., Flaherty, K. R., Hershenson, M. B., Murray, S., Martinez, F. J., and Moore, B. B. (2012) Periostin promotes fibrosis and predicts progression in patients with idiopathic pulmonary fibrosis, *Am J Physiol Lung Cell Mol Physiol* 303, L1046-1056.
180. Tai, I. T., Dai, M., and Chen, L. B. (2005) Periostin induction in tumor cell line explants and inhibition of in vitro cell growth by anti-periostin antibodies, *Carcinogenesis* 26, 908-915.
181. Howard, J. C., Varallo, V. M., Ross, D. C., Roth, J. H., Faber, K. J., Alman, B., and Gan, B. S. (2003) Elevated levels of beta-catenin and fibronectin in three-dimensional collagen cultures of Dupuytren's disease cells are regulated by tension in vitro, *BMC Musculoskelet Disord* 4, 16.
182. Tomasek, J., and Rayan, G. M. (1995) Correlation of alpha-smooth muscle actin expression and contraction in Dupuytren's disease fibroblasts, *J Hand Surg Am* 20, 450-455.
183. Dallan, J. C., and Ehrlich, H. P. (2008) A review of fibroblast-populated collagen lattices, *Wound Repair Regen* 16, 472-479.

184. Dugina, V., Fontao, L., Chaponnier, C., Vasiliev, J., and Gabbiani, G. (2001) Focal adhesion features during myofibroblastic differentiation are controlled by intracellular and extracellular factors, *J Cell Sci* 114, 3285-3296.
185. O'Leary, R., Wood, E. J., and Guillou, P. J. (2002) Pathological scarring: strategic interventions, *Eur J Surg* 168, 523-534.
186. Scott, P. G., Ghahary, A., and Tredget, E. E. (2000) Molecular and cellular aspects of fibrosis following thermal injury, *Hand Clin* 16, 271-287.
187. Ishikawa, K., Yoshida, S., Nakao, S., Nakama, T., Kita, T., Asato, R., Sassa, Y., Arita, R., Miyazaki, M., Enaida, H., Oshima, Y., Murakami, N., Niino, H., Ono, J., Matsuda, A., Goto, Y., Akashi, K., Izuhara, K., Kudo, A., Kono, T., Hafezi-Moghadam, A., and Ishibashi, T. (2014) Periostin promotes the generation of fibrous membranes in proliferative vitreoretinopathy, *FASEB J* 28, 131-142.
188. Litvin, J., Chen, X., Keleman, S., Zhu, S., and Autieri, M. (2007) Expression and function of periostin-like factor in vascular smooth muscle cells, *Am J Physiol Cell Physiol* 292, C1672-1680.
189. Kim, C. J., Isono, T., Tambe, Y., Chano, T., Okabe, H., Okada, Y., and Inoue, H. (2008) Role of alternative splicing of periostin in human bladder carcinogenesis, *Int J Oncol* 32, 161-169.
190. Litvin, J., Blagg, A., Mu, A., Matiwala, S., Montgomery, M., Berretta, R., Houser, S., and Margulies, K. (2006) Periostin and periostin-like factor in the human heart: possible therapeutic targets, *Cardiovasc Pathol* 15, 24-32.
191. Conte, E., Fruciano, M., Fagone, E., Gili, E., Caraci, F., Iemmolo, M., Crimi, N., and Vancheri, C. (2011) Inhibition of PI3K prevents the proliferation and differentiation of human lung fibroblasts into myofibroblasts: the role of class I P110 isoforms, *PLoS One* 6, e24663.
192. Kim, C. S., Kim, J. K., Nam, S. Y., Yang, K. H., Jeong, M., Kim, H. S., Jin, Y. W., and Kim, J. (2007) Low-dose radiation stimulates the proliferation of normal human lung fibroblasts via a transient activation of Raf and Akt, *Mol Cells* 24, 424-430.
193. Morel, J., Audo, R., Hahne, M., and Combe, B. (2005) Tumor necrosis factor-related apoptosis-inducing ligand (TRAIL) induces rheumatoid arthritis synovial fibroblast proliferation through mitogen-activated protein kinases and phosphatidylinositol 3-kinase/Akt, *J Biol Chem* 280, 15709-15718.
194. Bain, J., Plater, L., Elliott, M., Shpiro, N., Hastie, C. J., McLauchlan, H., Klevernic, I., Arthur, J. S., Alessi, D. R., and Cohen, P. (2007) The selectivity of protein kinase inhibitors: a further update, *Biochem J* 408, 297-315.

195. Tsuji, F., Setoguchi, C., Okamoto, M., Seki, I., Sasano, M., and Aono, H. (2012) Bucillamine inhibits CD40-mediated Akt activation and antibody production in mouse B-cell lymphoma, *Int Immunopharmacol* 14, 47-53.
196. Rinnab, L., Schutz, S. V., Diesch, J., Schmid, E., Kufer, R., Hautmann, R. E., Spindler, K. D., and Cronauer, M. V. (2008) Inhibition of glycogen synthase kinase-3 in androgen-responsive prostate cancer cell lines: are GSK inhibitors therapeutically useful?, *Neoplasia* 10, 624-634.
197. Croft, D. R., and Olson, M. F. (2006) The Rho GTPase effector ROCK regulates cyclin A, cyclin D1, and p27Kip1 levels by distinct mechanisms, *Mol Cell Biol* 26, 4612-4627.
198. Tanaka, M., Abe, T., and Hara, Y. (2009) Roles of focal adhesions and fibronectin-mediated cohesion in proliferation of confluent fibroblasts, *J Cell Physiol* 219, 194-201.
199. Yin, J., Lu, J., and Yu, F. S. (2008) Role of small GTPase Rho in regulating corneal epithelial wound healing, *Invest Ophthalmol Vis Sci* 49, 900-909.
200. Chen, J., Guerriero, E., Lathrop, K., and SundarRaj, N. (2008) Rho/ROCK signaling in regulation of corneal epithelial cell cycle progression, *Invest Ophthalmol Vis Sci* 49, 175-183.
201. Iwamoto, H., Nakamuta, M., Tada, S., Sugimoto, R., Enjoji, M., and Nawata, H. (2000) A p160ROCK-specific inhibitor, Y-27632, attenuates rat hepatic stellate cell growth, *J Hepatol* 32, 762-770.
202. Alessi, D. R., Cuenda, A., Cohen, P., Dudley, D. T., and Saltiel, A. R. (1995) PD 098059 is a specific inhibitor of the activation of mitogen-activated protein kinase kinase in vitro and in vivo, *J Biol Chem* 270, 27489-27494.
203. Kikuchi, Y., Kunita, A., Iwata, C., Komura, D., Nishiyama, T., Shimazu, K., Takeshita, K., Shibahara, J., Kii, I., Morishita, Y., Yashiro, M., Hirakawa, K., Miyazono, K., Kudo, A., Fukayama, M., and Kashima, T. G. (2014) The niche component periostin is produced by cancer-associated fibroblasts, supporting growth of gastric cancer through ERK activation, *Am J Pathol* 184, 859-870.
204. Chen, T., Kunnavatana, S. S., and Koch, R. J. (2006) Effects of mitomycin-C on normal dermal fibroblasts, *Laryngoscope* 116, 514-517.
205. Franke, T. F., Kaplan, D. R., Cantley, L. C., and Toker, A. (1997) Direct regulation of the Akt proto-oncogene product by phosphatidylinositol-3,4-bisphosphate, *Science* 275, 665-668.
206. Pages, G., Lenormand, P., L'Allemain, G., Chambard, J. C., Meloche, S., and Pouyssegur, J. (1993) Mitogen-activated protein kinases p42mapk and p44mapk are required for fibroblast proliferation, *Proc Natl Acad Sci U S A* 90, 8319-8323.

207. Grimes, C. A., and Jope, R. S. (2001) The multifaceted roles of glycogen synthase kinase 3beta in cellular signaling, *Prog Neurobiol* 65, 391-426.
208. Leung, T., Chen, X. Q., Manser, E., and Lim, L. (1996) The p160 RhoA-binding kinase ROK alpha is a member of a kinase family and is involved in the reorganization of the cytoskeleton, *Mol Cell Biol* 16, 5313-5327.
209. Riento, K., and Ridley, A. J. (2003) Rocks: multifunctional kinases in cell behaviour, *Nat Rev Mol Cell Biol* 4, 446-456.
210. Yin, J., and Yu, F. S. (2008) Rho kinases regulate corneal epithelial wound healing, *Am J Physiol Cell Physiol* 295, C378-387.
211. Boku, S., Nakagawa, S., Toda, H., Kato, A., Takamura, N., Omiya, Y., Inoue, T., and Koyama, T. (2013) ROCK2 regulates bFGF-induced proliferation of SH-SY5Y cells through GSK-3beta and beta-catenin pathway, *Brain Res* 1492, 7-17.
212. Miao, L., Dai, Y., and Zhang, J. (2002) Mechanism of RhoA/Rho kinase activation in endothelin-1- induced contraction in rabbit basilar artery, *Am J Physiol Heart Circ Physiol* 283, H983-989.
213. Reif, K., Nobes, C. D., Thomas, G., Hall, A., and Cantrell, D. A. (1996) Phosphatidylinositol 3-kinase signals activate a selective subset of Rac/Rho-dependent effector pathways, *Curr Biol* 6, 1445-1455.
214. Wehrwein, E. A., Northcott, C. A., Loberg, R. D., and Watts, S. W. (2004) Rho/Rho kinase and phosphoinositide 3-kinase are parallel pathways in the development of spontaneous arterial tone in deoxycorticosterone acetate-salt hypertension, *J Pharmacol Exp Ther* 309, 1011-1019.
215. Wang, Q., Nie, F. F., Zhao, X., and Qin, Z. L. (2007) [The expression of periostin in hyperplastic scars and the relations to TGF-beta1 and its receptors], *Zhonghua Zheng Xing Wai Ke Za Zhi* 23, 229-232.
216. Ehrlich, H. P., and Rajaratnam, J. B. (1990) Cell locomotion forces versus cell contraction forces for collagen lattice contraction: an in vitro model of wound contraction, *Tissue Cell* 22, 407-417.
217. Bell, E., Ivarsson, B., and Merrill, C. (1979) Production of a tissue-like structure by contraction of collagen lattices by human fibroblasts of different proliferative potential in vitro, *Proc Natl Acad Sci U S A* 76, 1274-1278.
218. Hinz, B., Pittet, P., Smith-Clerc, J., Chaponnier, C., and Meister, J. J. (2004) Myofibroblast development is characterized by specific cell-cell adherens junctions, *Mol Biol Cell* 15, 4310-4320.

219. Jiang, H., Rhee, S., Ho, C. H., and Grinnell, F. (2008) Distinguishing fibroblast promigratory and procontractile growth factor environments in 3-D collagen matrices, *FASEB J* 22, 2151-2160.
220. Schultz, G. S., and Wysocki, A. (2009) Interactions between extracellular matrix and growth factors in wound healing, *Wound Repair Regen* 17, 153-162.
221. Okazaki, M., Takeshita, S., Kawai, S., Kikuno, R., Tsujimura, A., Kudo, A., and Amann, E. (1994) Molecular cloning and characterization of OB-cadherin, a new member of cadherin family expressed in osteoblasts, *J Biol Chem* 269, 12092-12098.
222. Michaylira, C. Z., Wong, G. S., Miller, C. G., Gutierrez, C. M., Nakagawa, H., Hammond, R., Klein-Szanto, A. J., Lee, J. S., Kim, S. B., Herlyn, M., Diehl, J. A., Gimotty, P., and Rustgi, A. K. (2010) Periostin, a cell adhesion molecule, facilitates invasion in the tumor microenvironment and annotates a novel tumor-invasive signature in esophageal cancer, *Cancer Res* 70, 5281-5292.
223. Colwell, A. S., Phan, T. T., Kong, W., Longaker, M. T., and Lorenz, P. H. (2005) Hypertrophic scar fibroblasts have increased connective tissue growth factor expression after transforming growth factor-beta stimulation, *Plast Reconstr Surg* 116, 1387-1390; discussion 1391-1382.
224. Hanks, S. K., Calalb, M. B., Harper, M. C., and Patel, S. K. (1992) Focal adhesion protein-tyrosine kinase phosphorylated in response to cell attachment to fibronectin, *Proc Natl Acad Sci U S A* 89, 8487-8491.
225. Schaller, M. D., Borgman, C. A., Cobb, B. S., Vines, R. R., Reynolds, A. B., and Parsons, J. T. (1992) pp125FAK a structurally distinctive protein-tyrosine kinase associated with focal adhesions, *Proc Natl Acad Sci U S A* 89, 5192-5196.
226. Thannickal, V. J., Lee, D. Y., White, E. S., Cui, Z., Larios, J. M., Chacon, R., Horowitz, J. C., Day, R. M., and Thomas, P. E. (2003) Myofibroblast differentiation by transforming growth factor-beta1 is dependent on cell adhesion and integrin signaling via focal adhesion kinase, *J Biol Chem* 278, 12384-12389.
227. Lappalainen, P., and Drubin, D. G. (1997) Cofilin promotes rapid actin filament turnover in vivo, *Nature* 388, 78-82.
228. Maekawa, M., Ishizaki, T., Boku, S., Watanabe, N., Fujita, A., Iwamatsu, A., Obinata, T., Ohashi, K., Mizuno, K., and Narumiya, S. (1999) Signaling from Rho to the actin cytoskeleton through protein kinases ROCK and LIM-kinase, *Science* 285, 895-898.
229. Tamariz, E., and Grinnell, F. (2002) Modulation of fibroblast morphology and adhesion during collagen matrix remodeling, *Mol Biol Cell* 13, 3915-3929.

230. Hinz, B., Dugina, V., Ballestrem, C., Wehrle-Haller, B., and Chaponnier, C. (2003) Alpha-smooth muscle actin is crucial for focal adhesion maturation in myofibroblasts, *Mol Biol Cell* 14, 2508-2519.
231. Geiger, B., Bershadsky, A., Pankov, R., and Yamada, K. M. (2001) Transmembrane crosstalk between the extracellular matrix--cytoskeleton crosstalk, *Nat Rev Mol Cell Biol* 2, 793-805.
232. Vi, L., de Lasa, C., DiGuglielmo, G. M., and Dagnino, L. (2011) Integrin-linked kinase is required for TGF-beta1 induction of dermal myofibroblast differentiation, *J Invest Dermatol* 131, 586-593.
233. Markham, K., Bai, Y., and Schmitt-Ulms, G. (2007) Co-immunoprecipitations revisited: an update on experimental concepts and their implementation for sensitive interactome investigations of endogenous proteins, *Anal Bioanal Chem* 389, 461-473.
234. Klockenbusch, C., and Kast, J. (2010) Optimization of formaldehyde cross-linking for protein interaction analysis of non-tagged integrin beta1, *J Biomed Biotechnol* 2010, 927585.
235. Nelson, C. M., and Bissell, M. J. (2006) Of extracellular matrix, scaffolds, and signaling: tissue architecture regulates development, homeostasis, and cancer, *Annu Rev Cell Dev Biol* 22, 287-309.
236. Mitra, S. K., Hanson, D. A., and Schlaepfer, D. D. (2005) Focal adhesion kinase: in command and control of cell motility, *Nat Rev Mol Cell Biol* 6, 56-68.
237. Yamashita, O., Yoshimura, K., Nagasawa, A., Ueda, K., Morikage, N., Ikeda, Y., and Hamano, K. (2013) Periostin links mechanical strain to inflammation in abdominal aortic aneurysm, *PLoS One* 8, e79753.
238. Ghatak, S., Misra, S., Norris, R. A., Rodriguez, R. M., Hoffman, S., Levine, R. A., Hascall, V. C., and Markwald, R. R. (2014) Periostin induces intracellular cross talk between kinases and hyaluronan in atrioventricular valvulogenesis, *J Biol Chem*.
239. Schlaepfer, D. D., Mitra, S. K., and Ilic, D. (2004) Control of motile and invasive cell phenotypes by focal adhesion kinase, *Biochim Biophys Acta* 1692, 77-102.
240. Hsia, D. A., Mitra, S. K., Hauck, C. R., Streblov, D. N., Nelson, J. A., Ilic, D., Huang, S., Li, E., Nemerow, G. R., Leng, J., Spencer, K. S., Cheresch, D. A., and Schlaepfer, D. D. (2003) Differential regulation of cell motility and invasion by FAK, *J Cell Biol* 160, 753-767.
241. Zhai, J., Lin, H., Nie, Z., Wu, J., Canete-Soler, R., Schlaepfer, W. W., and Schlaepfer, D. D. (2003) Direct interaction of focal adhesion kinase with p190RhoGEF, *J Biol Chem* 278, 24865-24873.

242. van Horck, F. P., Ahmadian, M. R., Haeusler, L. C., Moolenaar, W. H., and Kranenburg, O. (2001) Characterization of p190RhoGEF, a RhoA-specific guanine nucleotide exchange factor that interacts with microtubules, *J Biol Chem* 276, 4948-4956.
243. Gebbink, M. F., Kranenburg, O., Poland, M., van Horck, F. P., Houssa, B., and Moolenaar, W. H. (1997) Identification of a novel, putative Rho-specific GDP/GTP exchange factor and a RhoA-binding protein: control of neuronal morphology, *J Cell Biol* 137, 1603-1613.
244. Morgan-Fisher, M., Wewer, U. M., and Yoneda, A. (2013) Regulation of ROCK activity in cancer, *J Histochem Cytochem* 61, 185-198.
245. Amano, M., Chihara, K., Nakamura, N., Kaneko, T., Matsuura, Y., and Kaibuchi, K. (1999) The COOH terminus of Rho-kinase negatively regulates rho-kinase activity, *J Biol Chem* 274, 32418-32424.
246. Holinstat, M., Knezevic, N., Broman, M., Samarel, A. M., Malik, A. B., and Mehta, D. (2006) Suppression of RhoA activity by focal adhesion kinase-induced activation of p190RhoGAP: role in regulation of endothelial permeability, *J Biol Chem* 281, 2296-2305.
247. Narumiya, S., Ishizaki, T., and Watanabe, N. (1997) Rho effectors and reorganization of actin cytoskeleton, *FEBS Lett* 410, 68-72.
248. Sund, B. (2000) *New Developments in Wound Care*, PJB Publication, London.
249. Harding, K. G., Morris, H. L., and Patel, G. K. (2002) Science, medicine and the future: healing chronic wounds, *BMJ* 324, 160-163.
250. Woodbury MG, H. P. (2005) The extent of chronic wounds in Canada, *Wound Care Canada* 3, 18-22.
251. Wu, S. C., Driver, V. R., Wrobel, J. S., and Armstrong, D. G. (2007) Foot ulcers in the diabetic patient, prevention and treatment, *Vasc Health Risk Manag* 3, 65-76.
252. Liu, S., Herault, Y., Pavlovic, G., and Leask, A. (2014) Skin progenitor cells contribute to bleomycin-induced skin fibrosis, *Arthritis Rheumatol* 66, 707-713.
253. Gudjonsson, J. E., Johnston, A., Dyson, M., Valdimarsson, H., and Elder, J. T. (2007) Mouse models of psoriasis, *J Invest Dermatol* 127, 1292-1308.
254. Swindell, W. R., Johnston, A., Carbajal, S., Han, G., Wohn, C., Lu, J., Xing, X., Nair, R. P., Voorhees, J. J., Elder, J. T., Wang, X. J., Sano, S., Prens, E. P., DiGiovanni, J., Pittelkow, M. R., Ward, N. L., and Gudjonsson, J. E. (2011) Genome-wide expression profiling of five mouse models identifies similarities and differences with human psoriasis, *PLoS One* 6, e18266.

255. Harunari, N., Zhu, K. Q., Armendariz, R. T., Deubner, H., Muangman, P., Carrougher, G. J., Isik, F. F., Gibran, N. S., and Engrav, L. H. (2006) Histology of the thick scar on the female, red Duroc pig: final similarities to human hypertrophic scar, *Burns* 32, 669-677.
256. Xie, Y., Zhu, K. Q., Deubner, H., Emerson, D. A., Carrougher, G. J., Gibran, N. S., and Engrav, L. H. (2007) The microvasculature in cutaneous wound healing in the female red Duroc pig is similar to that in human hypertrophic scars and different from that in the female Yorkshire pig, *J Burn Care Res* 28, 500-506.
257. Zhu, K. Q., Carrougher, G. J., Gibran, N. S., Isik, F. F., and Engrav, L. H. (2007) Review of the female Duroc/Yorkshire pig model of human fibroproliferative scarring, *Wound Repair Regen* 15 Suppl 1, S32-39.
258. Sullivan, T. P., Eaglstein, W. H., Davis, S. C., and Mertz, P. (2001) The pig as a model for human wound healing, *Wound Repair Regen* 9, 66-76.
259. Gallant, C. L., Olson, M. E., and Hart, D. A. (2004) Molecular, histologic, and gross phenotype of skin wound healing in red Duroc pigs reveals an abnormal healing phenotype of hypercontracted, hyperpigmented scarring, *Wound Repair Regen* 12, 305-319.
260. Pohjolainen, V., Rysa, J., Napankangas, J., Koobi, P., Eraranta, A., Ilves, M., Serpi, R., Porsti, I., and Ruskoaho, H. (2012) Left ventricular periostin gene expression is associated with fibrogenesis in experimental renal insufficiency, *Nephrol Dial Transplant* 27, 115-122.
261. Okamoto, M., Hoshino, T., Kitasato, Y., Sakazaki, Y., Kawayama, T., Fujimoto, K., Ohshima, K., Shiraishi, H., Uchida, M., Ono, J., Ohta, S., Kato, S., Izuhara, K., and Aizawa, H. (2011) Periostin, a matrix protein, is a novel biomarker for idiopathic interstitial pneumonias, *Eur Respir J* 37, 1119-1127.
262. Sen, K., Lindenmeyer, M. T., Gaspert, A., Eichinger, F., Neusser, M. A., Kretzler, M., Segerer, S., and Cohen, C. D. (2011) Periostin is induced in glomerular injury and expressed de novo in interstitial renal fibrosis, *Am J Pathol* 179, 1756-1767.
263. Wallace, D. P., White, C., Savinkova, L., Nivens, E., Reif, G. A., Pinto, C. S., Raman, A., Parnell, S. C., Conway, S. J., and Fields, T. A. (2014) Periostin promotes renal cyst growth and interstitial fibrosis in polycystic kidney disease, *Kidney Int* 85, 845-854.
264. Aggeler, J., Ward, J., Blackie, L. M., Barcellos-Hoff, M. H., Streuli, C. H., and Bissell, M. J. (1991) Cytodifferentiation of mouse mammary epithelial cells cultured on a reconstituted basement membrane reveals striking similarities to development in vivo, *J Cell Sci* 99 (Pt 2), 407-417.

265. Barcellos-Hoff, M. H., Aggeler, J., Ram, T. G., and Bissell, M. J. (1989) Functional differentiation and alveolar morphogenesis of primary mammary cultures on reconstituted basement membrane, *Development* 105, 223-235.
266. Streuli, C. H., Schmidhauser, C., Bailey, N., Yurchenco, P., Skubitz, A. P., Roskelley, C., and Bissell, M. J. (1995) Laminin mediates tissue-specific gene expression in mammary epithelia, *J Cell Biol* 129, 591-603.
267. Weaver, V. M., Lelievre, S., Lakins, J. N., Chrenek, M. A., Jones, J. C., Giancotti, F., Werb, Z., and Bissell, M. J. (2002) beta4 integrin-dependent formation of polarized three-dimensional architecture confers resistance to apoptosis in normal and malignant mammary epithelium, *Cancer Cell* 2, 205-216.
268. Weigelt, B., Lo, A. T., Park, C. C., Gray, J. W., and Bissell, M. J. (2010) HER2 signaling pathway activation and response of breast cancer cells to HER2-targeting agents is dependent strongly on the 3D microenvironment, *Breast Cancer Res Treat* 122, 35-43.
269. Polo, M. L., Arnoni, M. V., Riggio, M., Wargon, V., Lanari, C., and Novaro, V. (2010) Responsiveness to PI3K and MEK inhibitors in breast cancer. Use of a 3D culture system to study pathways related to hormone independence in mice, *PLoS One* 5, e10786.
270. Prinz, F., Schlange, T., and Asadullah, K. (2011) Believe it or not: how much can we rely on published data on potential drug targets?, *Nat Rev Drug Discov* 10, 712.
271. Bissell, M. J., and Hines, W. C. (2011) Why don't we get more cancer? A proposed role of the microenvironment in restraining cancer progression, *Nat Med* 17, 320-329.
272. Dolberg, D. S., Hollingsworth, R., Hertle, M., and Bissell, M. J. (1985) Wounding and its role in RSV-mediated tumor formation, *Science* 230, 676-678.
273. Maher, J. J., and Bissell, D. M. (1993) Cell-matrix interactions in liver, *Semin Cell Biol* 4, 189-201.
274. Boyd, N. F., Guo, H., Martin, L. J., Sun, L., Stone, J., Fishell, E., Jong, R. A., Hislop, G., Chiarelli, A., Minkin, S., and Yaffe, M. J. (2007) Mammographic density and the risk and detection of breast cancer, *N Engl J Med* 356, 227-236.
275. Provenzano, P. P., Inman, D. R., Eliceiri, K. W., Knittel, J. G., Yan, L., Rueden, C. T., White, J. G., and Keely, P. J. (2008) Collagen density promotes mammary tumor initiation and progression, *BMC Med* 6, 11.

276. Wang, W., Wyckoff, J. B., Frohlich, V. C., Oleynikov, Y., Huttelmaier, S., Zavadil, J., Cermak, L., Bottinger, E. P., Singer, R. H., White, J. G., Segall, J. E., and Condeelis, J. S. (2002) Single cell behavior in metastatic primary mammary tumors correlated with gene expression patterns revealed by molecular profiling, *Cancer Res* 62, 6278-6288.
277. Provenzano, P. P., Eliceiri, K. W., Campbell, J. M., Inman, D. R., White, J. G., and Keely, P. J. (2006) Collagen reorganization at the tumor-stromal interface facilitates local invasion, *BMC Med* 4, 38.
278. Wozniak, M. A., Desai, R., Solski, P. A., Der, C. J., and Keely, P. J. (2003) ROCK-generated contractility regulates breast epithelial cell differentiation in response to the physical properties of a three-dimensional collagen matrix, *J Cell Biol* 163, 583-595.
279. Paszek, M. J., Zahir, N., Johnson, K. R., Lakins, J. N., Rozenberg, G. I., Gefen, A., Reinhart-King, C. A., Margulies, S. S., Dembo, M., Boettiger, D., Hammer, D. A., and Weaver, V. M. (2005) Tensional homeostasis and the malignant phenotype, *Cancer Cell* 8, 241-254.
280. Croft, D. R., Sahai, E., Mavria, G., Li, S., Tsai, J., Lee, W. M., Marshall, C. J., and Olson, M. F. (2004) Conditional ROCK activation in vivo induces tumor cell dissemination and angiogenesis, *Cancer Res* 64, 8994-9001.
281. Malanchi, I., Santamaria-Martinez, A., Susanto, E., Peng, H., Lehr, H. A., Delaloye, J. F., and Huelsken, J. (2012) Interactions between cancer stem cells and their niche govern metastatic colonization, *Nature* 481, 85-89.
282. Howlett, A. R., Petersen, O. W., Steeg, P. S., and Bissell, M. J. (1994) A novel function for the nm23-H1 gene: overexpression in human breast carcinoma cells leads to the formation of basement membrane and growth arrest, *J Natl Cancer Inst* 86, 1838-1844.
283. Choi, J. W., Arai, C., Ishikawa, M., Shimoda, S., and Nakamura, Y. (2011) Fiber system degradation, and periostin and connective tissue growth factor level reduction, in the periodontal ligament of teeth in the absence of masticatory load, *J Periodontal Res* 46, 513-521.
284. Bonnefoy, A., and Legrand, C. (2000) Proteolysis of subendothelial adhesive glycoproteins (fibronectin, thrombospondin, and von Willebrand factor) by plasmin, leukocyte cathepsin G, and elastase, *Thromb Res* 98, 323-332.
285. Patterson, J., and Hubbell, J. A. (2011) SPARC-derived protease substrates to enhance the plasmin sensitivity of molecularly engineered PEG hydrogels, *Biomaterials* 32, 1301-1310.

286. Choi, J., Lin, A., Shrier, E., Lau, L. F., Grant, M. B., and Chaqour, B. (2013) Degradome products of the matricellular protein CCN1 as modulators of pathological angiogenesis in the retina, *J Biol Chem* 288, 23075-23089.
287. Eto, H., Suga, H., Aoi, N., Kato, H., Doi, K., Kuno, S., Tabata, Y., and Yoshimura, K. (2012) Therapeutic potential of fibroblast growth factor-2 for hypertrophic scars: upregulation of MMP-1 and HGF expression, *Lab Invest* 92, 214-223.
288. Neely, A. N., Clendening, C. E., Gardner, J., Greenhalgh, D. G., and Warden, G. D. (1999) Gelatinase activity in keloids and hypertrophic scars, *Wound Repair Regen* 7, 166-171.
289. Burd, A., and Huang, L. (2005) Hypertrophic response and keloid diathesis: two very different forms of scar, *Plast Reconstr Surg* 116, 150e-157e.
290. Kzhyshkowska, J., Workman, G., Cardo-Vila, M., Arap, W., Pasqualini, R., Gratchev, A., Krusell, L., Goerdts, S., and Sage, E. H. (2006) Novel function of alternatively activated macrophages: stabilin-1-mediated clearance of SPARC, *J Immunol* 176, 5825-5832.
291. Kzhyshkowska, J., Gratchev, A., and Goerdts, S. (2006) Stabilin-1, a homeostatic scavenger receptor with multiple functions, *J Cell Mol Med* 10, 635-649.

Appendix

Appendix A - Ethics Approval Notice



Use of Human Participants - Ethics Approval Notice

Principal Investigator: Dr. Bing Siang Gan
Review Number: 08222E
Review Level: Delegated
Approved Local Adult Participants: 1000
Approved Local Minor Participants: 0
Protocol Title: Molecular mechanisms of Dupuytren's Contracture, related fibroproliferative diseases and other human disorders.
Department & Institution: Surgery,
Sponsor:
Ethics Approval Date: November 08, 2011 **Expiry Date:** December 31, 2016
Documents Reviewed & Approved & Documents Received for Information:

Document Name	Comments	Version Date
Addition of Co-investigator	A new co-investigator has been added - Dr. Roel Ophoff from UCLA.	
Revised Study End Date	The researcher has requested a 5 year extension on this study - December 31, 2016.	
Revised UWO Protocol	With this new co-investigator samples will now be sent off site. This has been revised in the letter of information.	
Revised Letter of Information & Consent	September 2011 - Controls	
Revised Letter of Information & Consent	September 2011 - Study Subjects	

This is to notify you that The University of Western Ontario Research Ethics Board for Health Sciences Research Involving Human Subjects (HSREB) which is organized and operates according to the Tri-Council Policy Statement: Ethical Conduct of Research Involving Humans and the Health Canada/ICH Good Clinical Practice Practices: Consolidated Guidelines; and the applicable laws and regulations of Ontario has reviewed and granted approval to the above referenced revision(s) or amendment(s) on the approval date noted above. The membership of this REB also complies with the membership requirements for REB's as defined in Division 5 of the Food and Drug Regulations.

The ethics approval for this study shall remain valid until the expiry date noted above assuming timely and acceptable responses to the HSREB's periodic requests for surveillance and monitoring information. If you require an updated approval notice prior to that time you must request it using the UWO Updated Approval Request Form.

Members of the HSREB who are named as investigators in research studies, or declare a conflict of interest, do not participate in discussion related to, nor vote on, such studies when they are presented to the HSREB.

The Chair of the HSREB is Dr. Joseph Gilbert. The UWO HSREB is registered with the U.S. Department of Health & Human Services under the IRB registration number IRB 00000940.

Curriculum Vitae

Justin David Crawford

EDUCATION

- September 2009 – August 2014 **Doctor of Philosophy (PhD)**
 Department of Biochemistry
 Schulich School of Medicine & Dentistry
 University of Western Ontario, London, Ontario,
 Canada
- September 2005 – April 2009 **Bachelor of Medical Sciences (BMSc)**
 Honour Specialization in Clinical Biochemistry
 with distinction
 Schulich School of Medicine & Dentistry
 University of Western Ontario, London, Ontario,
 Canada

EXPERIENCE

- September 2009 – August 2014 **Graduate Research Assistantship**
 Cell and Molecular Biology Laboratory,
 Roth|McFarlane Hand and Upper Limb Centre,
 St. Joseph's Health Care, Lawson Health
 Research Institute, London, Ontario, Canada
 Supervisor: Dr. D.B. O'Gorman
- January 2012 – April 2014 **Graduate Teaching Assistant**
 University of Western Ontario, London, Ontario,
 Canada
 Biochemistry 3386b – Clinical Biochemistry
 Course Coordinator: Dr. Norman Smith
- September 2013 – December 2013 **Graduate Teaching Assistant**
 University of Western Ontario, London, Ontario,
 Canada
 Biochemistry 4450a – Molecular genetics of
 human cancer
 Course Coordinator: Dr. David Rodenhiser
- May 2009 – August 2009 **CIHR Summer Student**
 Cell and Molecular Biology Laboratory,
 Roth|McFarlane Hand and Upper Limb Centre,
 St. Joseph's Health Care, Lawson Health
 Research Institute, London, Ontario, Canada
 Supervisor: Dr D.B. O'Gorman

October 2008 – April 2009

Undergraduate Research Student.

Cell and Molecular Biology Laboratory,
Roth/McFarlane Hand and Upper Limb Centre,
St. Joseph's Health Care, Lawson Health
Research Institute, London, Ontario, Canada
Supervisor: Dr. D.B. O'Gorman

DISTINCTIONS, HONORS, AWARDS RECEIVED

Institute Community Support Travel Award

Canadian Institutes of Health Research, August 2012

Periostin: A potential mediator of myofibroblast contraction and survival in a 3-D model of hypertrophic scarring

Value: \$1000

Young Investigators Award

European Tissue Repair Society. September 2010

Value: 500 €

Western Graduate Research Scholarship

University of Western Ontario, 2009 – 2012

Value: Covers tuition

Western Scholarship of Distinction

University of Western Ontario, 2005

Value: \$1500

RESEARCH STUDENTSHIP AWARDS

September 2010 – August 2011

Frederick Banting and Charles Best Canada Graduate Scholarship – Master's Award

Canadian Institutes of Health Research
The role(s) of periostin in abnormal wound healing

Supervisor: Dr. David O'Gorman

Value: \$17,500

May 2009 – July 2009

IMHA Summer Studentship in Musculoskeletal Research

Canadian Institutes of Health Research
Generation of a lox-stop-lox *POSTN* cDNA transgene

Supervisors: Drs. D.B. O'Gorman and B.S. Gan

Value: \$4,950

BOOK CHAPTERS

Raykha C, Crawford J, Gan BS, O'Gorman DB. (2011) Insulin-like Growth Factor Binding Protein (IGFBP)-6: A mediator of myofibroblast differentiation in Dupuytren's Disease. In: Proceedings of the International Dupuytren's Symposium. Springer Verlag.

PUBLICATIONS

Crawford J, Nygard K., Gan BS and O'Gorman D. (2014) *Matrix-associated periostin promotes proliferation and differentiation of primary hypertrophic scar fibroblasts*, Manuscript submitted for publication.

Raykha C, **Crawford J**, Burry A, Drosdowech D, Faber K, Gan BS and O'Gorman D. (In press). IGF2 expression and β -catenin levels are increased in Frozen Shoulder Syndrome, *Clinical and Investigative Medicine*.

Raykha, C., **Crawford, J.**, Gan, B. S., Fu, P., Bach, L. A., and O'Gorman, D. B. (2013) IGF-II and IGFBP-6 regulate cellular contractility and proliferation in Dupuytren's disease, *Biochim Biophys Acta 1832*, 1511-1519.

PUBLISHED ABSTRACTS

Crawford JD*, Gan BS and O'Gorman DB
 Periostin: A mediator of myofibroblast contraction and survival in a 3-D model of hypertrophic scarring
 22nd European Tissue Repair Society Congress, 5 October 2012, Royal Olympic Hotel, Athens, Greece

Crawford JD*, Gan BS and O'Gorman DB
 Periostin induces the proliferation of primary hypertrophic scar fibroblasts and the GSK-3 β /beta-catenin signaling pathway
 21st European Tissue Repair Society Congress, 6 October 2011, Felix Meritis, Amsterdam, Netherlands

Raykha CN, **Crawford JD**, Gan BS and O'Gorman DB
 Is Insulin-like Growth Factor Binding Protein-6 a 'fibrosis suppressor' in Dupuytren's Disease?
 21st European Tissue Repair Society Congress, 6 October 2011, Felix Meritis, Amsterdam, Netherlands

Raykha CN, **Crawford JD**, Gan BS and O'Gorman DB
 IGFBP-6 and IGF-II: novel mediators of myofibroblast differentiation in Dupuytren's Disease?
 Fifth International Congress of the GRS and IGF Society, 6 October 2010, Sheraton Hotel, New York, NY

Crawford JD*, Gan BS and O'Gorman DB
 Periostin specifically induces fibroblast proliferation and myofibroblast differentiation in hypertrophic scarring
 20th European Tissue Repair Society Congress, 17 September 2010, Het Pand, Gent, Belgium

Raykha CN, **Crawford JD**, Gan BS and O'Gorman DB
 Insulin-like growth factor-II and insulin-like growth factor binding protein-6; previously unrecognized mediators of myofibroblast differentiation in Dupuytren's disease
 20th European Tissue Repair Society Congress, 17 September 2010, Het Pand, Gent, Belgium

Raykha CN, **Crawford JD**, Gan BS, O’Gorman DB
 IGFBP-6: A novel mediator of myofibroblast differentiation in Dupuytren’s Disease?
 International Dupuytren Symposium, InterContinental Hotel, 22 May 2010, Miami, FL

ORAL PRESENTATIONS

Crawford JD*, Gan BS and O’Gorman DB
 Periostin promotes and maintains myofibroblast differentiation in hypertrophic scarring
 Keystone Symposia, Fibrosis: From Bench to Bedside, 25 March 2014, Keystone Resort,
 Keystone, CO, USA

Crawford JD*, Gan BS and O’Gorman DB
 Periostin: A mediator of myofibroblast contraction and survival in a 3-D model of hypertrophic
 scarring
 22nd European Tissue Repair Society Congress, 5 October 2012, Royal Olympic Hotel, Athens,
 Greece

Crawford JD*, Gan BS and O’Gorman DB
 Periostin induces the proliferation of primary hypertrophic scar fibroblasts and the GSK-
 3beta/beta-catenin signaling pathway
 21st European Tissue Repair Society Congress, 6 October 2011, Felix Meritis, Amsterdam,
 Netherlands

Raykha CN, **Crawford JD**, Gan BS and O’Gorman DB
 Is Insulin-like Growth Factor Binding Protein-6 a 'fibrosis suppressor' in Dupuytren's Disease?
 21st European Tissue Repair Society Congress, 6 October 2011, Felix Meritis, Amsterdam,
 Netherlands

Raykha CN, **Crawford JD**, Gan BS and O’Gorman DB
 IGFBP-6 and IGF-II: novel mediators of myofibroblast differentiation in Dupuytren’s Disease?
 Fifth International Congress of the GRS and IGF Society, 6 October 2010, Sheraton Hotel, New
 York, NY

Crawford JD*, Gan BS and O’Gorman DB
 Periostin specifically induces fibroblast proliferation and myofibroblast differentiation in
 hypertrophic scarring
 20th European Tissue Repair Society Congress, 17 September 2010, Het Pand, Gent, Belgium

Raykha CN, **Crawford JD**, Gan BS and O’Gorman DB
 Insulin-like growth factor-II and insulin-like growth factor binding protein-6; previously
 unrecognized mediators of myofibroblast differentiation in Dupuytren’s disease
 20th European Tissue Repair Society Congress, 17th September 2010, Het Pand, Gent, Belgium

Raykha CN, **Crawford JD**, Gan BS, O’Gorman DB
 IGFBP-6: A novel mediator of myofibroblast differentiation in Dupuytren’s Disease?
 International Dupuytren Symposium, InterContinental Hotel, 22 May 2010, Miami, FL
 O’Gorman DB, **Crawford JD**, Raykha CN, and Gan BS
 Dupuytren's Disease: a model for dissecting the molecular components of fibrosis
 Kolling Institute of Medical Research, 18th March 2009, Royal North Shore Hospital, St,
 Leonards, Sydney, Australia

POSTER PRESENTATIONS

Crawford JD*, Gan BS and O’Gorman DB

Periostin: a matricellular inhibitor of apoptosis in hypertrophic scars?

London Health Research Day, London Convention Centre, 20 March 2012, London, ON, Canada

Crawford JD*, Gan BS and O’Gorman DB

Periostin induces fibroblast proliferation through a novel signalling pathway in hypertrophic scarring

Dr. Sandy Kirkley Musculoskeletal Research Day, Dr. Sandy Kirkley Centre for Musculoskeletal Research, 28 September 2011, London, ON, Canada

Crawford JD*, Gan BS and O’Gorman DB

Examining the Effects of Periostin on Hypertrophic Scar-Derived Fibroblasts

Margaret Moffat Research Day, University of Western Ontario, 30 March 2010, London, ON, Canada

Crawford JD*, Gan BS and O’Gorman DB

The Roles of Periostin in Keloid and Hypertrophic Scars

Western Research Forum, University of Western Ontario, 27 February 2010, London, ON, Canada

* Primary presenter